UNIVERSIDAD DE CHILE
FACULTAD DE CIENCIAS FISICAS Y MATEMATICAS
DEPARTAMENTO DE GEOLOGIA

ORIGEN DE LAS ROTACIONES TECTÓNICAS EN EL MARGEN OCCIDENTAL DE AMÉRICA DEL SUR: INFLUENCIA DE HETEROGENEIDADES EN LAS PLACA DE NAZCA Y SUDAMERICA.

TESIS PARA OPTAR AL GRADO DE DOCTOR EN CIENCIAS MENCION GEOLOGIA

MATIAS ALBERTO PEÑA GOMEZ

PROFESOR GUIA:
MARCELO FARIAS THIERS

MIEMBROS DE LA COMISION:
REYNALDO CHARRIER GONZÁLEZ
FERNANDO POBLETE GOMEZ
ANDRÉS TASSARA ODDO

SANTIAGO DE CHILE
2022

RESUMEN TESIS PARA OPTAR AL GRADO DE: Doctor en Ciencias, mención Geología
POR: Matias Alberto Peña Goez
FECHA: 2022
PROFESOR GUÍA: Dr. Marcelo Farias Thiers

Resumen

Uno de los rasgos más sobresalientes de los Andes Centrales es el Oroclino Boliviano, el que consiste en la curvatura de las principales estructuras y unidades morfotectónicas alrededor de un eje de simetría a los. 21°S. Este Oroclino ha sido estudiado desde los primeros datos paleomagnéticos obtenidos en 1984, denotando desde ya un patrón de rotaciones antihoraria, al norte del oroclino y rotaciones horarias, al sur de este. Aun cuando la densidad de datos aumenta día a día, el origen, límite y temporalidad de estas rotaciones continúa siendo materia de debate; así como su posible relación con eventos de deformación responsables de la orogenia andina.

En esta tesis, se presentarán los resultados de un estudio paleomagnético, junto con dataciones geocronológicas, y su correlación con eventos tectónicos del Meso-Cenozoico en los Andes Centrales. Para ello, se muestrearon más de 800 sitios paleomagnéticos entre 18,5° y 31°S, con una variabilidad meridiana entre 72° y 67°E. Estos fueron muestreados en la Precordillera chilena y Cordillera de Domeyko en rocas intrusivas y estratificadas desde el Paleozoico al Mioceno, así como también en rocas sedimentarias de edad paleozoica y terciaria en las Sierras Pampeanas.

Los resultados paleomagnéticos obtenidos en la Cordillera de la Costa y Cordillera de Domeyko entre 18° y 23°S se encuentran mayormente remagnetizados, ligados a los procesos magmáticos del Eoceno-Oligoceno responsables de la formación del mismo orógeno. Los datos de rotaciones muestran un patrón de rotaciones casi nulas, tanto para la Cordillera de Domeyko como para la Cordillera de la Costa. En el antearco chileno entre 26° y 29°S, los datos poseen una señal magnética primaria, mostrando una magnetización relacionada a su depositación (o intrusión), en algunos casos estando fuertemente ligada a procesos de depositación sintectónica. Estas muestras poseen un patrón sistemático de rotaciones horarias de alrededor de 30°, cambiando drásticamente este patrón al sur de los 29°S a una rotación de alrededor de 15°S. Las distintas rotaciones observadas son correlacionables a pulsos compresivos que van desde el Cretácico Superior en adelante, siendo el evento rotacional del Eoceno-Oligoceno el más fuerte de la zona de los Andes Centrales, y llevan a desafiar el concepto de Oroclino previamente establecido.

Palabras claves: *Andes Centrales, Oroclino Boliviano, Paleomagnetismo.*

Summary

One of the most outstanding features of the Central Andes is the Bolivian Orocline, which consists of the curvature of the main structures and morphotectonic units around an axis of symmetry at 21°S. This Orocline has been studied since the first paleomagnetic data obtained in 1984, already denoting a pattern of counterclockwise rotations, to the north of the orocline, and clockwise rotations, to the south of it. Even when data density increases day by day, the origin, limit and timing of these rotations continue to be a matter of debate; as well as its possible relationship with deformation events responsible for the Andean orogeny.

In this thesis, the results of a paleomagnetic study will be presented, plus some geochronological dating results, and their correlation with Meso-Cenozoic tectonic events in the Central Andes. To do this, more than 800 paleomagnetic sites were sampled between 18.5° and 31°S, with meridian variability between 72° and 67°E. These were sampled in rocks mainly from the Chilean Precordillera and Domeyko Range in intrusive and stratified rocks from the Paleozoic to Miocene, as well as in sedimentary rocks of Paleozoic and Tertiary age in the Sierras Pampeanas.

The paleomagnetic results obtained in the Coastal Range and Domeyko Range between 18° and 23°S are mostly remagnetized, linked to magmatic events in the Eocene-Oligocene. The rotational data show a pattern of almost null rotations, both for the Domeyko Range and for the Coastal Range. In the Chilean forearc between 26° and 29°S, the data have a primary magnetic nature, showing a magnetization related to its deposition (or intrusion), in some cases being strongly linked to syntectonic depositional processes. These samples have a systematic pattern of clockwise rotations around 30°, this pattern drastically changing south of 29°S to a clockwise rotation of about 15°. The different rotations observed are correlatable to compressive pulses that go from Late Cretaceous, being the Eocene-Oligocene rotational event the strongest in the Central Andes, and lead to challenge the previously established Oroclinal concept.

Agradecimientos

Me gustaria empezar esta cortina de agradecimientos primero que nada a quienes me dieron la oportunidad y me contagiaron las ganas respecto a este estudio. A Cesar Arriagada, por la amistad, por darme las dudas necesarias para plantear esta investigacion, por varios meses de salidas a terreno donde hablamos de lo humano, lo divino y lo avernal. A Pierrick Roperch, quien, en su estilo especial, me mostro ciertos secretos alquimicos del paleomagnetismo. A Fernando Martinez, de quien en esos primeros terrenos aprendi sobren arquitecturas e inversiones. A Marcelo Farias, quien me acogio (como a otros tantos), bajo su alero, y que me dio otra forma de ver las geologia, no solo a traves de este trabajo, sino que a lo largo de mil y un conversaciones y tazas de cafe, donde me hizo viajar desde los Andes a Mercurio, en una misma tarde de discusión. A Fernando Poblete, quien tambien me recogio bajo su alero, y me mostro los celestiales paisajes patagonicos, zonas llenas de aventuras para la mente y para el cuerpo, donde la avidez de conocimiento choca con la agreste naturaleza de islas y fiordos.

Los compañeros de trabajo fueron indispensables a la hora de poseer el animo para desarrollar y terminar este trabajo, por lo que un especial cariño debe ser mandado a la asociación R.A.P. (Razon Apoyo Perseverancia) cuyos integrantes son Javier Alvarez, Javier Reyes, Pablo Molina, Sebastian Bascuñan, Sebastian Herrera, Italo Payacan e Ivan Gomez. A los integrantes de la "Casa de Oliver": Yerko, Cristi y Rodrigo. A varios amigos de la Universidad: Feña, Vero, Ruso, Guagua, Chuncho, Jorquera, Mauro, Pelao, Galle, Seba Perroud, Martin, Waren, y muchos mas que se pueden quedar en el tintero. A los castores de isla Navarino: Tapia, Chala, Pajaro, Ricky, Joaco; amigos en el frio y en las aguas turbias. A mi familia, mis padres y hermanas, que han aguantado mis ñoñerias todos estos años. A mis primas, con las que comparti los años de U, y mis tia mariana y mi tio Carlos, que siempre recordare sus concejos y conversaciones, lo extrañaremos siempre, asi como a mis dos abuelitas.

A mi compañera, Alejandra, quien su amor, temple y apoyo han sido pilares fundamentales no solo para terminar este trabajo, sino para sobrevivir estos aciagos años de covid y de estruendo.

Al proyecto FONDECYT 1070964 y al Plan Nacional de SERNAGEOMIN por su financiamiento para la obtencion de muchas de las muestras de este trabajo.

Tabla de contenido

Índice de Figuras

1: Introducción

En esta sección se revisará, de forma historiográfica, la evolución del estado del arte del conocimiento del Oroclino Boliviano asi como ha avanzado el concepto de flexuramiento oroclinal en el tiempo. En base a estas problemáticas es como se propone la hipótesis y objetivos de este trabajo.

1.1.- Los Oroclinos: común en la arquitectura geodinámica.

Al observar el planeta Tierra desde el espacio es bastante notable que la gran mayoría de los cordones orogénicos poseen alguna flexura a lo largo de su rumbo. En su trabajo pionero de 1909 titulado "***Das Antlitz der Erde***" (La superficie terrestre), Eduard Suess describió conceptos aun utilizados hoy en día, como el supercontinente Gondwana, los valles del Rift Africano, y un término llamado "*Salientes*" con el que Suess describió los cambios de rumbo, a gran escala, de las distintas cordilleras alrededor del planeta (Suess, 1909). Esta lógica de curvaturas orogénicas fue retomada por Hobbs en 1914, quien relacionó esfuerzos compresivos asociados con eventos sísmicos como parte del proceso de formación de montañas, así como notó también que estas mismas deformaciones asociadas al levantamiento orogénico estaban siempre relegadas a "formas convexas", sobre todo al observar las líneas de islas y los cordones montañosos del Este de Asia y Oceania (Hobbs, 1914). Esta forma de ver los cinturones seria notada en detalle en las montañas Ouachita (Figura 1.1), en el estado de Oklahoma de los Estados Unidos, agregando conceptos como ejes de flexuramiento, el mayor acortamiento y densidad de fallamiento hacia el centro de los cinturones curvados y la asociación de estas salientes con cuerpos relógicamente más competentes que pueden haber ayudado a formarlas (Miser, 1929).

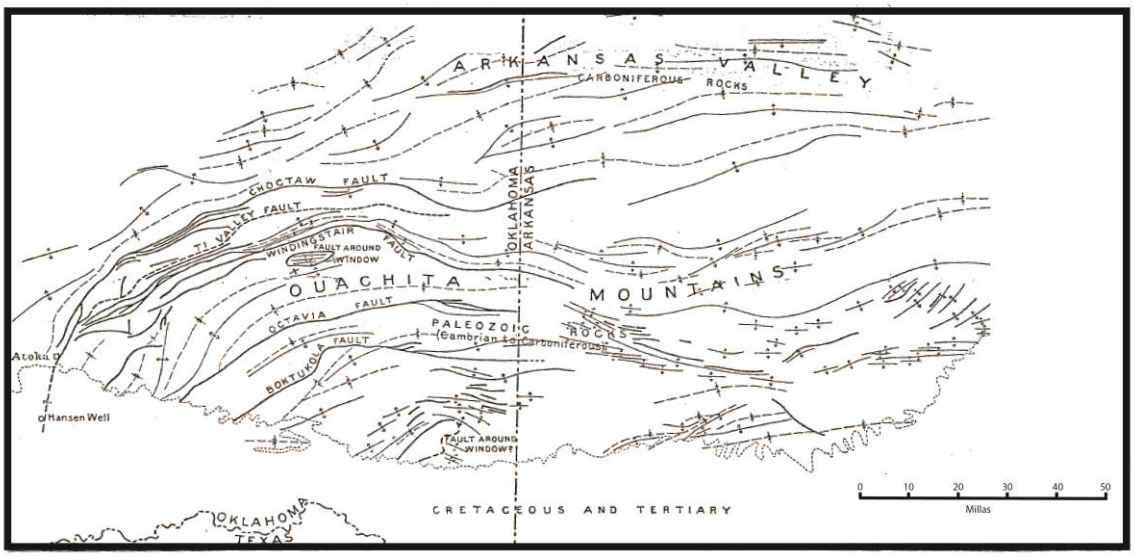

Figura 1.1 : Salientes de Montañas Oachita, en Oklahoma y Arkansas, estudiadas por Miser (1929).

El análisis de estos orogenos convexos con respecto a su edad de deformación fue complementado por datos a lo largo del planeta por Carey (Carey, 1955), redefiniendo posteriormente estos flexuramientos como "**Oroclinos**". Este término se refiere a "***cordones orogénicos curvados que adquirieron su curvatura después de su alzamiento***", sugiriendo que una de las características más relevantes para describir el desarrollo de esta curvatura es a través de la presencia de rotaciones de bloques tectónicos en planta (Figura 1.2).

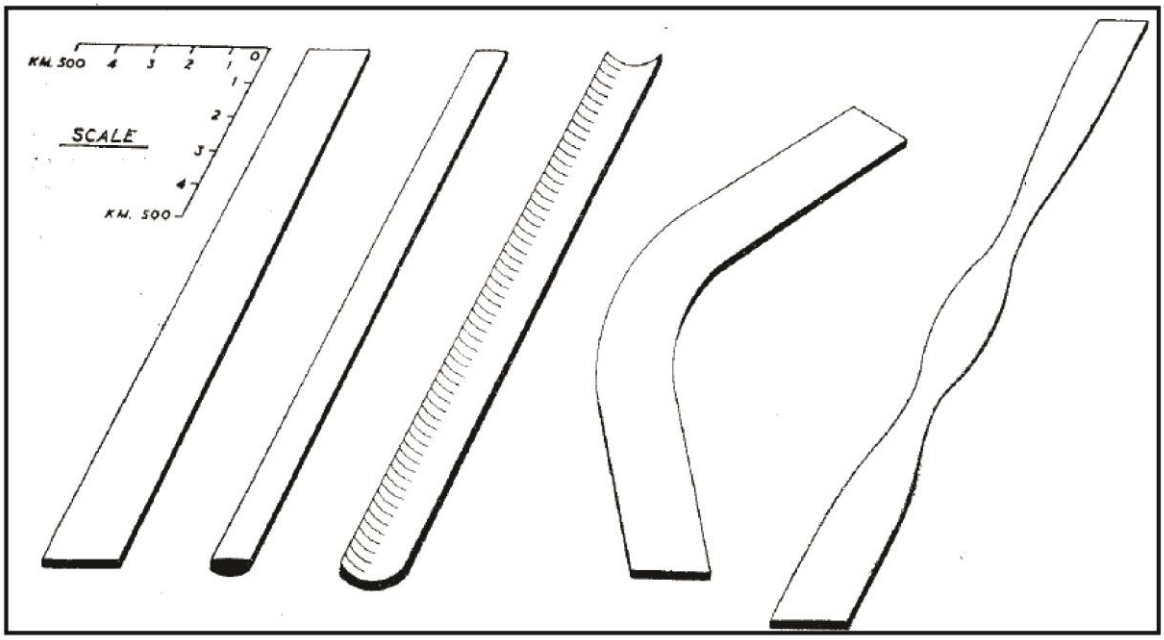

Figura 1.2: Modelos de curvamiento oroclinal según los planeamientos de Carey (1955).

Esta definición primigenia fue aumentada, siendo posible hoy clasificar los cinturones arqueados en tres categorías (Figura 1.3): El **arco primario** (Figura 1.3A), que adopta la curvatura durante la fase inicial de deformación del orógeno; el **Oroclino**, que adopta la curvatura luego de levantarse el orógeno; y el **arco progresivo**, que representa a aquellos orógenos que adquieren su curvatura sucesivamente durante su formación u orógenos que adquieren una porción de su curvatura durante una posterior fase de deformación (Weil y Sussman, 2004; Weil et al 2013).

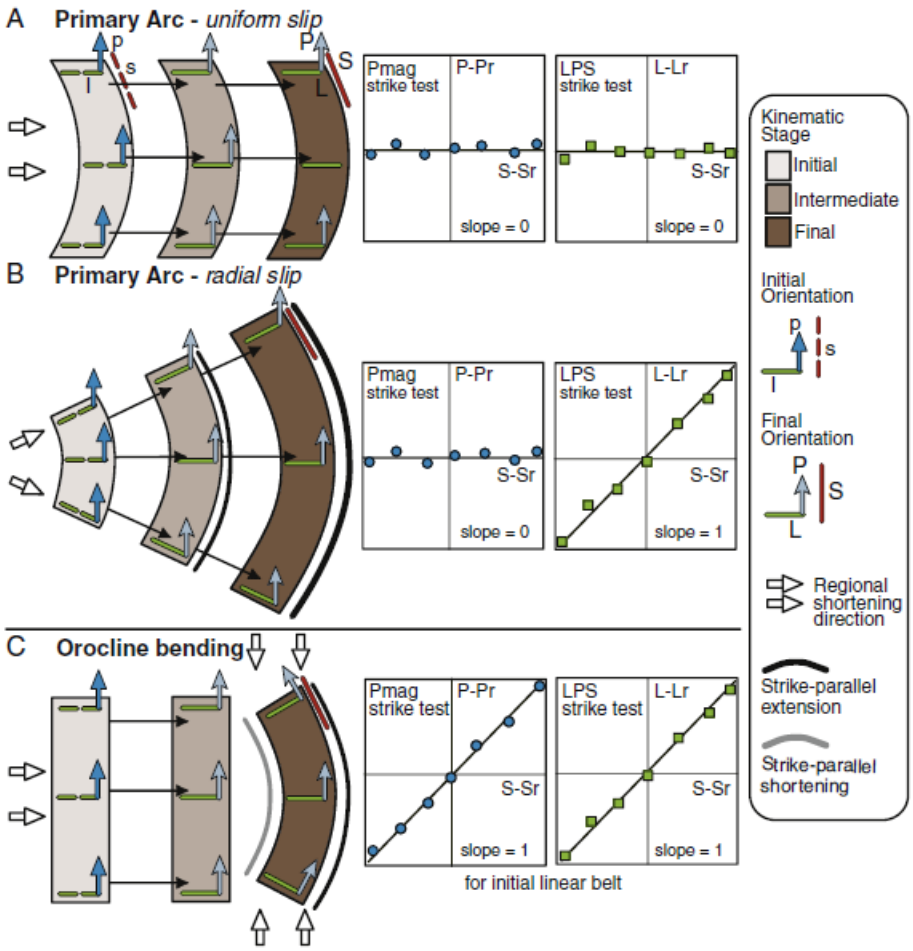

Figura 1.3: Clasificación de flexuras orogénicas. (A) corresponde a un arco primario con un vector de deformación uniforme, (B) un arco primario con un vector de deformación radia y (C) corresponde a un Oroclino. (Weil et al 2013).

Diversos procesos geológicos y geodinámicos han sido relacionados con la formación de oroclinos, siendo descritos por varios autores en tres categorías principales (figuras 1.3, 1.4 y 1.5): (a) Delaminación litosferica (Gutierrez-Alonso et al., 2012; Weil et al., 2013): el engrosamiento excesivo de la litosfera en el eje del flexuramiento oroclinal puede causar un colapso gravitacional de la litosfera inferior, adelgazando el manto litosferico, debilitando termalmente la corteza. (b) Procesos relacionados a deformación local en fajas plegadas y corridas de escama delgada (Marshak, 2004): La deformación diferencial, interacción con obstáculos, interacción con fallas de rumbo, intersección de dos fajas plegadas y corridas de distinto rumbo, y heterogeneidades heradadas por cuencas tectónicamente reactivadas; pueden generar deformación oroclinal de carácter regional. (c) Variaciones en el margen de

placas (Rosenbaum & Lister., 2004): Variaciones en los tipos de márgenes y curvamientos de los mismos propiciara deformación en la placa continental, curvando esta misma deformación de forma oroclinal. Estos diversos procesos han sido analizados para Oroclinos como el Varisco (Weil et al., 2013), las Tasmanides (Rosenmabun et al., 2012), el Oroclino Centro-Asiático (Xiao et al., 2010) y el conjunto de Oroclinos que circundan el Mediterraneo (Rosembaun, 2014). Dentro de estos procesos, la alternativa relacionada con la variación del margen de placas corresponde a una de las posibilidades más interesantes del último tiempo: enmarcada en esta opción se encuentra la subducción de heterogeneidades en la placa inferior (Capitanio et al., 2011; Martinod et al., 2010; O'Driscoll et al., 2012), la indentación de bloques tectónicos (Beltrando et al., 2010; Lickorish et al., 2002) y la acreción de pedazos de corteza continental que producen escapes tectónicos de masas a su alrededor (DeCelles et al., 2002; Jacobs y Thomas, 2004; Kuiper et al., 2011).

Los procesos de flexuramiento de un orógeno implican deformaciones a distintas escalas. A escala de una deformación de escama fina, ciertas heterogeneidades regionales pueden influenciar la formación de flexuras, pudiendo ser controladas por la anisotropía de cuencas extensionales previas a una deformación compresiva (figura 1.4), llamadas curvas "*controladas por cuencas*" (Macedo y Marshak, 1999, siendo estas heterogeneidades un actor importante para la existencia de curvaturas orgénicas de escala regional (Marshak et al., 1992; Mitra, 1997). De la misma forma, la presencia de cambios en las condiciones de los grandes *detachment* de los sistemas de fajas plegadas y corridas (como la presencia de evaporitas, cambios en el ángulo de la cuña compresiva, cambios en las condiciones de erosión o presencia de plutones) puede cambiar la respuesta a lo largo del rumbo de estos sistemas, produciendo curvaturas como respuestas a estos cambios (Macedo y Marshak, 1999).

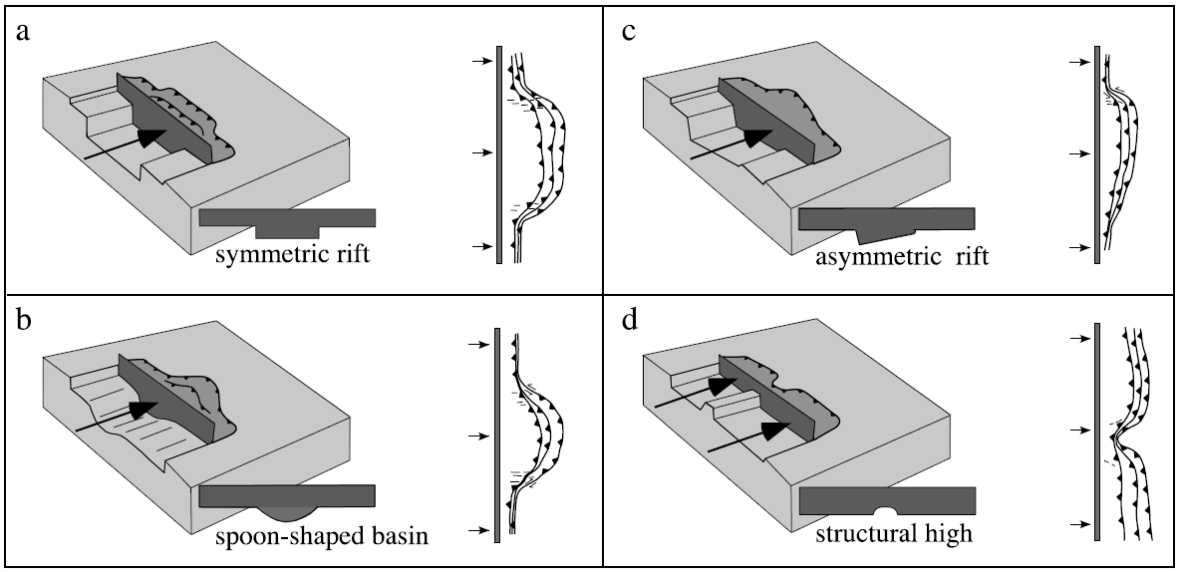

Figura 1.4: Curvaturas orogénicas formadas por heterogeneidades en los despegues de fajas plegadas y corridas según Marshak (2004).

A nivel de escama gruesa, o deformación de carácter geodinámico asociada con despegues profundos, pueden existir varios factores que propicien la creación de una flexura oroclinal. La acción de indentadores tectónicos es una de la más conocidas y estudiadas, sobre todo en los casos Alpinos (Lickorish et al., 2002) e Himalayos (Tapponier y Molnar, 1976), donde la colisión de grandes bloques continentales (o continentes enteros como el caso de los Himalayas) son usados para explicar las flexuras, escapes tectónicos y deformación de escama gruesa o despegues profundos (Davy y Cobbold, 1988; Jacobs y Thomas, 2004). Siguiendo el mismo razonamiento de choques continentales, la forma irregular de un bloque continental (Figura 1.5) puede inducir de forma específica la formación de curvaturas orogénicas (Dana, 1866; Thomas, 1977). Un último, pero no menos importante, caso donde es posible inducir flexuras corresponde a aquellas controladas por obstáculos, pudiendo darse dos casos específicos: uno donde una faja plegada y corrida interactúe con bloques de basamento en su antepais, obligándola a cambiar su rumbo (Paulsen y Marshak, 1998); o cuando montes submarinos o heterogeneidades positivas en la placa subductante interactúan con

la placa superior, produciendo cambios en el rumbo de la deformación (Dominguez et al., 1998)

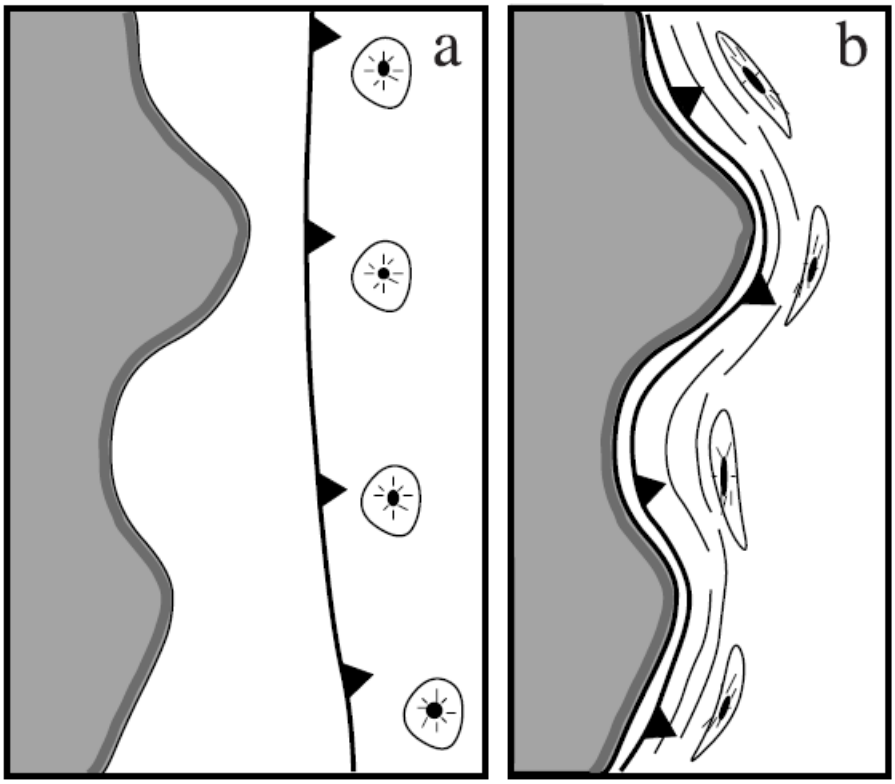

Figura 1.5: Flexuramientos producidos por irregularidades en el margen (Marshak, 2004).

1.2.- Oroclinos en Sudamérica: Andes centrales

El estudio de los oroclinos en distintas partes del planeta comparte metodologías similares: el establecimiento de las edades de deformación y el control de las rotaciones tectónicas que se producen a un lado y otro del su eje de simetría. Estas metodologías han sido fundamentales par entender las 4 grandes curvaturas que se encuentran a lo largo del margen occidental de Sudamérica, que de norte a sur son Huancabamba (Mitouard et al., 1990); Abancay (Roperch et al., 2011); Arica, u Oroclino Boliviano (Heki, 1985; Somoza et al., 1996; Arriagada et al., 2008); y Patagonia (Cunningham, 1993; Poblete et al., 2014; 2016). En un primer orden, el

más notable de estos oroclinos es el **Oroclino Boliviano** (Figura 1.6), ubicado alrededor de los 18º de latitud sur.

Siendo mas específicos, en los Andes Centrales podemos observar al menos 4 deflexiones además del Oroclino Boliviano, donde el margen continental cambia su rumbo, y las principales estructuras también lo hacen (Figura 1.6). Junto con ello, datos paleomagnéticos tomados desde hace más de 30 años apoyan estos cambios de rumbo como rotaciones tectónicas, mostrando como éstas poseían otras orientaciones respecto a las actuales (e.g., Arriagada et al., 2008). Las 4 principales deflexiones que podemos encontrar en estas zonas son: La deflexión de Abancay, el Oroclino de Vallenar, el Oroclino del Maipo y el Oroclino de Arauco.

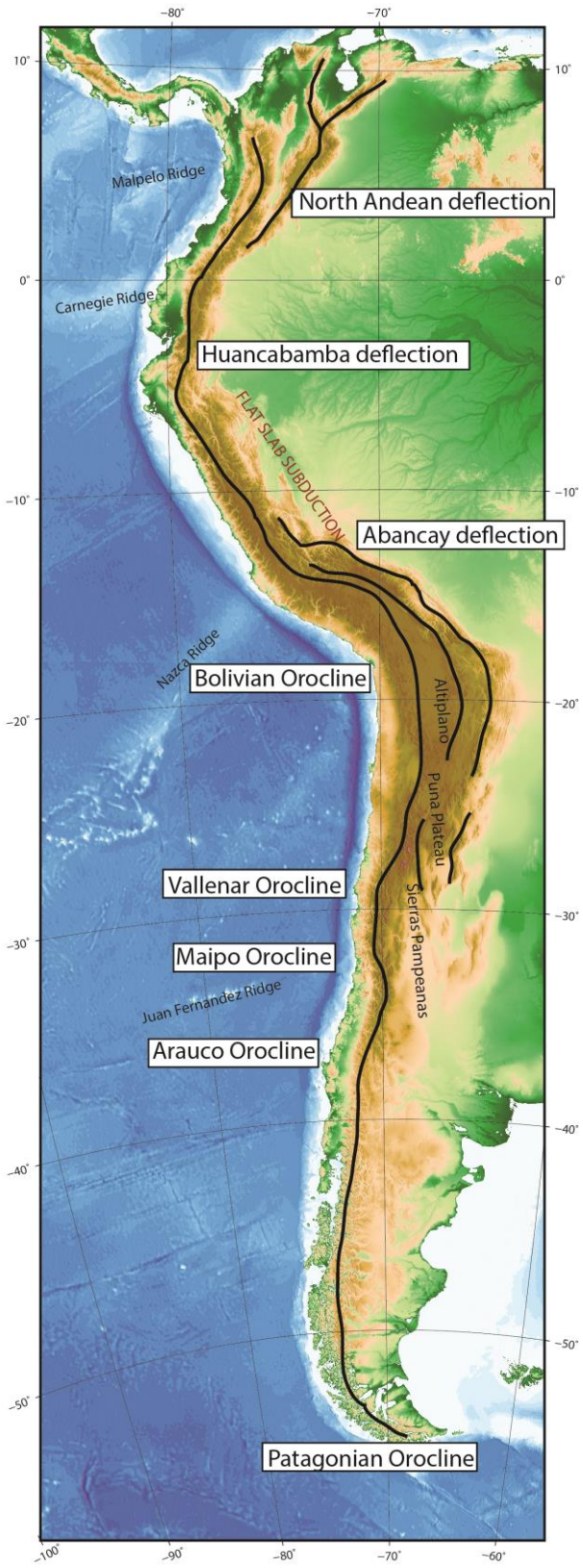

Figura 1.6: Principales Flexuras de América del Sur a lo largo de la cadena Andina.

Distintos estudios (Heki, 1985; Isacks, 1988; Somoza et al., 1999; Taylor et al., 2005; Arriagada et al., 2003; 2006; Roperch et al., 2006; 2011) han manejado, con distintos datos y metodologías, una hipótesis cuya estructura medular es similar: el Oroclino Boliviano es consecuencia de las restricciones geométricas impuestas por el acortamiento a lo largo de los Andes. Muchos de estos trabajos consideraban los efectos de las rotaciones tectónicas, determinadas por el método paleomagnético, sectorizando dos patrones importantes: Uno entre Arica y el Sur de Perú, de rotaciones anti horarias; y otro al sur de Arica hasta Vallenar, de rotaciones horarias, este último es conocido como el CARP, acrónimo de “Central Andean Rotation Pattern” (Somoza et al., 1996).

El conocimiento sobre el CARP ha evolucionado (Figura 1.7), desde asignarle una edad neógena de formación (Heki, 1983; Isacks, 1988), hasta asociarlos a una edad Paleógena, relacionado principalmente al evento tectónico Incaico (Roperch et al., 2006; Taylor et al., 2007; Arriagada et al., 2008), donde las mayores rotaciones en los Andes Centrales se produjeron durante un gran evento compresivo de escala regional, que ha sido asociado a la subducción de un ridge en la actual zona axial del Oroclino (Ramos y Folguera 2009; Eichelberger et al., 2015). Sin embargo, estudios más recientes han mostrado edades de rotación más antiguas, relacionadas con deformación compresiva del Cretácico Superior, y mostrando que el Oroclino Boliviano pudo tener una edad de inicio de formación más antigua que la asociada al evento Incaico (Somoza et al., 2012; Puigdomenech et al., 2020). Estas rotaciones son mayores que las que se puedan explicar por meras diferencias de acortamiento y/o estar acrecentadas por estructuras locales, como en Perú, donde el desplazamiento sinestral acomoda en gran parte las rotaciones ahí presentes (Roperch et al., 2011).

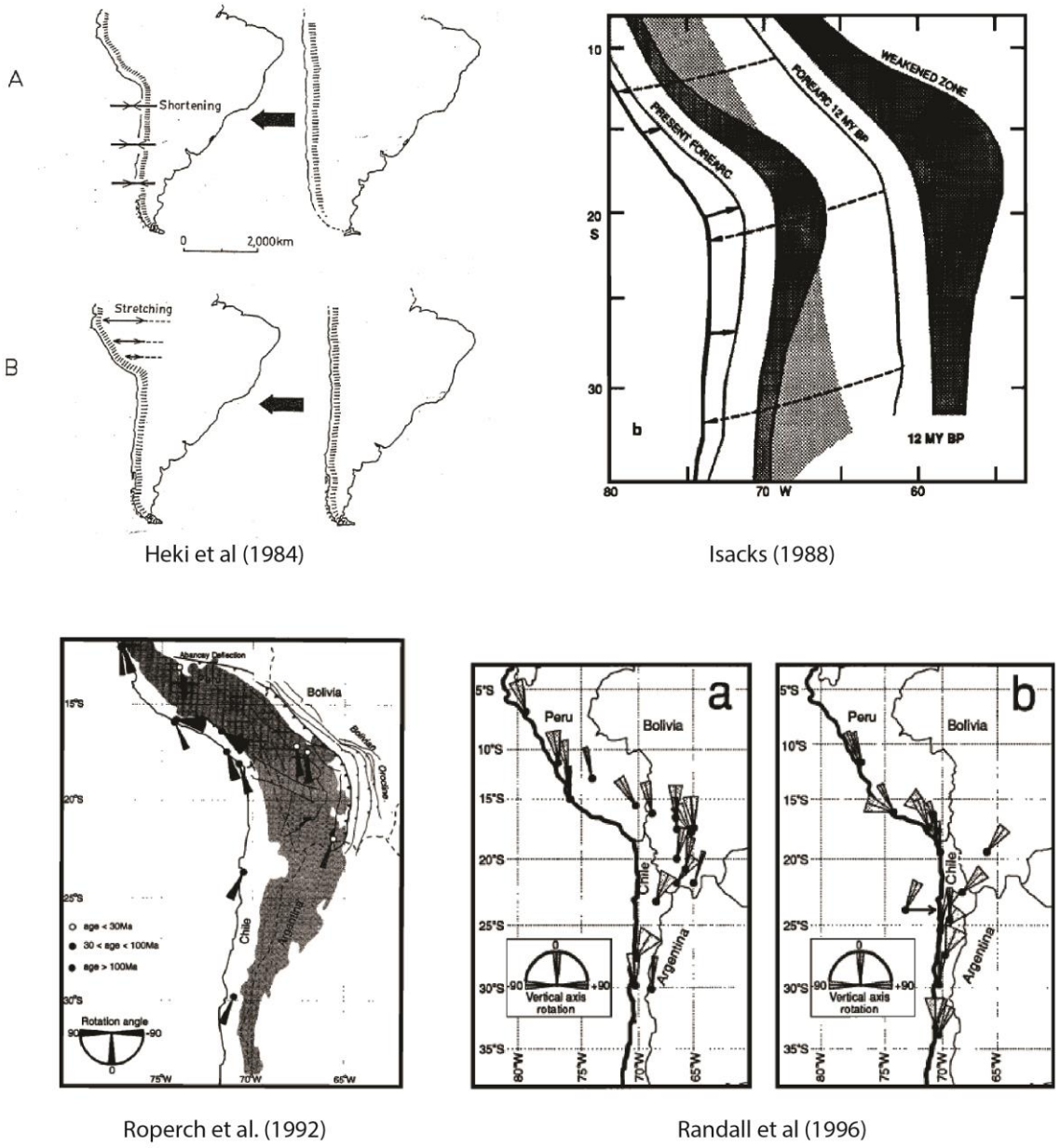

Figura 1.7: Evolución del entendimiento del Oroclino Boliviano a través del entendimiento de las rotaciones tectónicas. Primero como un patron de rotaciones con un modelo de un orógeno previo totalmente recto (Heki et al., 1984), para luego entender los Andes pre-oroclinales como una cadena montañosa levemente arqueada, con una edad de deformación propuesta alrededor de los 12 My (Isacks, 1988), luego propuesta para el Cenozoico (Roperch et al., 1992), y luego para el Cretácico, enaltesiendo el rol de sistemas de fallas de rumbo (Randall et al., 1996).

De los oroclinos mayores pertenecientes a los Andes Centrales mencionados anteriormente, podemos mencionar los siguientes de Norte a Sur:

La deflexión de Abancay representa un cambio en las magnitudes de rotación antihoraria, donde las rotaciones aumentan hasta más de 60º entre las localidades de Chalhuanca y Abancay (Roperch et al., 2011) en rocas de edad eocena. Este gran cambio de magnitud, desde datos cercanos a Cuzco, que poseen alrededor de 35º de rotación antihoraria, hacia las zonas fuertemente rotadas cerca de Abancay implican la presencia de una fuerte componente sinestral a lo largo de ella, deformación sinestral relacionada principalmente a la deformación incaica del Eoceno-Oligoceno (Roperch et al., 2011).

Alrededor de 29ºS se encuentra el Oroclino de Vallenar (Arriagada et al 2009; Capitulo 2), y corresponde a un cambio del patrón paleomagnetico de rotaciones horarias asociadas al Oroclino Boliviano, hacia el norte, (Arriagada et al., 2006) a un patrón de rotaciones leves o nulas hacia el sur, así como un cambio en el rumbo de las estructuras de primer orden desde NNE-SSW a N-S, no obstante, sin un notorio cambio en la orientación de la actual línea de costa.

Aproximadamente desde el extremo sur del segmento de subducción plana Pampeano (Barazangi y Isacks, 1976), en conjunto con el resurgimiento hacia el sur de la Depresión Central, se encuentra el Oroclino del Maipo (Farias et al., 2008; Arriagada et al., 2013). Este oroclino supone un cambio en la orientación de las estructuras de primer orden, desde un rumbo N-S a un rumbo NNE-SSW. Sumado a esto se ha documentado un brusco cambio en el patrón de rotaciones, desde una zona con rotaciones entre 7-10º de rotación horaria, a una zona de entre 13 y 42º de rotación en el mismo sentido (Arriagada et al., 2013; Puigdomenech et al., 2021).

El “Oroclino” de Arauco (ca. 38ºS; Melnick et al., 2009) es una flexura enmarcada en el cambio de rumbo de la estructuras principales y zona de transición entre una zona norte controlada por fallas inversas en el antearco y el tras-arco a una zona donde la deformación de rumbo juega un rol principal, a través de la Zona de Falla

Liquiñe-Ofqui (Melnick et al., 2006). Sin emabargo hasta el dia de hoy, este “Oroclino” no ha sido sustentando con datos paleomagnéticos para su correcta definición.

1.4.-Problemáticas relacionadas al Oroclino Boliviano: Causas y Azares

Para entender al Oroclino Boliviano hay que considerar que es una combinación de factores en 4 dimensiones, acortamientos y sistemas de fallas (Eichelberger et al., 2015), que dan información y propuestas de geometrías en profundidad, rotaciones tectónicas, que muestran movimientos en planta (Heki et al., 1985), y procesos de carácter geodinámico, como delaminación cortical (Key et al., 2009), flujos astenosféricos (Davila et al., 2013), cambios en el ángulo de subducción (Manea et al., 2012) o subducción de heterogeneidades (Martinod et al., 2010).

Sumado a esta visión espacio-temporal, se deben tomar en cuenta los cambios en la cantidad y el estilo de acortamiento observado a lo largo del rumbo de la cordillera (Jordan et al., 1983; Allmendinger et al., 1997; McQuarrie et al., 2002; 2005), el tipo de comportamiento de la litosfera (Tassara et al., 2010), variaciones del acoplamiento entre las placas (Iaffaldano et al., 2012) o la presencia de distintos basamentos acrecionados (Ramos, 2010).

Temporalmente, desde el Cretácico Tardío, el margen occidental de Sudamérica ha sufrido periodos de acortamiento y formación de cuencas de antepaís (Bascuñan et al., 2015), que sumado a procesos de inversión tectónica (Kley y Monaldi, 2002; Arriagada et al., 2006b; Amilibia et al., 2008; Martínez et al., 2013) corresponden a los primeros procesos de deformación compresiva que continúan a los procesos de cuencas extensionales del Mesozoico temprano-medio (Vicente, 2006). Sin embargo, es durante el periodo comprendido entre el Eoceno-Oligoceno (Fase Incaica) donde se producen las mayores tasas de acortamiento (Lamb et al., 2001; Mpodozis et al., 2005; McQuarrie et al., 2005; Cobbold et al., 2007). Llegando al

Mioceno es donde los alzamientos se aceleran, construyendo los relieves actuales de las llanuras altiplánicas y de la Puna (Farias et al., 2005; Charrier et al., 2013; Eichelberger et al., 2015), acumulando las mayores tazas de acortamiento alrededor de la zona altiplánica (Figura 1.8), específicamente entre los 16-6 My (Victor et al., 2004; Farías et al., 2005; Jordan et al., 2010; Garzione et al., 2014; Kar et al., 2016).

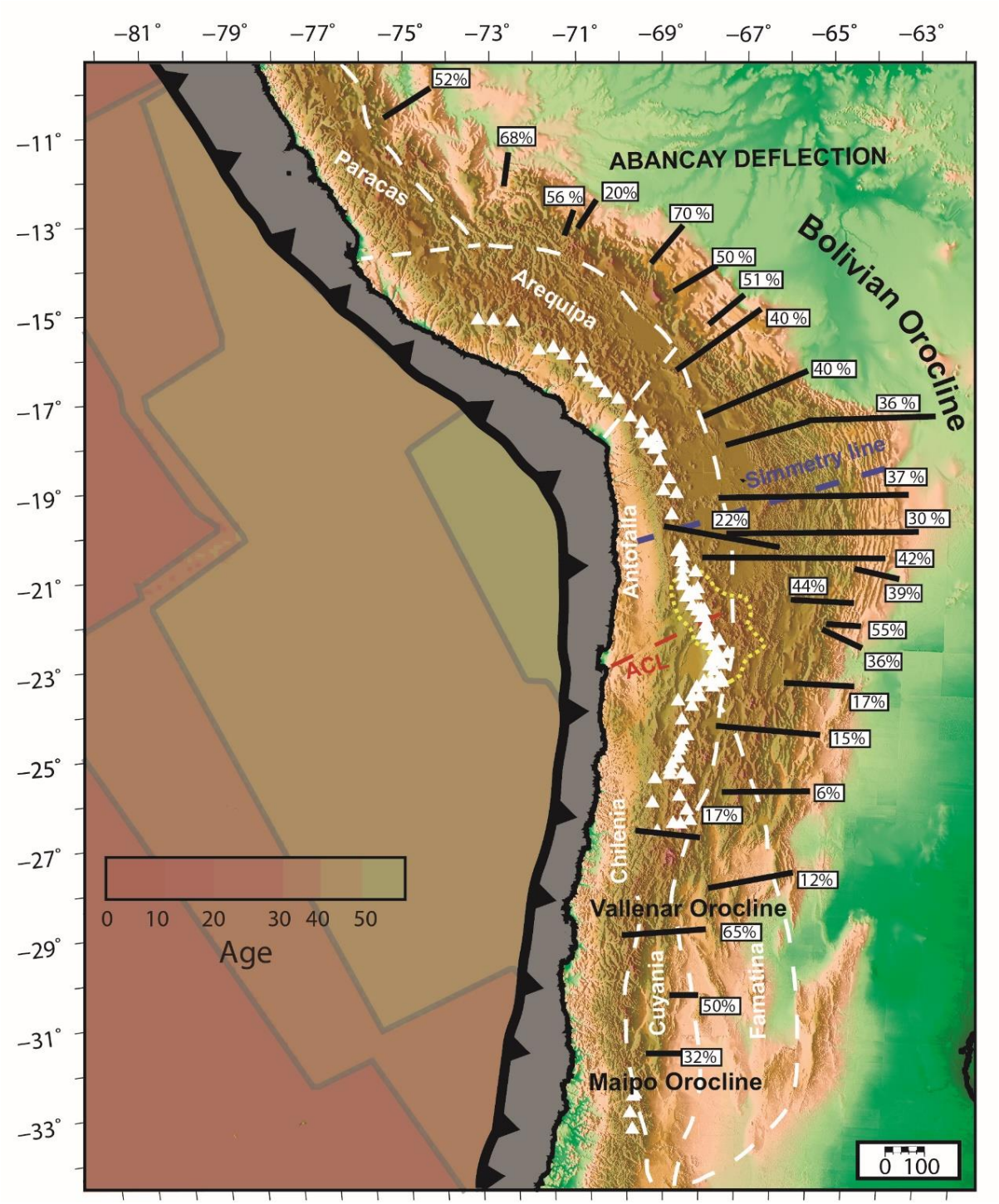

Figura 1.8: Acortamientos calculados alrededor del Oroclino Boliviano. Compilacion basadas en los trabajos de Arriagada et al. (2008), Eichelberger et al. (2015) y Martínez et al. (2017). Las líneas blancas corresponden a los limites de terrenos acrecionados según Ramos (2010).

1.5.-Las Heterogeneidades en la placa de Nazca y su relación con la placa Sudamericana

La placa de Nazca, placa oceanica que se encuentra al Oeste de la Placa Sudamericana desde la ruptura de la placa de Farallon a los 22.7Ma (Barckhausen et al., 2001), posee una gran variedad de montes submarinos (Figura 1.8), “ridges” y cadenas volcánicas relacionadas a Hot-spots, como la cadena de Juan Fernandez (Reyes et al., 2017), que han sido correlacionados a diversos procesos tectónicos. Entre ellos los mas destacados son:

Ridge de Nazca: Con un espesor cortical entre 14-17 Km (Contreras-Reyes et al., 2019) y unos 600-700 Kms de Ancho, esta gran heterogeneidad positiva en la placa de Nazca se le asigna una edad de alrededor de 37 My de Colisión con la placa Sudamericana.

Ridge de Iquique: Con un espesor cortical de alrededor de 10-15 Km, este ridge posee un ancho de alrededor de 200 Kms, siendo estimada su edad de contacto con la placa Sudamericana alrededor de los 45-50 My (Contreras-Reyes, et al., 2021)

Ridge de Taltal: Una cadena de montes submarino cuya expresión superficial puede relacionarse a las islas San Feliz y San Ambrosio. Esta cadena posee un ancho de menos de 100 Km, siendo su edad de colisión con la placa Sudamericana de alrededor de 50 My (Bello-Gonzalez et al., 2018).

Ridge de Copiapo: Esta cadena de montes submarinos es posible visibilizarla frente a las costas de Caldera, poseyendo un espesor cortical de alrededor de 15 Kms, menos de 100 kms de ancho, y una edad de colisión con la placa Sudamericana de alrededor de 42.5 My (Bello-Gonzalez et al., 2018).

Ridge de Juan Fernandez: La cadena de montes submarinos mas notoria del margen chileno posee una expresión superficila en el archipiélago del mismo nombre, con islas de edad entre los 8-4 My aproximadamente (Yañez et al., 2001; Reyes et al., 2017). Este ridge lleva subductando bajo la placa Sudamericana desde los 60 My (Bello-Gonzalez et al., 2018), sufriendo variaciones en su velocidad y obliquidad de convergencia en el tiempo.

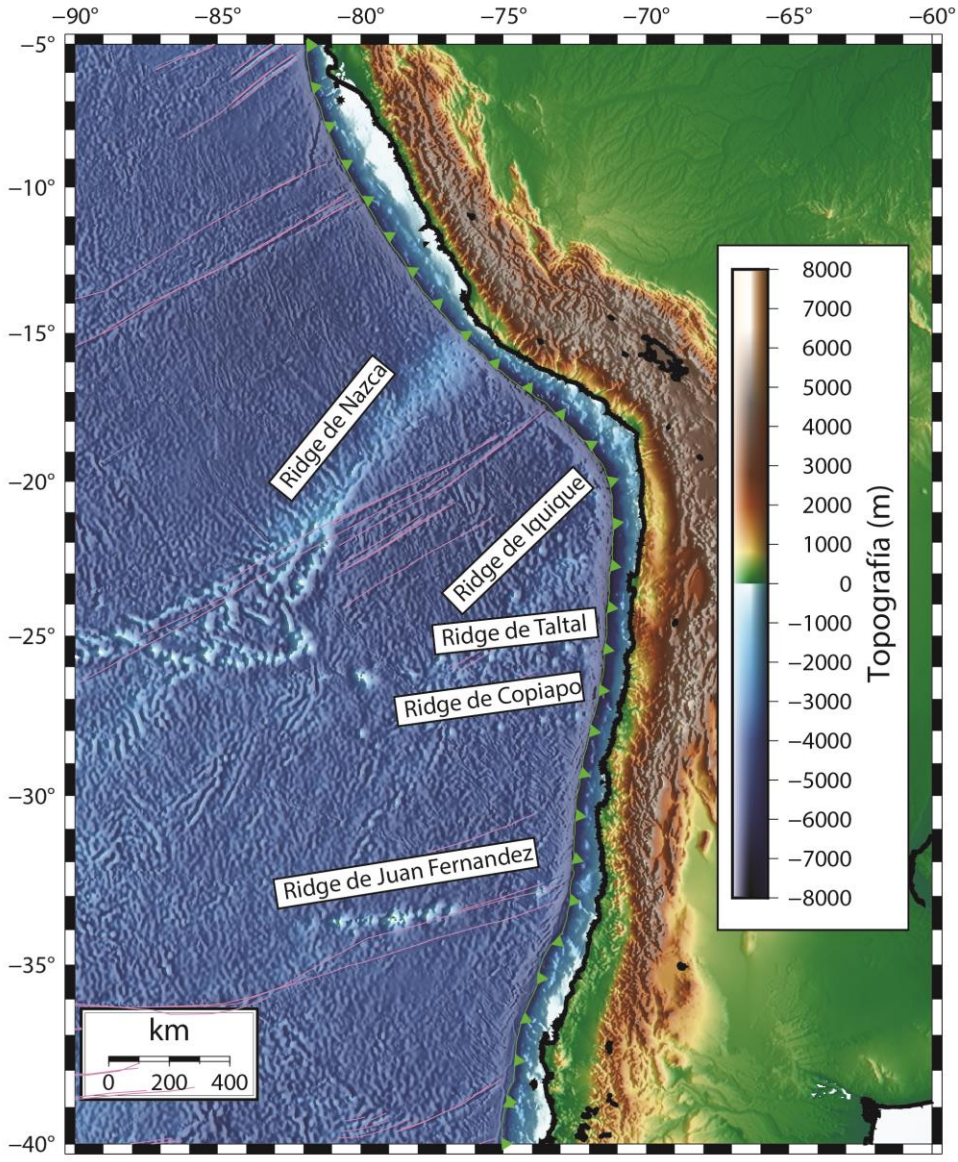

Figura 1.9: Posición de los distintos Ridges observables en la placa de Nazca, y su correlación latitudinal con la placa sudamericana.

1.6.- Problemática: ¿Qué propicia el flexuramiento?

En los últimos años, la formación del Oroclino Boliviano se ha asociado con factores geodinámicos relacionados a las distintas heterogeneidades y aspectos de la zona de subducción. Uno de estos factores es la ocurrencia y coincidencia de una hipotética subducción plana durante el Eoceno en la zona del Oroclino Boliviano,

que ejercería un control fundamental en el magmatismo y en el engrosamiento cortical del área (McQuarrie et al., 2005; Arriagada et al., 2008; Martinod et al., 2010). Esta subducción plana, y su asociación con la formación del Oroclino Boliviano, ha sido relacionada a una combinación de subducción de heterogeneidades en la placa de Nazca y de debilidades corticales heredadas de la corteza continental (Sdrolias y Müller, 2006; O'Driscoll et al., 2012; Martinod et al., 2013). En adición a las heterogeneidades de la Placa de Nazca, esta misma, durante el Eoceno, tuvo una distribución de edades tal que las más antiguas se ubicaron en la zona del Oroclino Boliviano, siendo otro factor más que habría colaborado en la formación del Oroclino (Sdrolias y Müller. 2006; Capitanio et al 2011).

Las heterogeneidades antes mencionadas han sido asociadas a un plateau oceánico (Sdrolias y Müller, 2006) producto de un ridge activo durante el Paleoceno, y emplazado en el hot-spot de Juan Fernández. Este plateau habría sido subductado durante el Eoceno, moviéndose de sur a norte con respecto al margen sudamericano desde el Eoceno-Oligoceno, y luego moviéndose hacia el sur del mismo margen durante el Neógeno (Yáñez et al., 2001; Sdrolias y Müller, 2006; Bello et al., 2018).

Tomando datos de una extensa bibliografía paleomagnética (Bayona et al., 2006; Roperch et al., 2006; Arriagada et al., 2008; Maffione et al., 2009; Roperch et al., 2011; Prezzi y Iglesias, 2012; Arriagada et al., 2013; Ferrando et al., 2014; Japas et al., 2016), así como datos propios, se ha podido delimitar, al menos, 5 bloques que poseen distintos patrones de declinación magnética, tomando las diferenciaciones de acuerdo a Arriagada (2018), que podemos separar en:

(1) Bloque Arequipa: Comprendido entre los 13 y los 18º de latitud sur, corresponde al bloque de rotaciones antihorarias de un promedio de alrededor de 35º (Roperch et al., 2006; 2011) relacionado, espacialmente, al terreno alóctono Grenvilliano de Arequipa (Ramos, V., 2010). El límite norte de este bloque correspondería a la Deflexión de Abancay (Roperch et al., 2011), donde confluyen

estructuras de rumbo que acomodan el movimiento lateral producido por un fuerte cambio en las rotaciones de sur a norte, teniendo hasta casi 65º de rotación en la franja magmática de Andahuaylas-Yauri (Roperch et al., 2011). El límite sur corresponde al Oroclino Boliviano, y marca el fin del patrón de rotaciones antihorarias.

(2) Bloque Antofalla: Comprendido entre los 18 y los 23º de latitud sur, corresponde a una zona de rotaciones leves a nulas, tanto en la Cordillera de la Costa como en la Precordillera chilena y el Altiplano. Espacialmente, ester bloque se encuentra relacionado al terreno alóctono de Antofalla (Ramos, V., 2010), así como correspondería a la zona afectada por la subducción plana durante el Eoceno (McQuarrie et al., 2005). Se encuentra limitada al sur con el Lineamiento Antofagasta Calama (LAC), que actúa como límite entre dos zonas de magnitudes rotacionales drásticamente distintas (Arriagada et al., 2003).

(3) Bloque Atacama: Corresponde a la zona del ante-arco comprendida entre 23 y 29º S, poseyendo rotaciones horarias de un promedio de ca. 35º que afectan a la Cordillera de la Costa, Depresión Central y Precordillera (flanco occidental de los Andes). Longitudinalmente, estas grandes rotaciones no siguen hacia el este, teniendo rotaciones bastante más leves (menores a 20º) en la Cordillera Frontal y en la zona de las Sierras Pampeanas (Coutand et al., 1999). Su límite sur corresponde al Oroclino de Vallenar, y marca el fin del patrón de rotaciones horarias fuertes en el antearco chileno.

(4) Bloque Elqui: Corresponde a una zona con rotaciones muy leves (entre 7 y 10º de rotación horaria, que teniendo el error en consideración se podría hablar de rotaciones casi nulas) ubicada en el antearco chileno entre 29 y 33ºS. Su límite sur corresponde al Oroclino del Maipo (Arriagada et al., 2013), el que marca el comienzo hacia el sur de un patrón de rotaciones horarias mayores que pueden alcanzar hasta 42º. Espacialmente, su límite sur coincide con el extremo sur de la zona de subducción Pampeana (Isacks, 1988), pero además con el cierre por norte de la Cuenca Neuquina del Mesozoico (Howell et al., 2005).

(5) Bloque Arauco: Corresponde a la zona de rotaciones horarias ubicada en el antearco chileno al sur de los 33°S, siendo su limite norte el Oroclino del Maipo, y su limite sur siendo, posiblemente, la flexura oroclinal propuesta por Melnick et al. (2006).

Tomando la delimitación anterior es factible preguntar **¿Cuál es el rol de las estructuras pre-Cenozoicas en la formación del Oroclino Boliviano? ¿Cuál es su grado de influencia en los procesos constructivos del orógeno andino? ¿Qué rol juegan las heterogeneidades de la placa oceánica en el arqueamiento de los Andes? ¿Podemos observar remanentes de las injerencias de estos factores?**

1.7.- Hipótesis de Trabajo

Se propone en este trabajo que existe una zonificación en planta de los distintos patrones de rotaciones tectónicas en los Andes Centrales. Estos patrones están relacionados con la formación del Oroclino Boliviano, de tal modo que la discretización de estas zonas refleja la presencia de distintos bloques tectónicos pre-existentes a la deformación del Cenozoico, en el margen occidental de Sudamérica. Estos bloques se distribuyen en distintas zonas tanto de Este a Oeste, como de Norte a Sur, y corresponden al bloque Peruano, de rotación antihoraria; al bloque central, de rotación nula y alta deformación compresiva; y al bloque Chileno, de rotación horaria (Figura 1.9). Se plantea que el comportamiento principal de estos bloques rotacionales está ligado a los procesos compresionales que afectaron al margen occidental de Sudamérica desde el Cretácico Medio-Tardío al Eoceno-Oligoceno, estando la zonificación de estos bloques influenciada por procesos tectónicos heredados, asi como sus limites podría estar delimitados por estructuras de carácter regional, como el lineamiento de Antofagasta-Calama (Figura 1.9).

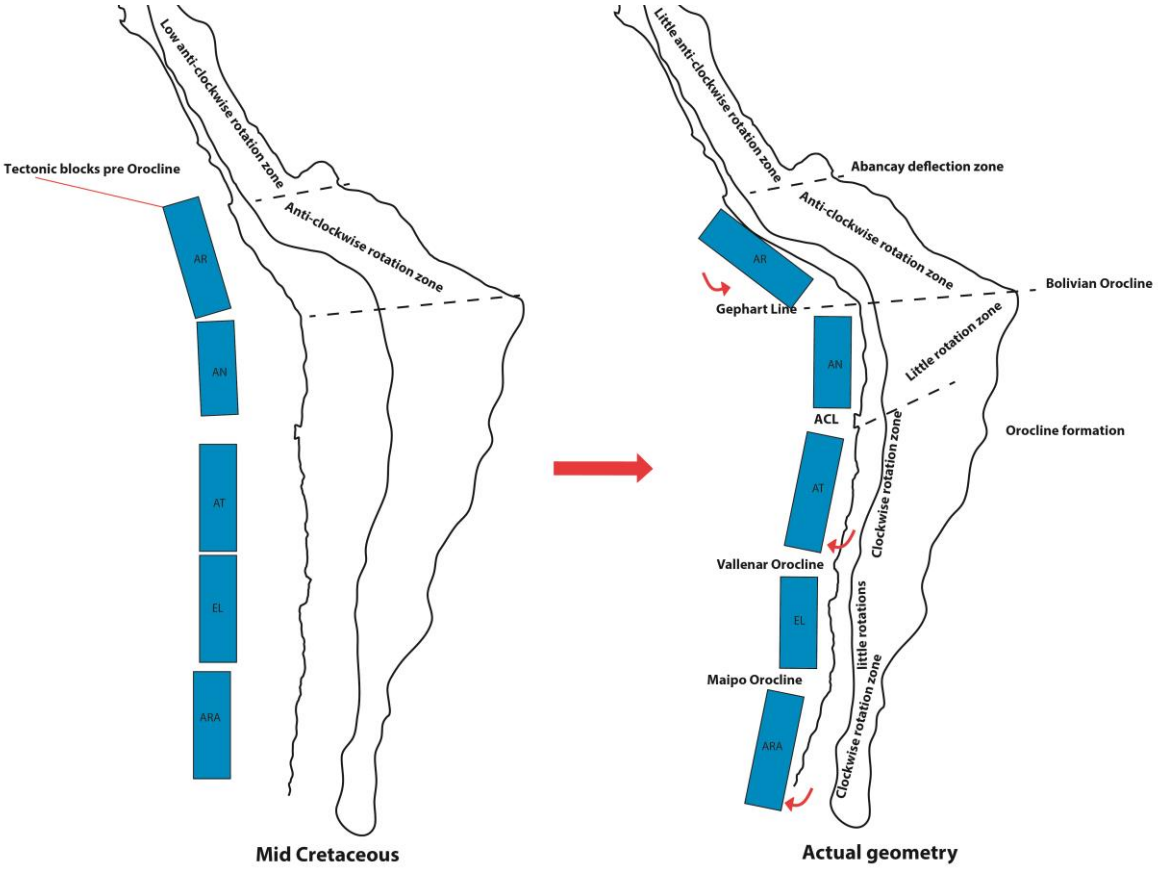

Figura 1.10: Hipótesis de deformación oroclinal, los bloques azules corresponden a una sectorización que representa las rotaciones de los distintos bloques antes mecionados: Bloque Arequipa (AR), Antofalla (AN), Atacama (AT), Elqui (EL) y Arauco (ARA).

1.8.- Objetivo general

El Objetivo principal de esta Tesis corresponderá a:

Comprender la causa de los distintos patrones rotacionales en los Andes Centrales, y el rol de los límites entre zonas de distinta magnitud y sentido de rotación tectónica generados durante la formación del Oroclino Boliviano.

1.9.- Objetivos específicos

- Delimitar espacialmente el patrón de rotaciones determinados paleomagnéticamente en torno a los Andes Centrales, concentrando el estudio en la parte chilena de los Andes Centrales.
- Determinar la edad y la magnitud de las rotaciones en los Andes Centrales.
- Analizar la relación entre los cambios latitudinales y longitudinales del patron de rotaciones tectónicas con cambios en las condiciones geodinámicas en el margen de subducción andino.
- Comprender la relación entre los grandes sistemas de fallas en los Andes Centrales y las rotaciones tectónicas asociadas a estas.

1.10.- Metodologías

-Reunir la información bibliográfica existente acerca de los datos paleomagnéticos de los Andes Centrales.
-Identificar los cambios de declinación magnética regional, de forma latitudinal y Longitudinal en la región de estudio.
-Identificar los principales lineamientos estructurales de los Andes Centrales
-Establecer una relación entre las principales fases tectónicas y los distintos eventos de deformación rotacional.
-Identificar zonas de falla que coincidan con grandes cambios en patrones de declinación magnética.

2: Estado del arte en el conocimiento del Oroclino Boliviano y los procesos tectónicos relacionados.

En esta sección se revisarán de forma resumida las contribuciones realizadas en distintas publicaciones, y como estas contribuciones se han enmarcado dentro de la evolución del conocimiento de los distintos procesos tectónicos ligados tanto a la formación del orógeno andino, como a las rotaciones asociadas a este proceso.

2.1- Estilos estructurales y edad de deformación en el flat-slab pampeano

Desde los estudios de Darwin (1835), pasando por las propuestas de Segerstrom (1967) y Jensen (1974), la región de Atacama de Chile ha sido una de las principales zonas de estudio para el entendimiento de la correlación entre la interacción de placas y la deformación producida en la placa superior (Figura 2.1). El plantamiento de zonas de subducción plana en los Andes Centrales (barazangi & isacks, 1976; 1979; Isacks, 1988), conllevo a interpretar que los estilos estructurales de escama gruesa en la zona de estudio podrían estar seriamente relacionados a la particular situación del plano de wadatti-benioff en esta zona (Jordan et al., 1983; Ramos et al., 1996; Giambiagi et al., 2002).

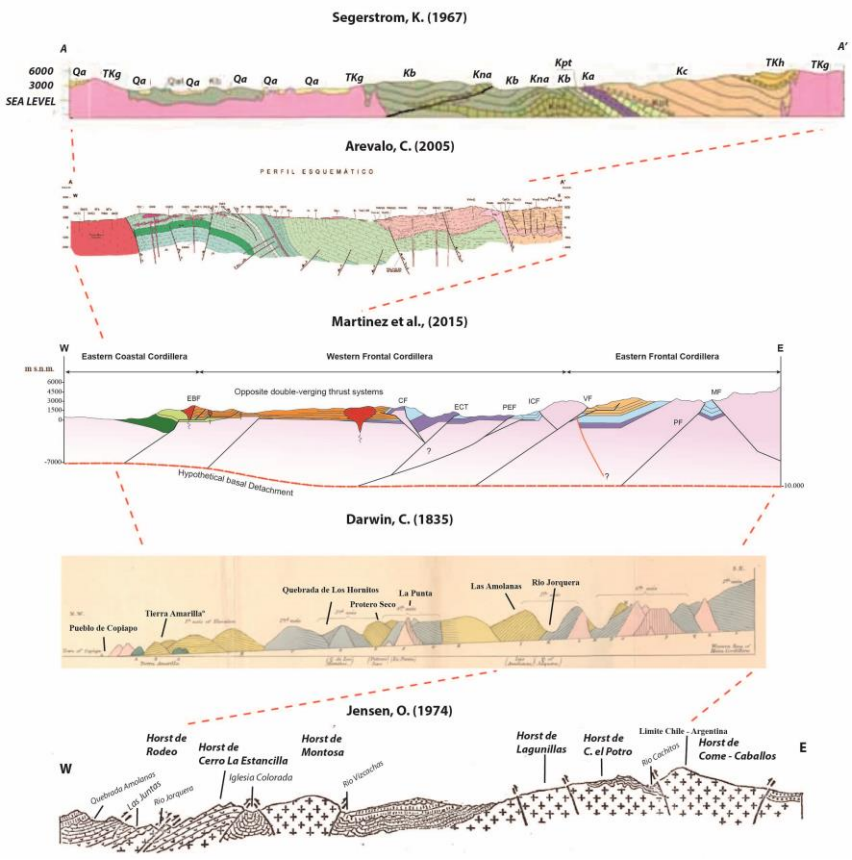

Figura 2.1: Distintas secciones estructurales a través del valle del rio Copiapo, denotando las geometrías similares, pero con interpretaciones disimiles.

La incorporación de los conceptos de inversión tectónica para describir una arquitectura de escama gruesa ha sido utilizada desde mas de 20 años en los Andes Centrales (Baby et al., 1997; Flint et al., 1993). Este tipo de estilo de deformación conlleva, generalmente, una deformación de tipo piel mixta (Copley & McKenzei, 2007), estilo de deformación que en los últimos años ha sido reconocido desde la región de Tarapaca (Fuentes et al., 2018) hasta la region Metropolitana (Mardones et al., 2021). En particular en la región de Atacama, los estudios en las cuenca que van desde el Triásico Medio hasta el Cretácico Inferior (varios martinez), estos estudios no solo han postulado la regularidad con que la arquitectura de escama mixta, relacionado a una inversión tectónica positiva, se encuentra en la región de Atacama, reconociendo no solamente estas geometrías, sino edades de deformación que van desde el Cretacicó Inferior Tardio hasta el Mioceno (Bascuñan et al., 2016; Martinez et al., 2015). El entendimiento de estos estilos es fundamental para el entendimiento de los procesos de rotaciones tectónicas, rotaciones tectónicas anomalas pueden encontrar explicación en las distintas heterogeneidades dentro de los procesos de inversión tectónica, como dentro de acortamientos diferenciales asociados a los procesos compresivos en los que se enmarcan estos procesos de inversión (Jara et al., 2015; Yamada & McClay, 2003).

En particular, dentro del marco de este trabajo de doctorado, diversas campañas fueron realizadas entre los valles del rio Copiapo y rio Huasco, donde los principales resultados publicados (Martinez et al., 2013; Martinez et al., 2015; Martinez et al., 2021) pueden resumirse en los siguientes puntos:

(a) Existe una vergencia general de la deformación hacia el Este, desde la inversión tectónica de la cuenca de Chañarcillo (Martinez et al., 2013) en el Cretácico Superior – Paleoceno, pasando por la inversión de la cuenca de Lautaro en el Cretácico Superior – Eoceno (Martinez et al., 2012), hasta el alzamiento de grandes bloques de basamento en la Cordillera Frontal en el Mioceno (Martinez et al., 2015).
(b) Los estilos estructurales corresponden a piel mixta, teniendo una expresión superficial en estilos de inversión tectónica, con retrocorrimientos y fallas de atajo. Este estilo estructural va cada vez mas migrando a un estilo de piel gruesa a medida que se avanza hacia el Este (Martinez et al., 2016).
(c) Las edades de exhumación obtenidas en rocas intrusivas del Cretácico Superior – Paleoceno, muestran que la zona entre la Cordillera de la Costa y la Cordillera Frontal presenta no solo edades de deformación relacionados al

limite Cretácico – Paleoceno, sino que existen edades de alzamientos que bordean esta misma edad (Martinez et al., 2021). Hacia la Cordillera Frontal, las principales edades de alzamiento de los intrusivos del Permico – Triásico, corresponden a edades Eocenas, mostrando como el evento “incaico” en la región sigue siendo el dominante (Martinez et al., 2017).

2.2 – Rotaciones tectónicas y su relación a la construcción del orógeno andino.

La actualización de nuevos datos (Figura 2.2), no solo de rotaciones tectónicas, sino de edades de deformación ha llevado a replantear el comienzo del Oroclino boliviano. Diversos autores (Somoza et al., 2015; Narea et al., 2015; Puigdomenech et al., 2020) han contribuido a ampliar la historia de las rotaciones tectónicas en el antearco de los Andes Centrales, sobre todo en la parte chilena del Oroclino boliviano, asignadole edades de rotaciones tectónicas mas cercanas al Cretácico Superior, y por lo tanto mas cercanas a un evento K-T o a una fase peruana Tardia. Esto sin embargo no merma los procesos rotacionales ocurridos en el Cenozoico, siendo las rotaciones asociadas al evento Eoceno-Oligoceno, de mayor magnitud que las rotaciones previas, estando en fuerte correlación con los mayores cálculos de acortamiento para la misma temporalidad en los Andes Centrales (Arriagada et al., 2008; Eichelberger et al., 2015).

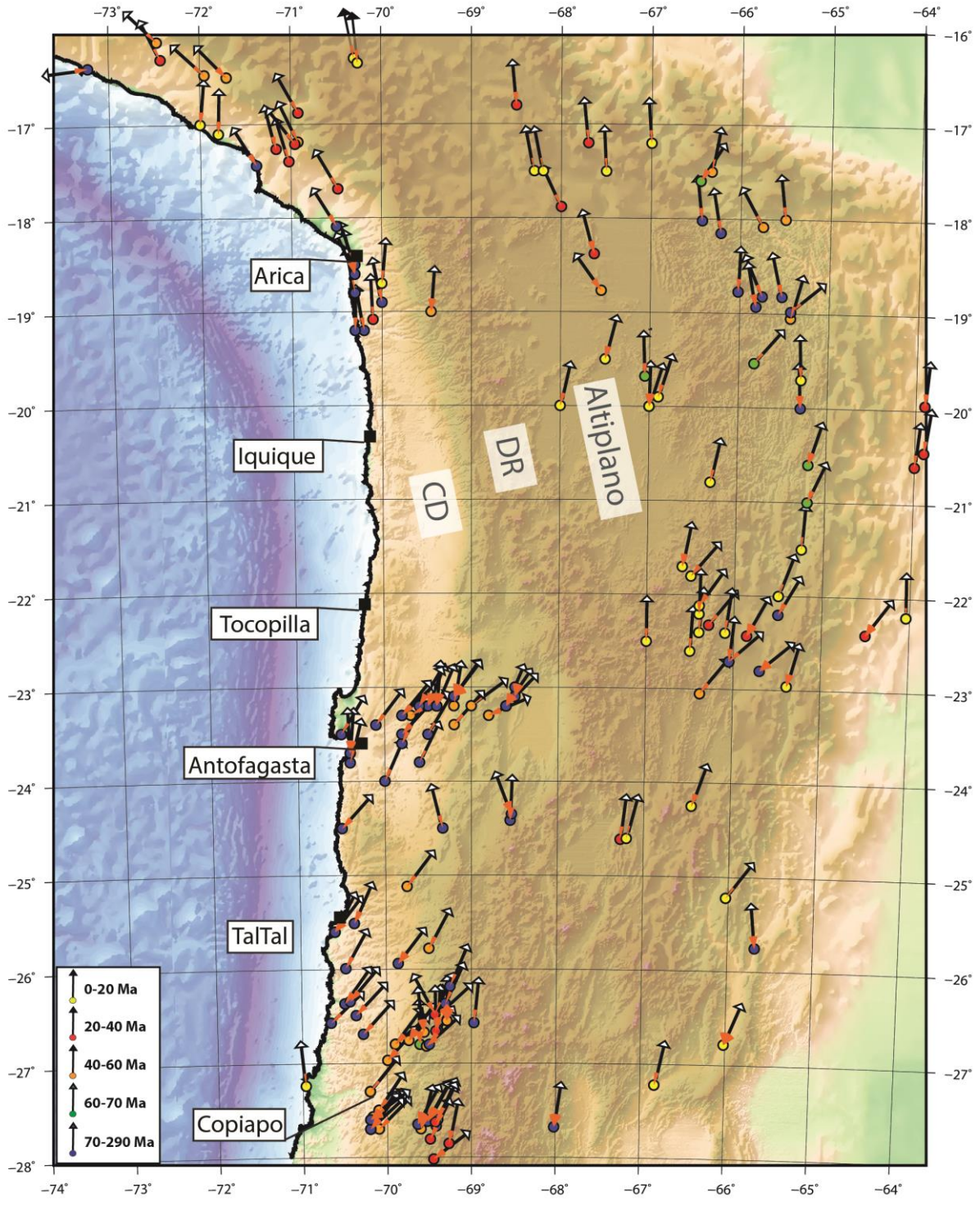

Figura 2.2: Rotaciones tectónicas en el los Andes Centrales de Chile. Los provienen de diversos estudios previos a este trabajo (Arriagada et al., 2006; Roperch et al., 2006; Somoza et al., 2015; Japas et al., 2016; Narea et al., 2015; Puigdomenech et al., 2020).

Esta evolución en el entendimiento de la temporalidad de los procesos ha llevado también a una evolución en la forma que se ha entendido el margen continental andino previo al proceso de flexión de este (Figura 2.3). Las primeras representaciones de este margen continental (Heki, et al., 1984) denotan un margen totalmente recto, y con una edad neógena de flexuramiento del margen. Posteriormente, diversos estudios bosquejaron un margen continental previo con cierta curvatura, curvatura que fue aumentando con respecto a la propuesta original a medida que se dispusieron de mayor cantidad de datos, siendo la edad también delimitada primero en el Mioceno (Isacks, 1988), hasta dar una edad Eocena-Oligocena al proceso mas fuerte de flexuramiento del margen (Roperch et al., 2006; Arriagada et al., 2008). La evolución de estas propuestas de margen es fundamental, no solo para comprender una paleogeografía, sino para entender como ciertos elementos de la placa oceanica interactuaron con la placa Sudamericana, como los ridges oceánicos (Bello et al., 2018).

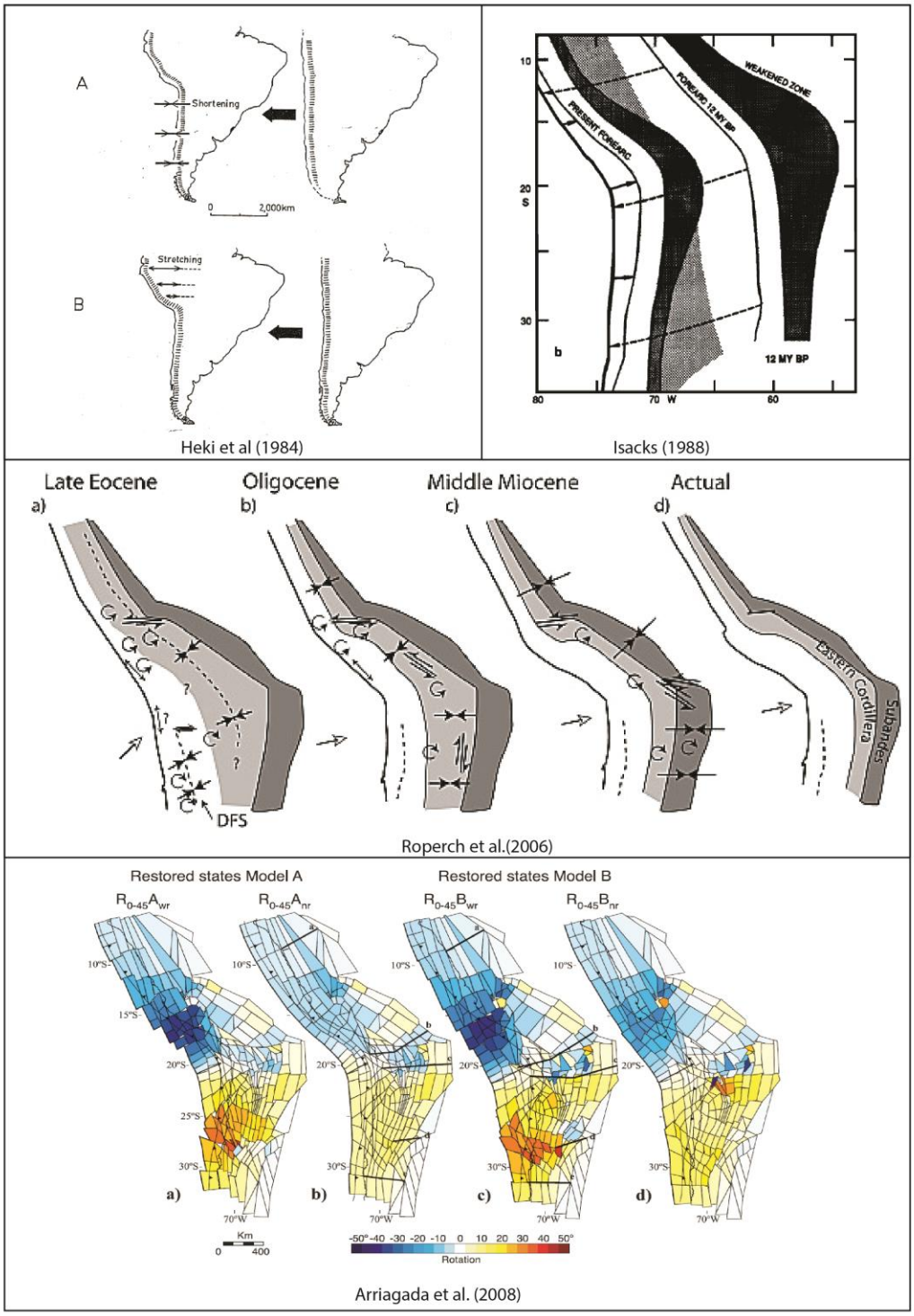

Figura 2.3: Distintos modelos de reconstrucción del margen continental de los Andes Centrales de acuerdo a datos de rotaciones tectónicas y acortamientos (Heki, et al., 1984; Isacks, 1988; Roperch et al., 2006; Arriagada et al., 2008).

En particular, en el marco del trabajo de este doctorado, aparte de variadas exposiciones en congresos, se han publicado dos trabajos relacionados a la técnica paleomagnética, cuyos aportes son:

(a) Determinar un exceso de rotación en una zona especifica al Norte del Salar de Atacama, de alrededor de 80° en sentido horario. Estas rotaciones pueden ser explicadas por una acumulación de eventos previos al evento rotacional Eoceno – Oligoceno, denotando la existencia de rotaciones tectónicas durante el Cretácico – Paleoceno (Narea et al., 2015).
(b) El análisis conjunto de anisotropía de susceptibilidad magnética (ASM) y de strain con indicadores cinemáticos en el limite Austral de la Puna, muestra cambios dramáticos en la dirección de contracción (Quiroga et al., 2021). Estos cambios de dirección de contracción están fuertemente controlados por el limite mismo del plateau de la Puna, estando de acuerdo con determinaciones anteriores a traves de datos paleomagnéticos y de strain (Aubry et al., 1996).

3: The southern limit of the Central Andean Rotation Pattern.

Con el fin de estudiar la continuidad del patrón de rotaciones paleomagnéticas entre los 24-33°S, se realizó un estudio a través de las distintas formaciónes geológicas del límite norte del Flat-Slab Pampeano, tanto en Chile como en Argentina. Este capítulo corresponde a un articulo aun en preparación, cuyas tablas de datos se encuentran en el capitulo de Anexos al final de esta tesis.

The southern limit of the Central Andean Rotation Pattern[1]

Peña, M[1,2], Roperch P. [3], Martínez, F.[4], Arriagada, C., Deckart, K.[1,5], Bascuñan,S[1].

(1) Departamento de Geología, Universidad de Chile, Casilla 13518, Correo 21, Santiago, Chile.

(2) Escuela de Geologia, Universidad Mayor, Manuel Montt 367, Santiago, Chile.

(3) IRD, LMTG & Géosciences Rennes, campus de Beaulieu, 35042, Rennes, France.

(4) Departamento de Ciencias Geológicas, Universidad Catolica del Norte, Angamos 0610, Antofagasta, Chile.

(5) Advanced Mining Technology Center, FCFM, Universidad de Chile, Av. Tupper 2007, Santiago, Chile

ABSTRACT. We report paleomagnetic results for more than 500 oriented samples, distributed in 67 sites, from the southern Atacama Desert, the modern Flat-slab of northern Chile and the southern Puna, in Argentina (25ºS to 33ºS). Remanent magnetization in volcanic and intrusive rocks is mostly primary, while a secondary magnetization is observed in few sedimentary rocks. Comparison of locality-mean directions with expected paleomagnetic directions indicates clockwise vertical axis rotations from 15,2 ± 13,7°, south of 29ºS, and 30,3 ± 14º, north of 29ºS and in the Andean Forearc. The magnitude of rotations changes from east to west, from an area with little clockwise rotations in the Puna-Altiplano, to a zone with more of 30º of clockwise rotations in the Andean Forearc. Between 27°30'-29ºS the tectonic rotations in the Andean forearc are strongly associated to the K-T sintectonic strata and its orogenesis, showing and anomalous pattern that correlates with the strike-changing structures of the area. The paleomagnetic data, added to previous studies,

[1] Manuscrito en preparación para ser enviado a Tectonics

and new U/Pb and $^{40}Ar/^{39}Ar$ ages, from this work, shows a range of tectonic rotations from the Upper Cretaceous to Eocene, for the rotations between 25-29ºS. There is a strong change in the magnitude of the clockwise rotations south of the 29ºS, making the Vallenar Orocline an end of the Central Andean Rotation Pattern (CARP) influence area. Block rotations within the Chilean Precordillera and Central Depression north of 29ºS are closely linked to the formation of the Bolivian Orocline, while the block rotations of the Altiplano-Puna block reflect the strong reology of the geological units affected by the tectonic rotations. Differences in longitude in the rotational deformation give the necessary space to the formation of Preandean Depressions, liking the timing of this process with the formation of the various Miocene-Oligocene Depressions in the north of Chile.

Keywords: Central Andes, Vallenar Orocline, Bolivian Orocline, Flat-Slab, Paleomagnetism.

3.1- Introduction

The present-day Andean margin between 30° and 28ºS (Figure 3.1), is characterized by two main features: Its lack of volcanism, due to the "Pampean" flat-slab subduction (Barazangi and Isacks, 1976), and its concave shape, where structural lineaments change their strike from mainly NS, south of 29ºS to NNE-SSW, to the north (Figure 3.1). The Bolivian Orocline, has been studied through several years, constraining its deformation and exhumation ages (McQuarrie et al., 2008; Eichelberger et al., 2015), defining its structural styles and geometries(Anderson et al., 2017; Herrera et al., 2017), understanding trench parallel flow (Gerbault et al., 2005; Kay et al., 2009), the influence of subducted heterogeneities an its influence in the andean deformation (Yáñez et al., 2003; Capitanio et al., 2012; O'Driscoll et al., 2012) and the origin of tectonic rotations along its limbs (Heki et al., 1985; Isacks, 1988; MacFadden et al, 1995; Randall et al, 1996; Somoza et al., 1996; 1998; Abels

and Bischoff, 1999; Arriagada et al, 2000, 2003, 2006, 2008; Roperch and Carlier, 1992; Roperch et al., 2006, 2011; Taylor et al., 1998, 2007; Maffione et al., 2012).

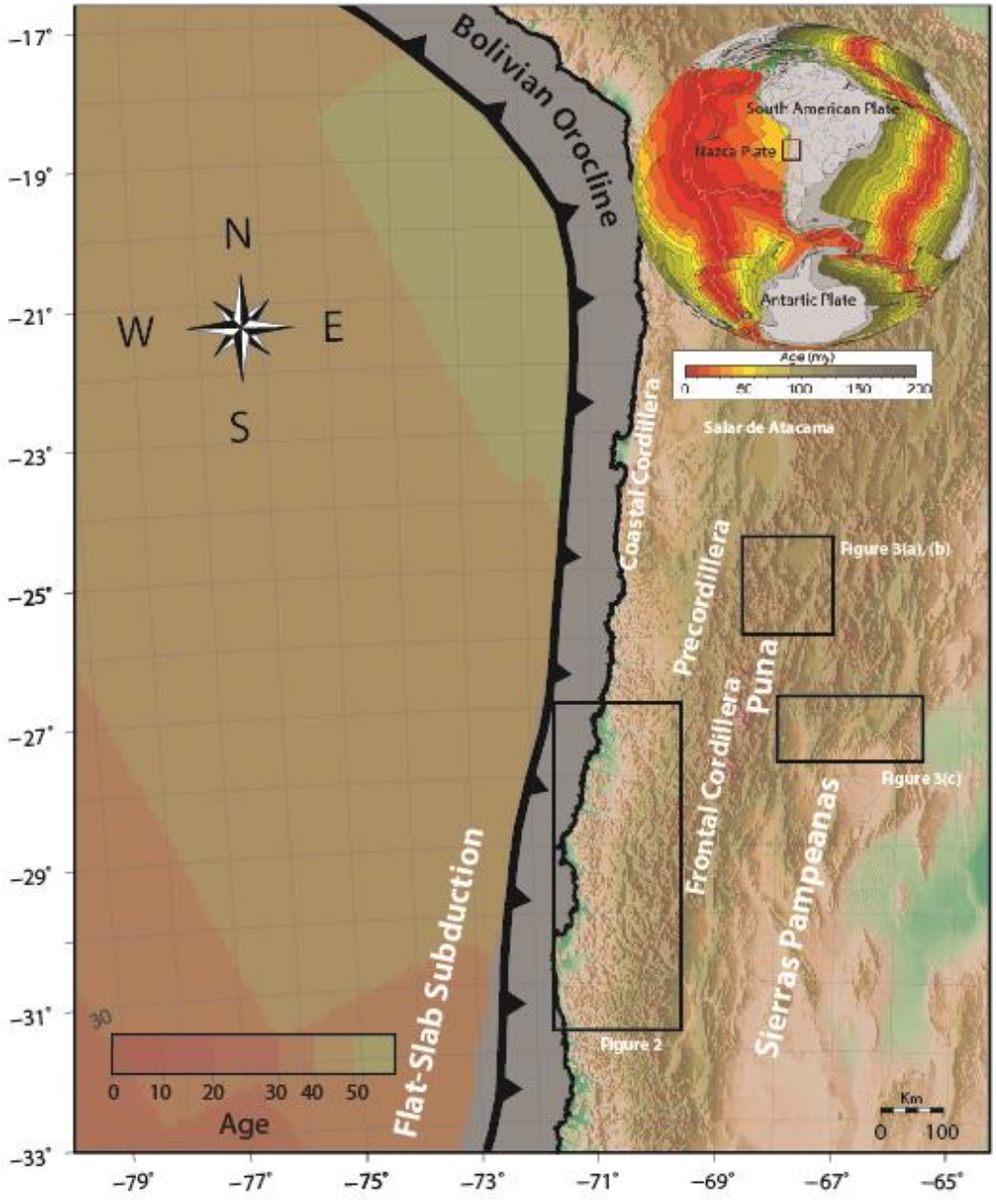

Figure 3.1: Central Andes and its. mains morphotectonic provinces. The black rectangles marks the locations of the paleomagnetic sites showed in figures 2 and 3.

Previous paleomagnetic studies suggest that the bending of the Central Andes induced clockwise block rotations along the chilean Andes from ~22°S to ~28°S

(Arriagada et al., 2006, 2008; Taylor et al., 2007). The proposed mechanisms of these rotations were different, some suggesting domino style blocks rotations (Randall et al., 1996; Beck, 1998; Grocott & Taylor, 2002; Taylor et al., 2007;2008), the influence of strike slip faults or shear zones (Beck, 1998; Kuhn & Reuther, 1999; Randal et al., 2001), or differential deformation combined with localized small-sized tectonic blocks (Arriagada et al., 2006b). From 28ºS to 31ºS there is no evidence of tectonic rotation (Ferrando et al., 2014). Clockwise rotations have been also reported for Central Chile south of ~31ºS, but the local bending of the margin in this area seems to be related to the subduction of the Juan Fernández ridge since the late Miocene (Arriagada et al., 2013, Puigdomenech et al., 2020). The transition from a zone of high rotations to a zone of little to no rotations and the timing and origin of tectonic rotations in the transitional zone remains unclear.

The timing of the tectonic rotations is another open matter. Being its deformation age first proposed in the Neogene (Heki et al., 1985; MacFadden et al., 1995), to an Eoceno-Oligocene age (Arriagada et al., 2003; 2006b), Upper Cretaceous-Early Paleocene (Somoza et al., 2012) to Upper Cretaceous (Puigdomenech et al., 2020). Being the age of the tectonic rotations associated to a different stage of deformations, or an accumulation of these, there is a need to place the different tectonic rotations in its propper tectonic region, associating the deformation ages in these specific areas to the tectonic rotation event.

In this contribution, we present the results of a regional scale paleomagnetic study with more than 500 samples collected from the Coastal Cordillera to the Principal Cordillera between 25° S to 31° S (Figures 3.1 and 3.2). Complementary to the paleomagnetic data, 6 U-Pb zircon and 5 Ar-Ar biotite ages have been obtained for a better understanding of the origin and timing of this regional feature, previously defined as the Vallenar Orocline (Arriagada et al., 2009).

3.2- Geological and tectonic setting between 25-31ºS

The studied region is located between 25º-33ºS, and 66º - 71º W. This area can be divided into two longitudinal zones: a western zone located in the Coastal Cordillera, Central Depression, Precordillera and the begininng of the Principal Cordillera; and an eastern zone, situated in the Frontal Cordillera and Sierras Pampeanas domain (Figures 3.1, 3.2, 3.3 and 3.4).

The western zone is located in the "Pampean flat-slab subduction" segment of central Chile and Argentina (Cahill and Isacks, 1992). This area is characterized by the absence of the Central Atacama Depression, which has its southern limit around 28º30'S (Farias et al., 2008).

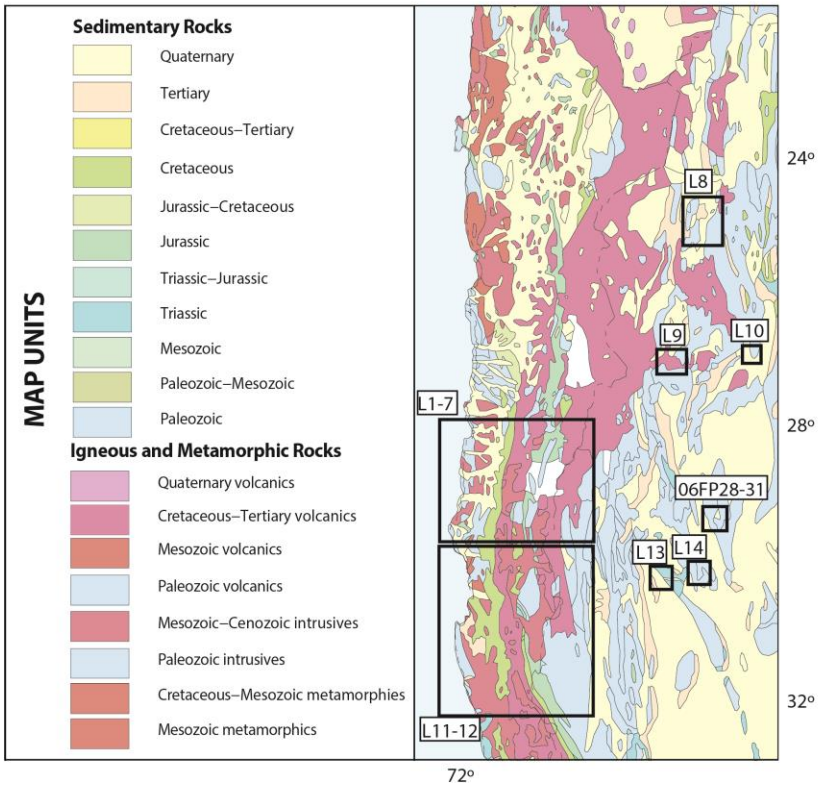

Figure 3.2: Simplified geological map of the Andes in the flat-slab subduction zone, modified from SERNAGEOMIN (2003) and Gomez et al. (2019). The black squares represent paleomagnetic localities, or group of localities.

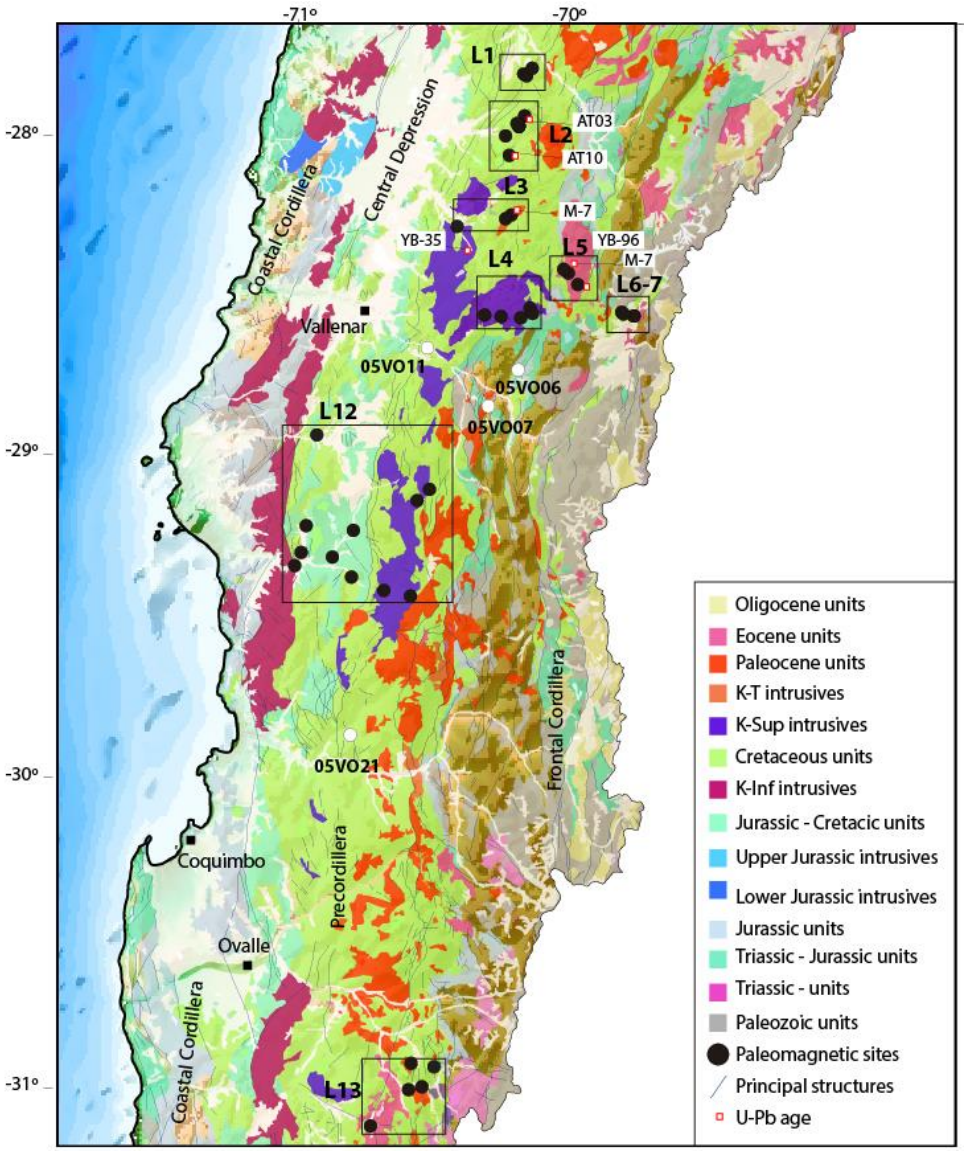

Figure 3.3: Simplified geological map of the Chilean Andes in the flat-slab subduction zone, modified from SERNAGEOMIN (2003). The black circles represent paleomagnetic sites, organized in localities (black squares), and the red squares correspond to the U-Pb samples from this work.

3.2.1- Forearc Section

From the Coastal Cordillera to Frontal Cordillera, there is a long strip of Paleozoic rocks related to both accretional processes of allochthonous and para-autochthonous terranes, and a metamorphic belt corresponding to a former accretionary prism (Mpodozis and Cornejo, 1988; Ramos, 2009; Alvarez et al., 2013; Herve et al., 2013). Volcanic and plutonic rhyolitic rocks related to the Choyoi magmatism are respectively covering or intruding the Paleozoic basement (Kleiman

and Japas, 2009). Since middle Triassic, extensional deformation occurred in this area, producing a series of extensional structures in the back-arc that accommodated volcano-clastic deposits from the Middle Triassic to the Early Jurassic, and sediments, both clastic and marine, during the Early Jurassic to the Middle-Late Jurassic (Jensen, 1976; Moscoso et al, 1982; Martínez et al, 2012). The early Mesozoic sedimentary rocks were deposited between the current Principal Cordillera and Precordillera, while a series of igneous bodies intruded the old Paleozoic metamorphic complexes of the Coastal Cordillera (Irwin et al., 1988).

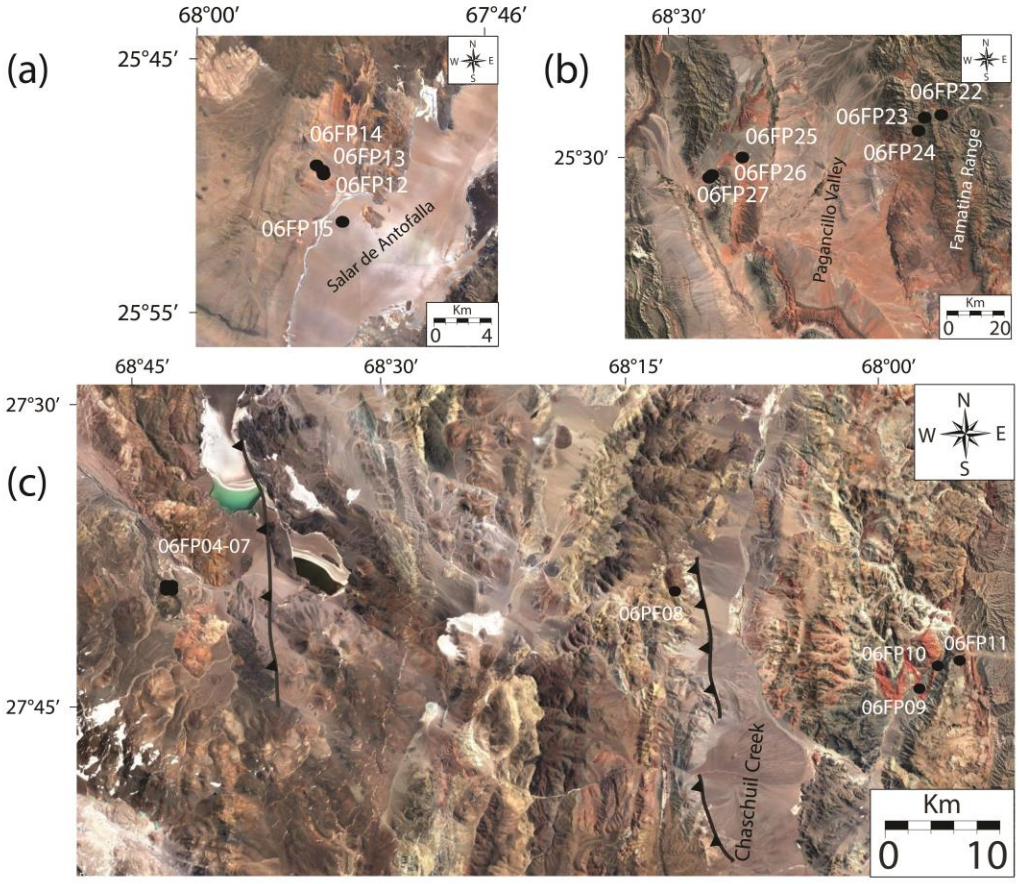

Figure 3.4: Location of some of the Southern Puna- Sierras Pampeanas paleomagnetic sites. (a) Corresponds to Antofalla locality, (b) Tambillos and Guandacol localities and (c) Laguna Verde and Chascuil localities.

The Upper Jurassic - Lower Cretaceous units are characterized by continental sedimentary and bimodal volcanic sequences (Dedios, 1967, Jensen, 1976; Iriarte

et al. 1999; Charrier et al., 2007; Oliveros et al., 2012), which are covering the Triassic-Jurassic basins (Martínez et al, 2012; Oliveros et al., 2012). At the western part of the Precordillera domain, a series of marine sedimentary rocks were deposited on top of these volcanic rocks, as part of the Lower Cretaceous Chañarcillo Basin, which records the last Mesozoic extensional pulse in the study area (Mourges, 2004; Martinez et al., 2013). These sequences are overlain by volcano-sedimentary rocks of the Upper Cretaceous and Paleocene, representing a volcanism whose igneous bodies intrude throughout the Precordillera area (Iriarte et al., 1999; Maksaev et al., 2009; Peña et al., 2013; Salazar et al., 2013; Creixell et al., 2013). Explosive volcanic deposits, with sedimentary interbeds and related intrusives, are the main representatives of the Eocene in the study area (Peña et al., 2013; Salazar et al., 2013). The unconsolidated deposits of the Atacama Gravels cover the latter deposits, in both the Frontal Range and in the foothills - Coastal Cordillera (Nalpas et al., 2008; Peña et al., 2013; Martinez et al., 2015).

3.2.2- Sierras Pampeanas Section

The eastern zone of this work (Figures 3.1, 3.2 and 3.4) comprehends a zone between various morphotectonic terrains, including the southern section of the Puna domain, the middle section of the Sierras Pampeanas domain, the Precordillera, the Sierra Famatina and the Frontal Cordillera (Ramos et al., 1993). The geology is characterized by Ordovician sedimentary and volcanic rocks, linked to the Puna eruptive belt in the southern Puna area (Ramos and Keppie, 1999), and Preacambrian and early Paleozoic basament rocks in the Sierras Pampeanas area (Salfity and Gorustovich, 1983), overlain by Devonian to Permian marine deposits and mid-Carboniferous to Permian terrigenous sedimentary rocks, respectively. These rocks are overlain by Cenozoic volcanic, synorogenic sediments (Horton et al., 2001) and evaporitic deposits in saline basins (Ramos, 1999). The Cenozoic units are affected by a series of N-S striking thrusts, generally propagating eastwards, that lift the older Paleozoic units over Cenozoic sediments, generating a series of ranges that caracterize the Sierras Pampeanas foreland deformation (Jordan and Allmendinger, 1986).

3.3.- U-Pb LA-ICPMS and Ar-Ar Geochronology

3.3.1- Sampling and methodology

Four samples in intrusives, were sampled in the forearc andean region, between 28-29ºS (Figures 3.2 and 3.3) for U-Pb dating on zircons, which were separated under the standard mineral separation method in the Department of Geology, University of Chile, using a Gemini table, a Frantz magnetic separator and heavy liquids procedures. The final selection of grains was made by hand, using a binocular. The mineral samples were sent to the Laboratory for Isotope Studies (LEI), Geoscience Center, Universidad Autonoma de Mexico (UNAM), Mexico.

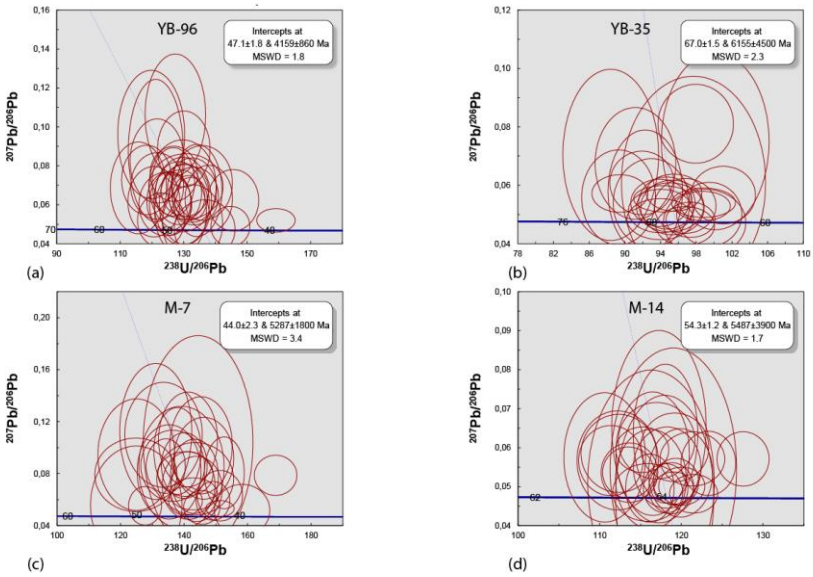

Figure 3.5: U/Pb age plots. Tera-Wasserburg plots are used for the intrusives, and Tuff-zircon plots for tuffs.

The analytical work was made using *Resonetic Resolution M50* with an *Excimer* laser of 193 mm connected to a *Thermo Xii Series Quadrupole Mass Scpectrometer* following analytical and technical procedures showed by Solari et al. (2010). A diameter of laser ablation of 34 micrometers was employed. The ages of tuffs were calculated using the TuffZirc algorithm and the intrusive ages were analized with Tera-Wasserburg plots included in the Isoplot 3.7 (Ludwig, 2008) software to select an age population (n> 10) for each zircon sample analyzed, when its free of Pb loss

and possible heritage problems (Figure 3.5). The age obtained represents the median age of the dominant group in a population of analyzed zircons (Table 1).

Additionaly, 3 sites from locality 4 were dated using the $^{40}Ar/^{39}Ar$ dating method (Table 1). Analyses were performed on individual grains of biotite, amphibole and K-feldspar (Figure 3.6). Samples were analysed with an $^{40}Ar/^{39}Ar$ laser probe and a Map 215 mass spectrometer. Irradiation of samples was performed at McMaster Nuclear Reactor (Hamilton, Ontario, Canada) in the 8F facility and lasted 66.667 h with a global efficiency (J/h) of $9.767 \times 10^{-5}\ h^{-1}$. The irradiation standard was sanidine TCRs (28.608 ± 0.033 Ma (Renne et al., 1998, 2010, 2011). Apparent age errors are plotted at the 1σ level and do not include the errors on the $^{40}Ar^{*}/^{39}Ar_K$ ratio and age of the monitor and decay constant. Plateau ages were calculated if 70% or more of the $^{39}Ar_K$ was released in at least three or more contiguous steps, the apparent ages of which agreeing to within 1σ of the integrated age of the plateau segment. Pseudo-plateau ages can be defined with less than 70% of the $^{39}Ar_K$ released and possibly less than three contiguous steps. The errors on the $^{40}Ar^{*}/^{39}Ar_K$ ratio and age of the monitor and decay constant are included in the final calculation of the error margins on the (pseudo) plateau ages.

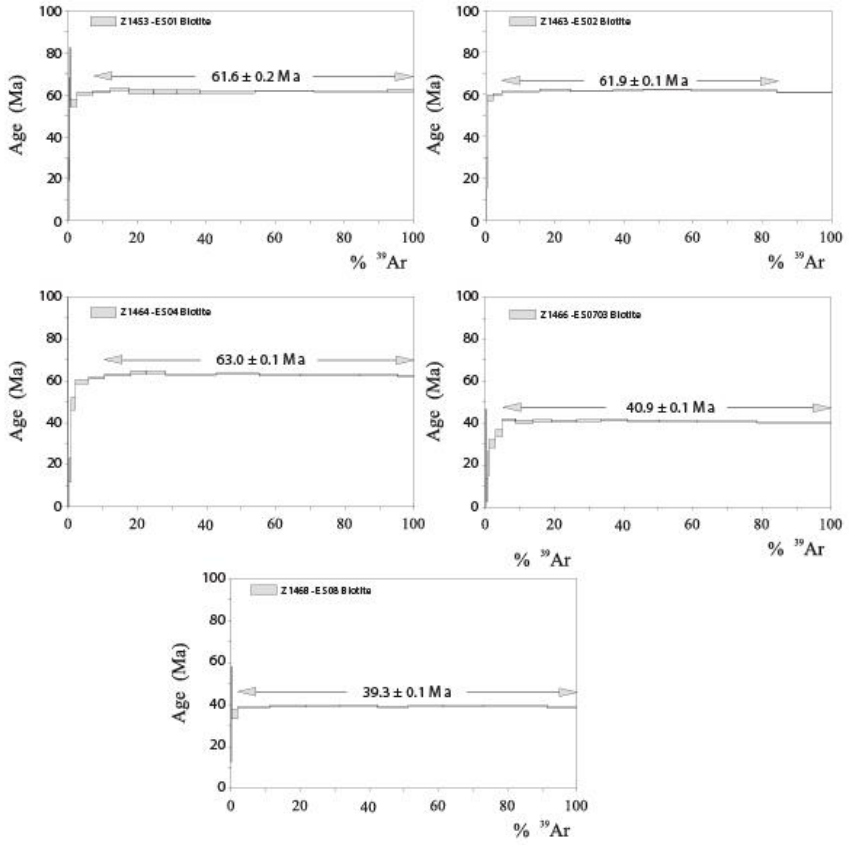

Figure 3.6: The 40Ar/39Ar age spectra of selected samples. The thickness of the gray rectangles for each step corresponds to 1σ uncertainty of apparent ages.

3.4- Paleomagnetism

3.4.1- Sampling and paleomagnetic techniques

The paleomagnetic sampling was conducted in several field campaigns during which more than 500 oriented samples were collected (Table 2). Samples were collected mainly in the Chilean Precordillera, and in the Sierras Pampeanas domain. The samples were taken mostly from Upper Cretaceous – Paleocene volcano-sedimentary rocks (Localities 1-2), Upper Cretaceous – Paleocene intrusives (Localities 3-4), Eocene intrusives (Locality 5), Jurassic lavas and sandstones

(Locality 7), Permian Sandstone (Localities 14-15) and a mixture of differente ages. Localities from 1 to 7 were drilled in folded and thrusted area, bounded by two large Mesozoic basins (Martinez et al., 2017). All sites were drilled using a portable gasoline-powered drill, and samples were oriented using magnetic and solar compasses when possible.

Remanent magnetization was measured with spinner magnetometers (Molspin and JR5 of AGICO), while magnetic susceptibility was measured with a Bartington susceptibilimeter at the Paleomagnetism Laboratory, Geology Department, Universidad de Chile. For sites with low Natural Remanent Magnetization (NRM) intensity, magnetic measurements were made with the 2G cryogenic magnetometer at the University of Rennes 1. To better characterize the magnetic carriers, we analyzed the acquisition of isothermal remanent magnetization (IRM), and the variation of susceptibility during heating (K-T) on some samples. IRM's were given with an ASC pulse magnetizer and K-T experiments were done with the AGICO KLY3-CS3 instrument. For most cores, one specimen was subjected to stepwise thermal demagnetization (steps 10 to 15) in an ASC furnace where the residual field was less than 10 nT. Magnetic susceptibility was measured after each thermal demagnetization step, to check changes in the magnetic mineralogy during heating. Stepwise alternating field (AF) demagnetization using the Molspin AF instrument was also performed on some samples. Magnetization directions were determined with a "least squares lines and planes" program following Kirschvink (1980). Evidence of secondary overprint magnetization due to lightning were found in some sites in volcanic rocks. In these cases, the AF demagnetization was preferred to thermal. Statistics combining directions and planes (McFadden and McElhinny, 1988) were used to determine the mean characteristic remanent magnetization (ChRM) directions for each site.

Tectonic rotation and flattening values with respect to stable South America for the individual sites were evaluated according to Demarest (1983), using reference South

American paleopoles from Torsvik *et al.* (2012). The site-mean directions for each locality and the tectonic rotations and inclination errors are given in Table 2.

3.4.2- Magnetic properties

3.4.2.1- Magnetization in volcanic rocks and intrusives

Most sites show natural remanent magnetization (NRM) intensities around 0.5 Am^{-1} and magnetic susceptibilities of 0.02 SI, typical of volcanic rocks with magnetite as the main ferromagnetic mineral (Dunlop & Ozdemir, 2001). Sites with lower susceptibility correspond to ignimbrites. Most sites from Cretaceous to Eocene outcrops show stable magnetizations and principal components of magnetization going through the origin during thermal or AF demagnetization. Magnetite is the main magnetic carrier in intrusive rocks (Figure 3.7). In volcanics, the magnetization left above 580°C show the same ChRM direction than the ChRM carried by magnetite indicating that oxidation during emplacement produced a small amount of hematite or stable maghemite as often observed in ryolitic rocks (Paquereau-Lebti et al., 2008) (Figure 3.7). During IRM acquisitions, saturation was often incomplete at 300 mT, especially in ignimbrites, in agreement with unblocking temperatures above 580°C (Figure 3.7). Demagnetization through AF of Upper Cretaceous to Eocene intrusives show stable magnetization (Localities 3-5) with, in some samples, an overprint likely related to lightning strikes (07ES04), which was easily removed by AF demagnetization. Evidence of low temperature oxidation were observed at some sites (08TX13) with a notable decline in magnetic susceptibility in the temperature range 250°-400°C, indicating reversal of titanomaghemite to hematite during heating.

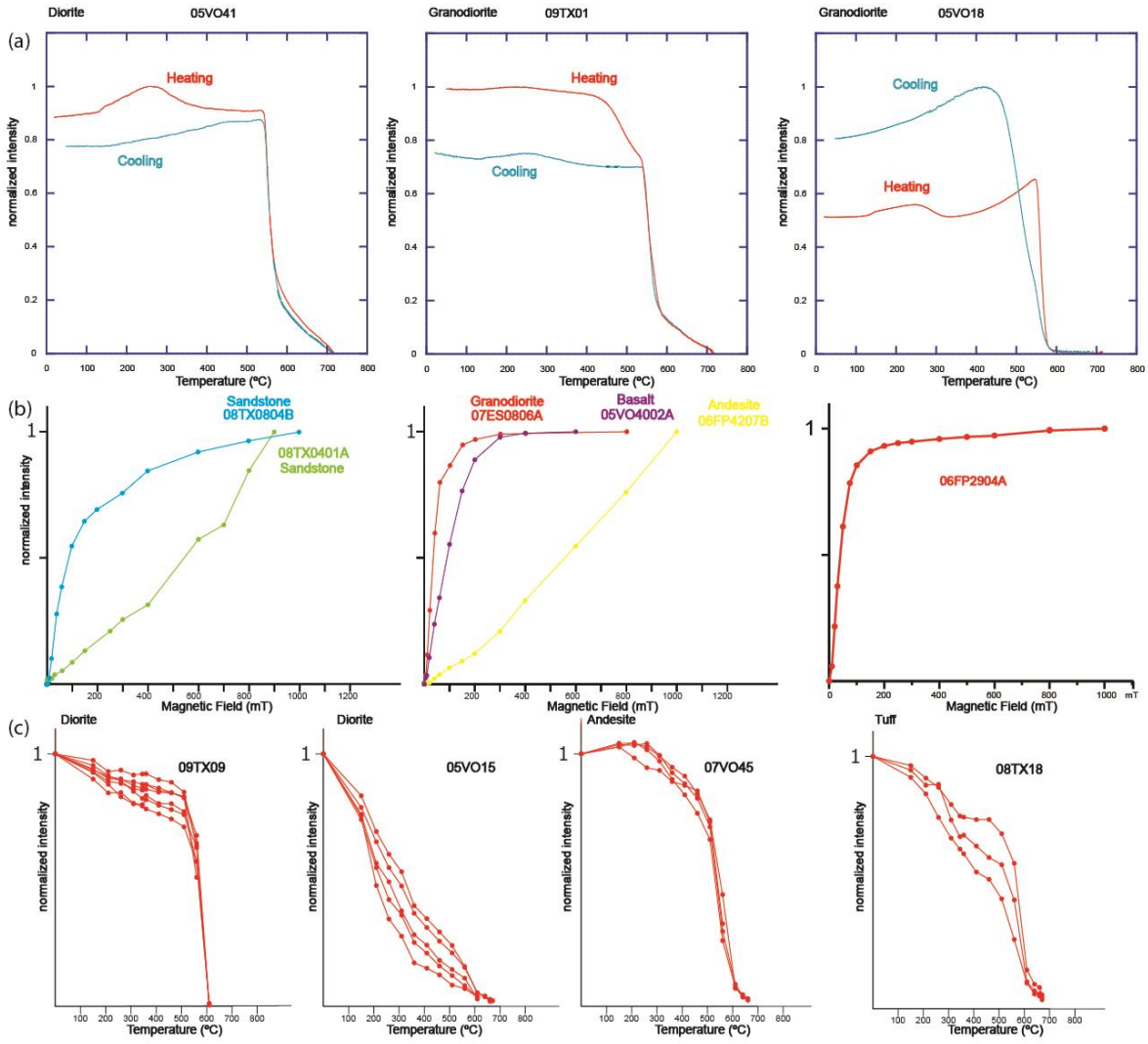

Figure 3.7: (a) Variation of magnetic susceptibility versus temperature, showing an important amount of magnetite carrying the magnetization, with an minor amount of hematite. (b) Normalized intensity of IRM versus magnetic field, the left one shows hematite as the main magnetic carrier in red beds, with some amounts of magnetite; the right one shows magnetite as the main magnetic carrier in extrusive rocks and intrusives, although there is a strong influence of hematite in tuffs. (c) Variation of magnetic intensity versus temperature, the rapid fall of intensity around 650ºC shows hematite as an important magnetic carrier, but others show magnetite, pirrotine and maghemite as secondary magnetic carriers.

3.4.2.2- Magnetization in Sedimentary rocks

The ChRMs identified in red beds correspond to a magnetization with unblocking temperatures almost linearly distributed in the temperature range 150–560°C up to 670°C. In most cases, the ChRM vectors are going through the origin during thermal

demagnetization (Figure 3.8) but there are some specific behaviors related to remagnetizations at some localities that will be further discussed during the description of the paleomagnetic data for each locality.

3.4.3- Characteristic Directions

3.4.3.1 Northern Andean Forearc

L1: Hornitos

4 sites were sampled (08TX15-08TX18) in ignimbrites belonging to the Hornitos Formation (Peña et al., 2013), of K-T age (Table 2). Sites 08TX15, 16 & 18 have similar magnetic properties with NRM intensities (0.01-01 Am^{-1}) and low susceptibility (0.0001 SI). The ChRM is carried by magnetite and hematite. Site 08TX17 has a strong NRM (~5 Am^{-1}) with stable ChRM carried mainly by pure magnetite. All sites have reverse polarity. The fold test reveals a better groupping of the site-mean ChRMs after tilt correction (Figure 3.9). The steep magnetic inclinations around 70º, suggests however that secular variation is not well averaged for this locality (Figure 3.8).

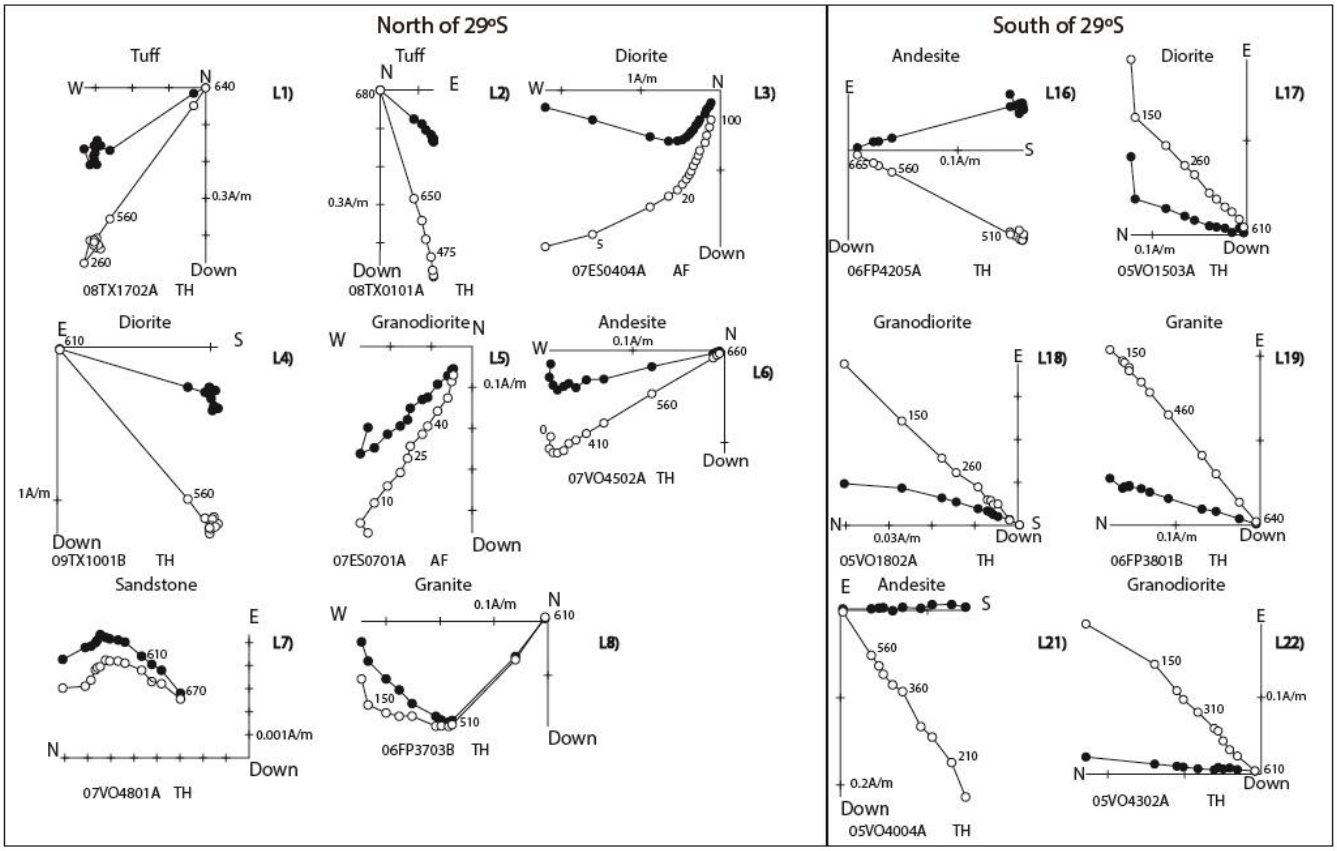

Figure 3.8: Orthogonal projections (in situ) of thermal (temperatures in °C) or alternating field (steps in mT) demagnetization diagrams for samples from volcanic, sedimentary or intrusive rocks for each locality. The projections represent the paleomagnetic locations described in the text. The viscous overprint is removed during the first steps of demagnetization, and the ChRM component is defined linearly through the origin. Solid (open) circles correspond to the projection onto the horizontal (vertical) plane.

L2: La Higuera

Around the La Higuera Synclinal, 8 sites were sampled (08TX01, 08TX03-06, 08TX08, 08TX10, 08TX13) in Upper Cretaceous rocks (Figure 3.3). Five sites were sampled in ignimbrites, two in fine-grained sandstones and one in andesitic lava. The sites 08TX03, 08TX04, 08TX05 were drilled in a vertical section of the same ignimbrite. These sites provided the same ChRM directions, which were combined to provide a mean direction for the same cooling unit. Site 08TX01 may correspond to the same ignimbrite but with a slightly different direction possibly due to uncertainties in the determination of the bedding direction. The two other sites in

volcanics (08TX01 and 08TX10) provided also a high temperature ChRM with respectively reverse and normal polarities.

The samples from the two sites in sandstones have two components of magnetization. A normal polarity magnetization was determined in the temperature range ~200-580°C with a reverse polarity magnetization recorded by hematite with unblocking temperatures above 600°C. The two components are nearly antipodal and better grouped after tilt correction. The low temperature magnetization likely corresponds to a remagnetization by hydrothermal activity related to the intense late Cretaceous magmatic activity before folding. Two U-Pb ages in tuffs were obtained in this locality, near sites 08TX05 and 08TX10 respectively, both of them with ages around 80 My (Table 2). The mean direction for the locality was calculated using the 4 volcanic units and the normal and reverse directions determined in the sediments.

L3: Salitral

3 sites (09TX01, 09TX09 and 09TX10) in Paleocene-Eocene intrusives (Peña et al., 2013) were sampled. One site (09TX01) in a granodiorite from a heterogeneous plutonic complex, and two (09TX09 and 09TX10) from a NNE-SSW striking Diorite. All sites show clear primary magnetic vectors through thermal demagnetization with magnetite being the principal mineralogical phase controling the magnetization. The 09TX01 and 09TX09 sites show normal polarity, while 09TX10 show reverse polarity. Two U-Pb ages were obtained, one in leuco-granodiorite with an age of 65.7 ± 1.3 My, near the site 09TX01 of this locality; and another with an age of 54.3 ± 0.7 My in a diorite, near the site 09TX09 (Table 2).

L4: Los Morteros

Five paleomagnetic sites were sampled in an intrusive complex of Late Cretaceous – Paleocene age (Peña et al., 2013) (Figure 3.3). Results were obtained at 5 sites, two from a granodiorite (07ES01 and 07ES02), one in a tonalite (07ES09) and two sites in dioritic rocks (07ES02, 07ES06). The ChRM were determined after AF

demagnetization. Site 07ES06 is the single site with a normal polarity. Three $^{40}Ar/^{39}Ar$ ages in biotite were obtained from sites 07ES01, 07ES02 and 07ES04, with ages of 61.2 ± 0.2, 61.9 ± 0.1 and 63 ± 0.1 Ma respectively (Figure 3.6). The reverse polarity observed for these sites is in agreement with the expected one from the Geomagnetic Polarity Time Scale for these ages (Table 2). Taking into account the reliability of the Argon ages, an Early Paleocene age is attributed to the mean ChRM.

L5: Tres Morros

Two sites were sampled in an Eocene granodiorite (07ES07-08) and two sites in a nearby foliated granodiorite (09TX03-04) of the same age (Figure 3.3). Sites 07ES07-08 have well defined ChRM of reverse polarity after AF demagnetization above 10 or 15 mT. A ChRM was also determined at site 09TX04 but no stable ChRM was recovered at site 09TX03. 40Ar/39Ar ages from site ES07 and site ES08 indicate cooling around 40Ma for the Manflas pluton and the Tres Morros locality. Two U-Pb samples were obtained in granites (Figure 3.5), with ages of 44.0 ± 2.3 Ma near site 07ES07, and 47.1 ± 1.8 Ma near site 09TX04.

L6: El Morro 1

Three sites were sampled in andesites (07VO45, 07VO46) and red sandstones 07VO47) from the Upper Cretaceous Viñita and Pucalume Formations (Figure 3.3; Salazar & Coloma, 2016).

Samples in the volcanic rocks have a stable single component of magnetization carried by magnetite and of reverse polarity. The magnetization is undoubtedly of primary origin. In contrast the sandstones at site 07VO47 have a more complex magnetization. The magnetic susceptibility (> 0.004SI) indicates that the sandstones are likely volcanoclastic sandstones. After the removal of a secondary component of magnetization, a component of magnetization of reverse polarity carried by magnetite was determined in the temperature interval ~460°C-610°C. This magnetization is likely acquired during sedimentation. Above 610°C there is a

component of magnetization of normal polarity carried by hematite but it is highly scattered and great circles are mainly controlled by the magnetization carried by magnetite. The mean ChRM for site 07VO47 is thus the magnetization carried by magnetite. The locality mean NRM is scattered probably because of secular variation recorded by the two sites in lava flows.

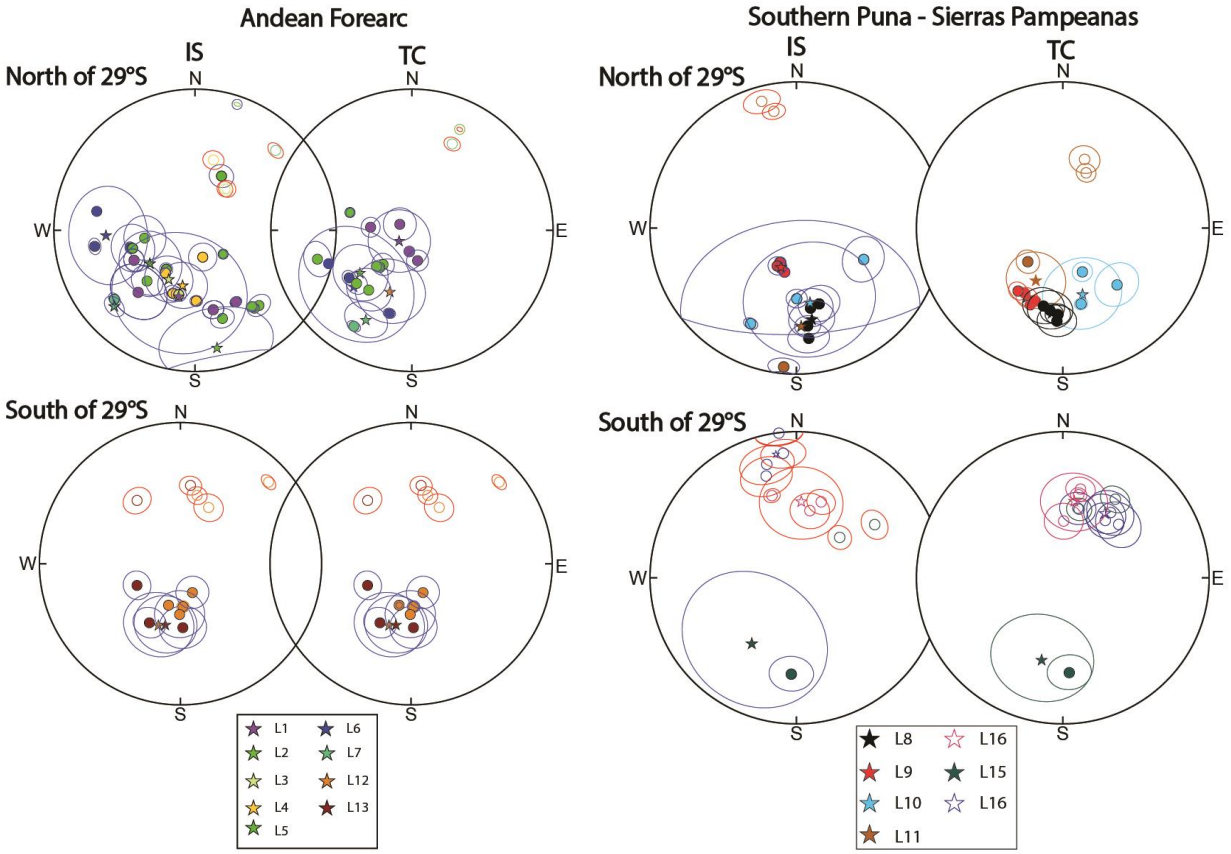

Figure 3.9: Equal-area projection of site-mean ChRM directions in situ (IS) and after tilt correction (TC) for localities listed in Table 2. Localities from 1 to 11 are in the north of the studied area, while 12-16 are in the south. Open (solid) symbols correspond to the projection in the upper (lower) hemisphere.

L7: El Morro 2

2 sites were drilled in red sandstones (07VO48 and 07VO49) of Early Cretaceous age (Salazar & Coloma, 2016). A high temperature component (unblocking temperatures >600°C) carried by hematite was determined at sites VO48 and VO49 with normal and reverse polarities respectively. At site 07VO49, a ChRM not

anchored to the origin with unblocking temperatures in the range (410-660°C) was determined in 4 specimens. Normal and reverse polarity directions are nearly anti-parallel and the ChRMs are likely of pre-tectonic origin.

Northern Andean Forearc Isolated sites.

Two lava flows were sampled around the Huasco River, near the city of Vallenar, one in Upper Trassic – Lower Jurassic andesitic lavas (05VO06) from La Totora Formation (Salazar et al., 2014), and another from (05VO11) an Upper Cretaceous andesitic lava (Arevalo et al., 2009). A Late Cretaceous ignimbrite was sampled at site 05VO07. The ChRM at site 05VO06 is carried by hematite and is of reverse polarity. Magnetite and hematite carry the ChRM at site 05VO11 while Ti poor titanomagnetite is the main carrier at site 05VO07. In all three cases, the ChRM was likely recorded during volcanic emplacement and cooling.

3.4.3.2 Sierras Pampeanas

L8: Antofalla

Southwest of the Salar de Antofalla (Figures 3.2 and 3.4), four sites in Oligocene red sandstones (06FP12, 06FP13, 06FP14 and 06FP15) were drilled in the Quiñoas Formation (Kraemer et al., 1999). The magnetic susceptibility values (geometric mean of 0.003 SI) indicate that these sediments are magnetite-rich volcanoclastic sediments. After removal of a low temperature present-day field overprint, the ChRMs were determined above ~250°C. Magnetite and hematite are respectively the main and minor magnetic carriers. The ChRM at all sites is of reverse polarity. The scatter decreases upon unfolding despite the small variation in bedding

L9: Laguna Verde

Four sites (06FP04, 06FP05, 06FP06 and 06FP07) were sampled in Oligocene red sandstones, south of Laguna Verde (Figure 3.3) from the Aparejos Formation (Rubiolo et al., 2001). Magnetic susceptibilities above 0.001SI indicate that

magnetite is the main magnetic mineral in the samples. The ChRMs of reverse polarity were determined in the temperature range 200-600°C but the vectors were not anchored to the origin because several samples have a poorly defined magnetization of normal polarity carried by hematite. The scatter in *in situ* coordinates at the site level as well as between the four sites is very low.

The scatter slightly increases upon tilt correction but the test is not significative since all sites have similar bedding dips, and there is several intercalations of mudstone and cross stratification in the unit. The ChRM is probably not a detrital magnetization acquired during sediment deposition but possibly a chemical magnetization. The *in situ* mean inclination is steep (66.4°) and the tilt-corrected inclination (45.5°) is in better agreement with expected inclination for the late Oligocene - early Miocene. Pliocene volcanism is reported for a large volcanic center (Goss et al., 2009) located about 20 km to the south of Laguna Verde and a remagnetization related to hydrothermal activity cannot be completely discarded. We however prefer the interpretation that the ChRM was recorded before folding in the area.

L10: Vinchina

One site (06FP28) in Oligocene red sanstones near the Vinchina town was sampled, this was merged with two sites (20 & 21), from Vizan et al. (2012), sampled in red sandstones from Laguna Brava Formation. Magnetic suscpetibilites around 0.004 suggest hematite as the main magnetic mineral carrier, like suggested by Vizan et al. (2012) for the D21 and D20 samples. The scatter of the site decreases notably after applying the tectonic correction, suggesting that the magnetization is pre-tectonic for this locality. The site 06FP28 has reverse polarity, unlike the sites 20 and 21 that have normal polarity.

L11: Chasculi

Three sites were sampled in Permian aeolian red sandstones of the De la Cuesta Fm. creek (Spaletti et al., 2010) (06FP09, 06FP10 and 06FP11) in the Angosturas (Figure 3.3). These sites have hematite as the principal magnetic carriers. They have a reverse polarity magnetization in agreement with their Permian age and a

magnetization likely recorded during the Kiaman superchron, with its deposition age, around 275 Ma (Limarino and Spalleti, 1986).

Eastern cordillera/Sierras Pampeanas Isolated sites

Two sites were sampled in red sandstone beds around the locality of Jahue. One in Triassic (06FP31) and another in Miocene (06FP28) outcrops. 06FP31 has normal polarity ChRMs with hematite as the main magnetic carrier. *S*amples from site 06FP28 have magnetic susceptibility (~0.004 SI) showing that magnetite is the main magnetic mineral in these sediments. A normal overprint in the present-day field was well defined in the temperature range (150-310°C). A reverse polarity magnetization was recovered at high temperature.

3.4.3.3 Southern Andean Forearc

L11: La Campana

8 Sites around the Domeyko depression (Rodriguez et al., 2015) were sampled (Figure 3.3). Sites 06FP42, VO19 and 06FP39, were sampled in Upper Cretaceous andesites. Sites 06FP40, 06FP38, O5VO18 were sampled in Upper Cretaceous intrusive rocks (SERNAGEOMIN, 2003)., One site (05VO16) was drilled in Upper Paleocene diorites. A single site (06FP37) is in Lower Cretaceous granites (Arevalo et al., 2009). Sites 06FP42, 06FP40, 05VO16 and 06FP37 have ChRMs of reverse polarity and high unlocking temperatures. ChRM of normal polarity and high unblocking temperatures are found at site 06FP38. Both polarities are observed at site 05VO18. The magnetization of these 6 sites is likely primary and were combined for the calculation of a mean direction for the locality. The ChRMs at the three other sites correspond to vectors not anchored to the origin and intermediate unblocking temperatures. The tilt-corrected direction is unlikely at site 06FP39. The age of remagnetization for these three sites is uncertain.

L12: Tulahuen

Five sites were drilled near the Cogotí River (Figure 3.3), belonging to Eocene diorites and granodiorites (05VO41, 05VO42 and 05VO43), Jurassic lavas (05VO37) and Upper Cretaceous andesitic lavas (05VO40). Sites 05VO40 and 05VO42 have reverse polarity, while 05VO41 and 05VO40 display normal polarity (Figure 3.9). The reverse polarity ChRM at site 05VO37 was determined with vectors not anchored to the origin. The magnetization is likely of secondary origin and was not taken into account in the mean calculation. The fold test is slightly negative but based on only one site with bedding correction. The difference in direction before and after bedding correction is not significant. We use the in situ direction and we attribute an Eocene magnetization age (ca. 40 Ma) to this direction (Figure 3.9).

Isolated Southern Andean Forearc

Three sites were drilled north of the town of La Serena. Site (05VO21) was sampled in mid-Cretaceous andesites (Emparan and Pineda, 1999); site 05VO20 in Late Cretaceous red beds and site 05VO22 in a Neocomian conglomerate. There is no evidence for a remagnetization in the conglomerate. A stable magnetization with high unblocking temperature is determined suggesting a primary magnetization for both sites VO20 and VO21.

3.4.3.4 Sierras Pampeanas – Permian Triassic rocks

L14: Los Tambillos

Three sites (06FP22, 06FP23 and 06FP24) were sampled in Permian red sandstones (Figure 3.4), between the localities of Miranda and Los Tambillos (Zhang et al., 1998, Gulbranson et al., 2015). Site 06FP23 has a well-defined reverse polarity magnetization carried by hematite as in sites FP09-10-11. In contrast, the magnetization at site FP22 is scattered. Only site FP24 provides a well-defined ChRM of normal polarity.

L15: Guandacol

Three sites (06FP25, 06FP26 and 06FP27) were sampled in Permian red sandstones, west of of Guandacol (Figure 3.4), associated with glacial and postglacial deposits (Alonso-Muruaga et al., 2018). Sites (06FP26 and 06FP27), have distributed unblocking temperature with a ChRM of normal polarity. In contrast the ChRM of site 06FP25, with reverse polarity, is mainly carried by hematite with high unblocking temperatures close to 670ºC. The fold test shows a better grouping after applying it (Figure 3.9), associating the age of magnetization with the deposition of these sandstones (Cesare and Limarino, 2008).

L16: Santo Domingo

One site (06FP31) was merged with three sites from Vizan et al. (2012), in Triassic red sandstones from Santo Domingo Formation. All sites have normal polarity and have a better grouping after applying tectonic correction, suggesting that the age of magnetization is around 200 My. ChRM for all samples is defined between 410-650°C, suggesting hematite as the principal magnetic carrier.

3.5.- Tectonic rotations in the South-Central Andes.

Tectonic rotations and inclination anomalies have been calculated for Paleozoic to Cenozoic units using an estimated age of magnetization and reference poles from Torsvik et al. (2012). The average direction for each sampled locality, tectonic rotations and tilt errors are found in Table 3.

All the paleomagnetic results come from areas that have registered a complex history of late Cretaceous – Cenozoic deformation. The rotations may vary spatially and with time.

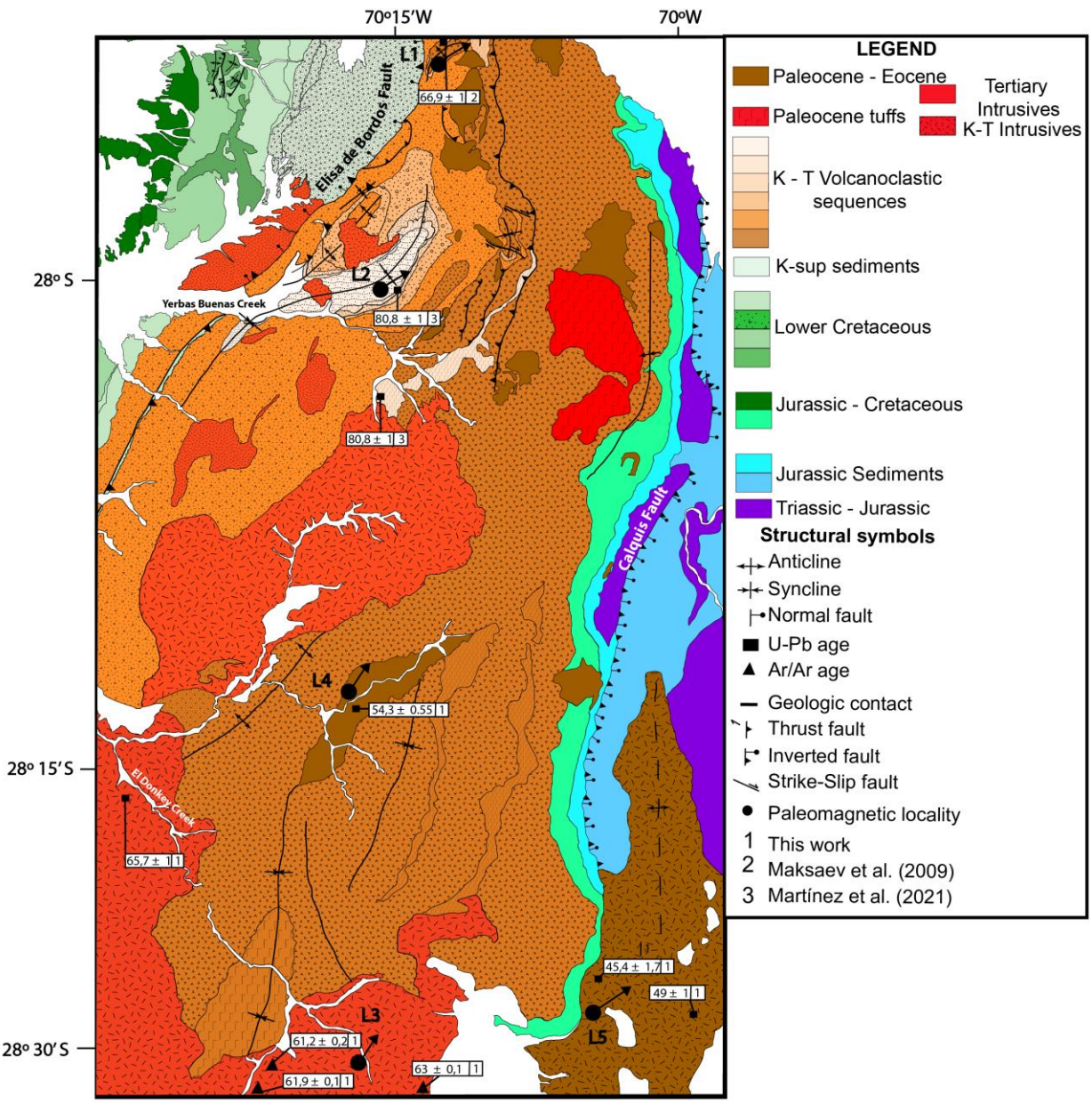

Figure 3.10: Simplified map of the Chilean Andes in the flat-slab subduction zone, modified from Martínez *et al.* (2013), with the paleomagnetic results of this work.

3.5.1 Spatial variations.

3.5.1.1 Tectonic rotations in the Andean forearc.

Adding our new data to previousy published studies (Taylor et al., 2007; Arriagada et al., 2008; 2013; Maffione et al., 2009; Somoza et al., 2012; Ferrando et al., 2014; Prezzi et al., 2014; Japas et al., 2016), and grouping sites of similar lithologies, belonging to a common structural block, in the same paleomagnetic locality, for

which we can calculate a tectonic rotation. We note one remarkable change in the rotational pattern. There is a noticeable difference in the tectonic rotations south of 25ºS and north of 29°S in the Andean Forearc (Figure 3.11), which shows an average clockwise tectonic rotation of 30,3 ± 14º with a low inclination error (0,9 ± 9,9°). Between 29ºS and 33°S, there is a clockwise rotation of 15,2 ± 13,7°, with also has a low inclination error (-1,7 ± 9,5º). The median rotation value for the area between 25°S and 29°S (35.13º) is slightly different to the arithmetic mean, indicating that the mean rotation is affected by large values, but not in great percentage.

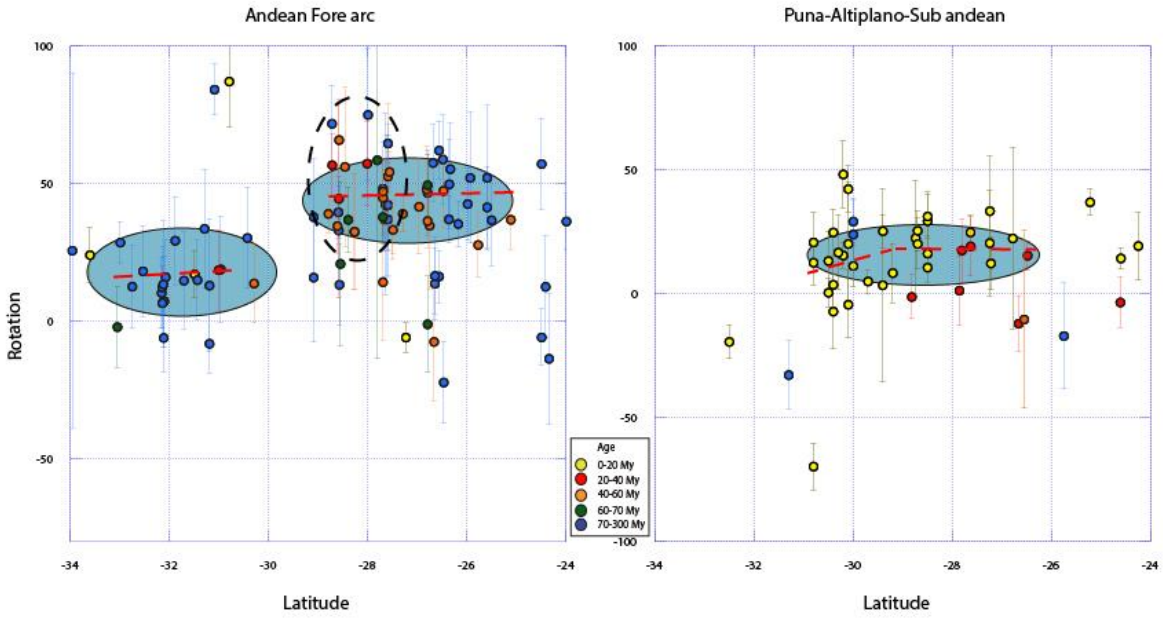

Figure 3.11: Variation in rotation in latitude and longitude for different age groups of samples, separated in the northern and southern domains.

However, there is a variation in the mean and the median value beetwen 27°30'-29ºS, with a mean rotation of 38.2 ± 13.6º and a median value of 38°, showing here the relevance of the weight of large rotation values in the mean value. In this particular area, the magnitude of rotations matches with the orientation of the main structures of the region, and the general orientation of the fault-bounded Paleozoic basement blocks, correlating these high values in the rotational data with the drastic

changes in strike of the faults and folds in the area (Figure 3.10), thus pointing to the importance of inherited structures in rotational deformation.

3.5.1.2 Tectonic rotations in Southern Puna - Sierras Pampeanas.

In the Southern Puna and Sierras Pampeanas area, north of 29ºS, rotations are also clockwise, but smaller than the forearc, with a magnitude of 18,6 ± 12,9°. South of 29ºS, in the same domain, clockwise rotations are bigger (23.8 ± 12°) than the north, and also bigger than its forearc counterpart. The change between north and south of 29°S talks about the presence of more strike-slip structures in the Sierras Pampeanas domain and reflects the big strike changes around Catamarca ranges (De Urreiztieta et al., 1992; Riller et al., 2003). The lower number of rotations north of 29°S, compared to the forearc, is strongly linked to the broken foreland structural styles inbetween the Sierras Pampeanas (Strecker et al., 2011; Davila et al., 2012; Del Papa et al., 2013), but with still some amount of strike-slip deformation (Mpodozis et al., 1997).

3.5.2 Temporal variations

The southern border of the Atacama Desert has been shaped by a series of tectonic events, such as the Mesozoic extensional events, which controlled overall basin configuration, and the Late Cretaceous-Tertiary compressional and oblique tectonic events, responsible for the uplift and deformation of the Andean chain (Charrier et al., 2007; Martínez et al., 2016). In addition, the episodic eastward migration of the Andean magmatic arc since Jurassic to its actual position may also have helped to produce the rotational patterns as a consequence of a thermally weakened crust, making the latitudinal changes more perceptible in the Andean Forearc. Rotations in the Coastal Cordillera and Central Valley may have been linked to the oldest early Late Cretaceous and early Paleocene phases of compressional-oblique

deformation, traditionally linked to strike-slip fault zones (Forsythe and Chisholm, 1994; Randall et al., 1996; Taylor et al., 1998, 2007), while rotations in the Precordillera have been related to the compressional-transpressional deformation mainly associated with the Incaic tectonic phase (Randall et al., 2001; Arriagada et al., 2000, 2003, 2006). Our new paleomagnetic data and geochronology, between 27,5-29ºS, shows in the forearc area (Figure 3.10) a cluster of large clockwise rotations (38,2± 13,6°), in the age range between 80-55 Ma (Table 2 and 3). Contrasting this new data with previous analysis (Arriagada et al., 2006; Taylor et al., 2007), and synorogenic strata observed in field (Martínez et al., 2013), we can suggest the existence of a rotational event around the Late Cretaceous to Late Cretaceous-Paleocene. The cluster of high rotations observed in the forearc between 27,5-29°S (Figure 3.10) are strongly linked to the Mesozoic inverted basins and the Upper Cretaceous-Paleocene syntectonic Volcano-sedimentary sequences, with a maximun deformation age of Late Cretaceous (Martínez et al., 2013), and a series of syntectonic intrusives and synorogenic strata (Martínez et al., 2013; Peña et al., 2013). We propose, in accordance with the new U-Pb ages obtained in this study, that this event may have occurred around 67 ± 1,5 Ma (Table 2) and 66,9 ± 1 Ma (Maksaev et al., 2009). The syntectonic volcanosedimentary sequences, where localities 1 and 2 were sampled, showed the largest clockwise rotations, pointing to the K-T syntectonic strata to the rotations obtained in the same sites, sites that are surrounded by local structures with strong strike changes (figure 3.10), but the high rotations in locality 5, in a plutonic complex with ages between 44-47 Ma, suggest that is not only a matter of time in the rotational pattern, but maybe are local tectonics producing these anomalous rotations.

Our new data from an Eocene plutonic complex, locality 5, give a mean clockwise rotation of 56,3 ± 28,9º, suggesting that the clockwise rotation event, linked to the Incaic Event (Arriagada et al., 2006), continued to be active after the Eocene in this area.

In the eastern localities, like Laguna Verde, there is evidence for post-Miocene clockwise rotations, but much smaller than the forearc ones. This new data suggest that the tectonic rotational defomation in the Precordillera and Central Depression

extended to the Oligocene, in agreement with data collected north of the studied area (Somoza et al., 1999; Arriagada et al., 2003; 2006), and suggesting that the rotational deformation extended into the Miocene in the eastern morphostructural units of the Andean chain, but with a decrease in its magnitude (Table 3).

3.6.- Local variations in rotations and their relation to structural heterogeneities

Traditionally, the rotational pattern has been associated with the largest strike-slip fault systems of Chile, like the Atacama Fault Zone, the Domeyko Fault Zone and the Liquiñe-Ofqui Fault Zone (Randall & Taylor, 1996; Beck et al., 2000; Roseneau et al., 2006). However, paleomagnetic studies have shown that some of these fault systems, or some sections of these, did not contribute significantly to local rotation patterns (Randall & Taylor et al., 1996; Arriagada et al., 2006), making the structural analysis of tetctonic rotations a sum of several factors: shortening partitioning, thermal weakened crust, inherited basament anisotropies, shear zones, tectonic extrusion, etc. (Poblete et al., 2014; Huang et al., 2015; Weil et al., 2016; Li et al., 2017).

Beetwen 27,5-29ºS there are two first order structures in the Chilean Precordillera, the Elisa de Bordos fault, that acomodated compressional and transpressional deformation related to the Early Cretaceous Chañarcillo basin inversion, with a reactivation age related to the K-T orogeny (Cornejo et al., 2003; Martínez et al., 2013); and the Calquis fault, which controlled the accomodation of a Triassic-Jurassic basin, reactivated through a positive tectonic inversion, mostly linked to Late Cretaceous-Eocene deformation (Martínez et al., 2012; 2013). There is a strong spatial, temporal and structural correlation beetwen these structures and large rotations in this area (Figure 3.10), since the localities with large rotations are found in folds that are related to shortcuts originated with the Elisa de Bordos fault and the inversion of the Chañarcillo Basin, the inversion of the Calquis fault and a triangle-

zone bordered by these two major faults (Martínez et al., 2016). In this scenario, the rotations beewtwen 27,5-29ºS could be explained by a local tectonic transpressional tectonic conditions explained by the change in the strike of the Elisa de Bordos and Calquis faults, and their “triangle zone” architecture (Figures 3.10 and 3.12). The unusual big rotations in K-T units between these two major faults add more evidence to the argument for a compressional behavior beetwen 27,5º-29ºS simultaneous to the deposition of the volcano-sedimentary sequences, from the Hornitos Formation, and the intrusion of large syntectonic complexes (Peña et al., 2013). The addition of a magmatic event coeval with the K-T deformation, that thermally weakened the surface, on the mentioned triangle-zone bounded between two regional fault systems, that could have facilitated the extra clockwise rotations in this particular area. These are not the only rotations out of the regional trend, some localities, like 10 and 14, in the Southern Punta-Sierras Pampeanas domain show other tectonics rotations linked to the changing strike of Andean orogen, and to the presence of NNW-striking transpessional belts, evidence patitioning of the regional deformation (Japas et al., 2016).

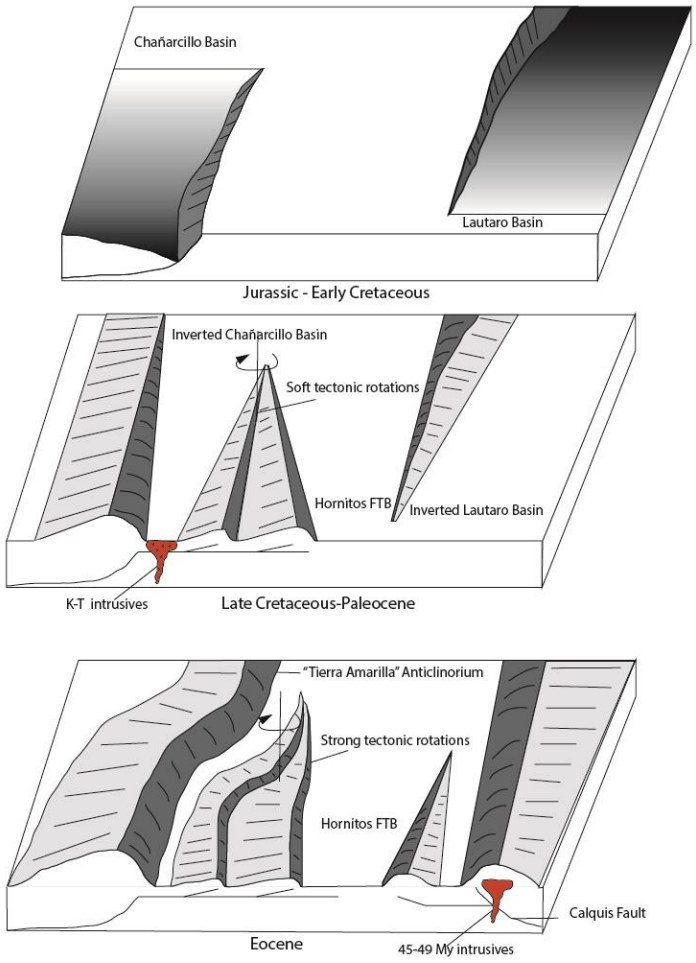

Figure 3.12: Tectonic sketch of how the inversion of the Mesozoic basins added more rotations to the K-T volcanosedimentary deposits, related to localities 1 and 2. See figure 10 to correlate with a plant-view map.

3.7.- Discussion: The CARP and its limits.

Since Isacks (1988), it has been suggested that a variation in the tectonic rotation around the Arica Bend, with a predicted model of anticlockwise rotations of 10-15º in southern Peru, and clockwise rotations of 5-10º for northern Chile, is a Neogene event in the first studies in the zone (Heki et al., 1985). This model evolved to interpret the highest magnitude of rotations as a distribution of crustal shear in the forearc, due to oblique convergence (Beck, 1988). Other works suggested that rotation is a product of a "Domino style" model, bounded by NW-SE faults that cut

NS striking faults related to the Atacama Fault System (Forsythe and Chisholm, 1994; Taylor et al., 1998; 2007). This model of regional faults with NW strike, forming a domino-type deformation style, is not consistent with the different structural models constructed with surface and depth geophysical information (Naranjo and Puig, 1984; Cornejo et al., 1993, 1998; Arévalo, 1994; Cornejo and Mpodozis, 1996; Marinovic et al., 1995; Iriarte et al., 1996; Godoy and Lara, 1998; Matthews et al., 2006; Arriagada et al., 2006b; Amilibia et al., 2008; Martínez et al., 2012, 2013; 2016), where it has been observed that the strike-slip component is an order of magnitude smaller compared to the compressional deformation, for regional-scale tectonics.

The Eocene - Oligocene rotations in Peru (Roperch et al., 2006) and north of Chile (Arriagada et al., 2006a), related to the Incaic event, have been proposed to have occurred simultaneously, on both sides of the Arica Bend. However, the data presented in this work, added to the data located around the city of Calama (Somoza et al., 2012), show that the rotations that would have altered the strike of regional structures and the continental margin from 23ºS to 29ºS, would have started in the Late Cretaceous - Paleocene, revealing a large-scale rotational deformation pattern prior to the Incaic event. The age of deformation related to these rotations can be traced from Calama (22ºS), close to Antofagasta (24ºS), the Salar de Atacama (23ºS), El Salvador (27ºS), north (27º30'S) and south of Copiapo (28º30'S) where a series of unconformities, geochronological data, syntectonic beds and cross-cutting relationships showing events in the Upper Cretaceous and early Paleocene (Cornejo et al., 2003; Cornejo and Mathews, 2001; Arevalo 2005a; Maksaev et al., 2009; Somoza et al., 2012; Salazar, 2012; Martínez et al., 2012, 2013; 2016; Bascuñán et al., 2015). This suggests that, although the Eocene rotations are still the largest, the rotational deformation and construction of the Bolivian Orocline would have started earlier, in the Upper Paleocene, linked to the first shortening events that uplifted the western margin of South America between 18-29°S.

For the rotations south of 29ºS, previous works (Ferrando et al., 2014; Arriagada et al., 2013) show little amount of rotations until 33ºS, which Arriagada et al. (2013)

suggest that the Andean forearc between these latitudes could have rotated in a counter-clockwise sense since the Upper Miocene, making the Pampean flat-slab a tectonic barrier to the far field rotational pattern of the Bolivian Orocline. Also, the major occurrence of great plutonic bodies south of 29°S, like the Illapel plutonic complex (Ferrando et al., 2014), make the rheology of this area more rigid and harder to rotate. These previous results agree with our data, having a compiled mean clockwise rotation of 15,9 ± 17,3°, suggesting that this segment with small rotations in the Andean forearc extends from 29ºS to 33ºS (Figure 3.13).

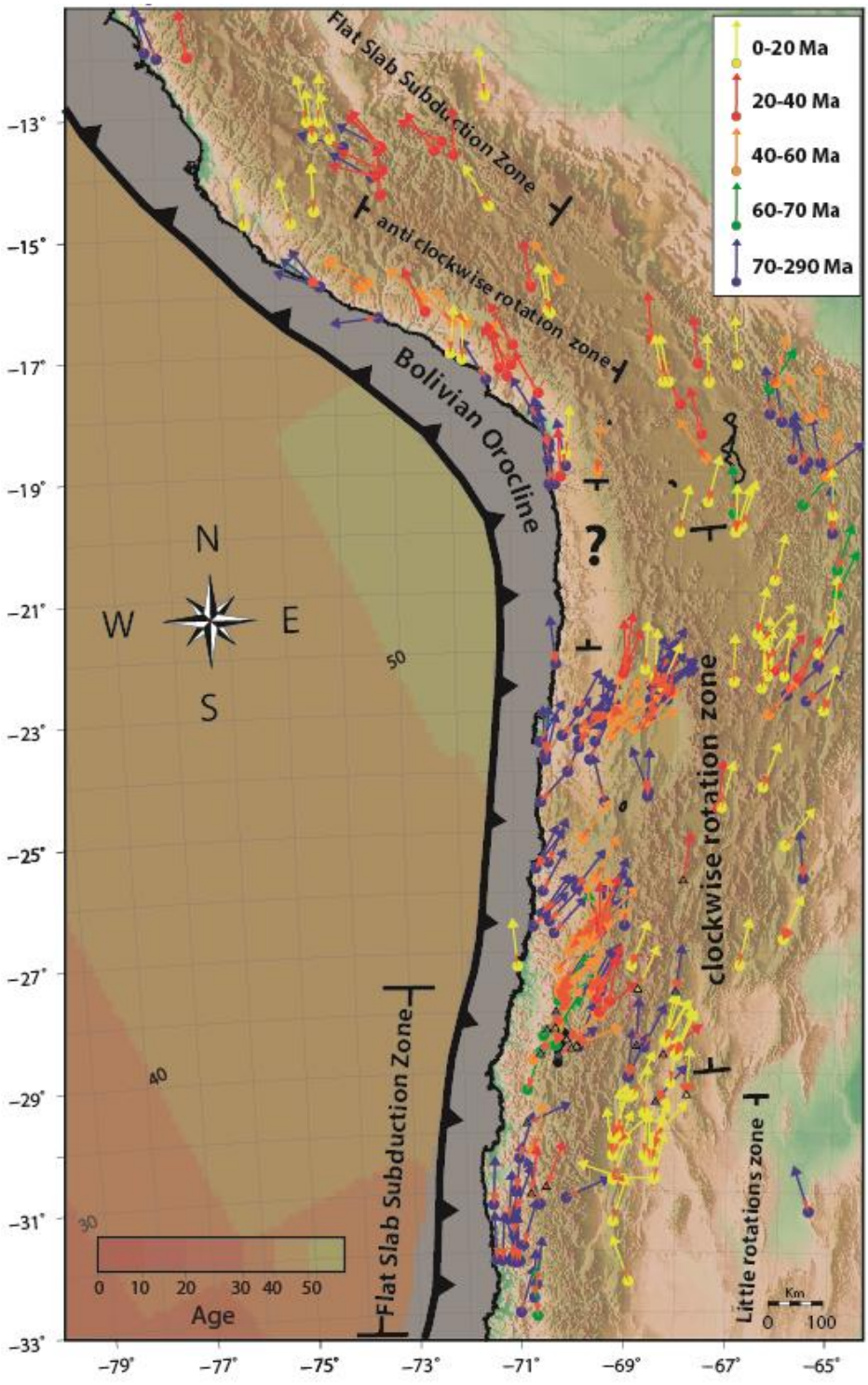

Figure 3.13: Paleomagnetic rotations in the South American western margin. Different colors represent different magnetization ages. The orange cone above the circles correspond to the error margin of the rotation.

From the continental point of view (Figure 3.13), a limit can be traced between the CARP zone and the zone of small rotations around 29ºS, marking a southern limit for the Bolivian Orocline clockwise rotational pattern. This limit shows a "hinge" like behavior for the western South American margin, relating a series of regional compressive tectonic events that shaped the Bolivian Orocline north of 29°S, represented by the large rotational pattern north of 29ºS; and little rotational deformation south of 29ºS, linked to the formation of the “Maipo Orocline” during the Oligocene-Miocene, and the subduction of the Juan Fernández Ridge (Arriagada et al., 2013). Also, there is a strong difference between the rotations in the Andean forearc and the Southern Puna-Sierras Pampeanas area (Figure 3.13), the second also showing north to south variations, but with lesser amount of rotations than the Andean forearc rotations, but with the same percentual difference north and south of 29°S. The longitudinal difference (Figure 3.13) points to contrasting mechanisms in the Southern Puna-Sierras Pampeanas domain when compared to the Andean Forearc, where the rheology of the former is more rigid than the volcano-sedimentary Mesozoic cover of the latter (Tassara & Yáñez, 2010; Ferrando et al., 2014; Del Rey et al., 2016). These reological differences could point to the crucial role of strong reologhy anisotropy, like the suture’s zones of the diverse accreted terranes in western South America (Ramos, 2008), or the shape of the Mesozoic basins (Vicente, J., 2006), that can play a significant role in the Cenozoic tectonic story of the western margin of South America (Ramos, V., 1994; Alvarez et al., 1999; Martínez et al., 2016).

The conceptual tectonic model made with these new rotational data allow us to draw a continuous model for the Andean Forearc between the Bolivian Orocline and the Maipo Orocline (Figure 3.14).

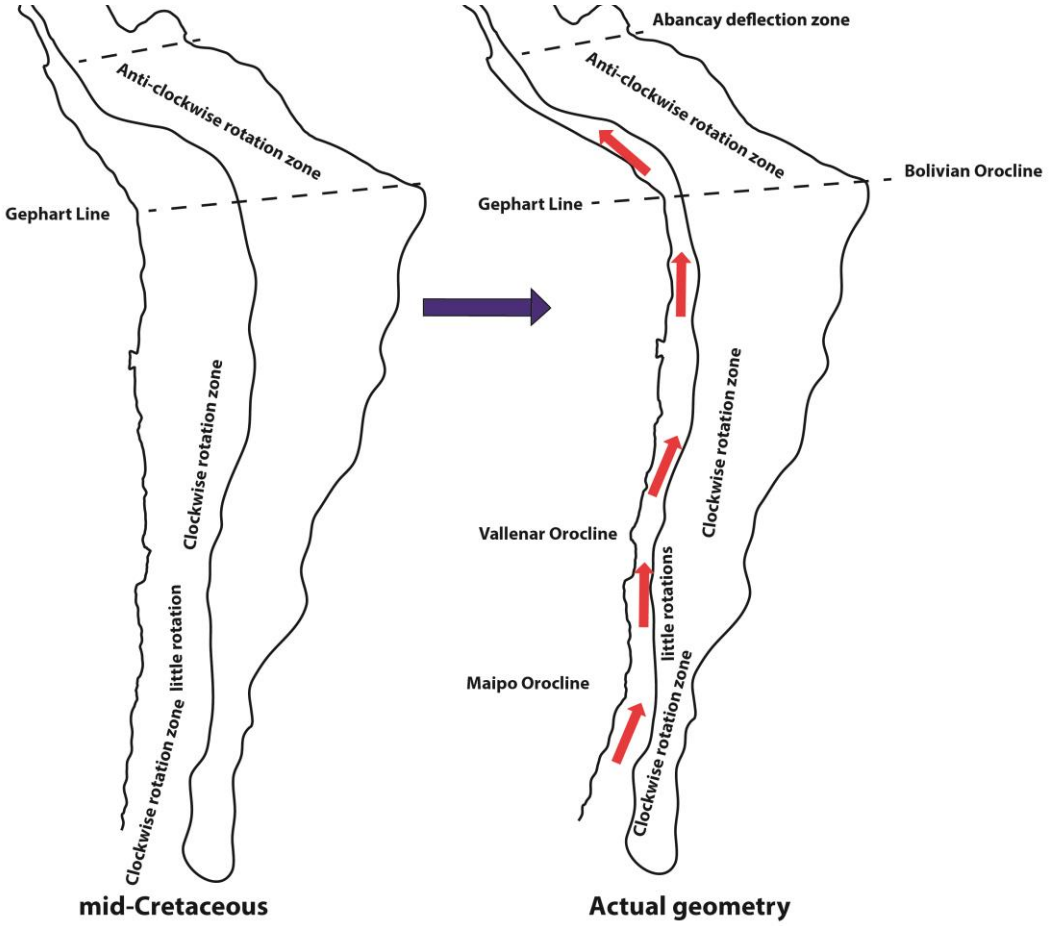

Figure 3.14: Schematic model of the rotational deformation segmentation and its consequences. The red arrows represent the different rotational domains north and south of 29°S, showing the latitudinal differences in the mean values.

3.10.- Conclusions

We have obtained paleomagnetic results for more than 500 paleomagnetic drillcores along the Pampean flat-slab region between 28°S and 31°S. Sixtyseven sites showed good magnetization, where magnetization in volcanic and intrusive rocks was mainly primary and acquired upon cooling. Tilt correction decreases the dispersion of the site mean directions at five localities, while post-tectonic magnetizations were observed at six localities, and four more localities with primary magnetization in intrusives. We interpret the remagnetization in the Central Depression, Precordillera and Frontal Cordillera as a result of local heating and hot fluid flow during Late Cretaceous-Paleogene magmatic arc activity.

Northern Chile, between 25º-29º, presents an average clockwise tectonic rotation around 30º, and the same section in the Puna-Sierras Pamepanas domain rotatedly around 18°. Our new data provide evidence that rotations ocurred since the Late Cretaceous, and continued during the Eocene-Oligocene until the Miocene (Arriagada et al., 2006a). Deformation of the Precordillera and clockwise block rotations in the forearc of northern Chile have been described as simultaneous with the forearc of southern Peru (Roperch et al., 2006). However, our new data, together with the structural data along the Precordillera, indicates that the K-T orogeny played a key factor in both the shortening (Cornejo et al., 2003; Maksaev et al., 2009; Martínez et al., 2013) and rotational events, showing that the formation of the Bolivian Orocline is older than previously though, and that K-T tectonics could have represented the initiation of the bending of the South American western margin. These results agree with previous data (Prezi and Alonso, 2002; Somoza et al., 2012), which suggests that an older rotational event, the K-T event, was the precursor of the main Eocene-Oligocene compressional event.

An orogen-scale mechanism, related to the construction of the Bolivian Orocline and combined with local tectonics, produced the rotation of tectonic blocks within the thermally weakened crust, due to the magmatic arcs from the Late Cretaceous to the Oligocene. This deformation style corresponds to a “hinge” mechanism around 29°S, responsible for the dramatic rotational differences in the Andean Forearc and the less obvious, but proportionally equal, rotational differences in the Southern Puna-Sierras Pampeanas. Deformation and block rotations within the forearc are not simply the consequence of shear-strain controlled by strike-slip faults, as there is no evidence for a difference in rotation induced by major strike-slip faults. These rotational pattern limits are strongly correlated with the changes in rheology and older structural limits, such as the suture zones of accreted terranes, and thus reaffirming the importance of structural inheritance in the process of tectonic rotations.

Acknowledgments

Matias Peña gratefully acknowledges a scholarship granted by the Chilean National Science Cooperation (CONICYT grant 21130668). Discussion with Marcelo Farías

and Fernando Poblete were fundamental. We would also like to thank Sergio Villagran and Marco Vaccaris for their field support.

4: Tectonic rotations in the northermost Chile: A continuous view of the Bolivian Orocline Forearc.

El patrón de rotaciones alrededor del eje Axial del Oroclino Boliviano ha sido uno de los mayores temas de estudio durante los últimos 40 años. Con el fin de comprender este patrón entre los 18-23°S en el ante-arco de Chile, así como relacionarlo con los distintos procesos compresivos en la región, se realizo un estudio paleomagnético entre estas latitudes. Este capítulo corresponde a un artículo sometido a la revista *Journal of American Earth Science,* cuyo manuscrito se presenta a continuación.

Tectonic rotations in the northermost Chile: A continuous view of the Bolivian Orocline Forearc.[1]

Peña, M[1,2], Martínez, F.[3], Arriagada, C[4]., Gomez, C[5].

(1) Departamento de Geología, Universidad de Chile, Casilla 13518, Correo 21, Santiago, Chile.

(2) Escuela de Geología, Universidad Mayor.

(3) Departamento de Ciencias Geológicas, Universidad Catolica del Norte, Angamos 0610, Antofagasta, Chile.

(4) Independant structural geology and andean tectonics consultat.

(5) Yastay consulting, Los Carrera 599, Oficina 14, Cuarto Piso, Copiapo, Chile.

ABSTRACT. We report paleomagnetic results for nearly 300 oriented samples, distributed in 44 sites, from the northern Atacama Desert to the Bolivian Orocline axis, between 18-23°S. Remanent magnetization in volcanic and intrusive rocks is mostly primary, while a secondary magnetization is observed in few sedimentary rocks. Comparison of locality-mean directions with expected paleomagnetic directions indicates a counterclockwise rotational pattern of 0.2 ± 13.9° between 18.5° and 22.5° S. The tectonic rotations in the Andean Forearc are linked to the Bolivian Orocline construction timing, with an emphasis of compressive deformation over strike-slip deformation in the Coastal Cordillera and the Domeyko Range. There is a strong change in the magnitude of the clockwise rotations associated with the Antofagasta-Calama Lineament, a structure that appears to play a key factor parating rotational blocks. The results point that the Atacama Fault System held more a compressional nature than a strike-slip nature, with no important difference in magnitude between the rotations in Coastal and Domeyko ranges. The longitudinal and latitudinal segmentation of the tectonic rotational pattern is in close

[1] Manuscrito en preparación para ser enviado a Journal of South American Earth Sciences

agreement with the longitudinal segmentation of the deformation events along the Andean chain, and can be related to latitudinal changes of pre-Cenozoic features in the Andean evolution.

4.1- Introduction

The present-day Andean margin of the Central Andes in northern Chile and Argentina, is characterized by two main features: a) the high topographic elevations of the Altiplano Plateau and b) the continental-scale Bolivian Orocline (Figure 4.1). The understanding of the Bolivian Orocline formation and the tectonic uplift of the Altiplano-Puna plateau has been studied during the last four decades through a combination of different approaches, such as, determination of tectonic rotation patterns, estimation of shortening rates, determination of timing of deformation, and exhumation processes, among others (Heki et al., 1983, 1985; Kley et al., 1999; McQuarrie et al., 2002; Heidbach et al., 2008). The Bolivian Orocline is understood as a continental-scale bending created from along-strike variations in the horizontal shortening of the Andean margin, thus producing an efficient mechanism to explain block rotations of the forearc region (McQuarrie, 2002; Hindle et al., 2005; Gotberg et al., 2010; Richards et al., 2004; Isacks, 1988; Arriagada et al., 2008). Block rotations in the continental margin are interpreted to be controlled by a series of kilometric-scale faults that allowed relief exhumation and latitudinal mass transfers through them (Glodny et al., 2006; Kukowski & Oncken ; 2006; Gerbault & Herailt, 2006; Eicherlberger et al., 2015) In this aproach, the paleomagnetic tool has been fundamental for the study of oroclines, evidencing timing and intensity of the deformation (Isacks, 1988;. MacFadden et al, 1995; Randall et al, 1996; Somoza et al., 1996; 1998; Abels and Bischoff, 1999; Arriagada et al, 2000, 2003, 2006, 2008,. Roperch et al., 2006; 2011, Taylor et al., 1998, 2005).

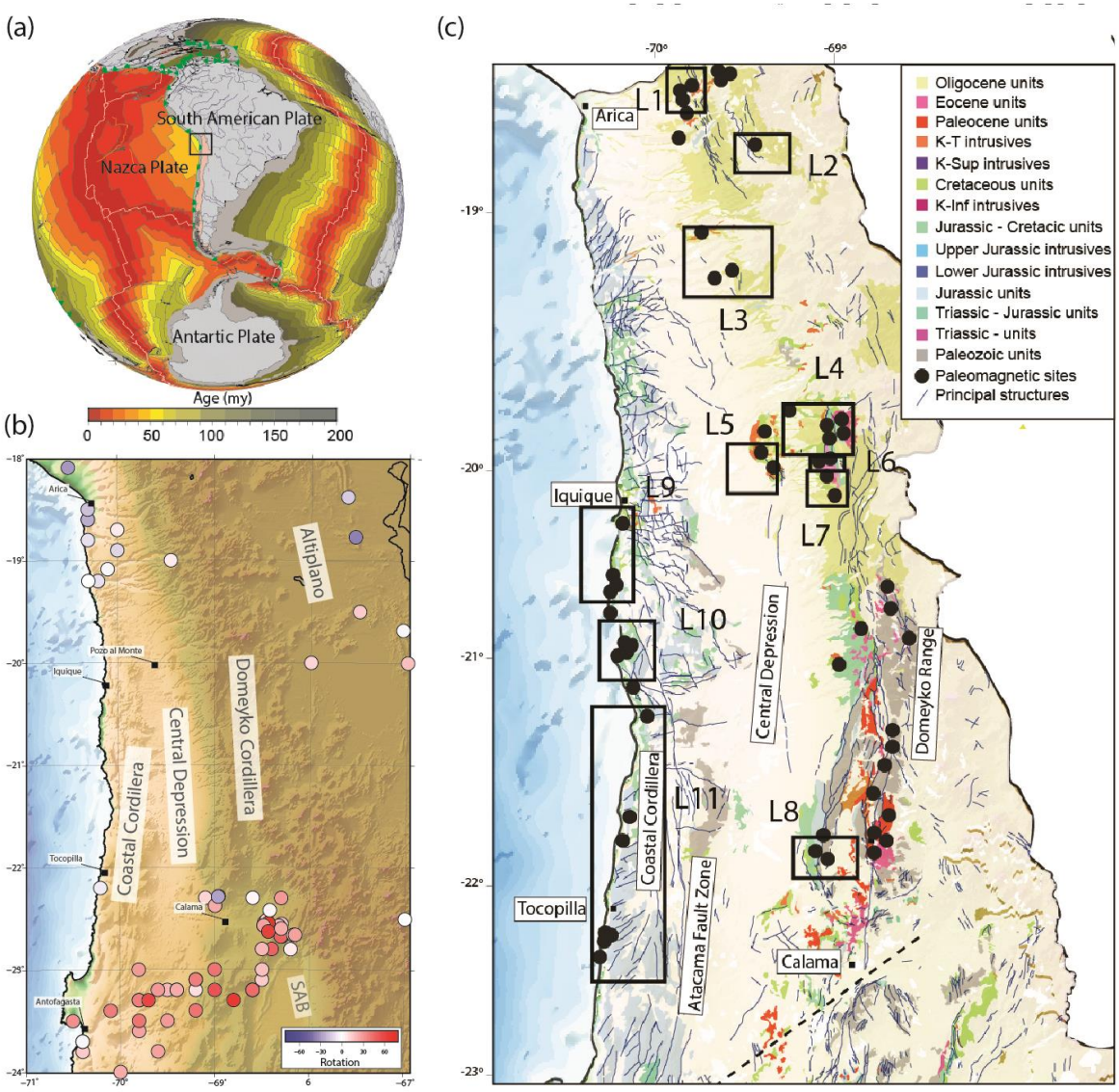

Figure 4.1: (a) Digital map of the ocean floor age (Muller et al., 2008) and principal tectonic plates in central-south South America. The black box represents the studied area. (b) Rotational data in the studied area from previous works (Roperch et al 2006; Arriagada et al., 2006; Prezzi et al., 2014). (c) Simplified geological map of Central Andes between 18°-23° South Latitude. The black circles represent the paleomagnetic sites, the black rectangles paleomagnetic localities and the segmented line the Antofagasta-Calama Lineament (ACL).

Previous paleomagnetic studies (Figure 4.1) showed that the bending of the Central Andes induced clockwise block rotations along the Chilean Andes (Arriagada et al., 2006, 2008; Taylor et al., 2005; Somoza et al., 2012; Narea et al., 2015) and countercolckwise rotations in the southern Peruvian Andes (Roperch et al., 2006; 2011). This rotational deformation has correlated with Cenozoic shortening

episodes, especially with an Eocene contractional pulse (Arriagada et al., 2008; Eichelberger et al., 2015), however; there is not a general consensus that the creation of the Bolivian Orocline resulted from a generalized Cenozoic contractional tectonic event, and therefore this is still matter of debate.

One of the principal problems related to rotational deformation along the Bolivian Orocline is the relationship between the latitudinal changes in tectonic shortening along the Andes and the amount and sense of expected rotations in both of its limbs. The expected rotations due to proposed jigsaw models (Arriagada et al., 2008) gives clockwise rotations around 20°, based in a palinpastic reconsctruction based on shortening data around 18°-22°S and a few paleomagnetic localities avaible (Victor et al., 2006; Roperch et al., 2006; Arriagada et al., 2006; 2008), being the understanding of the Andean range close to the Bolivian Orocline axis of extremely importance to the comprehension of the relationship between tectonic rotations and shortening. In order to understand this relationship, its necessary to fill this continuity data in the CARP database. Allowing us to understand how a series of different geological factors influence the different deformation styles in the region (Heki et al., 1985; Isacks et al., 1988; Gotberg et al., 2010; O'Driscoll et al., 2012; Eichelberger et al., 2015; Martinez et al., 2017)

In this contribution, we present the results of a regional scale paleomagnetic study, with more than 200 samples collected from the Coastal and Domeyko ranges between 18° S to 23° S along the western slope of the Central Andes in northern Chile (Figure 4.1), in order to understand the rotational pattern in the Andean forearc, and thus give us new ideas about the mechanism responsible for the creation of the Bolivian Orocline. We also examined the possible relationship between the growth of the Bolivian Orocline with others internal and external geological features present in the region, such as the presence of continental-scale structural lineaments, (Arriagada et al., 2003; Palacios et al., 2007) and heterogeneities in the Nazca Plate (Metois et al., 2016; Sailard et al., 2017).

4.2- Geological and tectonic setting between 18º and 23ºS

The study area involves two of the most notable tectonic provinces of the Chilean Cental Andes: The Coastal Range and the Domeyko Range (Figure 4.1). Surrounding the Domeyko Range, Proterozoic to lower Paleozoic (possibly pre-Silurian) metamorphic rocks are exposed along structural and topographic highs. They consist of mica-schists of the Choja Formation (Charrier et al., 2007), which are considered to be part of the Arequipa–Antofalla terrane (Ramos et al., 2010).

Upper Carboniferous to Triassic granitic plutons lies intruding into the metamorphic units along the Domeyko Range and these are assigned to the Collahuasi Formation and Cerro Jaspe intrusive Complex (Tomlinson et al., 1995) (Maksaev et a., 2014; Deckart et al., 2014). Both, Proterozoic to lower Mesozoic rocks have been interpreted as the basement rocks of the Andean forearc (Kato, 1985; Munizaga et al., 2008; Maksaev et al., 2014). These are frequently overlain by Triassic and Jurassic volcanic and sedimentary, mainly marine, successions with variable thicknesses and defined as La Ternera and El Profeta formations. They are interpreted as syn-rift deposits accumulated along basement-involved half-graben structures that resulted from the crustal extension episodes during Mesozoic times (Charrier, 1979; Suárez & Bell; 1992; Ardill et al, 1988; Amilibia et al., 2008; Espinoza et al., 2019)

Along the Coastal Cordillera Jurassic to lower Cretaceous Intrusive bodies and andesitic-basaltic lavas intrude and lie over Triassic successions respectivly. Both, have been interpreted as syn-extensional magmatic products also associated with Mesozoic crustal extensional episodes and volcanic-arc (Coira et al., 1982; Mpodozis and Ramos, 1989; Ardill et al., 1998; Charrier et al., 2007).

Many of Mesozoic extensional systems erlier in the Coastal and Domeyko Range were subsequently reactivated and tectonically inverted (Victor et al., 2004; Eltger et al., 2005; Charrier et al., 2007; Barnes and Ehlers, 2009) from middle Cretaceous to late Palaeocene (100 Ma–50 Ma). During this time spam the tectonic evolution of the Andean margin was marked by the eastward migration of the Mesozoic volcanic-

arc previously established in the Coastal Range, thus causing the tectonic inversion of the Mesozoic extensional systems. Upper Cretaceous and Paleocene synorogenic volcanic and sedimentary deposits usually cover the inverted Mesozoic syn-rift successions, thus indicating that the basin inversion occurred at least during two short pulses, one in the early-middle Cretaceous (Mpodozis et al., 2005; Amilibia et al., 2008; Bascuñán et al., 2015), and the other one close to the Cretaceous–Palaeocene boundary (Mpodozis et al., 2005; Arriagada et al., 2006; Charrier et al., 2007; Amilibia et al., 2008).

The basin inversion, corresponding to the so-called “Incaic phase” (Noble et al., 1979; Coira et al., 1982; Mégard, 1984; Charrier et al., 2007), was followed by major Eocene E-W shortening, crustal thickening and exhumation of kilometric portions of Paleozoic basement rocks. The “Incaic” shortening appears associated with subsidiary arc-parallel strike–slip deformation along the Domeyko Range and along the southern Peruvian forearc, related to the tectonic rotations in both limbs of the Bolivian Orocline (Roperch et al., 2006; 2011; Arriagada et al., 2008). Further, this deformation episode in northern Chile is characterized by exhumation of at least 4–5 km between 50 Ma and 30 Ma, as documented by apatite fission track thermochronology in those Palaeozoic crystalline basement rocks exposed in the Domeyko Range (Maksaev and Zentilli, 1999; Carrapa & DeCelles, 2008; Maksaev et al., 2009).

The Upper Paleogene-Neogene stratigraphy in the region is mostly exposed along intermontane basins located between topographic highs (Figure 4.1), being the Salar de Atacama Basin the most important of them. These deposits consist of continental volcanic and sedimentary successions, which report U-Pb ages that range between ~45-25 Ma with variable thicknesses and that unconformably cover the Upper Mesozoic and Paleocene deposits (Mpodozis et al., 2005; Arrigada et al., 2006). Important granitic emplaced in theres rocks also have been identified. The Oligocene rocks are mostly composed of folded assymetrical stratigraphic wedges of intercalated volcanoclastic and coarse, and fine, sedimentary deposits that cover older deformed Mesozoic and Lower Paleogene successions. These have been

interpreted as synorogenic deposits accumulated into contractional basins developed basement blocks (Martinez et al., 2017; 2018). The Miocene to Pliocene stratigraphic record is mainly characterized by volcanic rocks and some intercalated sedimentary deposits. Lavas related to two major volcanic clusters: the Altiplano-Puna Volcanic Complex (APVC) and the Aucanquilcha Volcanic Cluster (AVC) (Grunder et al., 2008; de Silva et al., 1989). The first one corresponds to the largest ignimbrite eruptions recorded located east of the Salar de Atcama (Gardeweg and Ramirez, 1987), with ages ranging from 11 Ma to the present, with more than 12000 Km^3 of erupted material (Salisbury et a., 2011) and related to a anomalous thin lithespohere related to its magma body (Zandt et al., 2003; Prezzi et al., 2009). The second one corresponds to a huge cluster of 700 Km^2 located around 21°S, with ages that ranged, also, from 11 Ma to present (Grunder et al., 2008).

4.3- Paleomagnetism

4.3.1- Sampling and paleomagnetic techniques

The paleomagnetic sampling was conducted in several field campaigns during which more than 300 oriented samples were collected (Table 1). All sites were drilled using a portable gasoline-powered drill and samples were oriented using magnetic and solar compasses when possible. Nearly 50 sites presented stable magnetization compoments, resulting in near 200 samples owning a reliable magnetic behavior.

Remanent magnetization was measured with spinner magnetometers (Molspin and JR5 of AGICO) while magnetic susceptibility was measured with a Bartington susceptibilimeter at the Tectonics and Paleomagnetism Laboratory, Geology Department, Universidad de Chile, in Santiago. For some sites, with low Natural Remanent Magnetization (NRM) intensity, magnetic measurements were made with the 2G cryogenic magnetometer at the University of Rennes. For most cores, one

specimen was subjected to stepwise thermal demagnetization (10 to 15 steps) in a ASC furnace where the residual field was less than 10 nT. Magnetic susceptibility was measured after each thermal demagnetization step, to check changes in the magnetic mineralogy during heating. Gradual alternating field (AF) demagnetization using the Molspin AF instrument was also performed on some samples. Magnetization directions were determined with "least squares lines and planes" program according to Kirschvink (1980). Evidence of secondary overprint magnetization due to lightning were found in some sites in volcanic rocks. In these cases, the AF demagnetization was preferred to thermal. Statistics combining directions and planes (McFadden and McElhinny, 1988) were used to determine the mean characteristic remanent magnetization (ChRM) directions for each site.

Tectonic rotation and flattening values with respect to stable South America for the individual sites were evaluated according to Demarest (1983), using reference South American paleopoles from Torsvik *et al.* (2012). The site-mean directions for each locality and the tectonic rotations and inclination errors are given in Table 1.

4.3.2- Magnetic properties

4.3.2.1- Magnetization in volcanic rocks and intrusives

Most sites show natural remanent magnetization (NRM) intensity around 0.5 Am^{-1} and magnetic susceptibility of 0.02 SI, typical of volcanic rocks with magnetite as the main ferromagnetic mineral. Sites with lower susceptibility correspond to ignimbrites with a more oxidized state. Most sites in Cretaceous to Eocene show stable magnetizations and the principal components of magnetization going through the origin during thermal or AF demagnetization. In most cases the maximum unblocking temperature was higher than 580°C, the blocking temperature of magnetite, the main magnetic carrier in intrusive rocks (Figures 4.2 & 4.3). All fractions of the

magnetization left above 580°C show the same ChRM direction than the ChRM carried by magnetite indicating that oxidation during emplacement produced a small amount of hematite or stable maghemite (Figure 4.2). Evidence of low temperature oxidation were observed at some sites (06DN53) with a notable decline in magnetic susceptibility in the temperature range 250°-400°C, indicating inversion of titanomaghemite to hematite during heating.

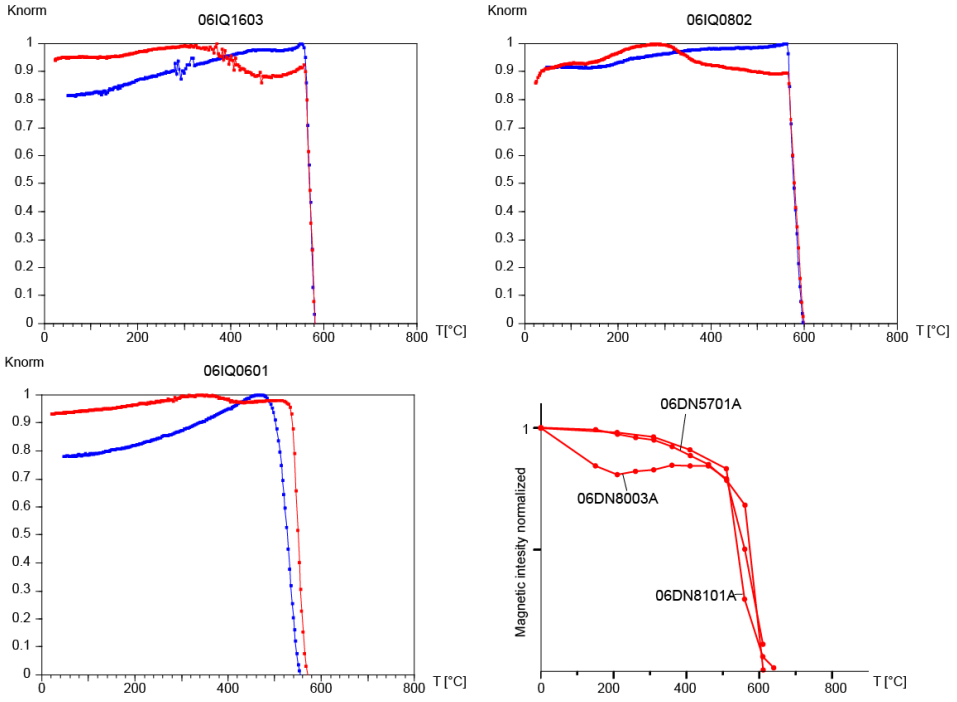

Figure 4.2 : Orthogonal projections (in situ) of thermal (temperatures in °C) or alternating field (steps in mT) demagnetization diagrams for samples from volcanic, sedimentary or intrusive rocks for each locality. The projections represent the paleomagnetic locations described in the text. The viscous overprint is removed during the first steps of demagnetization and the ChRM component is defined linearly through the origin. Solid (open) circles correspond to projection onto the horizontal (vertical) plane and blacks circles correspond to vertical plane projection.

4.3.2.2- Magnetization in Sedimentary rocks

The ChRMs identified in red beds correspond to a magnetization with unblocking temperatures almost linearly distributed in the temperature range 150–560°C up to 670°C and usually going through the origin during thermal demagnetization (Figure 4.2). The ChRMs were determined by least squares fit not anchored to the origin in the temperature interval 150–600°C.

4.3.3- Characteristic Directions

As discussed above, the CHRMs in most of our sedimentary sites is a secondary magnetization. Both polarities are observed, making a single short remagnetization event therefore discarded. The remagnetization of some samples, could be explained by the active magmatic arc, with massive intrusive such as the K-T intrusives near Calama (Somoza et al., 2012), with a thermoviscous overprint due to circulation of hot fluids. Porous sandstones with weak primary magnetization can be easily remagnetized during the emplacement of intrusives. Remagnetization may occur before, after or even during tilting of sedimentary beds. For each locality, the fold test is used to assess the origin of the ChRM.

In order to analyze spatial changes in magnetic declination and inclination, sites belonging to a homogeneous tectonic block were grouped into "localities" according to their age and structural context (Table 1). Tectonic rotations and inclination anomalies were calculated for Mesozoic- Cenozoic units, using the estimated age of magnetization and the BC02 APWP. The site-mean directions for each locality and the tectonic rotations and inclination errors are given in Table 1.

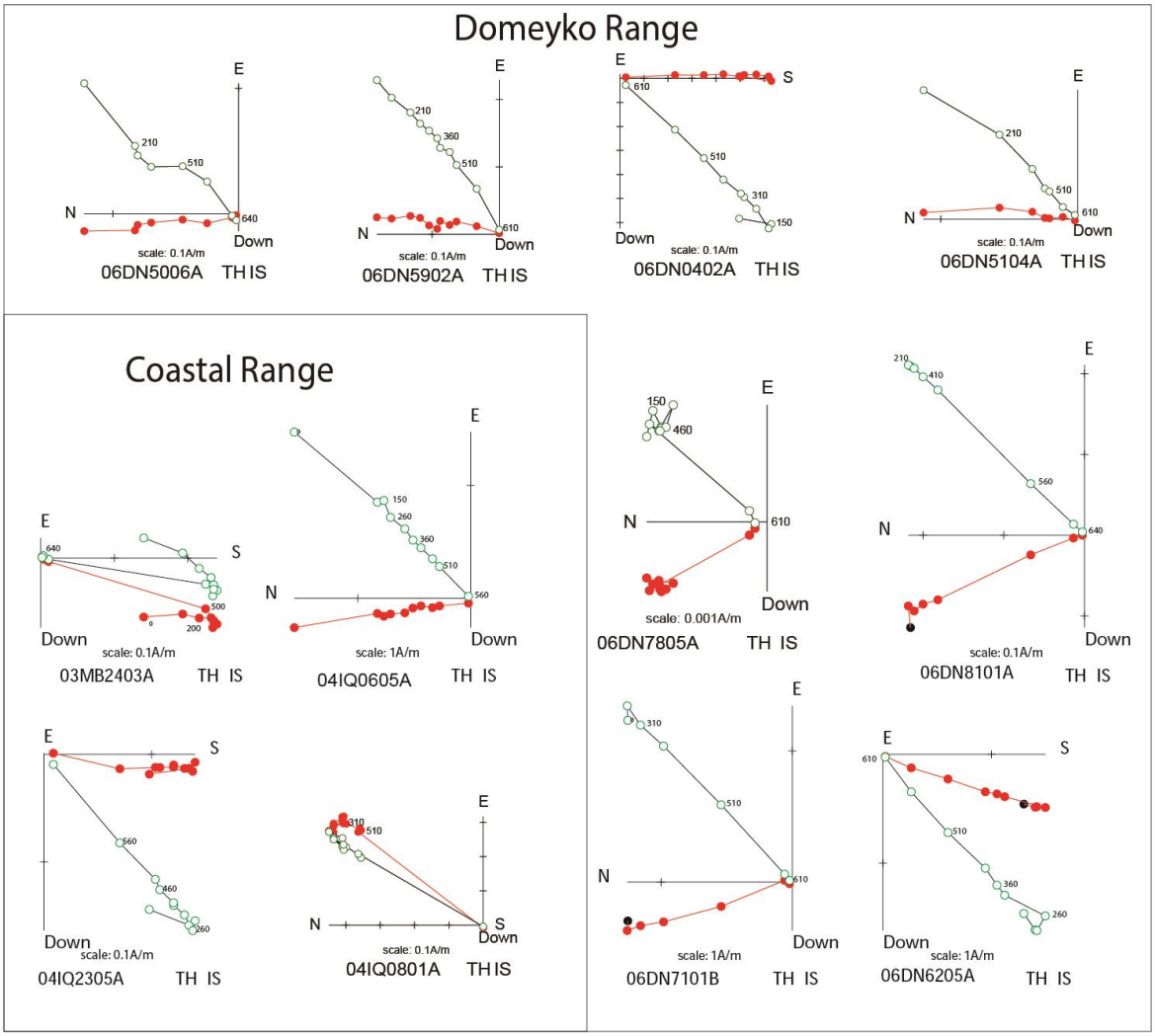

Figure 4.3: (a) Variation of magnetic susceptibility versus temperature (red heating and blue cooling), showing an important amount of magnetite carrying the magnetization, with a minor amount of hematite. (b) Variation of magnetic intensity versus temperature, the rapid fall of intensity around 650ºC shows hematite as an important magnetic carrier.

Locality 1: Lluta

3 were sites sampled near the Lluta valley (Garcia et al., 2004), in Upper Cretaceous – Paleocene sediments and granodiorites (06DN77, 06DN78 and 06DN80). Sites 06DN78 and 06DN80 have similar magnetic properties with NRM intensities in the range of 0.001 Am^{-1} ,and low magnetic susceptibility (0.0001 SI). The site 06DN77 has a stronger NRM (0.1 Am^{-1}) and susceptibility (0.01 SI). The folding test reveal a better grouping of the locality after applying it (Figure 4.4, Table 1), relating the age

of magnetization to Paleocene. Two sites had normal polarity (06DN78 and06DN80) and one has inverse polarity (06DN77). The three sites have a strong drop of magnetic intensity around 600ºC, suggesting magntite as the principal magnetic carrier, with a trace of hematite.

Locality 2: Cardones

Four sites in Paleocene intrusives (Garcia et al., 2004), two in granites (06DN81 and 06DN82) and two in granodiorites (06DN75 and 06DN76) near the Cardones creek were sampled. All four sites have moderate to strong NRM (0.01-0.1 Am^{-1}) and moderate susceptibility (0.001-0.01 SI).Three of the sites had normal polarity (06DN81, 06DN82 and 06DN75) and one has inverse polarity (06DN76). Three sites (06DN81, 06DN75 and 06DN76) have blocking temperature near 660ºC with little traces of secondary magnetic phases, while one site (06DN82) reveals a stepped drop of magnetic intensity until 580ºC, revealing magnetite and possible pirrothyne as secondary magnetic carriers.

Locality 3: Camiña

Two dacitic porphyries (06DN71 and 06DN72) were sampled and blended with three sites from Roperch et al. (2006). The polarity of both sites are normal, have a strong NRM (1-2 Am^{-1}), moderate susceptibility (0.01 SI) and their blocking temperature near 660ºC, with no visible traces of secondary mineralogy, reveals hematite as the principal magnetic carrier. The fold teast (Figure 4.4) reveal a better grouping before tilt correction, relating the magnetization age to the 15 My porhyry of 06DN71. Roperch *et al*. (2006) suggested that Paleocene-Eocene may be the appropriated magnetization age for these sites, but the large presence of miocene porphyries and dikes related to the Miocene volcanic activity in the region (Valenzuela et al., 2014), and the negative fold test points to a Miocene age of magnetization.

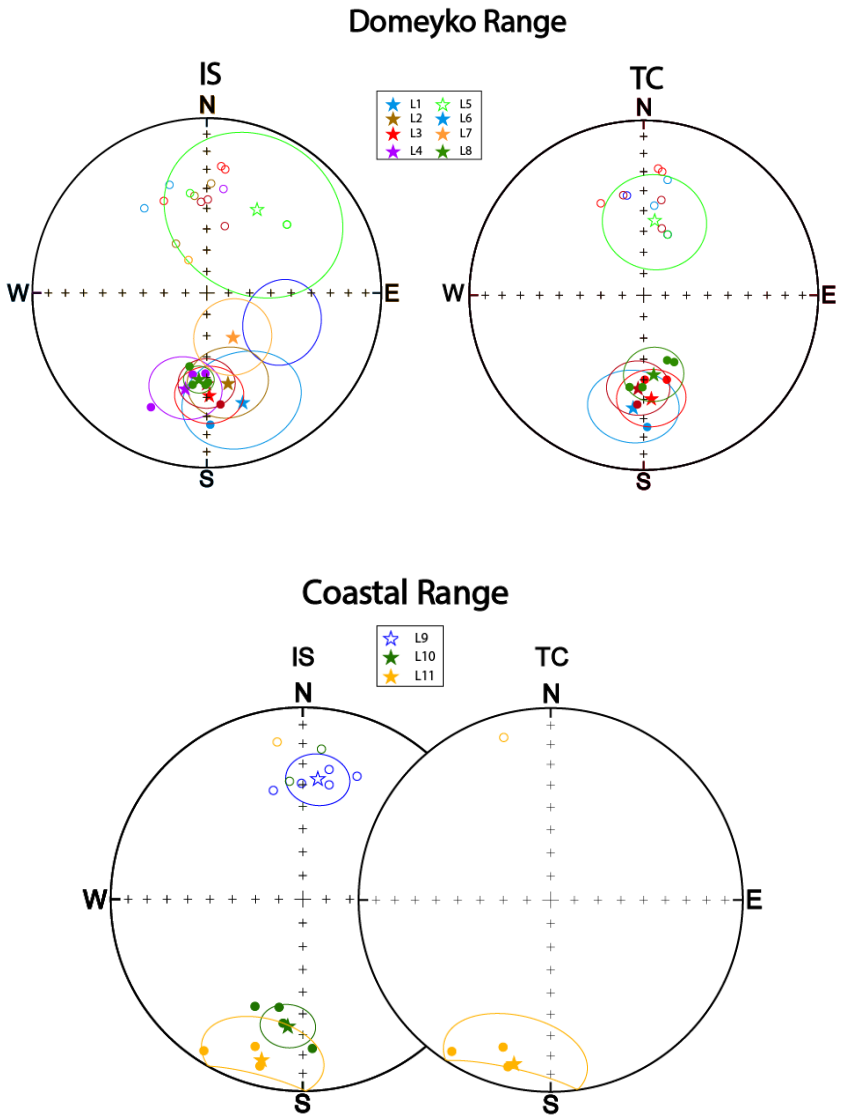

Figure 4.4: Equal-area projection of site-mean ChRM directions *in situ* and after tilt correction for Domeyko and Coastal Range localities listed in Table 1. The localities in situ (IS) are in the left stereogram and the ones after tilt correction (TC) are in the right. Open (solid) symbols correspond to projection in the upper (lower) hemisphere.

Locality 4: Chusmiza

Near the Elizabeth creek, four sites were sampled (06DN46, 06DN48, 06DN51 and 06DN53) in Eocene intrusives (Morande et al., 2015). All sites had reverse polarity, except site 06DN51 which have normal porlarity. The sites 06DN46 and 06DN48 had a blocking temperature near 600°C, revealing a mixture of magnetite and hematite as the principal magnetic carriers, and the sites 06DN51 and 06DN53 had

the same blocking temperature, but with a notable drop near 300°C, revealing the presence of secondary magnetic carriers, like maghemite and pirrothyne. The site 06DN46 have a weak NRM (0.001 Am^{-1}) and susceptibility (0.0001 SI), in contrast with the other sites that have a strong NRM (0.1 Am^{-1}) and moderately strong susceptibility (0.01 SI).

Locality 5: Lonzana

Near the town of Lonzana, in the Tarapaca Creek, one site (06DN50) was sampled in granites, from Cerro Jaspe Granodiorite (Morande et al., 2015), and other site (06DN49) was sampled in andesites from Upper Cretaceous - Paleocene age Cerro Empexa Formation. The fold test revealed a better grouping after aplying it, giving a magnetization age around the Cretaceous - Paleocene boundary. Both sites had normal polarity, a strong NRM (0.1 Am^{-1}), moderate susceptibility (0.01 SI), a blocking temperature near 600ºC that suggest a merge of hematite and magnetite as the principal magnetic mineralizaton.

Locality 6: Choja

Four sites were sampled around the Choja Creek (06DN52, 06DN57, 06DN58 and 06DN59), in sandstones from the Upper Cretaceous Cerro Empexa Formation (Morande et al., 2015) and sienogranites from the same age. The NRM of the sites 06DN59 and 06DN57 is strong (0.1-1 Am^{-1}), having a moderate susceptibility (0.01 SI). The other sites have a low NRM (0.001 Am^{-1}) and low susceptibility (0.0001 SI). The fold teast (Figura 3.4) reveal a better grouping before applying it, relating the magnetization age to the sienogranite intrusion. Three sites had normal polarity (06DN52, 06DN57 and 06DN59), while only one site (06DN58) had inverse polarity. The sites 06DN52 and 06DN58 had blocking temperature near 660ºC, showing hematite as the principal magnetic carrier, while the sites 06DN57 and 06DN59 had a blocking temperature near 600ºC, suggesting a possible blending of magnetite-hematite as the principal magnetic carriers. Only one site, the sienogranite (06DN59)

had an important drop of magnetic intensity around 300°C, revealing the possible presence of secondary magnetic phases like maghemite.

Locality 7: Pica

Near the town of Pica, three sites in monzodiorites and granodiorites (06DN63 and 06DN64) from the Paleocene plutonic complex Yabricoya (Tomlinson et al., 2015) were sampled. Both sites have a moderately strong NRM (0.01-0.1 Am^{-1}) and a moderately low susceptibility (0.01-0.0001 SI). The site 06DN63 had normal polarity while 06DN64 have inverse polarity. Both had blocking temperature near 600°C, suggesting a mixture of principal magnetic carriers, of magnetite and hematite.

Locality 8: Montecristo

One site in Paleocene andesite from Cerros of Montecristo locality was sampled and merged with 3 sites from Early Paleocene conglomerates and monzodiorite from Somoza et al. (2012). Appliying the fold test reveal a better groupping before doing it (Figure 4.4), linking the magnetization to the age of the intrusives, around 63 my, just like proposed by Somoza et al. (2012). 06DN04 had inverse polarity, strong NRM (0.1 Am^{-1}), moderately strong susceptibility (0.01 SI) and a blocking temperature near 600ºC.

Isolated sites in Domeyko Range

Three sites (06DN01, 06DN12 and 06DN22) were sampled along the domeyko range (Marinovic & Lahsen, 1984; Quezada et al., 2012; Blanco & Tomlinson, 2013) in Cerro Jaspe (06DN22), Guatacondo Creek (06DN12) and northe-east of Chuquicamata mine (06DN01). The sites were sampled in Granites and from Carboniferous (06DN22 and 06DN89), to Upper Cretaceous granites and Eocene granodiorites (06DN12 and 06DN01). The three sites have blocking temperatures above 600°C suggesting a hematite as the principal magnetic carrier. Results are presented in Table 1.

Locality 9: Chanabaya

Around the locality of Chanabaya, in the Coastal Cordillera, five sites were sampled, one site in andesites (04IQ04), and four sites in diorites (04IQ06, 04IQ08, 04IQ09 and 04IQ11) of Jurassic age (Quezada et al., 2014; Sepulveda et al., 2014) were sampled. The fold test (Figure 4.4) reveals a good grouping before applying it, relating the age of magnetization to the age of the diorite, near 155 My. 04IQ06 have strong NRM (0.1-1 Am^{-1}), being the other sites have a moderately strong NRM (0.01-0.1 Am^{-1}). Susceptibility in all sites is relatively similar, with values between 0.001-0.01 SI. All sites had normal polarity, and appears to have magnetite as the principal magnetic carrier, showing a blocking temperature near 560°C.

Locality 10: Loa

Six sites in Jurassic intrusives were sampled (Quezada et al., 2012; Medina et al., 2012). Three sites in diorites (04IQ16, 06IQ21 and 06IQ23), two in monzodiorites (04MB17 and 04MB18) and one in gabros (04IQ14). One site (04IQ14) had normal polarity, two sites had reverse polarity (04IQ16 and 04IQ23) and three sites (04MB17, 04MB18 and 04IQ21) had both polarities. Magnetite shows as principal magnetic carrier with blocking temperatures near 560°C in four sites (04IQ14, 04IQ16, 04IQ21 and 04IQ23) and hematite appears in two sites (04MB17 and 04MB18) with blocking temperatures near 660°C. All sites have relatively strong NRM (0.01-0.1 Am^{-1}) and moderate susceptibility (0.01 SI).

Locality 11: Gatico

Two sites in monzodiorites (04MB24 and 04MB25), one in diorites (04MB20) and one in andesites (04MB19), all of Jurassic age (Oliveros et a., 2006; Medina et al., 2012) were sampled. All sites have strong NRM (0.1 Am^{-1}) and moderately strong susceptibility (0.1-0.01 SI). The fold test revealed a better grouping after applying it, taking the age of the Cerro Carrasco intrusive complex (ca. 155 my) as the age of magnetization (Figure 4.4). All sites showed inverse polarity and blocking temperature near 580°C, relating magnetite as the principal magnetic carrier.

Isolated sites in Coastal Range

Two sites in Jurassic diorites, from the Barriles intrusive unit (04MB21 and 04MB27), near the town of Gatico and Hornitos, and one site in Andesites from Caleta Ligate Formation, near the locality of Chanabaya, were drilled (Oliveros et al., 2006; Sepulveda et al., 2009; Medina et al., 2012; Vasquez et al., 2015;). The three sites show high magnetic inclinations, suggesting the near precensse of faults that tilted its tectonic blocks (Table 1), and not blend well with sites of the same age because of this.

4.4.- Discusion

4.4.1.-Tectonic rotations in the southern limb of Bolivian Orocline.

Tectonic rotations and inclination anomalies have been calculated for Paleozoic to Cenozoic units, using an estimated age of magnetization and reference poles from Thorsvick et al. (2012). The average direction for each sampled locality, tectonic rotations and tilt errors are found in Table 1.

Assuming that the sites of similar age belong to the same tectonic block, for which we can calculate a tectonic rotation, we note that there is a marked difference in the magnetic declinations south of 22.8°S and north of 18.32°S, as well as a similar pattern in the Domeyko Range and Coastal Range between these latitudes (Figure 4.5). Between 22.5°S and 29°S (Arriagada et al., 2006b; Taylor et al., 2005; Somoza et al., 2012; Narea et al., 2015) there is an average of clockwise tectonic rotations in

the Andean forearc of about 29.1 ± 13.8°, with a low inclination error, near 0.1 ± 11° (Figure 4.5) and around 22.5°S and 18.32°S, (Roperch et al., 2006; Arriagada et al., 2006b; Goguitchaichvili et al., 2003), there is an average countercolckwise rotation of 0.2 ± 13.9°, with a low inclination error, near 2.4 ± 11.3°. The median rotation value for the area between 22.8°S and 18.32°S is 1.2° and similar to the arithmetic mean in the same area, indicating that the mean rotation is weakly affected by a large value. From north to south, the magnitude of rotation mainly coincides with the orientation of the main structures of the region related to fault bounded Paleozoic basement blocks (Figure 4.1).

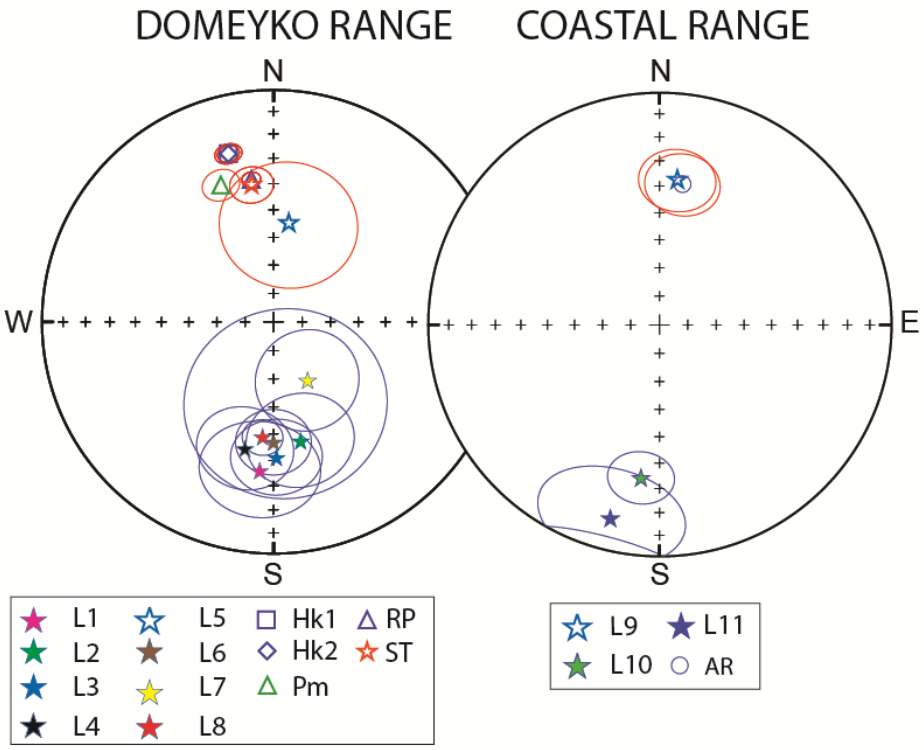

Figure 4.5: Equal area projection of site mean directions for all the localities, plus localities from other works. PM= Palmer et al. (1980); HK=Heki et al.(1985); ST=Scalan and Turner (1992); RP= Roperch et al. (2006); AR= Arriagada et al. (2006b).

The Altiplano rotational pattern, between 21°S (Figure 4.6), can be described with a change around the simetry axis of the Orocline (Gephart, 1994). The pattern changes from an average rotation around of 21.7 ± 12.1° of clockwise rotation between 21°S, and 22.5°S, and with an average of 6.6 ± 11.9° clockwise rotations

between 18.4° and 21°S (Arriagada et al., 2008; Maffione et al., 2011; Prezzi et al., 2012; Japas et al., 2014; 2016). This rotational pattern totally differs from the pattern in the Forearc, where the change is negligible around 21°S. These data show the longitudinal variations in tectonic rotations, being the greatest rotation in the Altiplano-Subandean range a marker of the migration of compressional deformation, from the little rotational pattern in the Forearc, affected by Late Mesozoic – Early Cenozoic shortening deformation, to the Miocene-Oligocene deformation that generated the Altiplano – Subandean range.

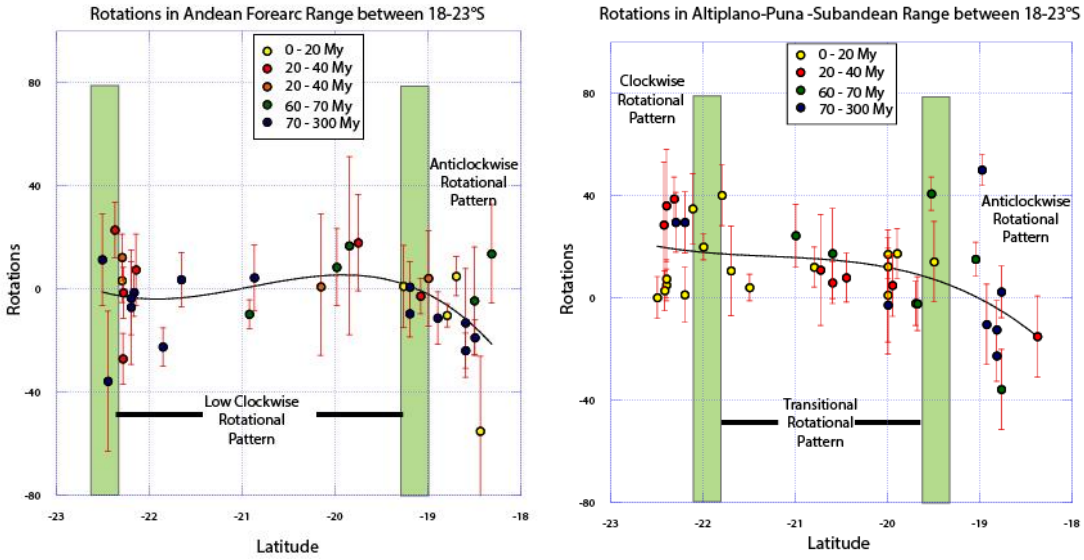

Figure 4.6: Variation of tectonic rotations versus latitude For the Andean forearc and for the Altiplano and Subandean Range domain, for different age groups of samples. The black smooth line shows a third-degree polynomial interpolation. The green rectangles shows the limit of the different patterns.

4.4.2.- Age of the tectonic block rotations

The northern boundary of the Atacama Desert has been shaped by a series of tectonic events, the Mesozoic extensional events, who controls the basin configurations, and the late Cretaceous-Tertiary compressional tectonic events that controlled deformation of the andean chain and the uplift of the Altiplano Plateau (Charrier et al., 2013; Eichelberger et al., 2015; Fuentes et al., 2018). Previous works (Arriagada et al., 2008; Maffione et al., 2011; Prezzi et al., 2012; Japas et al., 2014;

2016), shows that the strongest rotational deformation, between 22.5°S and 18.32°S, appears to happened around Miocene in the Altiplano domain, in agreement with the age of the Altiplano Uplift in the area (Eichenberger et al., 2015). These rotations are higher than the ones observed in Jurassic - Eocene rocks, along the Andean forearc, pointing that the “Incaic” event that is responsible for the great clockwise rotations south of 22.5°S and north of 18.32°S (Heki et al., 1984; Roperch et al., 2006; Arriagada et al., 2006b; Taylor et al., 2007; Somoza et al., 2012), is absent here on its common expression of larger tectonic rotations. This low rotational block, it is affected by the highest shortening rates in the Bolivian Orocline (Figure 4.7), suggesting that the deformation responsable of this shortening produced mainly compressional strain in this region. The Andean-building events in this latitude can relate to the compressional events of the Early Upper Cretaceous (Bascuñan et al 2015), and following the K-T and Eocene-Oligocene compressional deformation in the area (Garcia et al., 2005; Arriagada et al., 2006; Narea et al., 2015, Herrera et al., 2017).

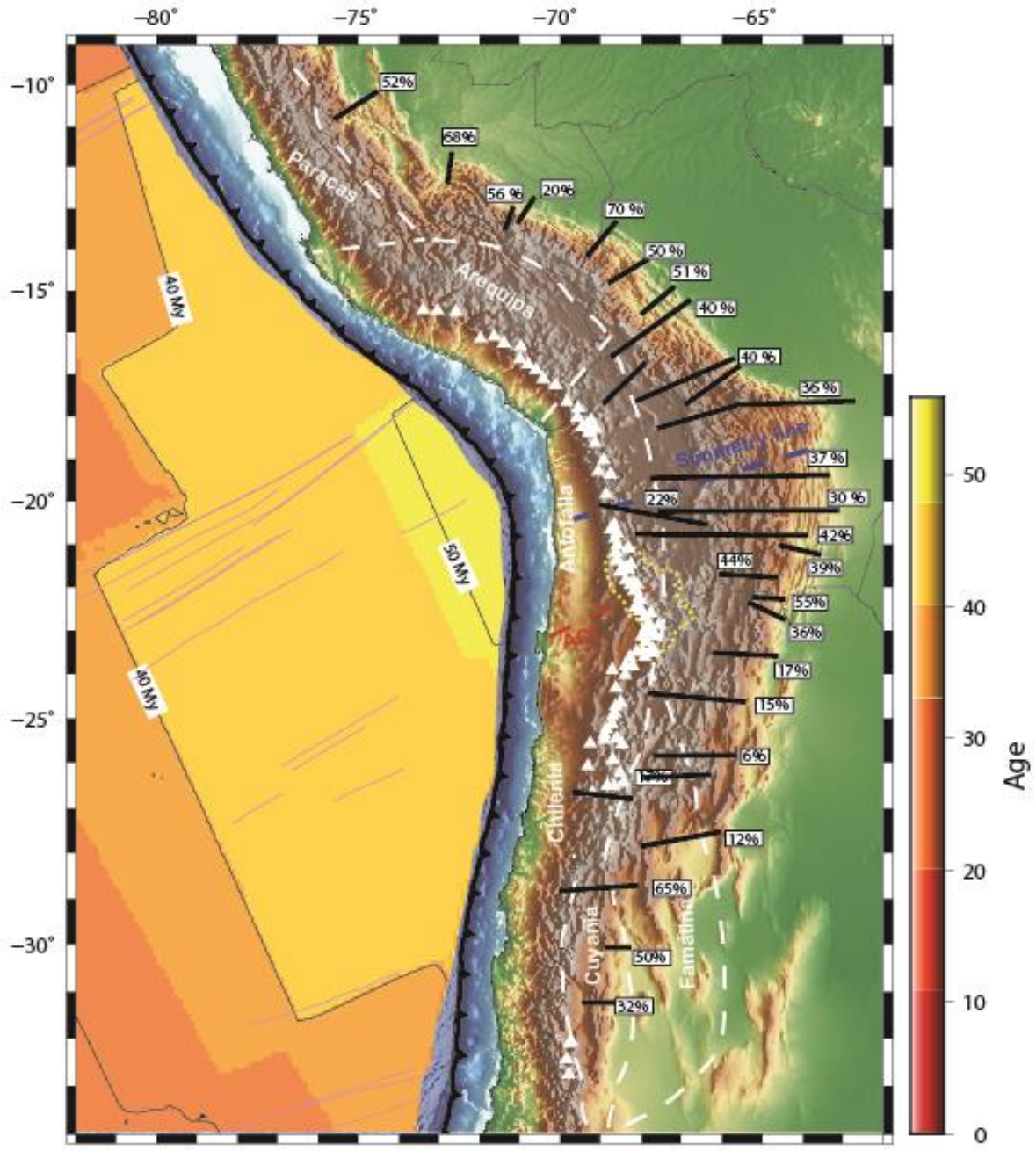

Figure 4.7: Compilation of balanced cross-sections in the Central Andes (Arriagada et al., 2008; Eichelberger 2015; McGroder et al., 2015; Martinez et al., 2016), and its shortening associated.

4.4.3.- Rotations around the Atacama Fault System

The Atacama Fault System (AFS) is one of the largest fault system in northern Chile, and usually showed as an example of strike-slip tectonics that resulted from variations of the obliquity between the subducted and the upper plate since the mid-

Mesozoic (Cembrano et al., 2005; Scheuber and Gonzalez, 1999). Much of the studies of the SFA have been realized south of Antofagasta, around the Coloso Fault System (Scheuber and Gonzalez, 1999; Cembrano et al., 2005; Jensen et al., 2011; Mitchell & Faulkner, 2009; Veloso et al., 2015) predicting notable clockwise rotations for the tectonic blocks adhered to a sinestral strike-slip fault zone. Analyzing paleomagnetic data from our localities and previous works (Arriagada et al., 2003; Goguitchaichvili et al., 2003), between 22.5°S and 18.32°S, there is an average mean of countercolckwise tectonic rotations of 5.2 ± 10.6° in the Coastal Cordillera, meanwhile the Domeyko Cordillera has an average of 1.7° ± 15 clockwise rotation (Figure 4.8). Expanding this analysis to the south, between 23-27°S, the Coastal Cordillera cumulated an average of 29.8 ± 13.2 of clockwise tectonic rotations, and the Domeyko Cordillera has an average of 26.4 ± 13.5 of clockwise tectonic rotations (Figure 4.8).These similarities between the Coastal Cordillera and the Domeyko Range-Precordillera at different latitudes shows that the strike-slip behavior of the Atacama Fault System is minimal, is increased in zones where its strike changes, partitioning the deformation (Cembrano et al., 2005; Veloso et al., 2011), sometimes reciving help of NW faults with a notorious strike-slip mechanism (Veloso et al., 2011; Contreras, 2018). We suggest that, the strike-slip movements recorded in Caleta Coloso (Cembrano et al., 2005; Veloso et al., 2015) are product of an anisotropy in the geometry of the fault system, mostly linked to the extensional process in early-mid Mesozoic (Oliveros et al., 2006) and strongly linked to compressional movements in the Upper Cretaceous (Bascuñan et al., 2015), where the strain partitioning changes from a compressive zone, where the AFS has a N-S strike, to a transpresive zone, where the AFS changes its strike. These way of understanding the AFS, underline a positive tectonic inverted nature as its principal characteristic, but with a transpressional character in some localized regions.

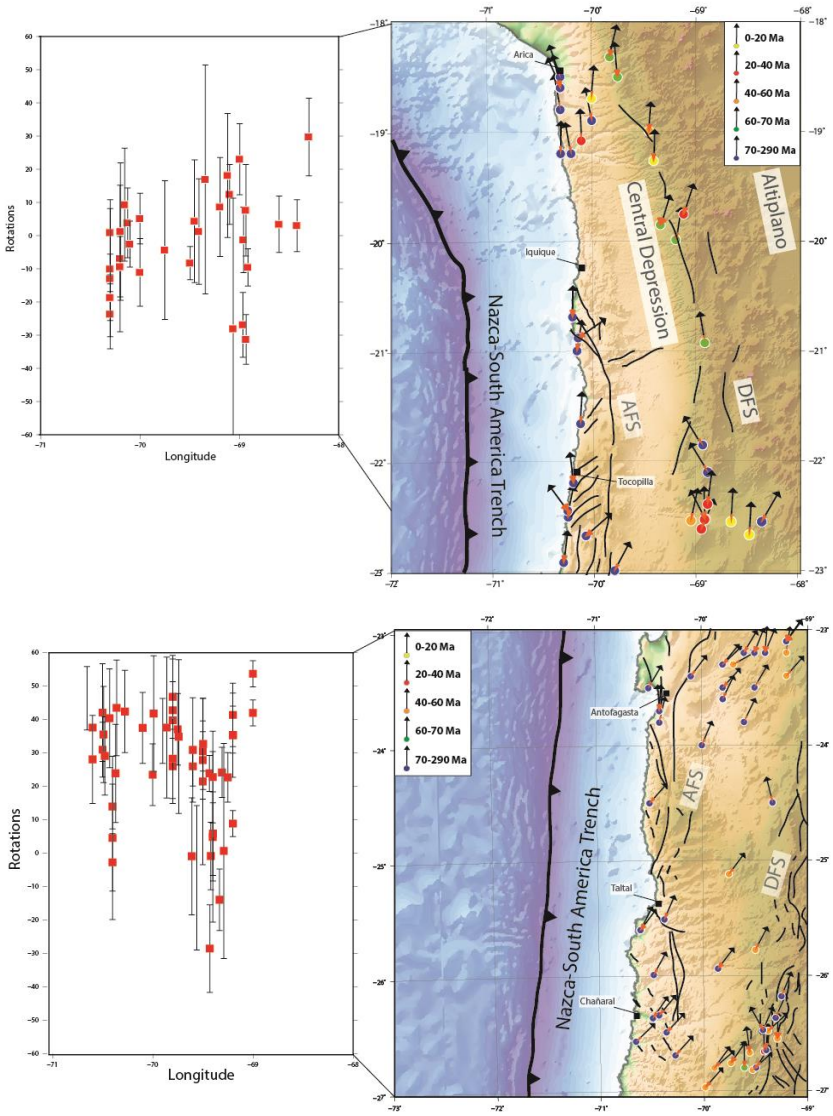

Figure 4.8: Variation of tectonic rotations versus longitude for the Andean Forearc between 18-22,5°S. and between 23-27°S. Both zones show likeness in the amount of rotations in Coastal and Domeyko ranges.

4.4.4 The segmentation of the CARP.

The understanding of the variation of the rotational tectonic pattern in the Andean Forearc has evolved from a clockwise rotational pattern around 10-15°, of Neogene age, around the Bolivian Orocline (Isacks,1988) to a pattern from around 30° of countercolckwise rotation in the forearc in the north of the Arica bending (Roperch

et al 2006; 2011) and around 30° of clockwise to the southern (Arriagada et al., 2006; Taylor et al., 2007; Somoza et al., 2012; Narea et al., 2015). The Eocene - Oligocene rotations in Peru (Roperch et al., 2006) and north of Chile (Arriagada et al., 2006a), related to the “Incaic” event, have been proposed simultaneous for both sides of Arica elbow, beginning the process as earlier in the so-called K-T or late Cretaceous-Paleocene tectonic phase (Cornejo et al., 2003; Somoza et al., 2012). The age of rotation for the forearc region, between 22.5°S and 18.32°S, is contemporaneous with a Late Eocene-Oligocene compressional deformation (Victor et al., 2004; Herrera et al., 2017) and with the tectonic rotations around the Antofagasta-Calama Lineament (Arriagada et al., 2003; Somoza et al., 2012; Narea et al., 2015). The area surrounding this lineament appears to act as a tectonic limit between two very different regional rotational beahaviors in the Andean forearc. To the north of it, the rotations are little, and south of it the rotations increasy dramatically. Moreover, the strike of the same structural lineament goes through the emplacement zone of the APVC (Salisbury et al., 2011; Lynner et al., 2016), can act as a czone of weakness between the crustal thicker Altiplano to the Puna plateau (Allmendinger et al., 1997); and also appears to be strongly related to the emplacement of large ore-bodies along the lineament strike (Palacios et al., 2007). Added to these, there is a increase in the magnitude of the tectonic rotations around the lineament (Figure 4.9). The strongest clockwise tectonic rotations related to this lineament ca be traced to the Upper Cretaceous (Arriagada et al., 2000; Narea et al., 2015), like the begginig of the compressional phase at the same latitude (Bascuñan et al., 2015), this gives the Antofagasta-Calama lineament a crucial role in the behavior and origin of the CARP. The distinc role as a tectonic limit, the high concentration of tectonic rotations of great magnitude and the special correlationship with various ore bodies suggest that this lineament is an inherited feature, possible correlated to Paleozoic acretted terrain limits (Ramos et al., 2010), or a tectonic limit of the Triassic basins in western South America (Espinoza et al, 2019), reactivated in the beginning of the compressional phase of the Andean Range.

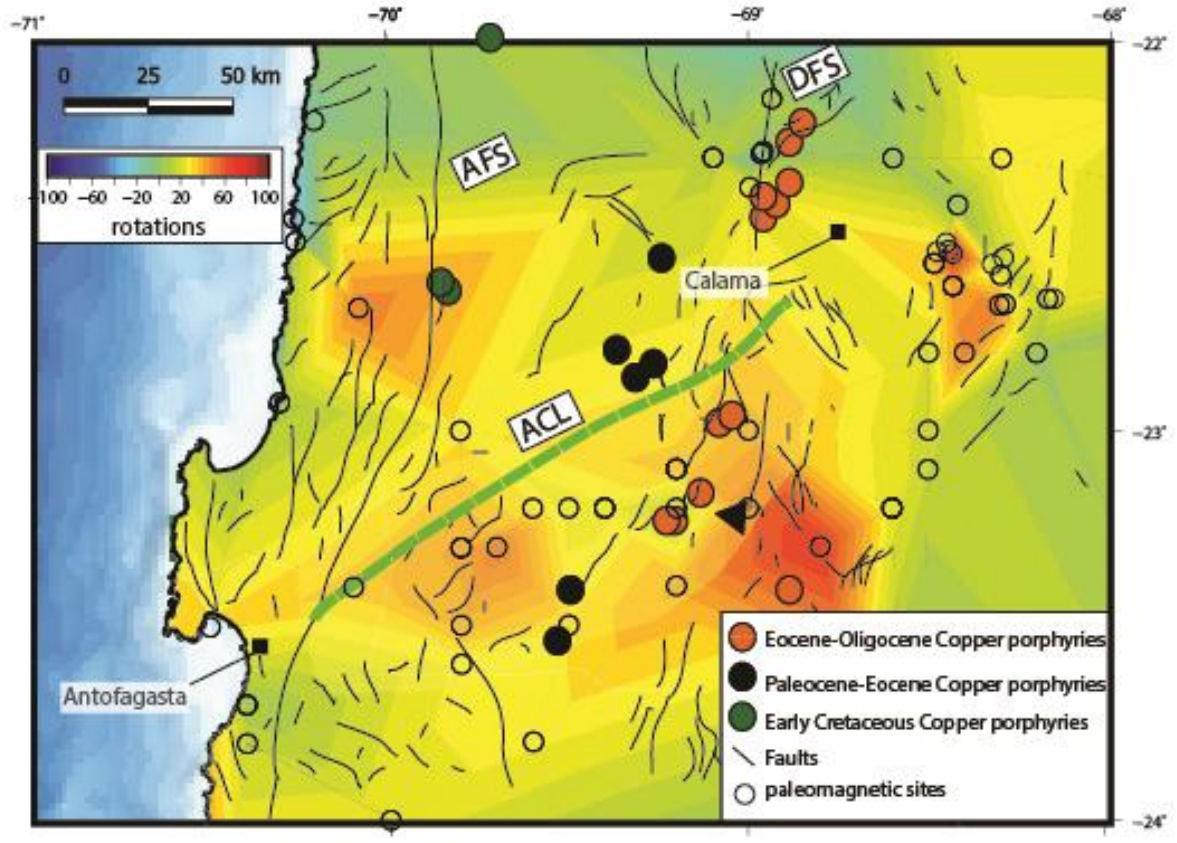

Figure 4.9: Tectonic rotations around the Antofagasta-Calama Lineament. The different colors are made by a triangulation in the software GMT, based in the paleomagnetic data represented in the small circles. The big circles are the copper porphyries, separated by age due to distinc colors.

Adding the above, we can separete 2 significants latitudinal changes in the rotational pattern of the Andean Forearc around its central region (Figure 4.10): the change around southern Peru and the Bolivian Orocline itself (Roperch et al., 2006; 2011); and in the ACL, around the 29°S (Arriagada et al., 2009; Salazar E., 2012). The shortening related to the Bolivian Orocline, can be linked to a large mechanical coupling along the subduction zone linked to Eocene-Oligocene flat-slab subduction process (Mamani et al., 2010; O'Driscoll et al., 2012). This coupled subduction mechanics could have helped to produce a major shortening and uplifting of the upper crust of the continental margin and little rotational deformation in the section between 22.5°S and 18.32°S, rotating the tectonic blocks to the north and south of it, with the help of some mayor structural lineaments, like the ACL, to divide the rotational patterns (Figure 4.11). This little rotational zone could have acted like and

intender, spreading deformation to the East, accumulating high shortening rates and developing very little rotation in the Forearc and the Western limit of the Altiplano domain.

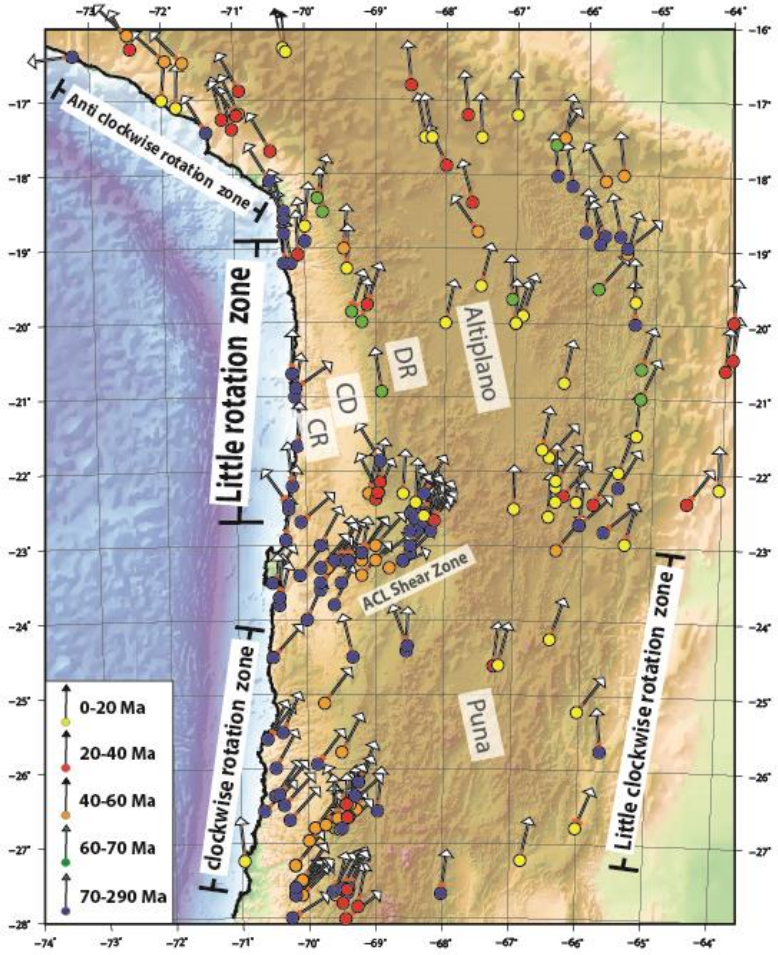

Figure 4.10: Tectonic rotations around the Bolivian Orocline, denoting the changes between the clockwise rotational pattern (south of 22-23°S) in the forearc, the countercolckwise rotational pattern (north of 19°S), also in the forearc, and the little rotational pattern between both previous ones**.**

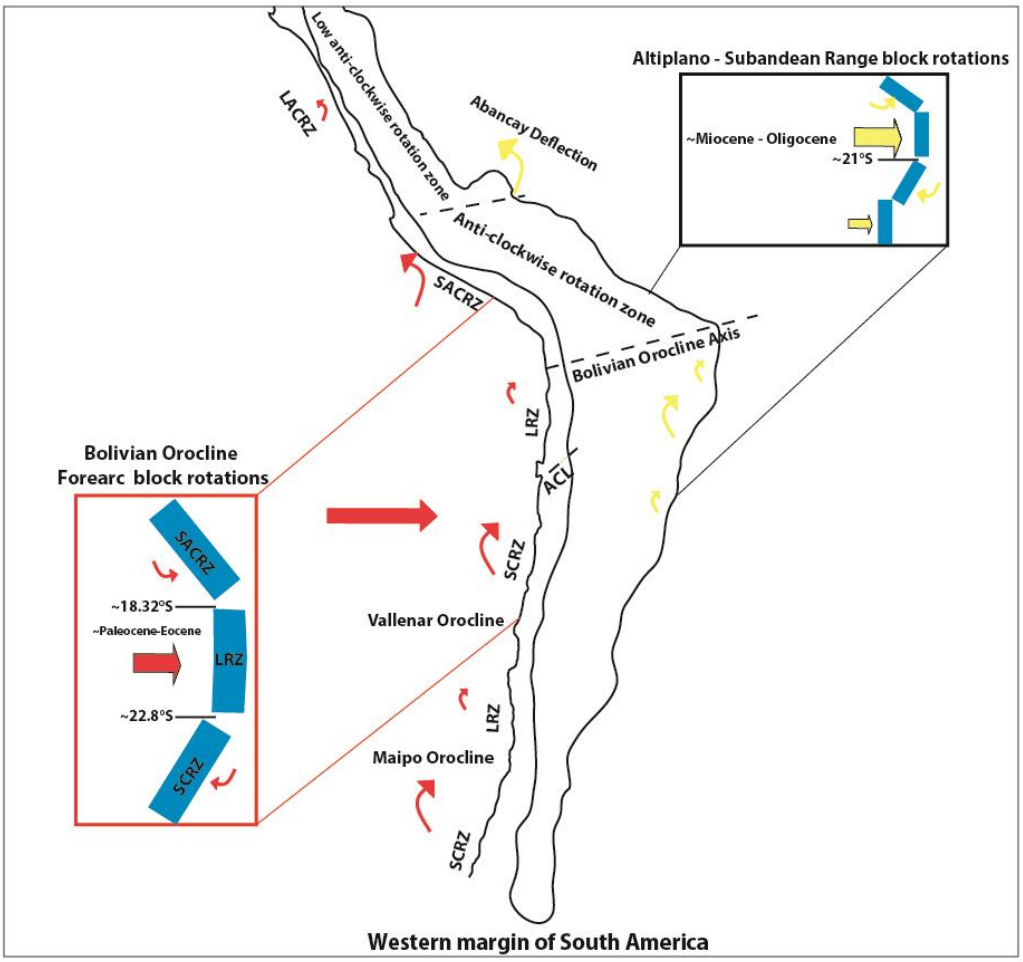

Figure 4.11: Schematic model of the rotational deformation segmentation and its consequences. The blue blocks represent the different domains of rotational changes, showing the latitudinal differences in the mean values, both in the Forearc and the Altiplano-Subandean Range. The red rotations in the western South American margin represents the Eocene-Oligocene rotational pattern of the CARP, and the yellow ones corresponds to the Miocene-Oligocene pattern

4.5.- Conclusions

We have obtained paleomagnetic results for 44 paleomagnetic sites along the Andean Forearc between 18°S and 23°S. Magnetization in volcanic and intrusive rocks is mainly primary and was acquired upon cooling. Tilt correction decreases the dispersion of the mean-site directions at two localities while postectonic magnetizations were observed at five localities, and four more localities with primary magnetization only in intrusives. We interpret the remagnetization in the Domeyko

Range as a result of local heating and hot fluid flow during Upper Cretaceous-Paleogene magmatic arc activity, like the Chusmisa locality.

The Chilean Andean Forearc around 22.5°S-18.5°S presents a mean countercolckwise rotation of 0.2 ± 13.9° in our 11 new localities, plus sites and localities for previuos works (Roperch et al., 2006; Arriagada et al., 2006; Somoza et al., 2012; 2015). Our compiled data support the idea that rotations ocurred during the Eocene-Oligocene in the Forearc, and migrated to the Eastern ranges like the Altiplano-Subandean range in the Miocene (Arriagada et al., 2006a; Roperch et al., 2006; 2011), with the magnitude of rotation being of similar magnitude both in the Coastal Cordillera and Domeyko Range in the Andean Forearc. Our new data contrast with the Altiplano-Subandean range data, with an average of 12.2 ± 12° clockwise rotation, with a strong change around 21° in the simetry axis of the Orocline.

Deformation and block rotations within the Coastal Cordillera are not simply the consequence of by strike-slip movement, as there is no important difference in the rotational pattern between the Coastal Cordillera and the Domeyko Range, thus dreceasing the relevance of the strike-skip character of the great fault sytems in both mountain chains.

The abrupt change from a little rotational pattern north of 22°40’ in the Andean Forearc to a strong clockwise rotational pattern around the ACL suggest that this is a first order structure, not only controlling the emplacement of ore bodies, but acting like a tectonic limit for the rotational deformation north and south of it.

An orogen-scale mechanism is needed to explain the formation of the Andean western margin, related to the construction of the Bolivian Orocline, the rotation of tectonic blocks south of. 22.5°S and north of 18.5°S within the thermally weakened crust of the Upper Cretaceous to Eocene magmatic arc. These results agree with previuous data (Prezzi and Alonso, 2002; Japas et al., 2015; Arriagada et al., 2008), that points to a latitudinal and longitudinal segmentation of the tectonic rotations of the central Andes. The continuos paleomagnetic data of the Bolivian Orocline

illustrate its many latitudinal changes linked to several tectonic features that need to be studied in detail, like the Antofagasta-Calama Lineament, in order to recognize its true nature.

Acknowledgments

Matias Peña gratefully acknowledges a scholarship granted by the Chilean National Science Cooperation (CONICYT grant 21130668). Dicussions with Fernando Poblete and Sebastian Bascuñan were fundamental. We would also like to thank Sergio Villagran and Marco Vaccaris for their field support.

5: Relaciones de heterogeneidades de la placa continental y oceánica en la deformación rotacional.

El estudio paleomagnético de los Andes Centrales permite correlacionar estos datos con su evolución tectónica, así como proponer posibles causas para el origen del Oroclino. En este capitulo se presentan las distintas discusiones que nacen de todo el conjunto de este trabajo.

Uno de los grandes misterios con respecto a la formación del Oroclino Boliviano corresponde al origen de su patrón de rotaciones. En este capítulo se discutirá este origen, tomando en consideración los datos analizados anteriormente, con el fin de: (1) Organizar los distintos patrones de rotaciones tectónicas en distintas áreas; (2) Relacionar estas áreas con edades de deformación especificas; (3) Analizar los límites de estas áreas y sus posibles orígenes; (4) Reconocer los notables efectos de las cuencas Mesozoicas en el patrón de rotaciones andino, (5) Analizar las posibles relaciones de heterogeneidades en la Placa de Nazca con los cambios en los patrones rotacionales y (6) Discutir sobre si el concepto de Oroclino se encuentra bien aplicado para la zona de estudio.

5.1.- Sectorización de los patrones de deformación rotacional

Los datos expresados en los capítulos anteriores muestran una serie de zonificaciones latitudinales y longitudinales referentes a los patrones de deformación rotacional. Estos dominios rotacionales han sido, tradicionalmente, agrupados en distintos bloques, o zonas, de escala continental. Desde los trabajos pioneros de Heki (1985), el Oroclino boliviano ha sido separado en dos bloques con deformación rotacional antihoraria, para el sur de Perú; y horaria, para el norte de Chile. Este patrón de rotaciones, bautizado como el ***Central Andean Rotation Pattern*** o **CARP** (Somoza et al., 1996), ha variado en gran medida según la densidad de datos agrupados y según su edad de deformación asociada. Los patrones de deformación rotacional no solo se han dado de forma latitudinal (Roperch et al., 2006; 2011; Arriagada et al., 2006) sino también de forma longitudinal (Maffione et al., 2009; Prezzi et al., 2012; 2014; Japas et al., 2016), denotando como estos patrones migran hacia el este, mientras la vergencia de la deformación posee una dirección también hacia el Este, de forma regional, al menos desde el Cretácico Superior (Victor et al., 2004; Arriagada et al., 2008; Eichelberger et al., 2015; Amilibia et al., 2008; Carrapa et al., 2015).

También pueden existir dominios rotacionales de menor escala, que corresponden a patrones rotacionales asociados a la respuesta de heterogeneidades estructurales locales (Somoza et al., 2012; Japas et al., 2016; Riller et al., 2017). Estos dominios pueden estar relacionados a la reactivación de estructuras pre-compresionales,

pudiendo controlar las rotaciones tectónicas durante eventos de reactivación de estas estructuras (Figura 5.1). La influencia de heterogeneidades estructurales es un concepto fundamental en el entendimiento de la tectónica andina, siendo la inversión tectónica uno de los estilos estructurales más comunes a lo largo de la Cordillera (Amilibia et al., 2008; Giambiagi et al., 2012; Jara et al., 2014; 2017; Tapia et al., 2015; Martínez et al., 2016), y pudiendo ser el efecto de estas inversiones tectónicas un actor importante para la formación de los distintos patrones rotacionales.

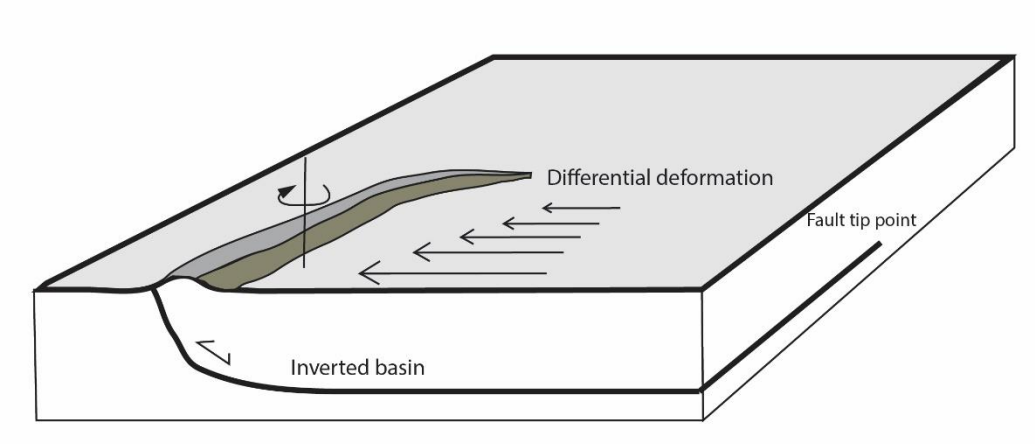

Figura 5.1: rotaciones tectónicas producidas por deformación diferencial controlada por una heterogeneidad estructural heredada.

Con respecto a los dominios de escala continental, a la hora de segmentar latitudinalmente los patrones rotacionales, es posible localizar zonas con patrones específicos a lo largo del antearco andino. En este caso (Figuras 5.2 y 5.3), podemos dividir los Andes Centrales en 5 dominios, de acuerdo con los datos vistos en capítulos anteriores: Un dominio de rotaciones antihorarias leves (LCCRZ) entre el sur de Ecuador y el Norte de Perú; un dominio de rotaciones antihorarias fuertes entre El Sur de Perú y Chile; un dominio de rotaciones horarias leves entre Arica y Antofagasta; un dominio de rotaciones horarias fuertes entre Antofagasta y Vallenar; y un dominio de rotaciones horarias leves entre Vallenar y Santiago.

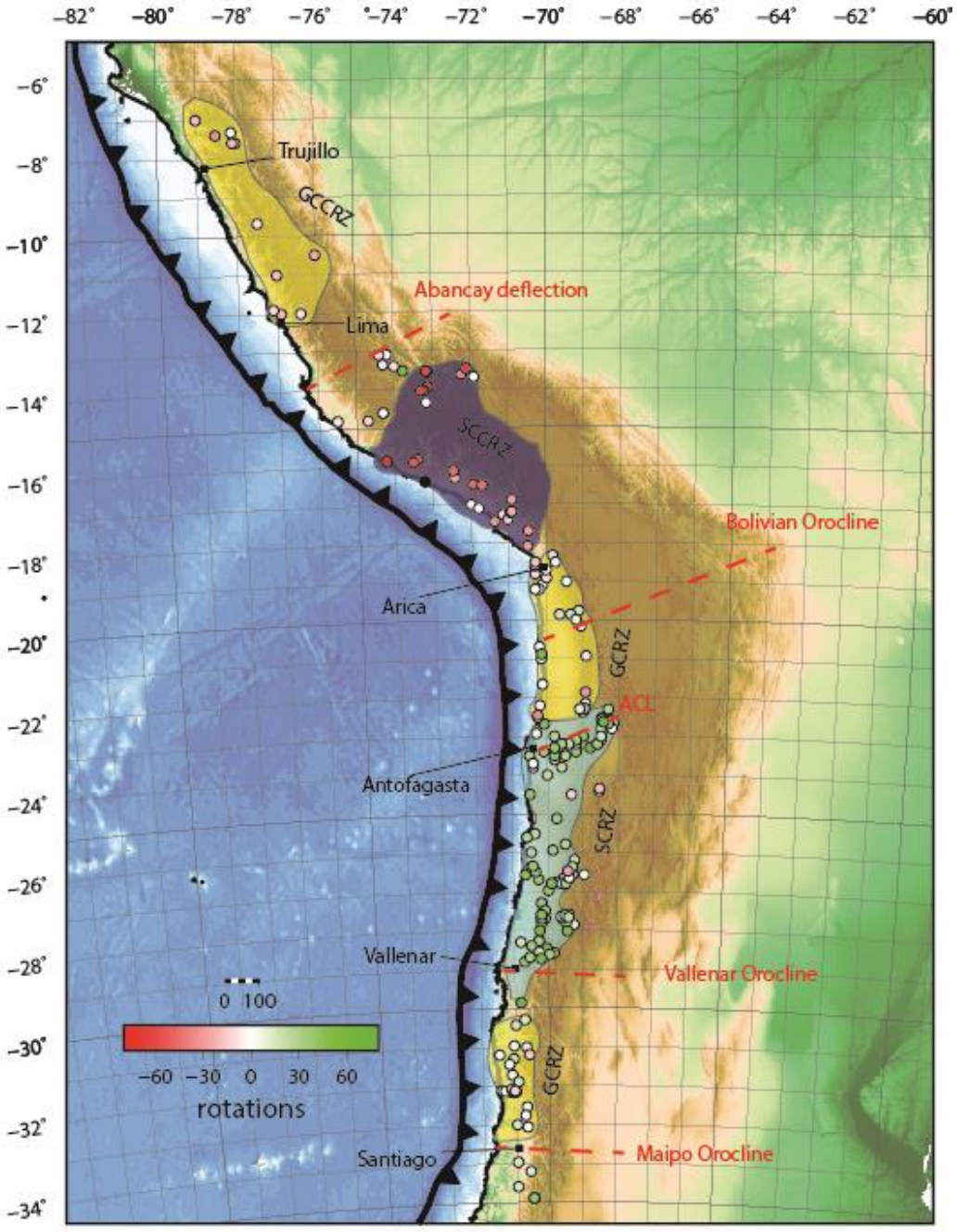

Figura 5.2: Rotaciones tectónicas en el ante arco Sudamericano. Cada circulo representa una localidad paleomagnética, con rotación según la escala de colores mostrada. Las localidades se encuentran agrupadas en las zonas de GCRZ (gentle clockwise rotations zone), SCRZ (strong clockwise rotations zone), SCCRZ (strong counterclockwise rotations zone) y LCCRZ (gentle-counterclockwise rotations zone).

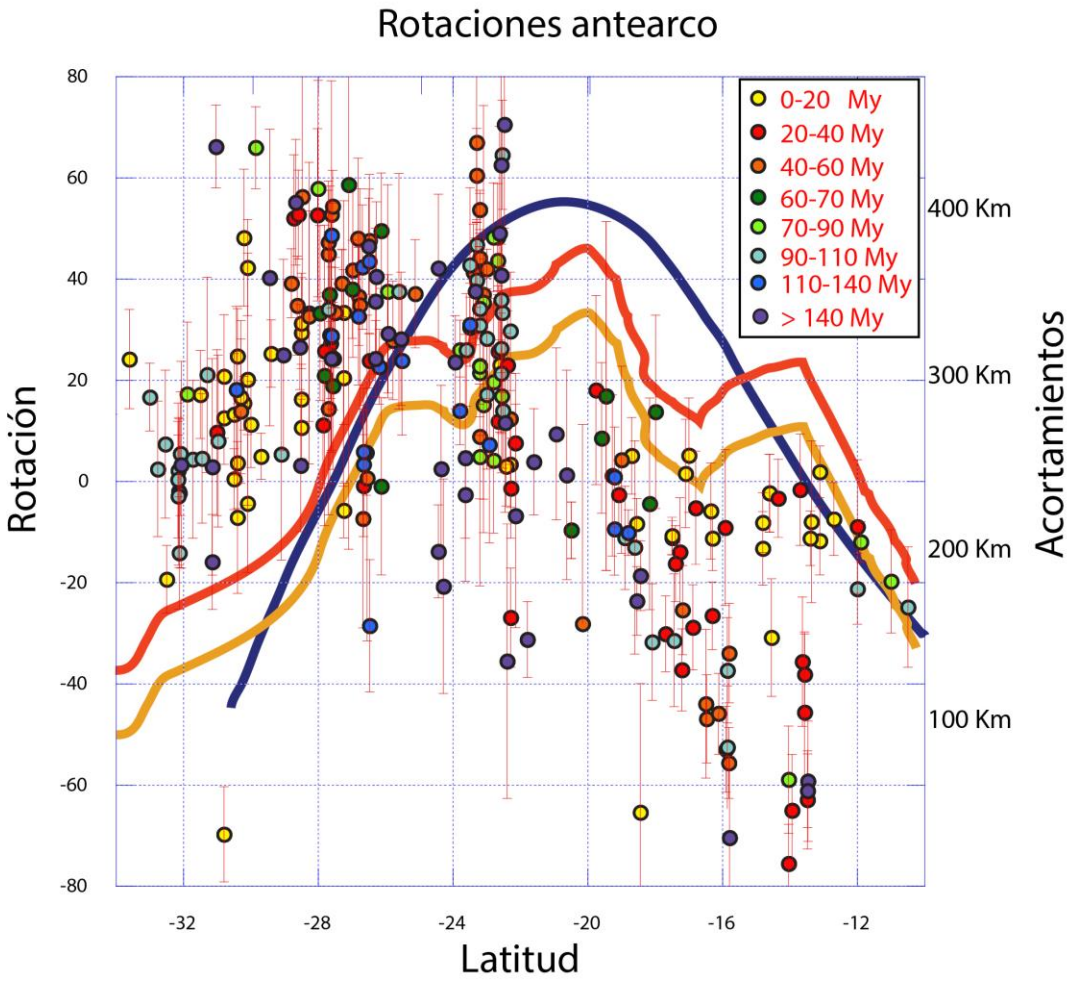

Figura 5.3: Rotaciones paleomagnéticas versus latitud para el antearco de los Andes Centrales. Comparado con curvas de acortamiento según Arriagada et al. (2008), línea azul, y Kleyy Monaldi (1998), curva roja para un modelo de 35 Km de espesor y cortical y curva amarilla para uno de 40 Km. Puede observarse de froma directa como la zona de nules rotaciones entre los 18-23°S corresponde a la zona de mayor acortamiento modelada.

De la misma forma, se puede realizar una segmentación en dominios orientales de la cordillera: Altiplano-Puna, Sierras Pampeanas y Sierra Subandina. Estas rotaciones suelen ser de menor magnitud, y fueron las que llevaron a definir, en un principio, la edad y magnitud de rotación propuesta por Heki (1985) y Isacks (1988). Al analizar estas primeras aproximaciones sobre la hipótesis de formación del

Oroclino Boliviano con respecto a datos modernos en las mismas zonas geomorfológicas (Maffione et al., 2009; Japas et al., 2016), podemos observar que, a pesar de que existe un patrón de rotaciones de mayor magnitud para la zona del ante-arco, la zona oriental del orógeno Andino posee dominios rotacionales cuyos cambios latitudinales son paralelos a los cambios latitudinales observados en el ante-arco, así como en ciertas ocasiones es posible observar más dominios latitudinales de deformación rotacional. (Figura 5.4).

La sectorización espacial de estos patrones rotacionales se encuentra íntimamente ligado a sus edades de deformación, relacionado a una deformación principalmente Eocena-Oligocena, y a un alzamiento principalmente Mioceno-Plioceno (Farías et al., 2010; García et al., 2011; Charrier et al., 2013; Carrapa et al., 2014; Eichelberger et al., 2015; Fuentes et al., 2019).

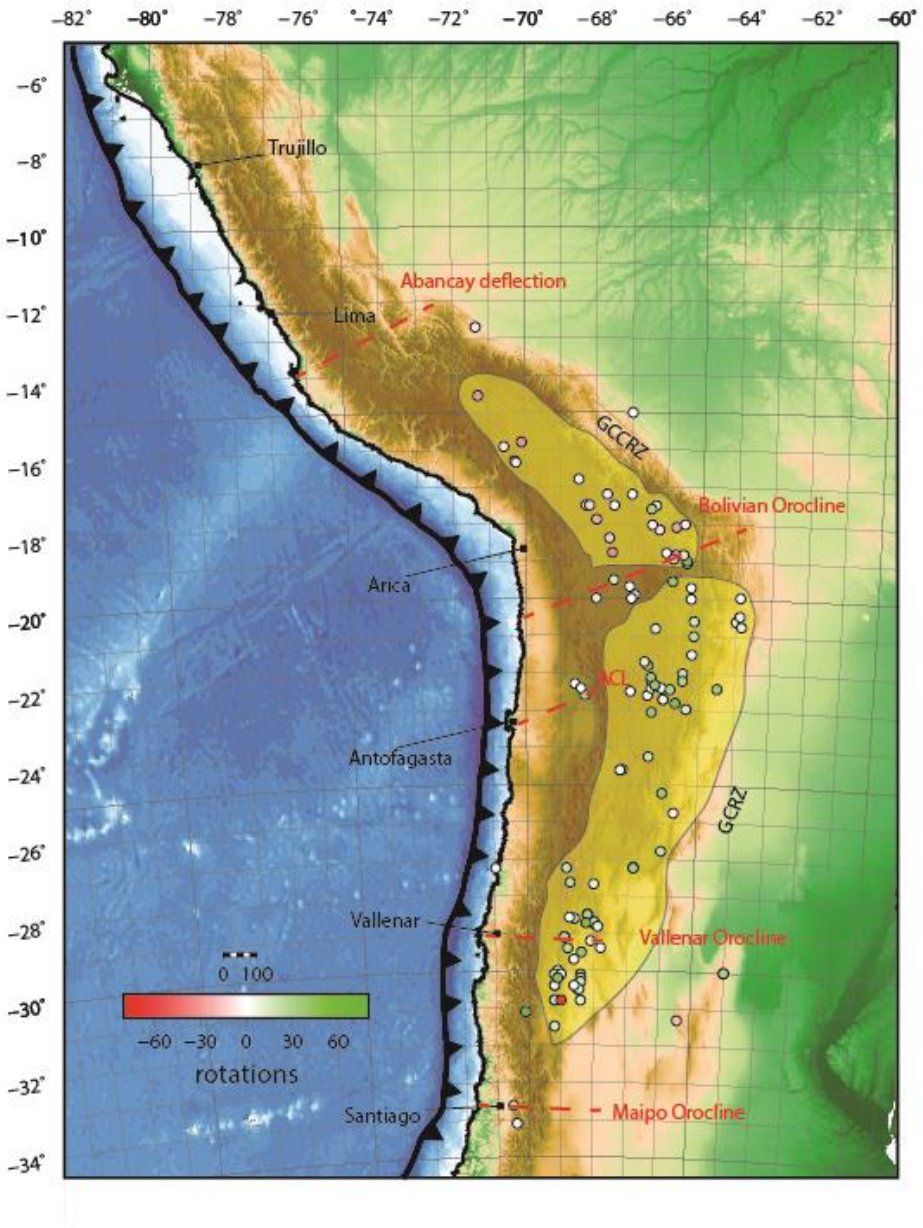

Figura 5.4: Rotaciones tectónicas en el ante arco Sudamericano. Cada circulo representa una localidad paleomagnética según la escala de colores mostrada. Las localidades se encuentran agrupadas en las zonas de LCRZ (little clockwise rotations zone) y LCCRZ (little counterclockwise rotations zone). Nótese la gran diferencia en magnitud con respecto a la figura 36 de las rotaciones en el ante-arco.

Con el fin de asimilar estos dominios rotacionales en áreas continuas, es posible realizar dos tipos de interpolaciones de los datos obtenidos: una triangulación de Delaunay (Schewchuck, J.R., 1996) o una superficie creada a partir de los datos (Smith & Wessel, 1990). Ambos métodos producen iso-superficies separadas según su magnitud y sentido de rotación tectónica, con el fin de observar cómo es esta relación latitudinal y longitudinal en la segmentación de los dominios rotacionales. Para ello es posible aproximarse a la triangulación en dos formas diferentes: (a) interpolando los datos paleomagnéticos totales de los Andes Centrales; o (b) Interpolando datos promediados por cuadrángulos móviles de 1° (Figuras 5.5 y 5.6). La primera aproximación podrá generarnos iso-superficies correctas con respecto a la cantidad y la posición de los datos, pero la segunda podrá ser de ayuda para la discretización de primer orden de los patrones de rotación.

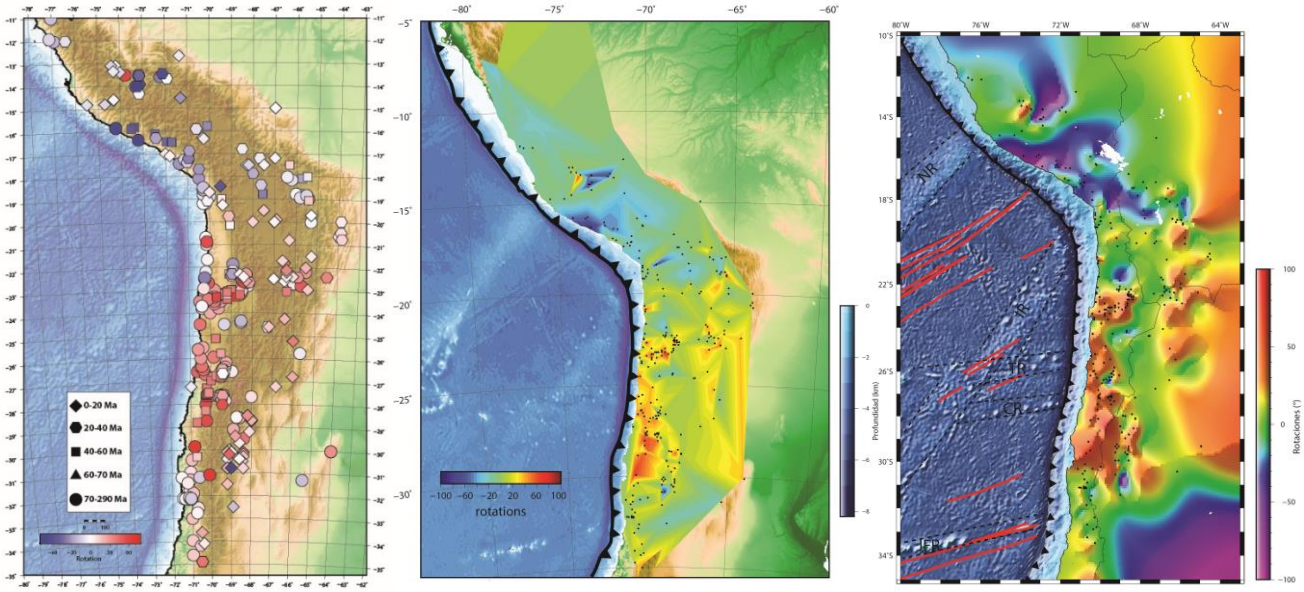

Figura 5.5: (a)Rotaciones tectónicas en los Andes Centrales, luego de los resultados de este trabajo, (b) Triangulación de Delaunay utilizando los mismos resultados, (c) Triangulación de superficie continua, también con los mismos datos. Los puntos negros en (b) y (c) muestran la ubicación de los datos.

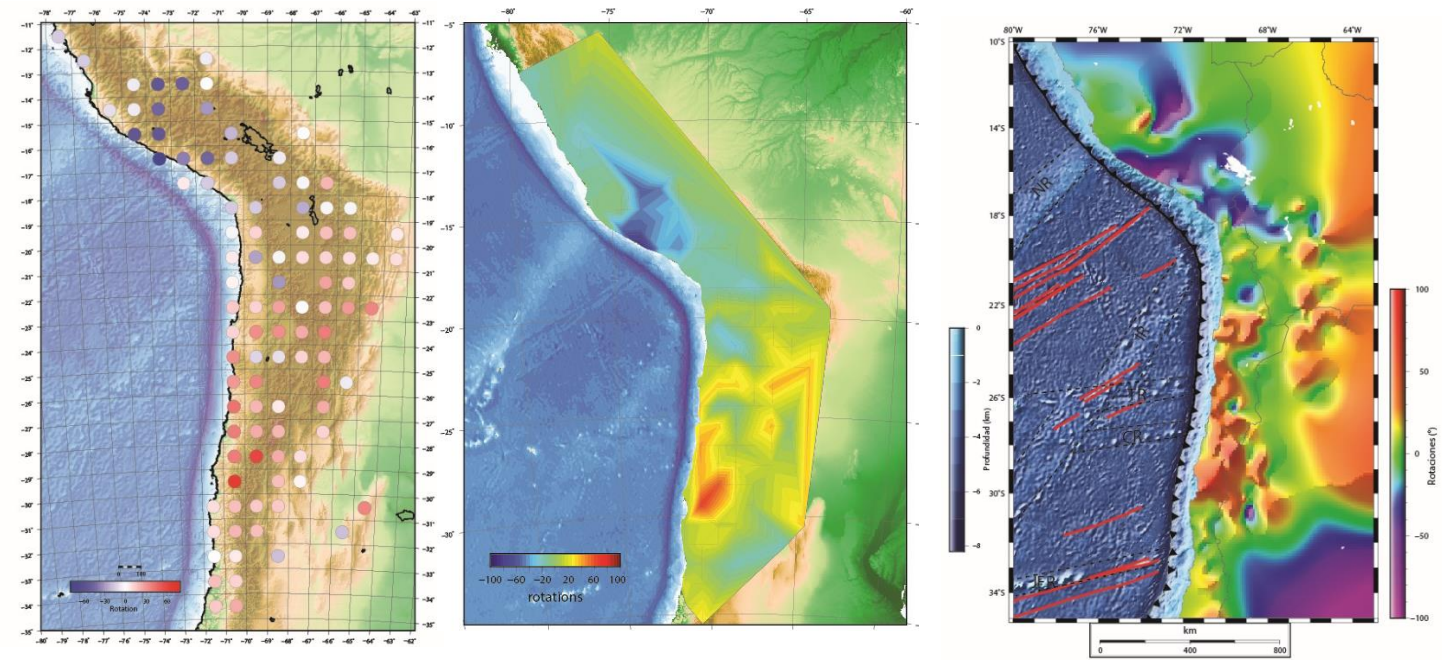

Figura 5.6: Rotaciones tectónicas medias para cada cuadrado Latitud-Longitud de los Andes Centrales. (a) Disposicion de cuadrángulos, (b) interpolación de datos por triangulación de Delaunay, (c) e interpolación de datos en superficie continua. Todos los gráficos utilizan los mismos datos.

Utilizando ambas discretizaciones, y fijándonos en el patrón regional que se desglosa de los datos promediados, se pueden observar claramente límites en los patrones rotacionales en el ante-arco chileno, que, sumado a los datos tabulados en los capítulos anteriores, podemos dividir exactamente en los siguientes dominios: (*Ia*) entre 18 y 23°S, con un patrón de rotaciones tectónicas casi nulo; (*IIa*) rotaciones horarias de alrededor de 30° entre 23 y 29°S; y (*IIIa*) rotaciones horarias de ca. 15° entre 29 y 33°S. Para la zona del Altiplano-Puna-Sierras pampeanas, es posible realizar la misma división, con dominios de rotaciones tectónicas: (*Ib*) horarias de alrededor de 14°, entre 18 y 23°S; (*IIb*) horarias de alrededor de 20° entre 24 y 29°S; y (*IIIb*) horarias de alrededor de 9° entre 30 y 34°S. Es necesario mencionar que en estas delimitaciones se realizaron siempre teniendo en consideración que todos estos dominios poseen sus propias heterogeneidades internas, como se mostró en los capítulos anteriores.

Observando y comparando esta interpolación con otras propuestas (c.f., Arriagada, 2018) podemos realizar el mismo tipo de análisis, comparándo cada dominio con los limites propuestos para los distintos terrenos acrecionados durante el Paleozoico Inferior en el margen occidental de Gondwana (Ramos, 2010). Esta forma de interpretar los distintos cambios en las rotaciones tectónicas, si bien parece amoldarse a los distintos límites de terrenos acrecionados, se encuentra limitada por falta de datos contínuos de estos límites, así como por la presencia de notorios cambios en los patrones rotacionales dentro de un mismo bloque, como los distintos cambios observados en el bloque Vallenar-Santiago (Figura 5.7).

Sin embargo, como se mencionó de forma anterior, estos dominios rotacionales están íntimamente ligados a edades de deformación específica para cada sector, por lo que es necesario analizar las relaciones de estos dominios con distintas edades de deformación.

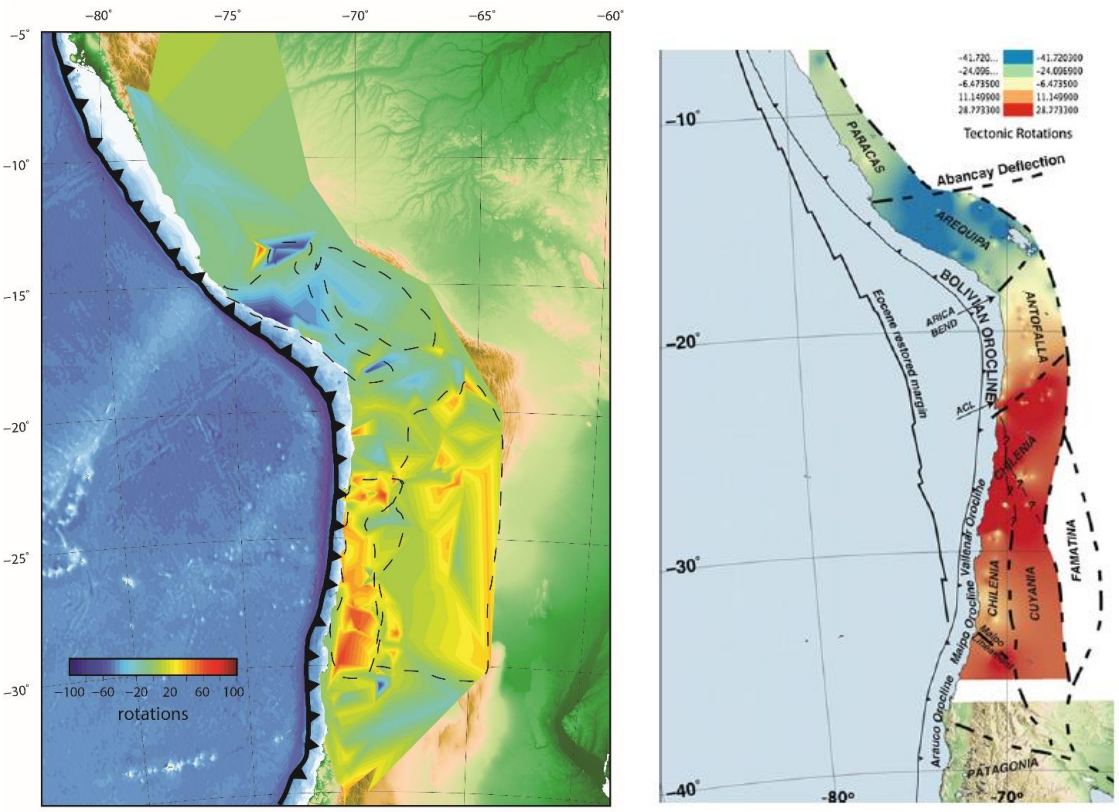

Figura 5.7: Triangulación de los datos de rotaciones tectónicas, realizados el software GMT 5 (Wessel et al., 2013) a la izquierda, y triangulación mostrada en Arriagada (2018). La triangulación muestra de forma continua no solo la segmentación latitudinal, sino que muestra una clara diferencia con la variación de las rotaciones longitudinalmente, así como ciertos patrones anómalos dentro de las grandes segmentaciones.

5.2.- Edad de las rotaciones en los andes Centrales.

Si anteriormente se mostró que era posible separar el patrón de rotaciones en el ante-arco de los Andes Centrales en 4 dominios mayores que poseen edades rotacionales específicas. Analizando las rotaciones respecto a su edad para todo el ante-arco del sector antes mencionado (Figura 5.8), se puede observar que no solo los mayores índices de rotaciones pertenecen a edades de magnetización mayores a 35 Ma, sino que hay una concentración de altas rotaciones para las edades entre 50-100 Ma.

En el capítulo 2, se estableció como los patrones de grandes rotaciones de rocas pre-Eocenas, asociados a rocas de edades Cretácico Superior y K-T, estuvieron sometidas a procesos de deformación compresiva desde, al menos, el Cretácico Superior Temprano (Bascuñan et al., 2015). Es por ello que la correlación edad/rotación, si bien no apunta a eventos rotacionales específicos, si nos asegura

que existe una acumulación de deformación rotacional desde el Cretácico Superior. Esta relación nos obliga a analizar, previo a los mayores eventos de deformación que forjaron el Oroclino Boliviano entre 45 y 35 Ma, la causa de estas rotaciones y el porqué de su alta magnitud acumulada.

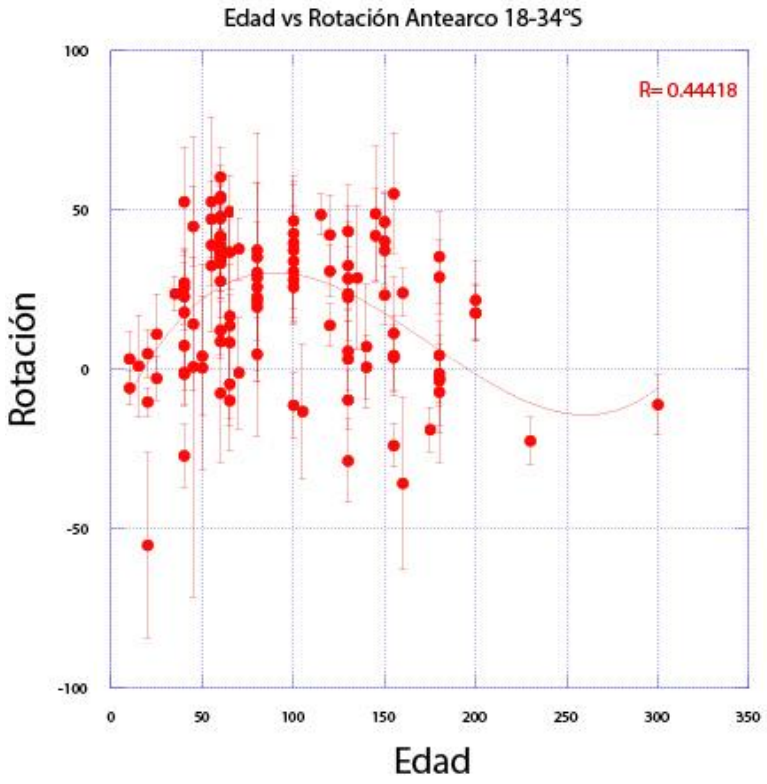

Figura 5.8: Rotaciones tectónicas versus Edad (en millones de años). La curva roja representa una regresión lineal con un coeficiente de correlación de 0.44418. Nótese la cima de la curva alrededor de los 80-90 My**.**

Con el fin de poder observar de manera detallada esta diferenciación en la edad de los procesos rotacionales, podemos es posible separar los datos del antearco (Figura 5.9) en rotaciones pre y pos 35 Ma, edad límite superior del evento “incaico”. Se puede observar bastante bien que el patron de rotaciones pos 35 My se encuentra bastante sectorizado, con zonas bien definidas para las rotaciones horarias y antihorarias, estando algunas zonas (como el ante arco chileno entre los 22-29°S) con una leve dispersión del patron de rotaciones, dispersión que puede

ser resultado de la baja cantidad de datos correspondiente a esa edad en la zona mas occidental del ante-arco. Al observar la zonificación de las rotaciones pre 35 My es cuando se observan zonificaciones bien interesantes. Si bien existe un alza e las grandes rotaciones alrededor de los 23°S, es posible observar fuertes alzas de rotaciones horarias, que se observab en los colores mas cercanos al rojo. Estas alzas se concentran entre los 23-29°S, siendo casi nulas al sur de este segmento. Entre los 10-17°S, las rotaciones observadas en Peru también muestran un alza notable, observándose una delimitación bien especifica para las mayores rotaciones antihorarias.

Si bien ambas figuras no son concluyentes, apuntan hacia la existencia de ciertas zonas con patrones bien definidos, estando algunos limites bastante demarcados y siendo otros bien difusos, por lo que es necesario discutir acerca de la naturaleza misma de estos posibles limites.

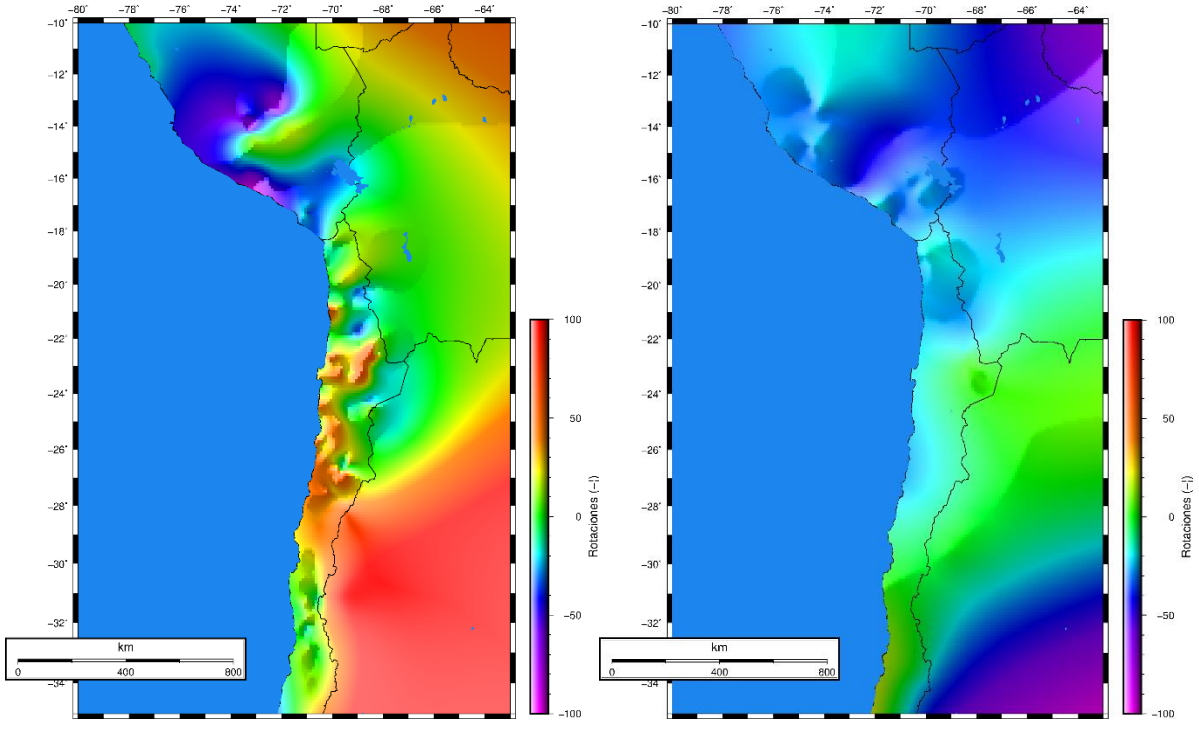

Figura 5.9: Superficie interpolada para magnitud de rotaciones tectónicas pre 35 My (izquierda) y pos 35 My (derecha). Puede observarse de forma clara las altas rotaciones horarias producidas el chile relacionado al evento incaico y anteriores.

Con el fin de aportar no solo a como se distribuye el patron de rotaciones previo a los 35 millones de años, sino que a observar como se alinea la forma del margen

continental, trabajos anteriores (Arriagada et al., 2008) utilizaron las bases de datos de acortamiento y rotaciones tectónicas para analizar la evolución de la deformación alrededor del Oroclino Boliviano. Si utlizamos el software Gplates, utilizando las mismas definiciones de bloques tectónicos definidas en trabajos anteriores, podemos comparar la forma del margen continental de forma clara, en un caso para el modelo previo a este estudio, y en otro para el modelo generado con los nuevos datos de rotaciones tectónicas mostrados anteriormente. Lo que puede observarse (Figura 5.10), es que la forma pre-Incaica del margen continental es bastante similar en ambos modelos, produciendo el modelo de Arriagada et al. (2008), la zona de no rotaciones como un artefacto por las mayores deformaciones en las latitudes entre los 18-22°S, asi como mostrando una zona de transición entre el dominio de las rotaciones tectónicas horarias al sur de los 23°S y el dominio de rotaciones nulas al norte de los 34°S.

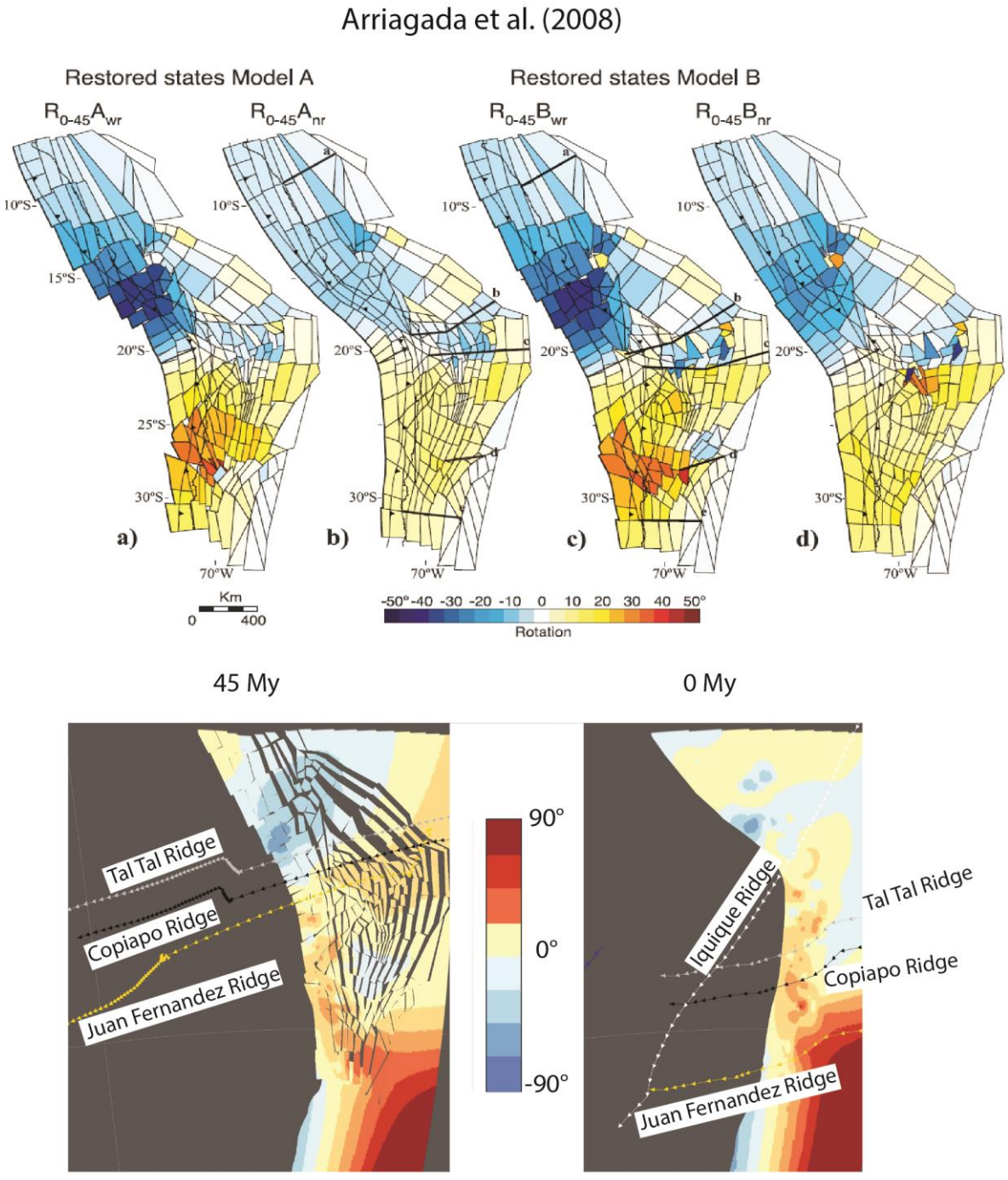

Figura 5.10: Comparación entre la reconstrucción del margen continental andino a los 45 millones de años de Arriagada et al. (2008), en la parte superior, y modelo propio generado por Gplates en la parte inferior.

5.3.- Limites de los patrones rotacionales: Lineamientos y debilidades corticales.

Una de las causas más comunes a las que fueron atribuidas las rotaciones tectónicas presentes en los Andes Centrales correspondió a la acción de sistemas de fallas definidas con movimientos de rumbo, siendo el caso del Sistema de Fallas de Atacama (SFA) y el Sistema de Fallas de Domeyko (SFD), supuestos actores principales al momento de darle un origen a los patrones de rotaciones en el antearco andino (e.g., Sheubber et al., 1990; Reutter et al., 1991; 1996; Taylor et al., 1998; Cembrano et al., 2005). Sin embargo, trabajos de distinta índole estructural realizados en la zona, no solo han discutido la naturaleza cinemática de estos grandes lineamientos (Arriagada et al., 2006b; Amilibia et al., 2008; Martínez et al., 2016; Contreras, 2018), sino que han optado por enmarcar a estos lineamientos dentro de estilos estructurales mayormente compresivos, con componentes de rumbo, pero principalmente relacionados a sistemas de inversión tectónica positiva y la posterior formación de fajas plegadas y corridas (Amilibia et al., 2008). Sin embargo, en algunas zonas pueden observarse estructuras de rumbo de escala regional, que incluso llegan a cortar algunos de estos grandes sistemas de fallas. (Contreras, 2018).

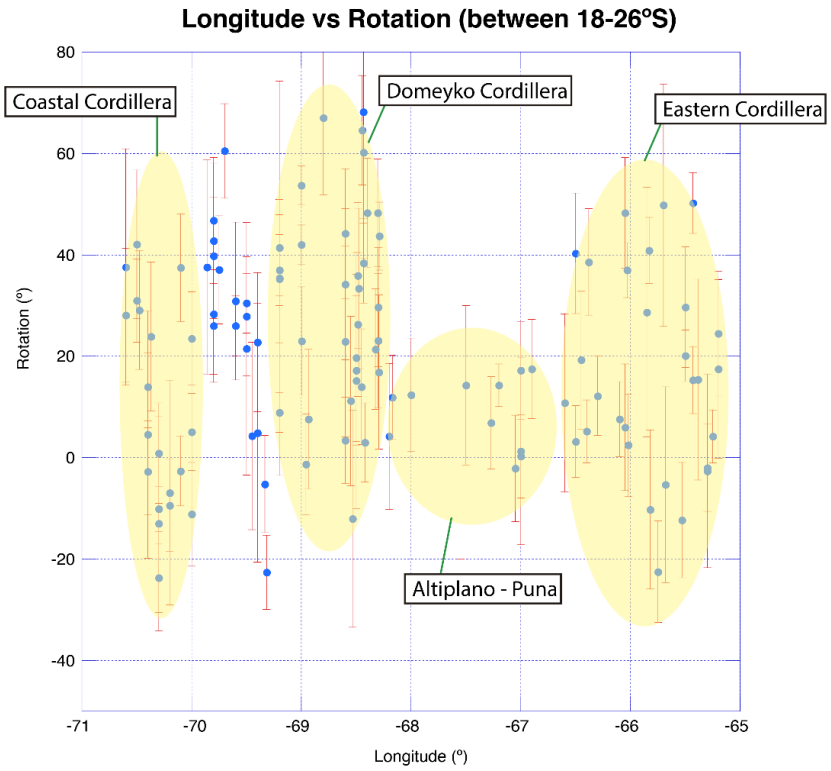

Figura 5.11: Cambios longitudinales en las rotaciones entre los 18° y 26°S, designando las rotaciones a las distintas geomorfologías andinas.

El Sistema de Fallas de Atacama corresponde sin duda a uno de estos grandes lineamientos donde aún está viva la discusión con respecto al carácter general de su movimiento, temporalidad y magnitud. Trabajos paleomagnéticos anteriores (Forsythe y Chisholm, 1994; Randall et al., 1996; Taylor et al., 1998; Arriagada et al., 2003; Taylor et al., 2005, Contreras, 2018) han discutido prolíficamente sobre la influencia de la zona de falla en las rotaciones tectónicas presentes en la Cordillera de la Costa, pero siempre poniendo en duda el nivel de influencia de este lineamiento versus la presencia, y acción, de otros lineamientos, como el sistema de fallas de Taltal, la falla Barazarte, el lineamiento de la carretera Antofagasta-Calama o la falla Paposo, todas estructuras que disectan la traza principal de SFA (Forsythe y Chisholm, 1994; Abels y Bischoff, 1999; Arriagada et al., 2000; Contreras; 2018). Observando los datos de rotaciones tectónicas previos, mas los de este trabajo, podemos observar (Figura 5.11) que los cambios mas drásticos asociados a rotaciones están mayormente ligados a los limites morfotectónicos, siendo la diferencia entre el ante-arco y las rotaciones producidas en el Altiplano-

Puna y la Cordillera Oriental, mucho mas marcada que la diferencia en el interior del mismo ante-arco. En el Capitulo 4 de este trabajo se mostro como los grandes lineamientos estructurales de rumbo N-S, como los Sistemas de Falla de Atacama y de Domeyko, no poseen grandes diferencias entre si en los distintos dominios rotacionales, actuando como un bloque cuasi homogeneo, con presencia de heterogeneidades puntuales, como las rotaciones asociadas a la Falla Paposo, al sur de la península de Mejillones (Figura 5.12).

La vista en planta de los datos de rotaciones tectónicas hasta la fecha (Figura 5.12) hace posible observar un par de patrones rotacionales a escala regional: (1) Existe una concentración de altas rotaciones horarias alrededor del lineamiento de la Carretera Antofagasta-Calama.(2) Al observar las rotaciones entre los tramos 26-24°S y 18.5-22°S, la diferencia entre las magnitudes de rotaciones a lo largo del antearco chileno es mínima, estando la Cordillera de la Costa comportándose de una manera similar a la Cordillera de Domeyko y a la Depresión Central.

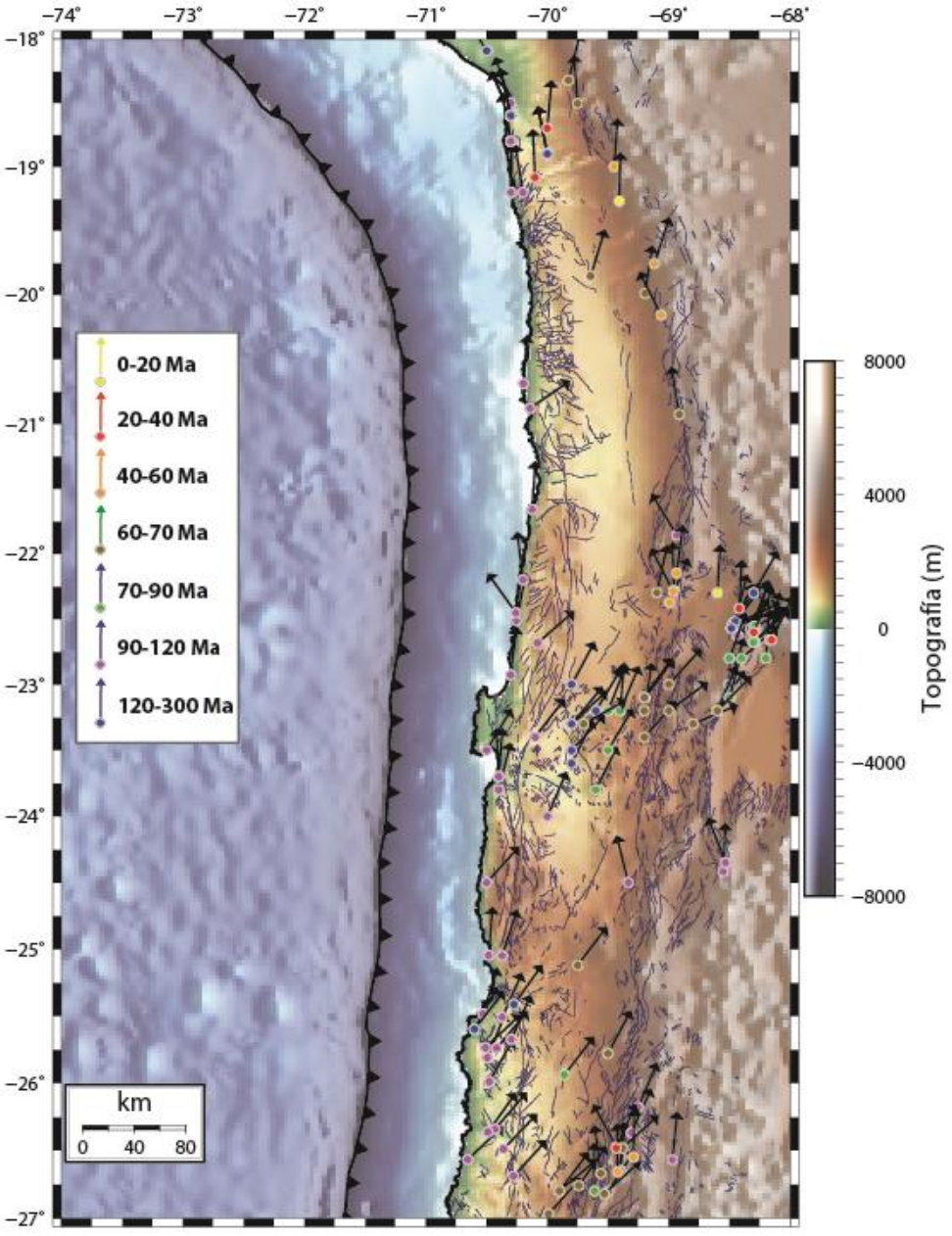

Figura 5.12: Principales sistemas de fallas N-S, siendo SFA el sistema de fallas de Atacama y SFD el sistema de fallas de Domeyko; junto con algunos lineamientos importantes, como la falla Barazarte (FB), la falla Taltal (FT) y el lineamiento de la carretera Antofagasta-Calama.

Muchos de los grandes lineamientos estructurales de margen occidental de Sudamerica poseen una historia multiple, estos pueden haber nacido como fallas normales para la creación de cuencas Mesozoicas (Espinoza et al., 2019) o Cenozoicas (Farias et al., 2010), que luego han sido reactivadas en épocas

posteriores. De la misma forma ciertos niveles de despegue de algunas fajas plegadas y corridas han sido consideradas antiguos limites de terrenos acrecionados (Cristalini y Ramos, 2000), cuyas zonas de sutura han sido postuladas a través de distintos argumentos, con menor y mayor claridad, para todo el margen occidental de Sudamerica (Figura 5.13). Si definimos estas estructuras como debilidades estructurales de carácter regional, es necesario observar como pueden correlacionarse estas grandes estructuras con los cambios en los patrones de rotaciones observados.

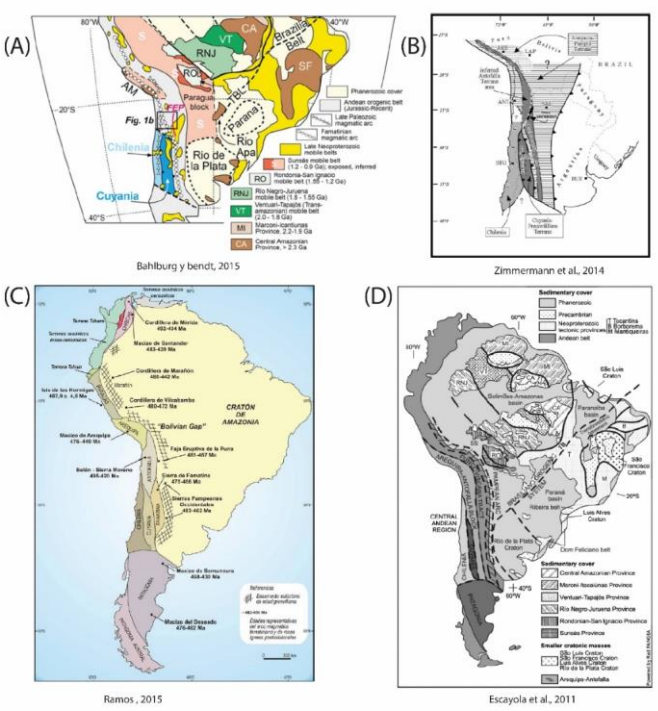

Figura 5.13: Definición y extensión área de terrenos acrecionados paleozoicos por distintos autores. Nótese la intensa diferencia entre la definición de los bloques de Arequipa y Antofalla (siendo incluso fusionados en algunas interpretaciones) y de la posición y extensión de Chilenia.

Al observar la correlación de los datos de rotaciones tectónicas interpoladas (Figura 5.14), comparando con áreas de dominio de cuencas Mesozoicas (Vicente, J.C., 2006) asi como con los limites postulados para los distintos terrenos acrecionados en el Paleozoico (Ramos, V., 2010), podemos observar cómo en ciertas zonas los supuestos límites paleozoicos parecen delimitar diferencias rotacionales (como

cerca de la península de Mejillones), y en otras zonas los límites de cuencas Mesozoicas también pueden correlacionarse con ciertos patrones (como los límites de las cuencas del Oxfordiano con el fin del patron de rotaciones horarias fuertes alrededor de los 31°S).

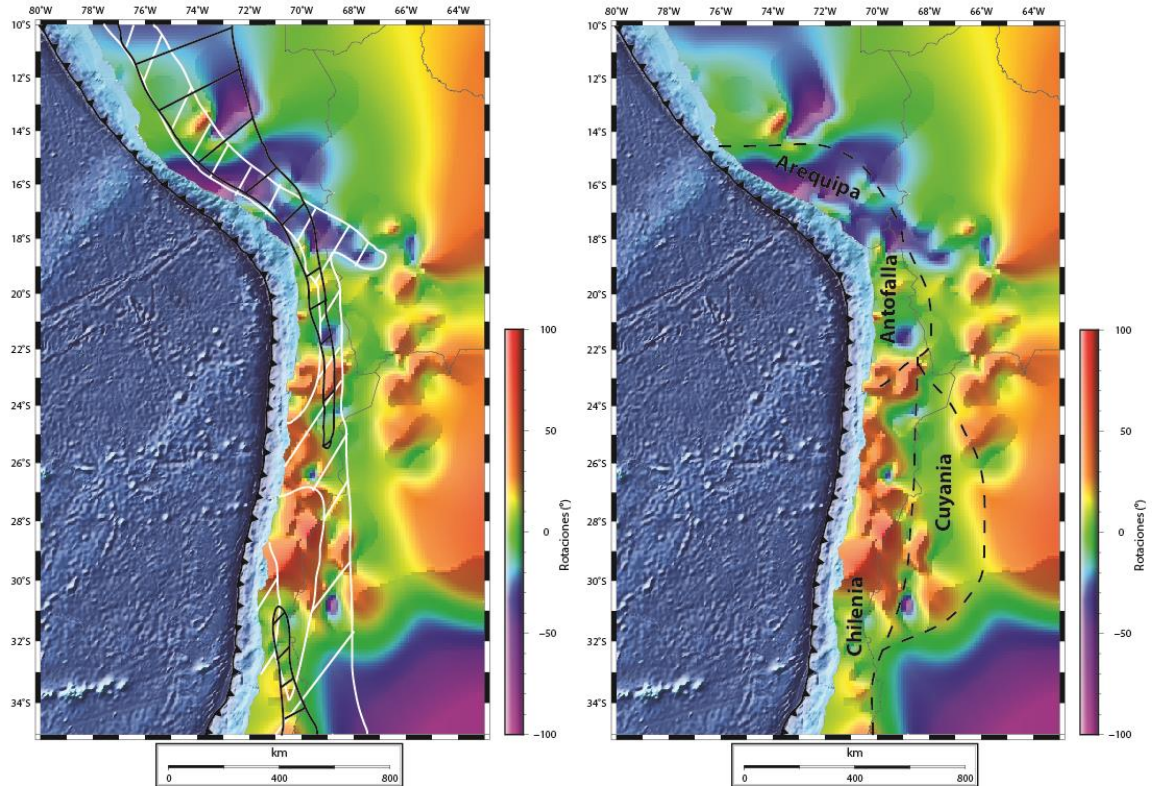

Figura 5.14: Datos de rotaciones interpolados en una superficie continua. Izquierda: el área achurada en negro corresponde a la zona interpretada para las cuencas del Oxfordiano, mientras el área en blanco corresponde a las cuencas del Pliensbachiano, según Vicente, J.C.(2006). Derecha: el área entre las líneas segmentadas correspondo a los límites de terrenos acrecionados definidos por Ramos, V. et al. (2010).

Es posible observar cómo estos límites (difusos) entre patrones rotacionales se observan no solo de forma paulatina, sino que en algunos casos, como en el límite entre el bloque de Antofalla y Chilenia, el límite en sí posee la mayor concentración de altas rotaciones horarias del norte de Chile (Arriagada et al., 2003; Arriagada et al., 2006; Somoza et al., 2015; Astudillo et al., 2008; Narea et al., 2015) apuntando a una fuerte relación entre el lineamiento de la carretera Antofagasta-Calama y este supuesto rasgo estructural Paleozoico, siendo interesante recalcar como ese limite

Paleozoico no ha sido reportado de forma filedigna, y pudiendo ser las rotaciones tectónicas anomalas y el cambio de patron de rotaciones al norte y al sur de este lineamiento, un aliciente para investigar en detalle su verdadera naturaleza.

No solo se pueden considerar estos lineamientos como limitantes de procesos de rotaciones tectónicas, los limites de espesor elástico (Perez-Gussinyé, et al., 2008), grosor cortical evidenciado por datos geoquímicos (Mamani et al., 2008) y de resistencia de la litosfera (Ibarra et al., 2021), evidencian un cambio en distintos tipos de comportamientos alrededor del LAC, demostrando que el cambio notado en los patrones de rotaciones tectónicas infiere un limite geológico de carácter regional.

5.4.- Heterogeneidades de la placa subductante y su relación con los patrones rotacionales.

Asi como se ha podido observar ciertos elementos geológicos que poseen una buena correlación espacial con las áreas de los bloques rotacionales, o con los limites de estos, es también importante analizar los efectos de la placa subductada en la deformación de la placa superior. Para ello es de vital importancia el análisis de heterogeneidades positivas presentes en ella. El caso más estudiado del margen continental chileno, y con más consecuencias relacionables por diversos autores, corresponde a la subducción del Ridge de Juan Fernández (Figura 5.15). Los efectos relacionados a la subducción de éste (Yañez et al., 2001; Ramos y Folguera, 2009) incluyen: supresión del volcanismo, deformación de escama gruesa por acoplamiento mecánico de placas, formación de elevadas geomorfologías debido a estas deformaciones y facilitamiento de formación de yacimientos metálicos relacionados al engrosamiento cortical, producido por estas deformaciones de escama gruesa (Ramos y Folguera, 2009; Martínez et al., 2016; Arriagada et al., 2013).

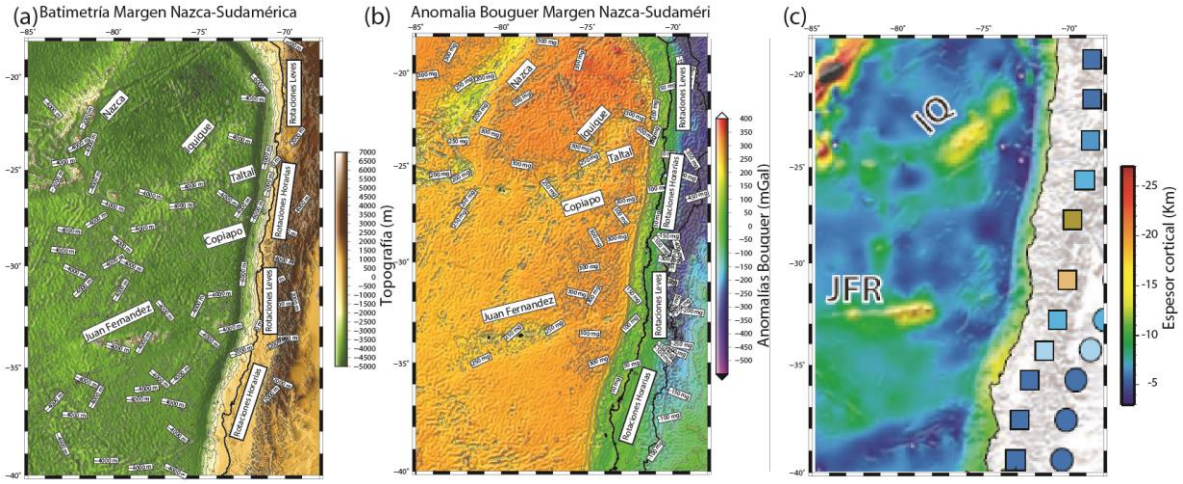

Figura 5.15: (a) Topografía y Batimetría del margen occidental Sudamericano; (b) Anomalia gravitacional de Bouguer según el modelo EIGEN-GRGS.RL04 (Lemoine et al., 2019), (c) Espesor cortical para la placa de Nazca según Pérez-Gussinyé et al.(2008). Se marca con el nombre los Ridges mas importantes reconocidos en la placa de nazca, junto con curvas de contorno para la topografía y anomalia gravitatoria.

Existen otras heterogeneidades dentro de la placa de Nazca que vale la pena señalar, como los Ridges de Iquique, Taltal y Copiapo (Figura 5.15), que si bien no se les ha relacionado a cambios importantes en la deformación de la placa Sudamericana, en comparación al Ridge de Juan Fernadez (Contreras-Reyes y Carrizo, 2011; Álvarez et al., 2015), se les ha correlacionado con los limites de la subducción plana Pampeana (Alvarez et al., 2015) y con los limites de zonas de ruptura de grandes eventos sísmicos (Maksymowicz, 2015). Estas correlaciones espaciales entran en discusión, a la hora de observar como no son necesariamiente exactas espacio-temporalmente (Mulcahy et al., 2014; Skinner y Clayton, 2015), o cuando se observa una migración de la actividad magmática no necesariamente relacionado con la subducción de estas heterogeneidades (Goss et al., 2013).

Si se desea analizar de forma correcta espacio-temporalmente la correlación de la subducción de estas heterogeneidades en el tiempo con los resultados de rotaciones tectónicas de este trabajo, es posible comparar reconstrucciones que conlleven la reconstrucción de la forma del margen (Bello et al., 2018) con lo obtenido en capítulos anteriores (Figuras 5.16 y 5.17). La correlación entre ambos eventos no es directa para la gran mayoría de los ridges, y puede observarse como

la zona de altas rotaciones horarias definida en el capitulo 3 de este trabajo no es mayormente afectada por el paso de estos ridges. La edad de las mayores rotaciones para la zona al sur de Copiapo, se encuentra entre los 65-40 My, siendo las rotaciones mas antiguas directamente no relacionados con estos ridges, a diferencia de las rotaciones mas nuevas que si podrían tener algún grado de correlación. Para la zona de “leves rotaciones”, entre los 29-33°S, definida al principio de este capitulo, se ha postulado que una rotación antihoraria revertiría rotaciones horarias producidas previos al paso del ridge de Juan Fernandez (Arriagada et al., 2013), esta misma situación puede observarse en modelos análogos (Martinod et al., 2013), donde la subducción oblicua de un ridge conduce a la rotación antihoraria de la placa superior a medida que este avanza de norte a sur. Esta propuesta de origen para la deformación rotacional no se ajusta cuando observamos el paso del mismo ridge de Juan Fernandez, asi como de otros ridges, según el modelo de Bello et al. (2018), lo que sugiere que la sola subducción del ridge no es suficiente explicación, y se necesita una compilación detallada de distintas caraceristicas de la corteza subducatada, asi como de la placa Sudamericana, un margen reconstruido, análisis de la oblicuidad de subducción, edad de la placa subductada, espesor elástico entre otros factores, para analizar de forma integral la influencia de la placa subductada en los eventos de deformación de la placa superior.

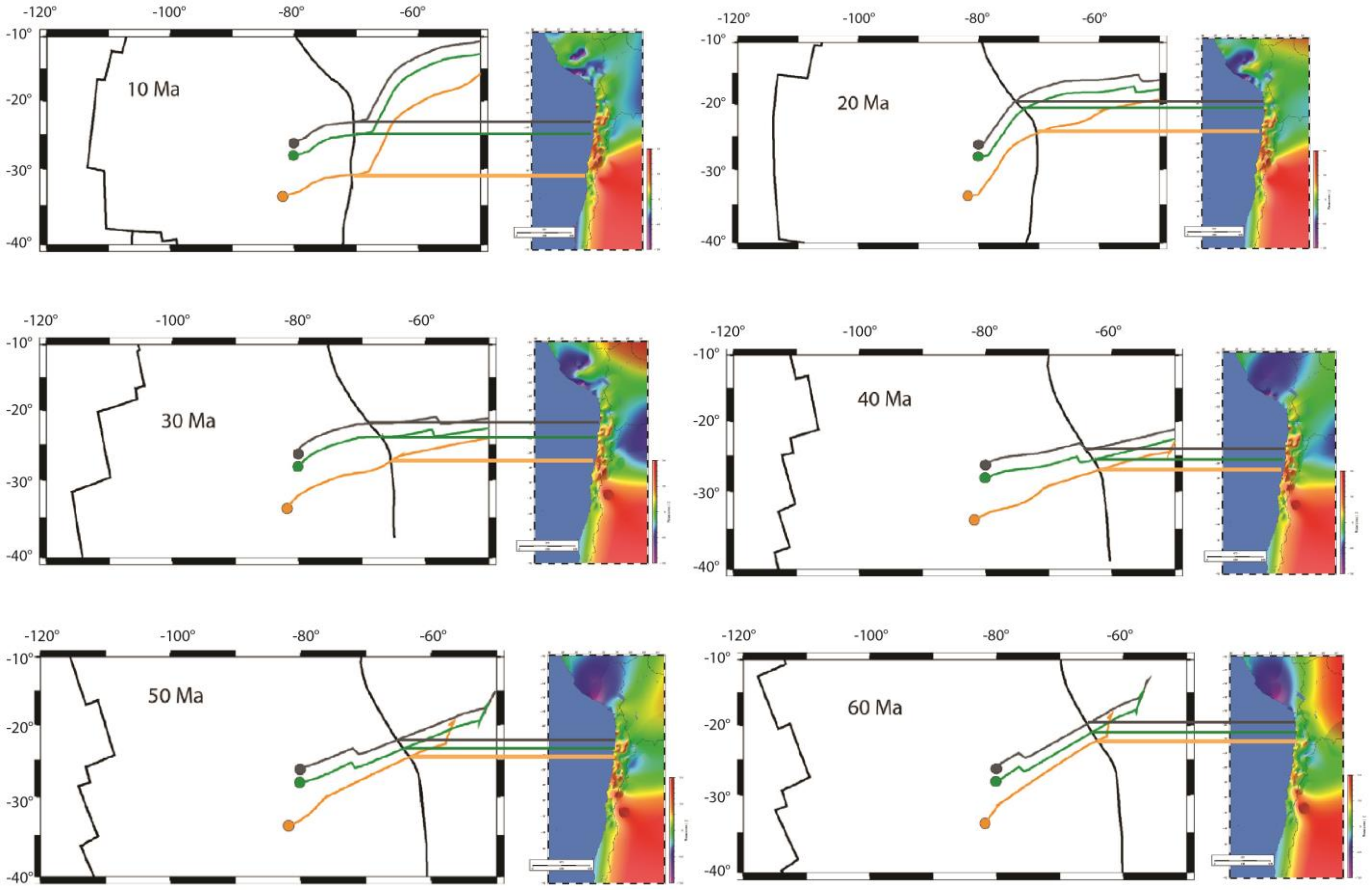

Figura 5.16: Comparación de las posiciones de distintos ridges subductados en el margen occidental de Sudamérica (negro Taltal, verde Copiapo y amarillo Juan Fernandez) comparado con una interpolación de datos de rotaciones en superficie continua para cada edad. Puede notarse a modo general, que las rotaciones altas se concentran en una zona que no necesariamente esta gatillado por el paso de estas heterogeneidades. La escala de colores de rotaciones es la misma de la Figura 5.14.

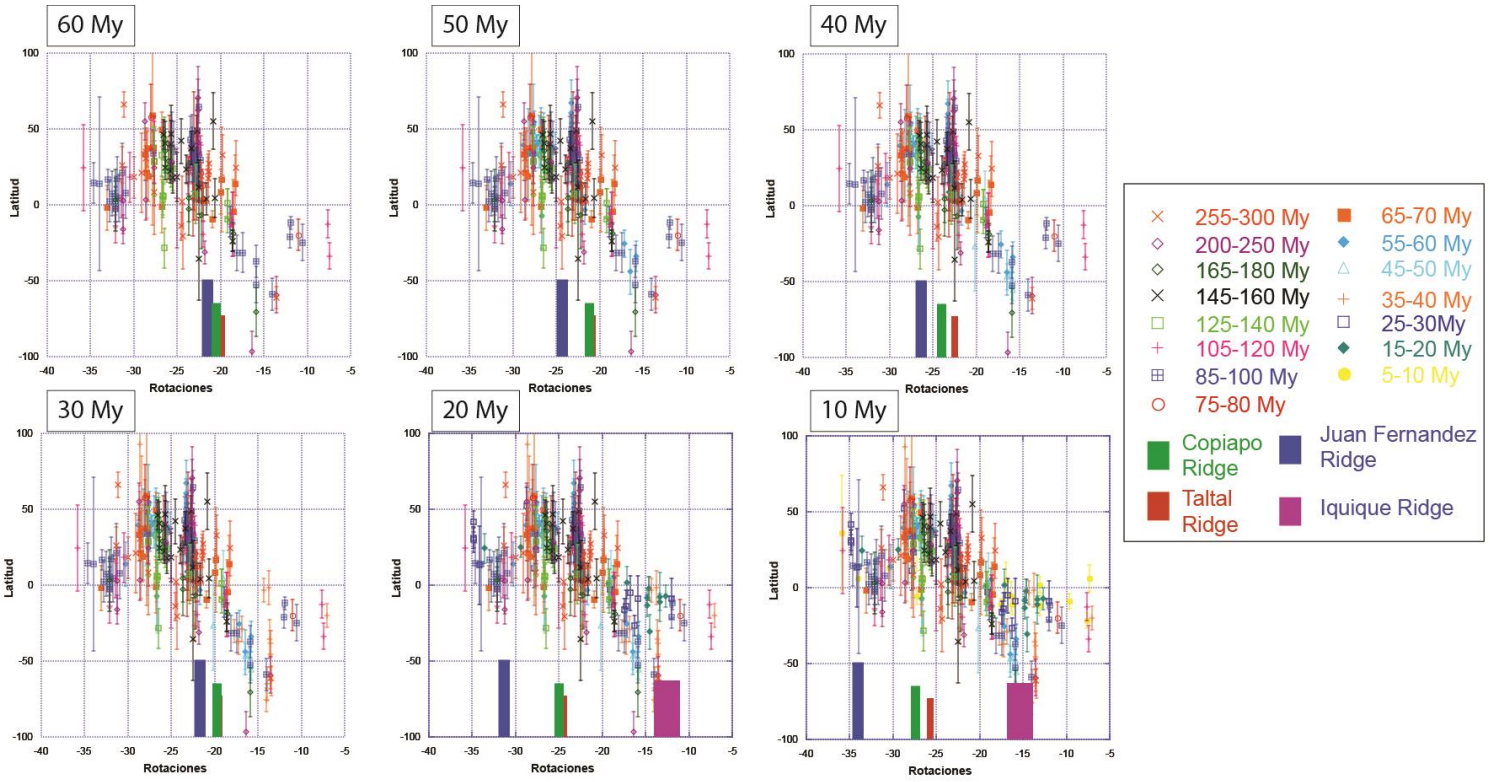

Figura 5.17: Comparación de las posiciones de distintos ridges subductados en el margen occidental de Sudamérica (negro Taltal, verde Copiapo y amarillo Juan Fernandez) comparado con graficos de cajas de rotaciones vs latitud. Otra forma de observar como el paso de estas heterogeneidades no produce un efecto notable en los patrones de rotaciones tectónicas.

Diversos autores han postulado a la influencia de una heterogeneidad subductada en los Andes Centrales como uno de los posibles mecanismos responsables del flexuramiento del Oroclino Boliviano (Martinod et al 2010; 2013; O'Driscoll et al., 2012). A través de reconstrucciones de placas, se ha propuesto la subducción de una heterogeneidad positiva, alrededor del actual eje del Oroclino Boliviano, hace ca. 45 Ma, siendo la subducción de esta heterogeneidad no solo responsable de la flexura, sino que del engrosamiento cortical y las grandes tasas de acortamiento del Eoceno. El producto de la subducción de este ridge no sólo se utiliza para explicar las zonas de rotación antihoraria y horaria, sino que provocaría una zona de pocas rotaciones, pero de intensa deformación compresiva

En otras configuraciones oroclinales a nivel mundial se ha observado que, efectivamente, existe una relación entre la deformación de la placa superior y la subducción de un ridge, siendo algunos incluso ligados a los cambios de curvatura

en la subducción (Florez-Rodriguez et al., 2019; Haynie y Jadamec, 2017; Wagner et al., 2017). Esta relación se encuentra supeditada a sus dimensiones y características mecánicas (Florez-Rodriguez et al., 2019). El análisis de estas correlaciones entre geometrías de subducción y su posible correlación con eventos de deformación rotacional, o los limites espaciales de estos, nos lleva a analizar si los últimos eventos rotacionales poseen alguna correlación con los cambios observables dentro del plano de Wadatti-Benioff.

5.5.- Heterogeneidades en el plano de Wadatti-Benioff: subducciones relictas.

Al analizar los distintos cambios en la evolución geológica Andina, vemos que el ángulo de subducción juega un rol fundamental en los procesos de la placa superior, pudiendo generar distintos procesos orogénicos, como cuencas de tras-arco u orógenos compresivos; todo controlado mayormente por la interacción entre la placa subductante y la placa subductada (Uyeda y Kanamori, 1979; Heuret y Lallemand, 2005; Sdrolias y Müller, 2006; Doglioni et al., 2007). Los Andes Centrales poseen variados cambios de ángulo de subducción a lo largo de su rumbo, asociandos con el decrecimiento de la actividad volcánica en ciertas zonas, el grado de acoplamiento, los estilos estructurales y la presencia de franjas metalogénicas en la región (Cahill y Isacks, 1992; Stern y Kilian, 1996; Gutscher, et al., 2000; Gutscher, 2002; Pardo et al., 2002; Yañez et al., 2001; Farías et al., 2010; Maksymowicz et al., 2012).

La subducción de heterogeneidades, como ridges asísmicos y zonas de fracturas, han mostrado tener cierto control sobre la sismicidad de mediana profundidad (Pardo et al., 2002) así como un rol más que importante en la definición de las zonas de fractura de terremotos (Contreras-Reyes y Carrizo, 2011; Maksymowicz, 2015). La correlación sugerida entre heterogeneidades subductadas y patrones de deformación (Yañez et al., 2001; Hampel et al., 2004; Arriagada et al., 2013; Álvarez et al., 2015; Maksymowicz, 2015) analizada anteriormente nos muestra que no siempre estas correlaciones son directas para los patrones de rotaciones tectónicas.

Esto incluso se puede observar al analizar las diferencias en los patrones de rotación de deformación pos 25 Ma, y su correlación con la subducción de distintas heterogeneidades de la placa de Nazca (Figura 5.18), donde no se ve claramente una correlación entre ambos elementos. Esta correlación si se observa con las distintas zonas de fracturas de los grandes terremotos (Maksymowicz, 2015), asi como se observa un cambio en el patron de rotaciones relacionado de mejor forma a los distintos cambios en la morfología del orógeno andino, como el paso desde las Sierras Pampeanas al limite austral de la Puna. Un ultimo análisis que es necesario realizar es que, si no se observan correlaciones claras con elementos que aun se observan en la placa de Nazca, hay que observar que sucede cuando esta esta subductada.

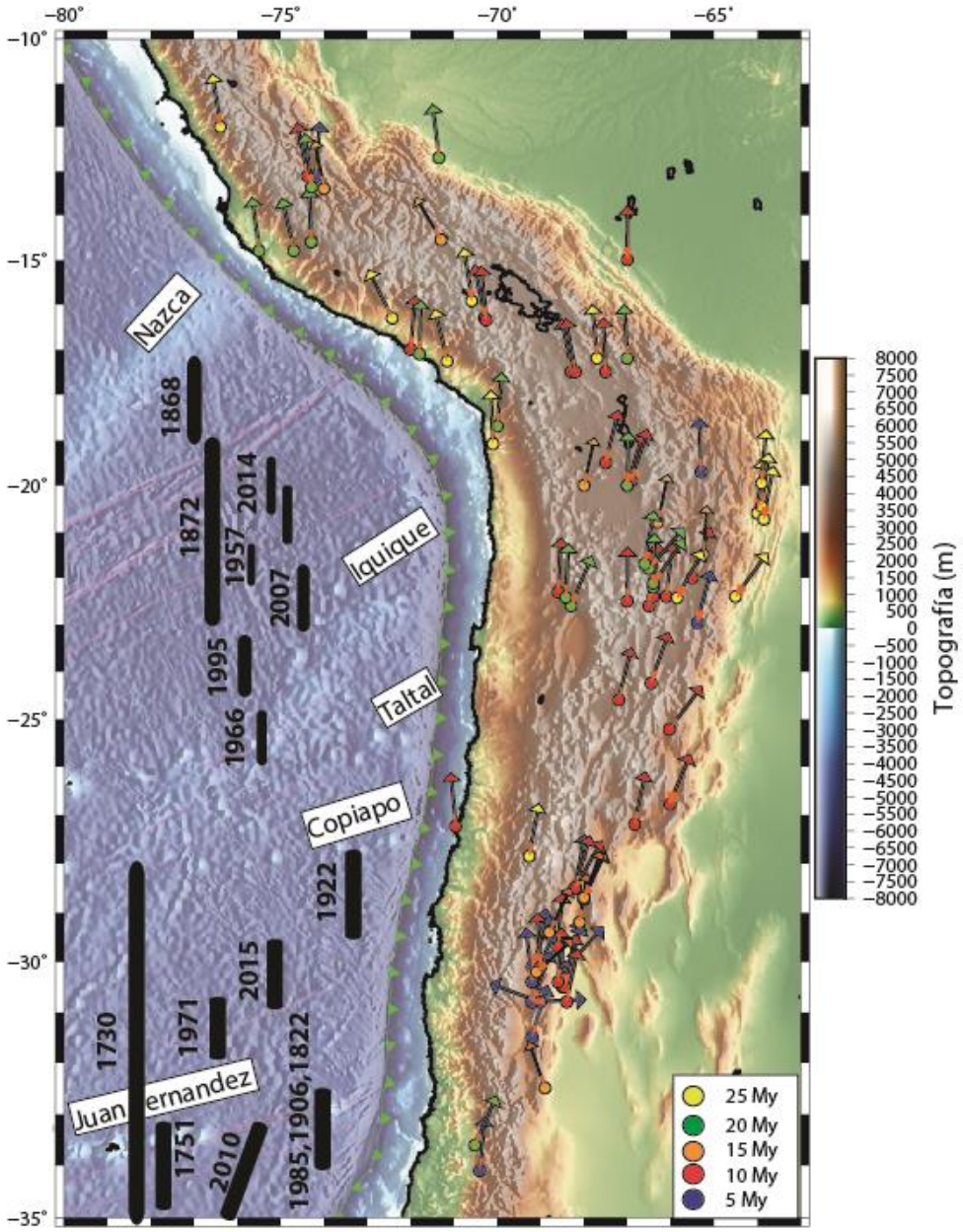

Figura 5.18: Rotaciones tectónicas entre 25-5 Ma alrededor de los Andes Centrales. Heterogeneidades de la placa de Nazca han sido graficadas en sus latitudes de subducción correspondientes, y se compara con las distintas extensiones latitudinales de ruptura de sismos (Ruiz y Madariaga, 2018).

Cuando se observan los cambios de la subducción en profundidad, podemos observar (Figura 5.19) ciertas ondulaciones en el plano de Waddati-Benioff, íntimamente relacionadas a la subducción de las zonas de fracturas, en especial la zona de fractura de Nazca y a la zona de subducción del ridge de Taltal. Mas aún,

estas mismas ondulaciones se relacionan espacialmente con el limite del Altiplano, siendo su límite sur relacionado a la zona de fractura de Mejillones. Estas ondulaciones no son nuevas a la hora de estudiar las zonas de subducción, siendo explicadas como una reacción del slab a los cambios de ángulo con respecto una reacción del manto litosférico, que tiende a levantar la placa subductada, compitiendo con el slab-pull de la misma (Heuret y Lallemand, 2005; Hu et al., 2016).

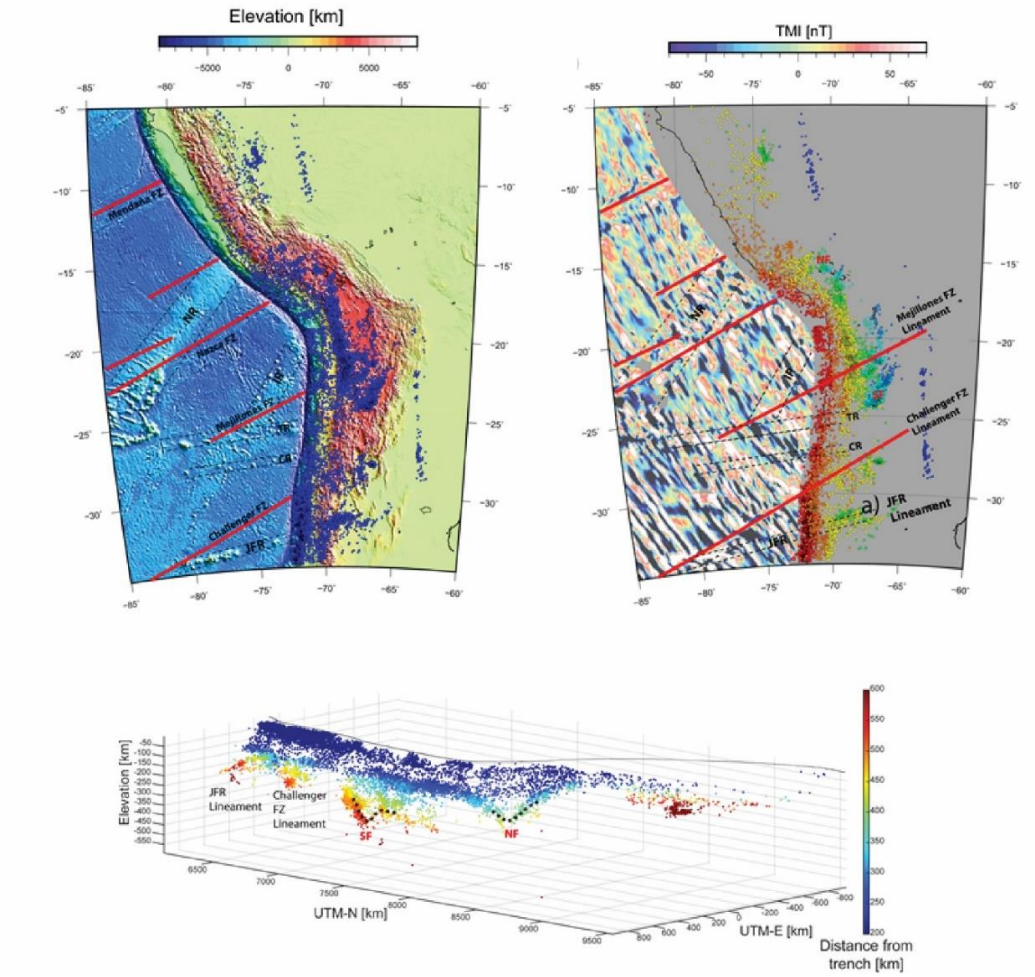

Figura 5.19: Sismicidad producida por la subducción de la placa de Nazca. El mapa superior izquierdo muestra el catálogo NEIC de profundidades mayores a 20 Km en puntos azules, en rojo se encuentran marcadas las zonas de fractura de la placa oceánica, y rodeadas por líneas negras segmentadas los distintos ridges (NR: Nazca Ridge; IR: Iquique Ridge; TR: Taltal Ridge; CR: Copiapó Ridge; JFR: Juan Fernández Ridge). SF y NF corresponden a un plegamiento al sur y norte del Oroclino, respectivamente. El Mapa superior derecho muestra los sismos en una escala de colores donde los azules son los más profundos, extendiendo las zonas de fractura en el continente desde una grilla de campo total magnético. El esquema inferior es una visión 3D del catálogo NEIC, relacionando las distintas heterogeneidades en profundidad.

Estas ondulaciones, si bien no pueden asociarse de forma directa a los grandes patrones rotacionales del antearco Andino, si poseen una correlación mayor con los patrones rotacionales de la zona oriental de la cordillera. La edad de rotación en esta zona, desde el Mioceno, coincide con la edad de las heterogeneidades subductadas, así como los cambios en los patrones de rotación latitudinal en este sector (Figura 5.20), cambios que se producen alrededor de la zona de mayor acortamiento del Oroclino, y donde el ondulamiento de la superficie de sismicidad efectivamente marca un cambio en los patrones rotacionales en la zona del Altiplano-Puna-Sierras Subandinas.

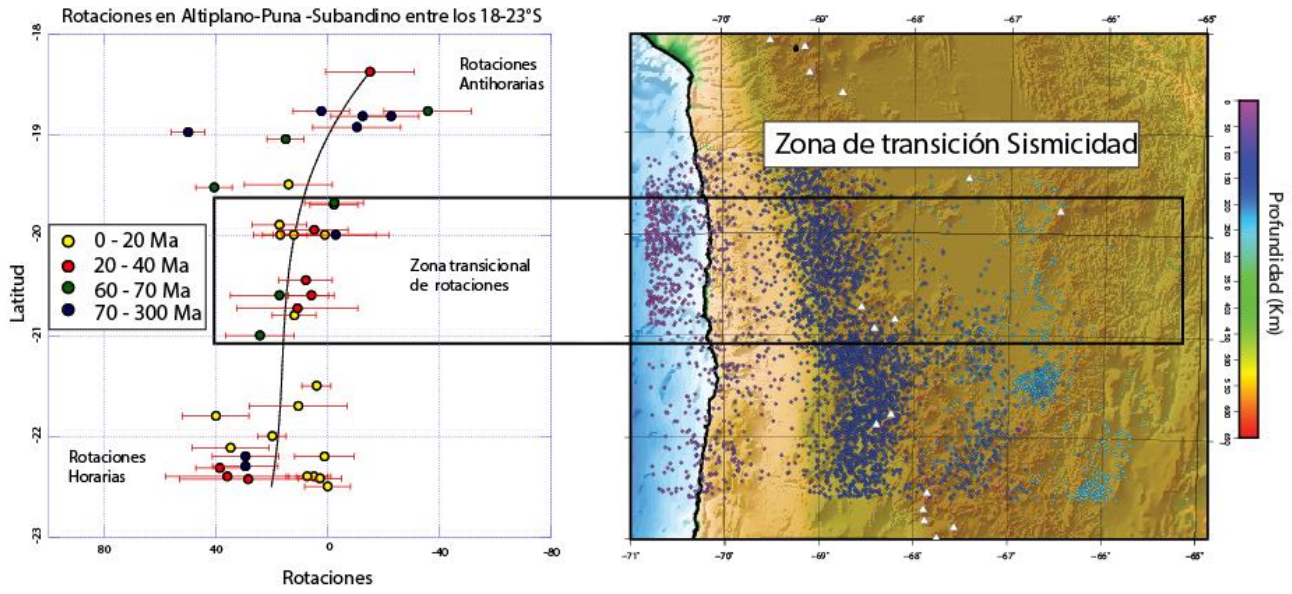

Figura 5.20: Rotaciones entre los 18-23°S de la región del Altiplano-Puna-Sierras Subandinas de Sudamérica, comparado con la profundidad de eventos sísmicos en la región. El área definida como “Tocopilla slab tear zone” corresponde a la línea segmentada en negro y nombrada como SF en la figura anterior.

Esta ultima correlación implica que es necesario elegir con sumo cuidado los modelos con los que entendemos los cambios en el angulo, velocidad y obliquidad de subducción, donde ciertos casos pueden proponerse correlaciones con efectos en la placa superior, pero estando siendo estas mismas propuestas de efectos no siempre sustentadas en los distintos tipos de deformación observable en la misma placa.

5.6.- ¿Oroclino Boliviano o Arco Progresivo?

A medida que avanza la densidad de datos y conocimientos en distintas áreas, conceptos establecidos en los primeros años de investigaciones son siempre desafiados, dada la enorme cantidad de datos disponible actualmente. El concepto oroclonical no es la excepción, siendo anteriormente desafiado en Sudamerica en la zona patagónica (Poblete, 2015). Al analizar el patron de rotaciones en los Andes Centrales podemos observar que existen al menos 3 eventos principales: Una primera etapa relacionada a la inversión tectónica de cuencas mesozoicas en el Cretácico Superior – Paleogeno; una segunda etapa relacionada al evento compresivo Eoceno – Oligoceno; y una tercera etapa relacionada al evento compresivo responsable del alzamiento del Altiplano – Puna en el Mioceno.

Tomando en consideración que desde el Cretácico Superior existen rotaciones tectónicas asociadas al surgimiento del orógeno andino, tanto en trabajos anteriores como en los resultados mostrados en este trabajo (Narea et al., 2015; Somoza et al., 2015; Puigdomenech et al 2020), podemos desafiar el nombre mismo del Oroclino Boliviano, hacia un “Arco Progresivo Boliviano” (Yonkee & Weil, 2010) tomando en consideración el crecimiento de la cordillera andina ha sido paralelo a los procesos de rotaciones tectónicas.

Sin embargo, estos procesos no son temporalmente coherentes en la cordillera de la Costa, cordillera cuya orogénesis esta asociada al Cretacico Inferior Tardio (Bascuñan et al., 2016), y teniendo esta cordillera rotaciones tectónicas de magnitud y sentido similar a las rotaciones observadas en la Cordillera de Domeyko (Capitulos 3 y 4). Esta cordillera, que primero es formada y luego flexurada, podría quedar en la categoría de oroclino, siendo un oroclino costero que, en este trabajo, nombraremos el “Oroclino de Arica” (Figura 5.21).

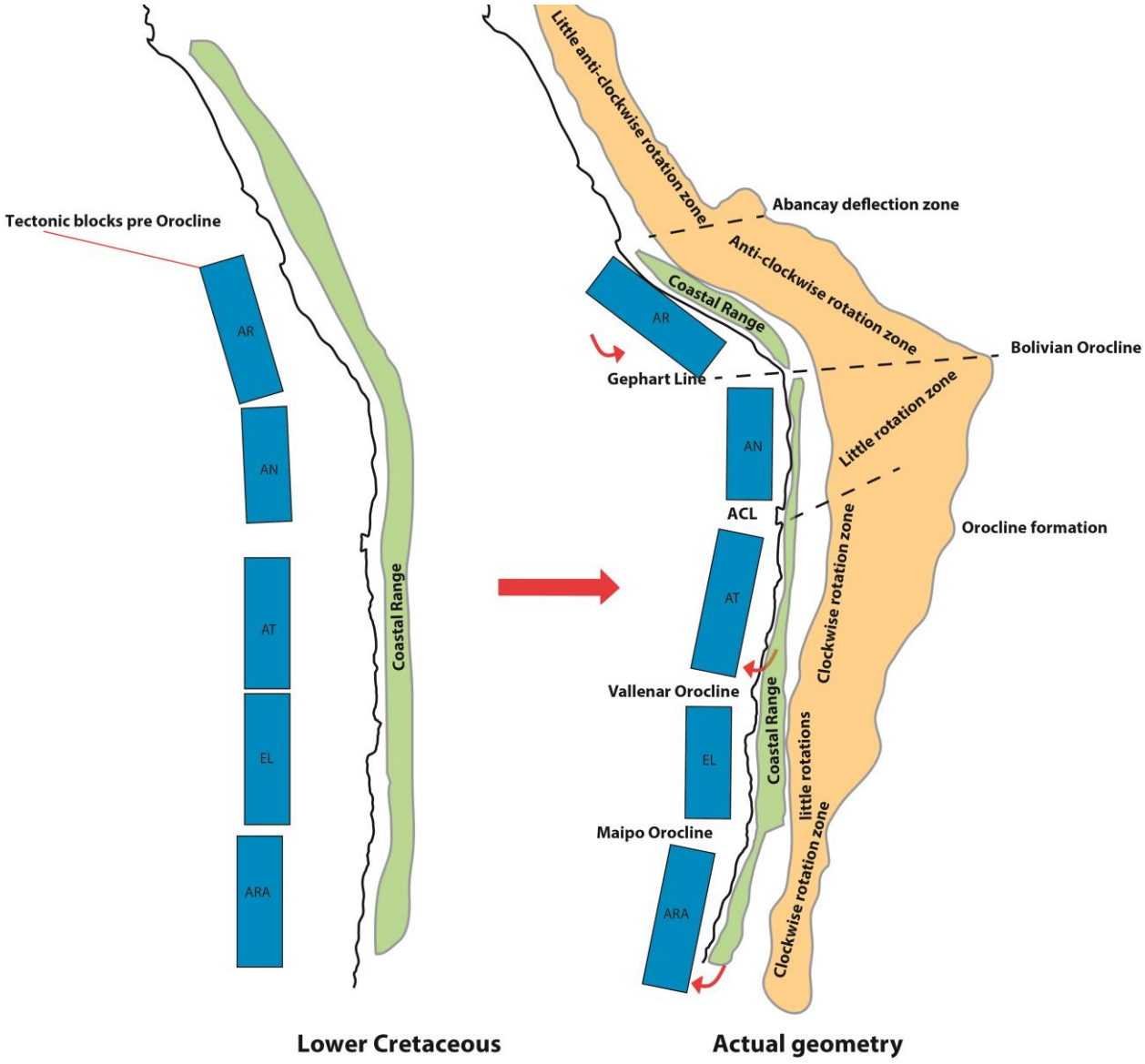

Figura 5.21: Formación de la Cordillera de la costa (en verde) en el Cetácico Inferior y su posterior flexuramiento en el Cretácico Superior en adelante. La posterior formación de la Cordillera de los Andes (en naranjo) sincronica a rotaciones tectónicas producidas en su interior, nos permite redefinir los conceptos oroclinales en los Andes Centrales.

5.7.- Sintesis de la discusión

A modo de síntesis de los distintos puntos discutidos antes, podemos resumir que:

(a) Existe efectivamente una sectorización latitudinal y longitudinal de los patrones de rotación tectónica, pudiendo ligar estos a distintas edades de deformación relacionados al orógeno Andino.

(b) Algunos de los limites de los patrones rotacionales parecen estar bien definidos en los datos, como el limite entre el patron de rotaciones leves al norte de los 23°S y el patron de rotaciones horarias fuertes al sur de la misma coordenada; asi como existen ciertos limites difusos, como el limite alrededor de los 33°S. Este ultimo limite pudiendo ser su limitante la falta de densidad de datos en la zona.

(c) Existe una relación de ciertos patrones estructurales, como limites de terrenos acrecionados propuestos y zonas de cuencas Mesozoicas, y patrones de rotaciones tectónicas. Estas correlaciones espaciales son en su mayoría difusas, pero ciertas estructuras, como el Lineamiento Antofagasta-Calama, muestran un rol principal en la segmentación del patron de rotaciones tectónicas.

(d) De la misma forma, la correlación entre heterogeneidades positivas de la placa subductada y de patrones de rotaciones tectónicas parece ser difusa, no pasando la prueba de una correlación espacio-temporal de forma clara. La propuesta de subducción de una gran heterogeneidad positiva que haya gatillado la formación del Oroclino Boliviano no puede descartarse, pero en este mismo trabajo se ha observado que rasgos estructurales heredados pueden jugar un rol mayor que ridges asísmicos o zonas de fracturas.

(e) El concepto de Oroclino puede ser revisado, con respecto a la cordillera Andina, estando la Cordillera de los Andes mas cercana al concepto de Arco Progresivo, el Arco Progresivo Boliviano, y la Cordillera de la Costa mas cercana a un Oroclino, el Oroclino de Arica.

6: Conclusiones

Dentro de las conclusiones que podemos obtener de los datos obtenidos están:

-Existe un patrón de rotaciones horarias en el antearco entre 23° y 29°S de una magnitud de aproximadamente 30°. Estas rotaciones están intrínsecamente relacionadas con los eventos de deformación compresional, debiendose no solo a los efectos del evento compresional Eoceno-Oligoceno, sino que evidenciando eventos anteriores, como los eventos del Cretácico Superior y del límite Cretácico-Paleoceno. Estos patrones no se mantienen hacia los dominios orientales de la Cordillera, siendo las rotaciones en el dominio austral de la Puna menores que las rotaciones del dominio de Sierras Pampeanas.

-Existe un patrón de rotaciones leves, casi nulas, entre los 18,5° y 23° de latitud sur del ante-arco. Este patrón de rotaciones leves afecta a rocas desde el Triásico en adelante, mostrando como esta zona no sufrió una mayor deformación rotacional en los eventos compresionales andinos. Sin embargo, es posible hacer una segmentación alrededor de los 21° de latitud sur para las rotaciones que se encuentran en los dominios de las Sierras Subandinas-Altiplano.

-Los patrones de rotaciones tectónicas no son afectados por movimientos de rumbo en los sistemas de fallas de Atacama y Domeyko, estando las rotaciones tectónicas de la cordillera de la costa acopladas con las de la precordillera-cordillera Principal en Chile.

-La edad de los eventos rotacionales en el ante-arco chileno se relaciona a eventos compresivos más antiguos que los relacionados al evento Incaico, siendo los eventos del Cretácico Superior y K-T, los primeros pasos para la deformación rotacional horaria entre la Cordillera de la Costa – Cordillera Frontal en el norte de Chile entre los 23°-29° de latitud Sur. Sin embargo, el evento Incaico sigue siendo el evento de deformación rotacional que mayor magnitud de deformación produce en el Oroclino Boliviano.

-Existe una fuerte correlación de rasgos estructurales y tectónicos mayores con los limites de los patrones rotacionales, siendo algunos rasgos mas importantes (como el LAC o ciertos limites de cuencas Mesozoicas) que otros.

-Las heterogeneidades de la placa subductante pueden producir cierta influencia en la deformación de la placa superior, pero de forma secundaria respecto a los rasgos heredados en la placa continental, observando que la correlación entre subducción de ridges asísmicos y cambios en la deformarción es baja, exceptuando por el ridge de Juan Fernandez.

Bibliografía

Abels, A., Bischoff, L. (1999). Clockwise block rotations in northern Chile: Indications for a large-scale domino mechanism during the middle-late Eocene. Geology, 27(8), 751-754.

Allmendinger, R. W., Jordan, T. E., Kay, S. M., Isacks, B. L. (1997). The evolution of the Altiplano-Puna plateau of the Central Andes. *Annual review of earth and planetary sciences*, *25*(1), 139-174.

Alonso-Muruaga, P. J., Limarino, C. O., Spalletti, L. A., & Piñol, F. C. (2018). Depositional settings and evolution of a fjord system during the carboniferous glaciation in Northwest Argentina. Sedimentary Geology, 369, 28-45.

Álvarez, J., Mpodozis, C., Blanco-Quintero, I., García-Casco, A., Arriagada, C., & Morata, D. (2013). U–Pb ages and metamorphic evolution of the La Pampa Gneisses: Implications for the evolution of the Chilenia Terrane and Permo-Triassic tectonics of north Central Chile. Journal of South American Earth Sciences, 47, 100-115.

Amilibia, A., Sàbat, F., McClay, K. R., Muñoz, J. A., Roca, E., Chong, G. (2008). The role of inherited tectono- sedimentary architecture in the development of the central Andean mountain belt: Insights from the Cordillera de Domeyko. Journal of Structural Geology, vol 30 (12), 1520-1539.

Ammirati, J. B., Alvarado, P., Beck, S. (2015). A lithospheric velocity model for the flat slab region of Argentina from joint inversion of Rayleigh wave phase velocity dispersion and teleseismic receiver functions. Geophysical Journal International, 202(1), 224-241.

Ardill, J., Flint, S., Chong, G., & Wilke, H. (1998). Sequence stratigraphy of the Mesozoic Domeyko basin, northern Chile. Journal of the Geological Society, 155(1), 71-88.

Arévalo, C. (1994). Mapa geológico del cuadrángulo Los Loros. Servicio Nacional de Geología y Minería, Documentos de Trabajo, (6).

Arévalo, C. (2005). Carta Copiapó, Región de Atacama. Servicio Nacional de Geología y Minería, Carta Geológica de Chile, Serie Geología Básica, 91, 54.

Arriagada, C., Roperch, P., & Mpodozis, C. (2000). Clockwise block rotations along the eastern border of the Cordillera de Domeyko, northern Chile (22 45′–23 30′ S). Tectonophysics, 326(1), 153-171.

Arriagada, C., Roperch, P., Mpodozis, C., Dupont-Nivet, G., Cobbold, P. R., Chauvin, A., Cortés, J. (2003). Paleogene clockwise tectonic rotations in the forearc of central Andes, Antofagasta region, northern Chile. *Journal of Geophysical Research: Solid Earth*, *108*(B1).

Arriagada, C., Roperch, P., Mpodozis, C., Fernandez, R. (2006a). Paleomagnetism and tectonics of the southern Atacama Desert (25–28 S), northern Chile. *Tectonics*, *25*(4).

Arriagada, C., Cobbold, P. R., Roperch, P. (2006b). Salar de Atacama basin: A record of compressional tectonics in the central Andes since the mid-Cretaceous. *Tectonics*, *25*(1).

Arriagada, C., Roperch, P., Mpodozis, C., Cobbold, P.R. (2008). Paleogene building of the Bolivian Orocline, Tectonic restoration. TECTONICS, VOL. 27, TC6014, doi:10.1029/2008TC002269.

Arriagada, C., Roperch, P., Mpodozis, C., Charrier, R., Yanez, G., & Farias, M. (2009, May). The Vallenar Discontinuity and the Maipo Orocline: Regional significance of clockwise vertical-axis rotations in the central Chilean Andes. In AGU Spring Meeting Abstracts.

Arriagada, C., Ferrando, R., Córdova, L., Morata, D., Roperch, P. (2013). The Maipo Orocline: a first scale structural feature in the Miocene to Recent geodynamic evolution in the central Chilean Andes. *Andean Geology*, *40*(3), 419-437.

Astudillo, N., Roperch, P., Townley, B., Arriagada, C., Maksaev, V. (2008). Importance of small-block rotations in damage zones along transcurrent faults. Evidence from the Chuquicamata open pit, Northern Chile. Tectonophysics, 450(1-4), 1-20.

Aubry, L., Roperch, P., de Urreiztieta, M., Rossello, E., Chauvin, A. (1996). Paleomagnetic study along the southeastern edge of the Altiplano-Puna Plateau: Neogene tectonic rotations. Journal of Geophysical Research: Solid Earth, 101(B8), 17883-17899.

Baby, P., Rochat, P., Mascle, G., Hérail, G. (1997). Neogene shortening contribution to crustal thickening in the back arc of the Central Andes. Geology, 25(10), 883-886.

Bahlburg, H., Berndt, J. (2016). Provenance from zircon U–Pb age distributions in crustally contaminated granitoids. Sedimentary geology, 336, 161-170.

Barazangi, M., Isacks, B. L. (1976). Spatial distribution of earthquakes and subduction of the Nazca plate beneath South America. *Geology*, *4*(11), 686-692.

Barazangi, M., Isacks, B. L. (1979). Subduction of the Nazca plate beneath Peru: evidence from spatial distribution of earthquakes. Geophysical Journal International, 57(3), 537-555.

Barckhausen, U., Ranero, C. R., von Huene, R., Cande, S. C., Roeser, H. A. (2001). Revised tectonic boundaries in the Cocos Plate off Costa Rica: Implications for the segmentation of the convergent margin and for plate tectonic models. Journal of Geophysical Research: Solid Earth, 106(B9), 19207-19220.

Bascuñán, S., Arriagada, C., Le Roux, J., Deckart, K. (2016). Unraveling the Peruvian Phase of the Central Andes: stratigraphy, sedimentology and geochronology of the Salar de Atacama Basin (22 30–23 S), northern Chile. Basin Research, 28(3), 365-392.

Barnes, J. B., Ehlers, T. A., McQuarrie, N., O'sullivan, P. B., & Tawackoli, S. (2008). Thermochronometer record of central Andean Plateau growth, Bolivia (19.5 S). Tectonics, 27(3).

Barnes, J. B., & Ehlers, T. A. (2009). End member models for Andean Plateau uplift. Earth-Science Reviews, 97(1-4), 105-132.

Bayona, G., Rapalini, A., Costanzo-Alvarez, V. (2006). Paleomagnetism in Mesozoic rocks of the northern Andes and its implications in Mesozoic tectonics of northwestern South America. *Earth, planets and space*, *58*(10), 1255-1272.

Beck, M. E. (1988). Analysis of Late Jurassic-Recent paleomagnetic data from active plate margins of South America. Journal of South American Earth Sciences, 1(1), 39-52.

Bellahsen, N., Sébrier, M., Siame, L. (2016). Crustal shortening at the Sierra Pie de Palo (Sierras Pampeanas, Argentina): near-surface basement folding and thrusting. Geological Magazine, 153(5-6), 992-1012.

Bello-González, J. P., Contreras-Reyes, E., Arriagada, C. (2018). Predicted path for hotspot tracks off South America since Paleocene times: Tectonic implications of ridge-trench collision along the Andean margin. Gondwana Research, 64, 216-234.

Beltrando, M., Lister, G. S., Rosenbaum, G., Richards, S., Forster, M. A. (2010). Recognizing episodic lithospheric thinning along a convergent plate margin: The example of the Early Oligocene Alps. *Earth-Science Reviews*, *103*(3-4), 81-98.

Besse, J., & Courtillot, V. (2002). Apparent and true polar wander and the geometry of the geomagnetic field over the last 200 Myr. Journal of Geophysical Research: Solid Earth (1978–2012), 107(B11), EPM-6.

Bishop, B. T., Beck, S. L., Zandt, G., Wagner, L., Long, M., Antonijevic, S. K., ... & Tavera, H. (2017). Causes and consequences of flat-slab subduction in southern Peru. Geosphere, 13(5), 1392-1407.

Blanco, N.; Vásquez, P.; Sepúlveda, F.A.; Tomlinson, A.J.; Quezada, A.; Ladino, M. 2012. Levantamiento geológico para el fomento de la exploración de recursos minerales e hídricos de la Cordillera de la Costa, Depresión Central y Precordillera de la Región de Tarapacá (20°-21°S). Servicio Nacional de Geología y Minería, Informe Registrado IR-12-50: 246 p., 7 mapas escala 1:100.000. Santiago.

Blanco, N., & Tomlinson, A. (2013). Carta Guatacondo. Región de Tarapacá. Servicio Nacional de Geología y Minería, Serie.

Boutelier, D. A., & Oncken, O. (2010). Role of the plate margin curvature in the plateau buildup: Consequences for the central Andes. Journal of Geophysical Research: Solid Earth, 115(B4).

Cahill, T., Isacks, B. L. (1992). Seismicity and shape of the subducted Nazca plate. Journal of Geophysical Research: Solid Earth, 97(B12), 17503-17529.

Carey, S. W. (1955). The orocline concept in geotectonics-Part I. In *Papers and proceedings of the Royal Society of Tasmania*(Vol. 89, pp. 255-288).

Capitanio, F. A., Faccenna, C., Zlotnik, S., Stegman, D. R. (2011). Subduction dynamics and the origin of Andean orogeny and the Bolivian orocline. *Nature*, *480*(7375), 83.

Carrapa, B., Strecker, M. R., & Sobel, E. R. (2006). Cenozoic orogenic growth in the Central Andes: Evidence from sedimentary rock provenance and apatite fission track thermochronology in the Fiambalá Basin, southernmost Puna Plateau margin (NW Argentina). Earth and Planetary Science Letters, 247(1-2), 82-100.

Carrapa, B., & DeCelles, P. G. (2008). Eocene exhumation and basin development in the Puna of northwestern Argentina. Tectonics, 27(1).

Carrapa, B., DeCelles, P. G. (2015). Regional exhumation and kinematic history of the central Andes in response to cyclical orogenic processes. Geol. Soc. Am. Mem, 212, 201-213.

Carrapa, B., Reyes-Bywater, S., Safipour, R., Sobel, E. R., Schoenbohm, L. M., DeCelles, P. G., Stockli, D. (2014). The effect of inherited paleotopography on exhumation of the Central Andes of NW Argentina. Bulletin, 126(1-2), 66-77.

Cembrano, J., González, G., Arancibia, G., Ahumada, I., Olivares, V., Herrera, V. (2005). Fault zone development and strain partitioning in an extensional strike-slip

duplex: A case study from the Mesozoic Atacama fault system, Northern Chile. Tectonophysics, 400(1-4), 105-125.

Césari, S. N., & Limarino, C. O. (2002). Palynology of glacial sediments from the Guandacol Formation (Middle Carboniferous) in the Cerro Bola area, Paganzo Basin, Argentina. Alcheringa, 26(1), 159-176.

Charrier, R., Baeza, O., Elgueta, S., Flynn, J. J., Gans, P., Kay, S. M., Zurita, E. (2002). Evidence for Cenozoic extensional basin development and tectonic inversion south of the flat-slab segment, southern Central Andes, Chile (33–36 SL). Journal of South American Earth Sciences, 15(1), 117-139.

Charrier, R., Pinto, L., & Rodríguez, M. P. (2007). Tectonostratigraphic evolution of the Andean Orogen in Chile. The geology of Chile (Moreno, T.; gibbons, W.; editors). The geological Society, 21-114.

Charrier, R., Hérail, G., Pinto, L., García, M., Riquelme, R., Farías, M., Muñoz, N. (2013). Cenozoic tectonic evolution in the Central Andes in northern Chile and west central Bolivia: implications for paleogeographic, magmatic and mountain building evolution. *International Journal of Earth Sciences*, *102*(1), 235-264.

Cobbold, P. R., Rossello, E. A., Roperch, P., Arriagada, C., Gómez, L.A., Lima, C. (2007). Distribution, timing, and causes of Andean deformation across South America. The Geological Society, London, Special Publications, 272, 321-343.

Coira, B., Davidson, J., Mpodozis, C., & Ramos, V. (1982). Tectonic and magmatic evolution of the Andes of northern Argentina and Chile. Earth-Science Reviews, 18(3-4), 303-332.

Contreras Figueroa, J. P. (2018). Segmentación de patrones de rotación tectónica delimitados por la falla Taltal: Cordillera de la Costa del Norte de Chile (25°-26° Latitud Sur). Tesis para optar al grado de Magíster en Ciencias, Mención Geología. Departamento de Geología, Universidad de Chile, Santiago, Chile.

Contreras-Reyes, E., Carrizo, D. (2011). Control of high oceanic features and subduction channel on earthquake ruptures along the Chile–Peru subduction zone. Physics of the Earth and Planetary Interiors, 186(1-2), 49-58.

Contreras-Reyes, E., Muñoz-Linford, P., Cortés-Rivas, V., Bello-González, J. P., Ruiz, J. A., Krabbenhoeft, A. (2019). Structure of the collision zone between the Nazca ridge and the Peruvian convergent margin: geodynamic and seismotectonic implications. Tectonics, 38(9), 3416-34

Contreras-Reyes, E., Obando-Orrego, S., Geersen, J., Bello-González, J. P. (2021). Density structure, flexure, and tectonics of the Iquique Ridge, northern Chile. Journal of South American Earth Sciences, 103423. 35.

Copley, A., McKenzie, D. (2007). Models of crustal flow in the India-Asia collision zone. Geophysical Journal International, 169(2), 683-698.

Cornejo, P. C., Mpodozis, C., Kay, S. M., Tomlinson, A. J., & Ramirez, C. F. (1993). Upper cretaceous-lower eocene potassic volcanism in an extensional regime in the precordillera of Copiapo, Chile.

Cornejo, P., & Mpodozis, C. (1996). Geología de la región de Sierra Exploradora (25-26 S). Servicio Nacional de Geología y Minería, Informe Registrado IR-96-09, 9.

Cornejo, P., Mpodozis, C., & Andrew J.. Tomlinson. (1998). Hoja Salar de Maricunga, Región de Atacama. Servicio nacional de geología y minería.

Cornejo, P., & Matthews, S. (2001). Evolution of Magmatism from the Uppermost Cretaceous to Oligocene, and its relationship to changing tectonic regime, in the Inca de Oro-El Salvador area (northern Chile).

Cornejo, R., Matthews, S., Pérez de Arce, C. (2003). The 'K-T' compressive deformation event in northern Chile (24-27°S). In Congreso Geológico Chileno, No. 10, Actas, CD-Rom, Sesión Temática 1. Concepción.

Creixell, C.; Labbé, M.; Arévalo, C.; Salazar, E. 2013. Geología del área Estación Chañar-Junta de Chingoles, Regiones de Atacama y Coquimbo. Servicio Nacional

de Geología y Minería, Carta Geológica de Chile, Serie Geología Básica, No. 150, 1 mapa escala 1:100.000. Santiago.

Cristallini, E. O., Ramos, V. A. (2000). Thick-skinned and thin-skinned thrusting in the La Ramada fold and thrust belt: crustal evolution of the High Andes of San Juan, Argentina (32 SL). Tectonophysics, 317(3-4), 205-235.

Coutand, I., Chauvin, A., Cobbold, P. R., Gautier, P., Roperch, P. (1999). Vertical axis rotations across the Puna plateau (northwestern Argentina) from paleomagnetic analysis of Cretaceous and Cenozoic rocks. *Journal of Geophysical Research: Solid Earth*, *104*(B10), 22965-22984.

Dana, J. D. (1866). Observations on the origin of some of the Earth's Features. *American Journal of Science and Arts (1820-1879)*, *42*(125), 205.

Darwin, C. (1846). Geological observations on South America: Being the third part of the geology of the voyage of the Beagle, under the command of Capt. Fitzroy, RN during the years 1832 to 1836. Smith, Elder and Company, 65, Cornhill.

Dávila, F. M., Giménez, M. E., Nóbile, J. C., & Martínez, M. P. (2012). The evolution of the high-elevated depocenters of the northern Sierras Pampeanas (ca. 28˚ SL), Argentine broken foreland, South-Central Andes: the Pipanaco Basin. Basin Research, 24(6), 615-636.

Dávila, F. M., Carter, A. (2013). Exhumation history of the Andean broken foreland revisited. *Geology*, *41*(4), 443-446.

Davy, P., Cobbold, P. R. (1988). Indentation tectonics in nature and experiment. 1. Experiments scaled for gravity. *Bull. Geol. Inst. Univ. Uppsala*, *14*, 129-141.

DeCelles, P. G., Robinson, D. M., Zandt, G. (2002). Implications of shortening in the Himalayan fold-thrust belt for uplift of the Tibetan Plateau. *Tectonics*, *21*(6), 12-1.

Dediós, P. (1967). Cuadrángulo Vicuña, Provincia de Coquimbo. Instituto de Investigaciones Geológicas, Carta Geológica de Chile, (16), 65.

Deckart, K., Hervé, F., Fanning, C. M., Ramírez, V., Calderón, M., & Godoy, E. (2014). Geocronología U-Pb e isótopos de Hf-O en circones del batolito de la Costa Pensilvaniana, Chile. Andean geology, 41(1), 49-82.

Del Papa, C., Hongn, F., Powell, J., Payrola, P., Do Campo, M., Strecker, M. R. & Pereyra, R. (2013). Middle Eocene-Oligocene broken-foreland evolution in the Andean Calchaqui Valley, NW Argentina: insights from stratigraphic, structural and provenance studies. Basin Research, 25(5), 574-593.

Demarest Jr, H. H. (1983). Error analysis for the determination of tectonic rotation from paleomagnetic data. Journal of Geophysical Research: Solid Earth, 88(B5), 4321-4328.

De Silva, S. L. (1989). Altiplano-Puna volcanic complex of the central Andes. Geology, 17(12), 1102-1106.

De Urreiztieta, M., Gapais, D., Le Corre, C., Cobbold, P. R., & Rossello, E. (1996). Cenozoic dextral transpression and basin development at the southern edge of the Puna Plateau, northwestern Argentina. Tectonophysics, 254(1-2), 17-39.

Dewey, J. F., Bird, J. M. (1970). Mountain belts and the new global tectonics. *Journal of Geophysical Research*, *75*(14), 2625-2647.

Doglioni, C., Carminati, E., Cuffaro, M., Scrocca, D. (2007). Subduction kinematics and dynamic constraints. Earth-Science Reviews, 83(3-4), 125-175.

Dominguez, S., Lallemand, S., Malavieille, J., Schnürle, P. (1998). Oblique subduction of the Gagua Ridge beneath the Ryukyu accretionary wedge system: Insights from marine observations and sandbox experiments. *Marine Geophysical Researches*, *20*(5), 383-402.

Eichelberger, N., McQuarrie, N., Ryan, J., Karimi, B., Beck, S., Zandt, G. (2015). Evolution of crustal thickening in the central Andes, Bolivia. *Earth and Planetary Science Letters*, *426*, 191-203.

Elger, K., Oncken, O., & Glodny, J. (2005). Plateau-style accumulation of deformation: Southern Altiplano. Tectonics, 24(4).

Emparan, C., & Pineda, G. (1999). Área Condoriaco-Rivadavia, Región de Coquimbo. Servicio nacional de geolog'ia y miner'ia.

Emparan, C., & Pineda, G. (2000). Área La Serena-La Higuera, Región de Coquimbo. Servicio Nacional de Geología y Minería, Mapas Geológicos, 18.

Escayola, M. P., van Staal, C. R., Davis, W. J. (2011). The age and tectonic setting of the Puncoviscana Formation in northwestern Argentina: An accretionary complex related to Early Cambrian closure of the Puncoviscana Ocean and accretion of the Arequipa-Antofalla block. Journal of South American Earth Sciences, 32(4), 438-459.

Farías, M., Charrier, R., Comte, D., Martinod, J., Hérail, G. (2005). Late Cenozoic deformation and uplift of the western flank of the Altiplano: Evidence from the depositional, tectonic, and geomorphologic evolution and shallow seismic activity (northern Chile at 19 30′ S). *Tectonics*, *24*(4).

Farías, M., Charrier, R., Carretier, S., Martinod, J., Fock, A., Campbell, D., Comte, D. (2008). Late Miocene high and rapid surface uplift and its erosional response in the Andes of central Chile (33–35 S). *Tectonics*, *27*(1).

Farías, M., Comte, D., Charrier, R., Martinod, J., David, C., Tassara, A., Fock, A. (2010). Crustal-scale structural architecture in central Chile based on seismicity and surface geology: Implications for Andean mountain building. Tectonics, 29(3).

Ferrando, R., Roperch, P., Morata, D., Arriagada, C., Ruffet, G., Córdova, M. L. (2014). A paleomagnetic and magnetic fabric study of the Illapel Plutonic Complex, Coastal Range, central Chile: Implications for emplacement mechanism and regional tectonic evolution during the mid-Cretaceous. *Journal of South American Earth Sciences*, *50*, 12-26.

Flint, S., Turner, P., Jolley, E. J., Hartley, A. J. (1993). Extensional tectonics in convergent margin basins: An example from the Salar de Atacama, Chilean Andes. Geological Society of America Bulletin, 105(5), 603-617.

Flórez-Rodríguez, A. G., Schellart, W. P., Strak, V. (2019). Impact of aseismic ridges on subduction systems: insights from analog modeling. Journal of Geophysical Research: Solid Earth, 124(6), 5951-5969.

Forsythe, R., Chisholm, L. (1994). Paleomagnetic and structural constraints on rotations in the north Chilean coast ranges. Journal of South American Earth Sciences, 7(3-4), 279-294.

Fuentes, G., Martínez, F., Bascuñan, S., Arriagada, C., Muñoz, R. (2018). Tectonic architecture of the Tarapacá Basin in the northern Central Andes: New constraints from field and 2D seismic data. Geosphere, 14(6), 2430-2446.

Gana, F. (1991). Mapa geológico de la cordillera de la costa entre La Serena y Quebrada El Teniente: Región de Coquimbo.

García, M., Gardeweg, M., Clavero, J., & Hérail, G. (2004). Hoja Arica, Región de Tarapacá, escala 1: 250.000, Carta Geológica de Chile Nº 84.

García, M., Riquelme, R., Farías, M., Hérail, G., Charrier, R. (2011). Late Miocene–Holocene canyon incision in the western Altiplano, northern Chile: tectonic or climatic forcing?. Journal of the Geological Society, 168(4), 1047-1060.

Gardeweg, M., & Ramírez, C. F. (1987). La Pacana caldera and the Atana ignimbrite—a major ash-flow and resurgent caldera complex in the Andes of northern Chile. Bulletin of Volcanology, 49(3), 547-566.

Garzione, C. N., Molnar, P., Libarkin, J. C., MacFadden, B. J. (2006). Rapid late Miocene rise of the Bolivian Altiplano: Evidence for removal of mantle lithosphere. Earth and Planetary Science Letters, 241(3-4), 543-556.

Gephart, J. W. (1994). Topography and subduction geometry in the central Andes: Clues to the mechanics of a noncollisional orogen. Journal of Geophysical Research: Solid Earth (1978–2012), 99(B6), 12279-12288.

Giambiagi, L. B., Ramos, V. A. (2002). Structural evolution of the Andes in a transitional zone between flat and normal subduction (33 30′–33 45′ S), Argentina and Chile. Journal of South American Earth Sciences, 15(1), 101-116.

Giambiagi, L. B., Alvarez, P. P., Godoy, E., Ramos, V. A. (2003). The control of pre-existing extensional structures on the evolution of the southern sector of the Aconcagua fold and thrust belt, southern Andes. Tectonophysics, 369(1-2), 1-19.

Giambiagi, L., Mescua, J., Bechis, F., Tassara, A., Hoke, G. (2012). Thrust belts of the southern Central Andes: Along-strike variations in shortening, topography, crustal geometry, and denudation. Bulletin, 124(7-8), 1339-1351.

Goguitchaichvili, A., Alva-Valdivia, L. M., & Urrutia-Fucugauchi, J. (2003). Paleomagnetism and rock magnetism of the Jurassic La Negra Formation, northern Chile: Implications for tectonics and volcanic stratigraphy. International Geology Review, 45(6), 563-573.

Gómez, J., Schobbenhaus, C. & Montes, N.E., compilers. 2019. Geological Map of South America 2019. Scale 1:5 000 000. Commission for the Geological Map of the World (CGMW), Colombian Geological Survey, and Geological Survey of Brazil. Paris. https://doi.org/10.32685/10.143.2019.929

González, D., Pinto, L., Peña, M., & Arriagada, C. (2012). 3D deformation in strike-slip systems: Analogue modelling and numerical restoration. Andean Geology, 39(2), 295-316.

Goss, A. R., Kay, S. M., Mpodozis, C. (2013). Andean adakite-like high-Mg andesites on the northern margin of the Chilean–Pampean flat-slab (27–28· 5° S) associated with frontal arc migration and fore-arc subduction erosion. Journal of Petrology, 54(11), 2193-2234.

Gotberg, N., McQuarrie, N., & Caillaux, V. C. (2010). Comparison of crustal thickening budget and shortening estimates in southern Peru (12–14 S): Implications for mass balance and rotations in the “Bolivian orocline”. Bulletin, 122(5-6), 727-742.

Graeber, F.M. & Asch, G. 1999. Three-dimensional models of P waves velocity and P-to-S velocity ratio in the southern central Andes by simultaneous inversion of local earthquake data. Journal of Geophysical Research B 104 (9), 20237-56.

Grunder, A. L., Klemetti, E. W., Feeley, T. C., & McKee, C. M. (2008). Eleven million years of arc volcanism at the Aucanquilcha Volcanic Cluster, northern Chilean Andes: implications for the life span and emplacement of plutons. Earth and Environmental Science Transactions of the Royal Society of Edinburgh, 97(4), 415-436.

Gutiérrez-Alonso, G., Johnston, S. T., Weil, A. B., Pastor-Galán, D., Fernández-Suárez, J. (2012). Buckling an orogen: the Cantabrian Orocline. *GSA Today*, *22*(7), 4-9.

Gutscher, M. A., Spakman, W., Bijwaard, H., Engdahl, E. R. (2000). Geodynamics of flat subduction: Seismicity and tomographic constraints from the Andean margin. Tectonics, 19(5), 814-833.

Gutscher, M. A. (2002). Andean subduction styles and their effect on thermal structure and interplate coupling. Journal of South American Earth Sciences, 15(1), 3-10.

Hampel, A., Kukowski, N., Bialas, J., Huebscher, C., Heinbockel, R. (2004). Ridge subduction at an erosive margin: The collision zone of the Nazca Ridge in southern Peru. Journal of Geophysical Research: Solid Earth, 109(B2).

Haynie, K. L., Jadamec, M. A. (2017). Tectonic drivers of the Wrangell block: Insights on fore-arc sliver processes from 3-D geodynamic models of Alaska. Tectonics, 36(7), 1180-1206.

Hayes, G., 2018, Slab2 - A Comprehensive Subduction Zone Geometry Model: U.S. Geological Survey data release, https://doi.org/10.5066/F7PV6JNV.

Heki, K., Hamano, Y., Kinoshita, H., Taira, A., Kono, M. (1984). Paleomagnetic study of Cretaceous rocks of Peru, South America: evidence for rotation of the Andes. *Tectonophysics*, *108*(3-4), 267-281.

Heki, K., Hamano, Y. O. Z. O., Kono, M., Ui, T. (1985). Palaeomagnetism of Neogene Ocros dyke swarm, the Peruvian Andes: implication for the Bolivian orocline. *Geophysical Journal of the Royal Astronomical Society*, *80*(2), 527-534.

Henriquez González, S. (2012). Estructura del salar de Atacama:|bimplicancias en la estructura cortical de los Andes Centrales. Disponible en http://www.tesis.uchile.cl/handle/2250/113550.

Hernandez-Moreno, C., Speranza, F., & Di Chiara, A. (2014). Understanding kinematics of intra-arc transcurrent deformation: Paleomagnetic evidence from the Liquiñe-Ofqui fault zone (Chile, 38–41 S). Tectonics, 33(10), 1964-1988.

Hervé, F., Calderón, M., Fanning, C. M., Pankhurst, R. J., & Godoy, E. (2013). Provenance variations in the Late Paleozoic accretionary complex of central Chile as indicated by detrital zircons. Gondwana Research, 23(3), 1122-1135.

Hobbs, W. H. (1914). Mechanics of formation of arcuate Mountains. *The Journal of Geology*, *22*(3), 193-208.

Hoke, G. D., Isacks, B. L., Jordan, T. E., Blanco, N., Tomlinson, A. J., Ramezani, J. (2007). Geomorphic evidence for post-10 Ma uplift of the western flank of the central Andes 18 30′–22 S. Tectonics, 26(5).

Howell, J. A., Schwarz, E., Spalletti, L. A., Veiga, G. D. (2005). The Neuquén basin: an overview. Geological Society, London, Special Publications, 252(1), 1-14.

Hu, J., Liu, L., Hermosillo, A., Zhou, Q. (2016). Simulation of late Cenozoic South American flat-slab subduction using geodynamic models with data assimilation. Earth and Planetary Science Letters, 438, 1-13.

Huang, X., Xu, Z., Li, H., & Cai, Z. (2015). Tectonic amalgamation of the Gaoligong shear zone and Lancangjiang shear zone, southeast of Eastern Himalayan Syntaxis. Journal of Asian Earth Sciences, 106, 64-78.

Hutchison, C. S. (2010). Oroclines and paleomagnetism in Borneo and south-east Asia. *Tectonophysics*, *496*(1-4), 53-67.

Iaffaldano, G., Di Giuseppe, E., Corbi, F., Funiciello, F., Faccenna, C., Bunge, H. P. (2012). Varying mechanical coupling along the Andean margin: Implications for trench curvature, shortening and topography. *Tectonophysics*, *526*, 16-23.

Ibarra, F., Prezzi, C. B., Bott, J., Scheck-Wenderoth, M., Strecker, M. R. (2021). Distribution of temperature and strength in the Central Andean lithosphere and its relationship to seismicity and active deformation. Journal of Geophysical Research: Solid Earth, e2020JB021231.

Iriarte, S., Arévalo, C., Mpodozis, C., & Rivera, O. (1996). Mapa Geológico de la Hoja Carrera Pinto, escala 1: 1.00. 000. Servicio Nacional de Geología y Minería (Chile), Mapas Geológicos, (3).

Iriarte, S., Arévalo, C., & Mpodozis, C. (1999). Hoja La Guardia, Región de Atacama. Servicio nacional de geología y minería.

Irwin, J. J., García, C., Hervé, F., & Brook, M. (1988). Geology of part of a long-lived dynamic plate margin: the coastal cordillera of north-central Chile, latitude 30 51'-31 S. Canadian Journal of Earth Sciences, 25(4), 603-624.

Isacks, B. L. (1988). Uplift of the central Andean plateau and bending of the Bolivian orocline. *Journal of Geophysical Research: Solid Earth*, *93*(B4), 3211-3231.

Jacobs, J., Thomas, R. J. (2004). Himalayan-type indenter-escape tectonics model for the southern part of the late Neoproterozoic–early Paleozoic East African–Antarctic orogen. *Geology*, *32*(8), 721-724.

Japas, M. S., Ré, G. H., Oriolo, S., Vilas, J. F. (2016). Palaeomagnetic data from the Precordillera fold and thrust belt constraining Neogene foreland evolution of the

Pampean flat-slab segment (Central Andes, Argentina). *Geological Society, London, Special Publications*, *425*(1), 81-105.

Jara, P., Likerman, J., Winocur, D., Ghiglione, M. C., Cristallini, E. O., Pinto, L., Charrier, R. (2015). Role of basin width variation in tectonic inversion: insight from analogue modelling and implications for the tectonic inversion of the Abanico Basin, 32°–34° S, Central Andes. Geological Society, London, Special Publications, 399(1), 83-107.

Jara, P., Likerman, J., Charrier, R., Herrera, S., Pinto, L., Villarroel, M., Winocur, D. (2017). Closure type effects on the structural pattern of an inverted extensional basin of variable width: Results from analogue models. Journal of South American Earth Sciences.

Jensen, O. 1976. Geología de las nacientes del río Copiapó entre los 27°53' y 28°20' Lat. sur, provincia de Atacama, Chile: Santiago, Universidad de Chile, Departamento de Geologia, Memoria de Titulo, 299 p.

Jordán, T. E., Isacks, B. L., Allmendinger, R. W., Brewer, J. A., Ramos, V. A., Ando, C. J. (1983). Andean tectonics related to geometry of subducted Nazca plate. Geological Society of America Bulletin, 94(3), 341-361.

Jordan, T. E., Isacks, B., Ramos, V. A., Allmendinger, R. W. (1983). Mountain building in the Central Andes. *Episodes*, *3*(3), 20-26.

Jordan, T. E., Mpodozis, C., Munoz, N., Blanco, N., Pananont, P., & Gardeweg, M. (2007). Cenozoic subsurface stratigraphy and structure of the Salar de Atacama Basin, northern Chile. Journal of South American Earth Sciences, 23(2-3), 122-146.

Jordan, T. E., Nester, P. L., Blanco, N., Hoke, G. D., Dávila, F., Tomlinson, A. J. (2010). Uplift of the Altiplano-Puna plateau: A view from the west. Tectonics, 29(5).

Johnston, S. T. (2001). The Great Alaskan Terrane Wreck: reconciliation of paleomagnetic and geological data in the northern Cordillera. *Earth and Planetary Science Letters*, *193*(3-4), 259-272.

Kay, S. M., Coira, B. L. (2009). Shallowing and steepening subduction zones, continental lithospheric loss, magmatism, and crustalflow under the Central Andean Altiplano-Puna Plateau. *Backbone of the Americas: shallow subduction, plateau uplift, and ridge and terrane collision*, *204*, 229.

Kay, S. M., Mpodozis, C., Coira, B. (1999). Neogene magmatism, tectonism, and mineral deposits of the Central Andes (22 to 33 S latitude). Geology and ore deposits of the Central Andes, 7, 27-59.

Kennan, L., Lamb, S. H., & Hoke, L. (1997). High-altitude palaeosurfaces in the Bolivian Andes: evidence for late Cenozoic surface uplift. Geological Society, London, Special Publications, 120(1), 307-323.

Kirschvink, J. L. (1980). The least-squares line and plane and the analysis of palaeomagnetic data. Geophysical Journal of the Royal Astronomical Society, 62(3), 699-718.

Kleiman, L. E., & Japas, M. S. (2009). The Choiyoi volcanic province at 34 S–36 S (San Rafael, Mendoza, Argentina): Implications for the Late Palaeozoic evolution of the southwestern margin of Gondwana. Tectonophysics, 473(3), 283-299.

Kley, J., Monaldi, C. R., Salfity, J. A. (1999). Along-strike segmentation of the Andean foreland: causes and consequences. *Tectonophysics*, *301*(1-2), 75-94.

Kley, J., Monaldi, C. R. (2002). Tectonic inversion in the Santa Barbara System of the central Andean foreland thrust belt, northwestern Argentina. *Tectonics*, *21*(6), 11-1.

Kraemer, B., Adelmann, D., Alten, M., Schnurr, W., Erpenstein, K., Kiefer, E., ... & Görler, K. (1999). Incorporation of the Paleogene foreland into the Neogene Puna plateau: the Salar de Antofalla area, NW Argentina. Journal of South American Earth Sciences, 12(2), 157-182.

Kuiper, Y. D., Lin, S., Böhm, C. O. (2011). Himalayan-type escape tectonics along the Superior Boundary Zone in Manitoba, Canada. *Precambrian Research*, *187*(3-4), 248-262.

Lallemand, S., Heuret, A., Boutelier, D. (2005). On the relationships between slab dip, back-arc stress, upper plate absolute motion, and crustal nature in subduction zones. Geochemistry, Geophysics, Geosystems, 6(9).

Lamb, S., Hoke, L. (1997). Origin of the high plateau in the Central Andes, Bolivia, South America. *Tectonics*, *16*(4), 623-649.

Lamb, S. (2001). Vertical axis rotation in the Bolivian orocline, South America: 2. Kinematic and dynamical implications. *Journal of Geophysical Research: Solid Earth*, *106*(B11), 26633-26653.

Le Roux, J. P., Gómez, C. A., Olivares, D. M., & Middleton, H. (2005). Determining the Neogene behavior of the Nazca plate by geohistory analysis. Geology, 33(3), 16Li, S., Yang, Z., Deng, C., He, H., Qin, H., Sun, L., ... & Pan, Y. (2017). Clockwise rotations recorded in redbeds from the Jinggu Basin of northwestern Indochina. GSA Bulletin, 129(9-10), 1100-1122.5-168.

Lickorish, W. H., Ford, M., Burgisser, J., Cobbold, P. R. (2002). Arcuate thrust systems in sandbox experiments: A comparison to the external arcs of the Western Alps. *Geological Society of America Bulletin*, *114*(9), 1089-1107.

Limarino, C. O., & Spalletti, L. A. (1986). Eolian Permian deposits in west and northwest Argentina. Sedimentary Geology, 49(1), 109-127.

Lossada, A. C., Giambiagi, L., Hoke, G., Mescua, J., Suriano, J., & Mazzitelli, M. (2018). Cenozoic Uplift and Exhumation of the Frontal Cordillera Between 30° and 35° S and the Influence of the Subduction Dynamics in the Flat Slab Subduction Context, South Central Andes. In The Evolution of the Chilean-Argentinean Andes (pp. 387-409). Springer, Cham.

Ludwig, K. (2008). Manual for Isoplot 3.7: Berkeley Geochronology Center Special Publication No. 4, rev. August, 26, 77.

Lynner, C., Anderson, M. L., Portner, D. E., Beck, S. L., & Gilbert, H. (2017). Mantle flow through a tear in the Nazca slab inferred from shear wave splitting. Geophysical Research Letters, 44(13), 6735-6742.

Lynner, C., Beck, S. L., Zandt, G., Porritt, R. W., Lin, F. C., & Eilon, Z. C. (2018). Midcrustal Deformation in the Central Andes Constrained by Radial Anisotropy. Journal of Geophysical Research: Solid Earth.

Macedo, J., Marshak, S. (1999). Controls on the geometry of fold-thrust belt salients. *Geological Society of America Bulletin*, *111*(12), 1808-1822.

McFadden, P. L., & McElhinny, M. W. (1988). The combined analysis of remagnetization circles and direct observations in palaeomagnetism. Earth and Planetary Science Letters, 87(1), 161-172.

MacFadden, B. J., Anaya, F., & Swisher, C. C. (1995). Neogene paleomagnetism and oroclinal bending of the central Andes of Bolivia. Journal of Geophysical Research: Solid Earth, 100(B5), 8153-8167.

Maffione, M., Speranza, F., Faccenna, C. (2009). Bending of the Bolivian orocline and growth of the central Andean plateau: Paleomagnetic and structural constraints from the Eastern Cordillera (22–24 S, NW Argentina). *Tectonics*, *28*(4).

Maksaev, V., & Zentilli, M. (1999). Fission track thermochronology of the Domeyko Cordillera, northern Chile: Implications for Andean tectonics and porphyry copper metallogenesis. Exploration and Mining Geology, 8(1/2), 65-90.

Maksaev, V., Munizaga, F., Zentilli, M., & Charrier, R. (2009). Fission track thermochronology of Neogene plutons in the Principal Andean Cordillera of central Chile (33-35 S): Implications for tectonic evolution and porphyry Cu-Mo mineralization. Andean Geology, 36(2).

Maksaev, V., Munizaga, F., & Tassinari, C. (2014). Temporalidad del magmatismo del borde paleo-Pacífico de Gondwana: geocronología U-Pb de rocas ígneas del Paleozoico tardío a Mesozoico temprano de los Andes del norte de Chile entre los 20° y 31° S. Andean geology, 41(3), 447-506.

Mamani, M., Tassara, A., Wörner, G. (2008). Composition and structural control of crustal domains in the central Andes. Geochemistry, Geophysics, Geosystems, 9(3).

Manea, V. C., Pérez-Gussinyé, M., Manea, M. (2012). Chilean flat slab subduction controlled by overriding plate thickness and trench rollback. *Geology*, *40*(1), 35-38.

Marshak, S., Wilkerson, M. S. (1992). Effect of overburden thickness on thrust belt geometry and development. *Tectonics*, *11*(3), 560-566.

Marshak, S. (2004). Salients, recesses, arcs, Oroclines, and Syntaxes A review of ideas concerning the formation of map-view curves in fold-thrust belts.

Mardones, V., Peña, M., Pairoa, S., Ammirati, J. B., Leisen, M. (2021). Architecture, Kinematics, and Tectonic Evolution of the Principal Cordillera of the Andes in Central Chile (∼ 33.5° S): Insights From Detrital Zircon U-Pb Geochronology and Seismotectonics Implications. Tectonics, 40(7), e2020TC006499.

Marinovic, N., & Lahsen, A. (1984). Hoja Calama, Regidn de Antofagasta: Carta Geoldgica de Chile, 1: 250000.

Martínez, F., Arriagada, C., Mpodozis, C., Peña, M. (2012). The Lautaro Basin: a record of inversion tectonics in northern Chile. Andean Geology 39 (2): 258-278.

Martínez, F., Arriagada, C., Peña, M., Del Real, I., Deckart, K. (2013). The structure of the Chañarcillo Basin: An example of tectonic inversion in the Atacama region, northern Chile, Journal of South American Earth Sciences, Volume 42, 1-16.

Martínez, F., Peña, M., & Arriagada, C. (2015). Geología de las áreas Iglesia Colorada-Cerro del Potro y Cerro Mondaquita, región de Atacama, Escala 1: 100.000.

Martínez, F., Arriagada, C., Peña, M., Deckart, K., Charrier, R. (2016). Tectonic styles and crustal shortening of the Central Andes “Pampean” flat-slab segment in northern Chile (27–29 S). Tectonophysics, 667, 144-162.

Martínez, F., Parra, M., Arriagada, C., Mora, A., Bascuñan, S., Peña, M. (2017). Late cretaceous to cenozoic deformation and exhumation of the chilean frontal cordillera (28°–29° S), Central Andes. Journal of Geodynamics, 111, 31-42.

Martínez, F., Gonzalez, R., Bascuñan, S., & Arriagada, C. (2017). Structural styles of the Salar de Punta Negra Basin in the Preandean Depression (24°-25° S) of the Central Andes. Journal of South American Earth Sciences.

Martínez, F., Montanari, D., Del Ventisette, C., Bonini, M., & Corti, G. (2018). Basin inversion and magma migration and emplacement: Insights from basins of northern Chile. Journal of Structural Geology.

Martínez, F., Peña, M., Parra, M., López, C. (2021). Contraction and exhumation of the western Central Andes induced by basin inversion: New evidence from “Pampean” subduction segment. Basin Research, 33(5), 2706-2724.

Martinod, J., Husson, L., Roperch, P., Guillaume, B., Espurt, N. (2010). Horizontal subduction zones, convergence velocity and the building of the Andes. *Earth and Planetary Science Letters*, *299*(3-4), 299-309.

Martinod, J., Guillaume, B., Espurt, N., Faccenna, C., Funiciello, F., Regard, V. (2013). Effect of aseismic ridge subduction on slab geometry and overriding plate deformation: Insights from analogue modeling. *Tectonophysics*, *588*, 39-55.

Matthews, S., Cornejo, P., & Riquelme, R. (2006). Carta Inca de Oro, Región de Atacama. Servicio Nacional de Geología y Minería. Carta Geológica de Chile, Serie Geología Básica, 102, 79.

Maksymowicz, A., Contreras-Reyes, E., Grevemeyer, I., Flueh, E. R. (2012). Structure and geodynamics of the post-collision zone between the Nazca–Antarctic spreading center and South America. Earth and Planetary Science Letters, 345, 27-37.

Maksymowicz, A. (2015). The geometry of the Chilean continental wedge: Tectonic segmentation of subduction processes off Chile. Tectonophysics, 659, 183-196.

McGroder, M. F., Lease, R. O., & Pearson, D. M. (2015). Along-strike variation in structural styles and hydrocarbon occurrences, Subandean fold-and-thrust belt and inner foreland, Colombia to Argentina. Geological Society of America Memoirs, 212, 79-113.

McQuarrie, N. (2002). The kinematic history of the central Andean fold-thrust belt, Bolivia: Implications for building a high plateau. *Geological Society of America Bulletin*, *114*(8), 950-963.

McQuarrie, N., Horton, B K., Zandt, G., Beck, S., DeCelles, P. G. (2005). Lithospheric evolution of the Andean fold-thrust belt, Bolivia, and the origin of the central Andean plateau, Tectonophysics, 399, 15 – 37, doi:10.1016/j.tecto.2004.12.013.

Medina, E.; Niemeyer, H.; Wilke, H.W.; Cembrano, J.; García, M.; Riquelme,R.; Espinoza, S.; Chong, G. 2012. Cartas Tocopilla y María Elena, Región de Antofagasta. Servicio Nacional de Geología y Minería, Carta Geológica de Chile, Serie Geología Básica 141 y 142 p., 1 mapa escala 1:100.000. Santiago.

Mégard, F., Noble, D. C., McKEE, E. H., & Bellon, H. (1984). Multiple pulses of Neogene compressive deformation in the Ayacucho intermontane basin, Andes of central Peru. Geological Society of America Bulletin, 95(9), 1108-1117.

Melnick, D., Folguera, A., Ramos, V. A. (2006). Structural control on arc volcanism: The Caviahue–Copahue complex, Central to Patagonian Andes transition (38 S). *Journal of South American Earth Sciences*, *22*(1-2), 66-88.

Melnick, D., Bookhagen, B., Strecker, M. R., Echtler, H. P. (2009). Segmentation of megathrust rupture zones from fore-arc deformation patterns over hundreds to millions of years, Arauco peninsula, Chile. *Journal of Geophysical Research: Solid Earth*, *114*(B1).

Mescua, J.F., Giambiagi, L.B. (2012). Fault inversion vs. new thrust generation: a case study in the Malargüe fold-and-thrust belt, Andes of Argentina. Journal of Structural Geology 35, 51e63.

Miser, H. D. (1929). Structure of the Ouachita Mountains of Oklahoma and Arkansas. *Oklahoma Geol. Survey Bull*, *50*(30), 7.

Métois, M., Vigny, C., & Socquet, A. (2016). Interseismic coupling, megathrust earthquakes and seismic swarms along the Chilean subduction zone (38–18 S). Pure and Applied Geophysics, 173(5), 1431-1449.

Mitchell, T. M., & Faulkner, D. R. (2009). The nature and origin of off-fault damage surrounding strike-slip fault zones with a wide range of displacements: A field study from the Atacama fault system, northern Chile. Journal of Structural Geology, 31(8), 802-816.

Mitouard, P., Kissel, C., Laj, C. (1990). Post-Oligocene rotations in southern Ecuador and northern Peru and the formation of the Huancabamba deflection in the Andean Cordillera. Earth and Planetary Science Letters, 98(3-4), 329-339.

Mitra, G. (1997). Evolution of salients in a fold-and-thrust belt: The effects of sedimentary basin geometry, strain distribution and critical taper. In *Evolution of geological structures in micro-to macro-scales* (pp. 59-90). Springer, Dordrecht.

Morandé, J.; Gallardo, F.; Farías, M. 2015. Carta Guaviña, Región de Tarapacá. Servicio Nacional de Geología y Minería, Carta Geológica de Chile, Serie Geología Básica 177. 1 mapa escala 1:100.000.

Moscoso, R., Padilla, H., Rivano, S. (1982). Hoja Los Andes. Instituto de Investigaciones Geologicas.

Mourgues, F. A. (2004). Advances in ammonite biostratigraphy of the marine Atacama basin (Lower Cretaceous), northern Chile, and its relationship with the Neuquén basin, Argentina. Journal of South American Earth Sciences, 17(1), 3-10.

Mpodozis, C., & Cornejo, P. (1988). Hoja Pisco Elqui: IV region de Coquimbo. Servicio nacional de geologia y mineria.

Mpodozis, C., Ramos, V. (1990). The Andes of Chile and Argentina.

Mpodozis, C., Kay, S. M., Gardeweg, M., & Coira, B. (1997). Geología de la región de Valle Ancho-Laguna Verde (Catamarca, Argentina): una ventana al basamento del extremo sur de la zona volcánica de los Andes Centrales. Actas, 3, 1689-1693.

Mpodozis, C., Arriagada, C., Basso, M., Roperch, P., Cobbold, P., Reich, M. (2005). Late Mesozoic to Paleogene stratigraphy of the Salar de Atacama Basin, Antofagasta, Northern Chile: implications for the tectonic evolution of the Central Andes. *Tectonophysics*, *399*(1-4), 125-154.

Mpodozis, C., & Ramos, V. A. (2008). Tectónica jurásica en Argentina y Chile: extensión, subducción oblicua, rifting, deriva y colisiones?. Revista de la Asociación geológica Argentina, 63(4), 481-497.

Müller, R. D., Sdrolias, M., Gaina, C., & Roest, W. R. (2008). Age, spreading rates, and spreading asymmetry of the world's ocean crust. Geochemistry, Geophysics, Geosystems, 9(4).

Mulcahy, P., Chen, C., Kay, S. M., Brown, L. D., Isacks, B. L., Sandvol, E., Coira, B. L. (2014). Central Andean mantle and crustal seismicity beneath the Southern Puna plateau and the northern margin of the Chilean-Pampean flat slab. Tectonics, 33(8), 1636-1658.

Nalpas, T., Dabard, M. P., Ruffet, G., Vernon, A., Mpodozis, C., Loi, A., & Hérail, G. (2008). Sedimentation and preservation of the Miocene Atacama Gravels in the Pedernales–Chañaral Area, Northern Chile: Climatic or tectonic control?. Tectonophysics, 459(1), 161-173.

Narea, K., Peña, M., Bascuñán, S., Becerra, J., Gómez, I., Deckart, K., Roperch, P. (2015). Paleomagnetism of Permo-Triassic and Cretaceous rocks from the Antofagasta region, northern Chile. Journal of South American Earth Sciences, 64, 261-272.

Noble, D. C., Farrar, E., & Cobbing, E. J. (1979). The Nazca Group of south-central Peru: Age, source, and regional volcanic and tectonic significance. Earth and Planetary Science Letters, 45(1), 80-86.

O'Driscoll, L. J., Richards, M. A., Humphreys, E. D. (2012). Nazca–South America interactions and the late Eocene–late Oligocene flat-slab episode in the central Andes. *Tectonics*, *31*(2).

Oliveros, V., Féraud, G., Aguirre, L., Fornari, M., & Morata, D. (2006). The Early Andean Magmatic Province (EAMP): 40Ar/39Ar dating on Mesozoic volcanic and plutonic rocks from the Coastal Cordillera, northern Chile. Journal of Volcanology and Geothermal Research, 157(4), 311-330.

Oliveros, V., Labbé, M., Rossel, P., Charrier, R., & Encinas, A. (2012). Late Jurassic paleogeographic evolution of the Andean back-arc basin: New constrains from the Lagunillas Formation, northern Chile (27° 30'–28° 30'S). Journal of South American Earth Sciences, 37, 25-40.

Oncken, O., Hindle, D., Kley, J., Elger, K., Victor, P., Schemmann, K. (2006). Deformation of the central Andean upper plate system—Facts, fiction, and constraints for plateau models. In The Andes (pp. 3-27). Springer, Berlin, Heidelberg.

Palacios, C., Ramírez, L. E., Townley, B., Solari, M., Guerra, N. (2007). The role of the Antofagasta–Calama Lineament in ore deposit deformation in the Andes of northern Chile. *Mineralium Deposita*, *42*(3), 301-308.

Palmer, H. C., Hayatsu, A., & MacDonald, W. D. (1980). Palaeomagnetic and K—Ar age studies of a 6 km-thick Cretaceous section from the Chilean Andes. Geophysical Journal International, 62(1), 133-153.

Pananont, P., Mpodozis, C., Blanco, N., Jordan, T. E., & Brown, L. D. (2004). Cenozoic evolution of the northwestern Salar de Atacama Basin, northern Chile. Tectonics, 23(6).

Parada, M. A., Rivano, S., Sepúlveda, P., Hervé, M., Hervé, F., Puig, A., Munizaga, F., Brook, M., Pankhurst, R., & Snelling, N. (1988). Mesozoic and Cenozoic plutonic development in the Andes of central Chile (30 30′–32 30′ S). Journal of South American Earth Sciences, 1(3), 249-260.

Pardo, M., Comte, D., Monfret, T. (2002). Seismotectonic and stress distribution in the central Chile subduction zone. Journal of South American Earth Sciences, 15(1), 11-22.

Paulsen, T., Marshak, S. (1998). Charleston transverse zone, Wasatch Mountains, Utah: Structure of the Provo salient's northern margin, Sevier fold-thrust belt. *Geological Society of America Bulletin*, *110*(4), 512-522.

Peña, M., Becerra, J., Martínez, F., Arriagada, C. (2013). Geología del Área Yerbas Buenas-Tres Morros Región de Atacama. Carta Geológica de Chile. Servicio Nacional de Geología y Minería. Escala: 1:100.000. Serie Geológica Básica, 155.

Pérez-Gussinyé, M., Lowry, A. R., Phipps Morgan, J., Tassara, A. (2008). Effective elastic thickness variations along the Andean margin and their relationship to subduction geometry. Geochemistry, Geophysics, Geosystems, 9(2).

Pineda, G., & Calderón, M. (2008). Geología del área Monte Patria-El Maqui: región de Coquimbo. Servicio Nacional de Geología y Minería.

Poblete, F., Roperch, P., Hervé, F., Diraison, M., Espinoza, M., Arriagada, C. (2014). The curved Magallanes fold and thrust belt: Tectonic insights from a paleomagnetic and anisotropy of magnetic susceptibility study. *Tectonics*, *33*(12), 2526-2551.

Poblete Gómez, F. A. (2015). Formación del Oroclino Patagónico y evolución paleogeográfica del sistema Patagonia-Península Antártica.

Prezzi, C. B., & Alonso, R. N. (2002). New paleomagnetic data from the northern Argentine Puna: Central Andes rotation pattern reanalyzed. Journal of Geophysical Research: Solid Earth, 107(B2).

Prezzi, C. B., Götze, H. J., & Schmidt, S. (2009). 3D density model of the Central Andes. Physics of the Earth and Planetary Interiors, 177(3-4), 217-234.

Prezzi, C., Iglesia, M. P. (2012). The Southern Central Andes vertical axis tectonic rotations: relations with the deformation pattern. *Andean Geology*, *39*(2), 279-294.

Prezzi, C. B., Caffe, P. J., Llanos, M. P. I., Orgeira, M. J. (2014). New paleomagnetic data from Upper Oligocene–Lower Miocene rocks of the Northern Argentine Puna–Southern Bolivian Altiplano: Constraining the age of vertical axis rotations. Journal of Geodynamics, 78, 42-52.

Proffett, J. M. (2003). Geology of the Bajo de la Alumbrera porphyry copper-gold deposit, Argentina. Economic Geology, 98(8), 1535-1574.

Puigdomenech, C., Somoza, R., Tomlinson, A., Renda, E. M. (2020). Paleomagnetic data from the Precordillera of northern Chile: A multiphase rotation history related to a multiphase deformational history. Tectonophysics, 791, 228569.

Quezada, A. J., Vasquez, P., Sepulveda, F., White, N., & Tomlinson, A. (2012). Mapa Compilacion Geologica Area Quillagua—Alar Grande. Region De Tarapaca, Chilean National Geology Branch, Scale, 1(100,000).

Quiroga, R., Peña, M., Poblete, F., Giambiagi, L., Mescua, J., Gómez, I., Echaurren, A., Perroud, S., Suriano, J., Martinez, F., Espinoza, D. (2021). Spatio-temporal variation of the strain field in the southern Central Andes broken-foreland (27 30′ S) during the late cenozoic. Journal of South American Earth Sciences, 106, 102981.

Ramos, V. A., Cegarra, M., Cristallini, E. (1996). Cenozoic tectonics of the High Andes of west-central Argentina (30–36 S latitude). Tectonophysics, 259(1-3), 185-200.

Ramos, V. A., Cristallini, E. O., Pérez, D. J. (2002). The Pampean flat-slab of the Central Andes. Journal of South American earth sciences, 15(1), 59-78.

Ramos, V. A., Folguera, A. (2009). Andean flat-slab subduction through time. *Geological Society, London, Special Publications*, *327*(1), 31-54.

Ramos, V. A. (2010). The Grenville-age basement of the Andes. *Journal of South American Earth Sciences*, *29*(1), 77-91.

Ramos, V. A. (2015). La orogenia famatiniana (Ordovícico medio a tardío) en el margen continental protoandino de América del Sur: nuevas evidencias y sus implicancias tectónicas. In XIV Congreso Geológico Chileno.

Randall, D. E., Taylor, G. K., Grocott, J. (1996). Major crustal rotations in the Andean margin: Paleomagnetic results from the Coastal Cordillera of northern Chile. *Journal of Geophysical Research: Solid Earth*, *101*(B7), 15783-15798.

Randall, D. E., Tomlinson, A. J., & Taylor, G. K. (2001). Paleomagnetically defined rotations from the Precordillera of northern Chile: Evidence of localized in situ fault-controlled rotations. Tectonics, 20(2), 235-254.

Renne, P. R. et al., (1998). Intercalibration of standards, absolute ages and uncertainties in 40Ar/39Ar dating. Chem. Geol. 145, 117–152.

Renne, P. R., Balco, G., Ludwig, K. R., Mundil, R. & Min, K. Response to the comment by W.H. Schwarz et al. on “Joint determination of 40K decay constants and 40Ar∗/40K for the Fish Canyon sanidine standard, and improved accuracy for 40Ar/39Ar geochronology” by P.R. Renne et al. (2010). Geochim. Cosmochim. Acta 75, 5097–5100 (2011).

Reutter, K. J., Scheuber, E., Helmcke, D. (1991). Structural evidence of orogen-parallel strike slip displacements in the Precordillera of northern Chile. Geologische Rundschau, 80(1), 135-153.

Reutter, K. J., Scheuber, E., Chong, G. (1996). The Precordilleran fault system of Chuquicamata, northern Chile: Evidence for reversals along arc-parallel strike-slip faults. Tectonophysics, 259(1-3), 213-228.

Reyes, J., Lara, L. E., Morata, D. (2017). Contrasting PT paths of shield and rejuvenated volcanism at Robinson Crusoe Island, Juan Fernández Ridge, SE Pacific. Journal of Volcanology and Geothermal Research, 341, 242-254.

Riller, U., Clark, M. D., Daxberger, H., Doman, D., Lenauer, I., Plath, S., Santimano, T. (2017). Fault-slip inversions: Their importance in terms of strain, heterogeneity, and kinematics of brittle deformation. Journal of Structural Geology, 101, 80-95.

Rivano, S., Sepúlveda, P., & Hervé, M. P. A. 1985. Geocronologia K—Ar de las rocas intrusivas entre los 31—32 S, Chile. Revista geológica de Chile, (24), 63-74.

Rodríguez, M. P., Aguilar, G., Urresty, C., & Charrier, R. (2015). Neogene landscape evolution in the Andes of north-central Chile between 28 and 32° S: interplay between tectonic and erosional processes. Geological Society, London, Special Publications, 399(1), 419-446.

Roperch, P., Carlier, G. (1992). Paleomagnetism of Mesozoic rocks from the central Andes of southern Peru: Importance of rotations in the development of the Bolivian orocline. *Journal of Geophysical Research: Solid Earth*, *97*(B12), 17233-17249.

Roperch, P., Sempere, T., Macedo, O., Arriagada, C., Fornari, M., Tapia, C., Garcia, M., Laj, C. (2006). Counterclockwise rotation of late Eocene–Oligocene fore-arc deposits in southern Peru and its significance for oroclinal bending in the central Andes. *Tectonics*, *25*(3).

Roperch, P., Carlotto, V., Ruffet, G., Fornari, M. (2011). Tectonic rotations and transcurrent deformation south of the Abancay deflection in the Andes of southern Peru. *Tectonics*, *30*(2).

Rosenbaum, G., Lister, G. S. (2004). Formation of arcuate orogenic belts in the western Mediterranean region. *Orogenic curvature: integrating paleomagnetic and structural analyses*, *383*, 41-56.

Rosenau, M., Melnick, D., & Echtler, H. (2006). Kinematic constraints on intra-arc shear and strain partitioning in the southern Andes between 38 S and 42 S latitude. Tectonics, 25(4).

Rosenbaum, G., Giles, D., Saxon, M., Betts, P. G., Weinberg, R. F., Duboz, C. (2005). Subduction of the Nazca Ridge and the Inca Plateau: Insights into the formation of ore deposits in Peru. Earth and Planetary Science Letters, 239(1-2), 18-32.

Rosenbaum, G. (2012). Oroclinal Bending in the southern New England Orogen (eastern Australia): a geological field excursion from Brisbane to Sydney. *J. Virtual Explorer*.

Rubilar, J., Martínez, F., Arriagada, C., Becerra, J., & Bascuñán, S. (2017). Structure of the Cordillera de la Sal: A key tectonic element for the Oligocene-Neogene evolution of the Salar de Atacama basin, Central Andes, northern Chile. Journal of South American Earth Sciences.

Ruiz, S., Madariaga, R. (2018). Historical and recent large megathrust earthquakes in Chile. Tectonophysics, 733, 37-56.

Saillard, M., Audin, L., Rousset, B., Avouac, J. P., Chlieh, M., Hall, S. R., ... & Farber, D. L. (2017). From the seismic cycle to long-term deformation: linking seismic coupling and Quaternary coastal geomorphology along the Andean megathrust. Tectonics, 36(2), 241-256.

Salazar, E. 2012. Evolución Tectono-Estratigráfica de la Cordillera de Vallenar: Implicancias en la construcción del Oroclino de Vallenar. Tesis para optar al grado de Magíster en Ciencias, Mención Geología. Departamento de Geología, Universidad de Chile, Santiago, Chile.

Salazar, E., Coloma, F., & Creixell, C. (2013). Geología del área El Tránsito-Lagunillas, Región de Atacama. Servicio Nacional de Geología y Minería. Carta Geológica de Chile, Serie Geología Básica, 149, 106.

Salazar P., Esteban ; Coloma B., Felipe ; SERNAGEOMIN. Geología del área Cerros de Cantaritos - Laguna Chica, región de Atacama, Escala 1:100.000 [monografías]. Santiago : SERNAGEOMIN, 2016. 171 p.: 1 mapa pleg. + 1 cd (Carta Geológica de Chile, Serie Geología Básica : 181)

Salisbury, M. J., Jicha, B. R., de Silva, S. L., Singer, B. S., Jiménez, N. C., & Ort, M. H. (2011). 40Ar/39Ar chronostratigraphy of Altiplano-Puna volcanic complex ignimbrites reveals the development of a major magmatic province. Bulletin, 123(5-6), 821-840.

Scanlan, P. M., & Turner, P. (1992). Structural constraints on palaeomagnetic rotations south of the Arica Bend, northern Chile: implications for the Bolivian Orocline. Tectonophysics, 205(1-3), 141-154.

Scheuber, E., & Gonzalez, G. (1999). Tectonics of the Jurassic-Early Cretaceous magmatic arc of the north Chilean Coastal Cordillera (22°–26° S): A story of crustal deformation along a convergent plate boundary. Tectonics, 18(5), 895-910.

Scheuber, E., Mertmann, D., Ege, H., Silva-González, P., Heubeck, C., Reutter, K. J., & Jacobshagen, V. (2006). Exhumation and basin development related to formation of the central Andean plateau, 21 S. In The Andes (pp. 285-301). Springer, Berlin, Heidelberg.

Segerstrom, K. (1967). Geology and ore deposits of central Atacama Province, Chile. Geological Society of America Bulletin, 78(3), 305-318.

Sempere, T., Carlier, G., Soler, P., Fornari, M., Carlotto, V., Jacay, J., ... & Jiménez, N. (2002). Late Permian–Middle Jurassic lithospheric thinning in Peru and Bolivia, and its bearing on Andean-age tectonics. Tectonophysics, 345(1-4), 153-181.

Sepúlveda, F. A., & Vásquez, P. (2009). The Jurassic-Cretaceous sequences of the Coastal Range near Iquique: reappraisal of the stratigraphy and new evidence for the Lower Cretaceous tectonic conditions. Santiago, 22, S9_083.

Servicio Nacional de Geología y Minería (Sernageomin) 2003. Mapa Geológico de Chile. Servicio Nacional de Geología y Minería, Carta Geológica de Chile 75, 1 mapa en 3 hojas, escala 1:1.000.000.

Sdrolias, M., Müller, R. D. (2006). Controls on back-arc basin formation. *Geochemistry, Geophysics, Geosystems*, *7*(4).

Shaw, J., Johnston, S. T., Gutiérrez-Alonso, G., Weil, A. B. (2012). Oroclines of the Variscan orogen of Iberia: Paleocurrent analysis and paleogeographic implications. *Earth and Planetary Science Letters*, *329*, 60-70.

Shewchuk, J. R. (1996, May). Triangle: Engineering a 2D quality mesh generator and Delaunay triangulator. In Workshop on Applied Computational Geometry (pp. 203-222). Springer, Berlin, Heidelberg.

Skinner, S. M., Clayton, R. W. (2013). The lack of correlation between flat slabs and bathymetric impactors in South America. Earth and Planetary Science Letters, 371, 1-5.

Smith, W. H. F., Wessel, P. (1990). Gridding with continuous curvature splines in tension. Geophysics, 55(3), 293-305.

Solari, L. A., Gómez-Tuena, A., Bernal, J. P., Pérez-Arvizu, O., & Tanner, M. (2010). U-Pb Zircon Geochronology with an Integrated LA-ICP-MS Microanalytical Workstation: Achievements in Precision and Accuracy. Geostandards and Geoanalytical Research, 34(1), 5-18.

Somoza, R., Singer, S., Coira, B. (1996). Paleomagnetism of upper Miocene ignimbrites at the Puna: An analysis of vertical-axis rotations in the Central Andes. Journal of Geophysical Research: Solid Earth, 101(B5), 11387-11400.

Somoza, R. (1998). Updated azca (Farallon)—South America relative motions during the last 40 My: implications for mountain building in the central Andean region. Journal of South American Earth Sciences, 11(3), 211-215.

Somoza, R., Singer, S., Tomlinson, A. (1999). Paleomagnetic study of upper Miocene rocks from northern Chile: Implications for the origin of Late Miocene-Recent tectonic rotations in the southern Central Andes. *Journal of Geophysical Research: Solid Earth*, *104*(B10), 22923-22936.

Somoza, R., Tomlinson, A. J., Caffe, P. J., Vilas, J. F. (2012). Paleomagnetic evidence of earliest Paleocene deformation in Calama (~ 22° S), northern Chile: Andean-type or ridge-collision tectonics?. Journal of South American Earth Sciences, 37, 208-213.

Somoza, R., Tomlinson, A. J., Zaffarana, C. B., Singer, S. E., Negre, C. P., Raposo, M. I. B., Dilles, J. H. (2015). Tectonic rotations and internal structure of Eocene plutons in Chuquicamata, northern Chile. Tectonophysics, 654, 113-130.

Stern, C. R., Kilian, R. (1996). Role of the subducted slab, mantle wedge and continental crust in the generation of adakites from the Andean Austral Volcanic Zone. Contributions to mineralogy and petrology, 123(3), 263-281.

Strecker, M. R., Hilley, G. E., Bookhagen, B., & Sobel, E. R. (2011). Structural, geomorphic, and depositional characteristics of contiguous and broken foreland

basins: examples from the eastern flanks of the central Andes in Bolivia and NW Argentina. Tectonics of sedimentary basins: Recent advances, 508-521.

Suess, E. (1909). *The face of the earth:(Das antlitz der erde)*(Vol. 4). Clarendon press.

Szaniawski, R., Mazzoli, S., Jankowski, L. (2017). Controls of structural inheritance on orogenic curvature and foreland basin sedimentation: Insights from the Przemyśl area, Western Carpathians. *Journal of Structural Geology*, *103*, 137-150.

Tapia, F., Farías, M., Naipauer, M., Puratich, J. (2015). Late Cenozoic contractional evolution of the current arc-volcanic region along the southern Central Andes (35° 20′ S). Journal of Geodynamics, 88, 36-51.

Tapponnier, P., Molnar, P. (1976). Slip-line field theory and large-scale continental tectonics. *Nature*, *264*(5584), 319.

Tassara, A., Yanez, G. (2010). Relationship between elastic thickness and the tectonic segmentation of the Andean margin (15-47° S). *Andean Geology*, *30*(2), 159-186.

Taylor, G. K., Grocott, J., Pope, A., Randall, D. E. (1998). Mesozoic fault systems, deformation and fault block rotation in the Andean forearc: a crustal scale strike-slip duplex in the Coastal Cordillera of northern Chile. Tectonophysics, 299(1-3), 93-109.

Taylor, G. K., Dashwood, B., Grocott, J. (2005). Central Andean rotation pattern: Evidence from paleomagnetic rotations of an anomalous domain in the forearc of northern Chile. *Geology*, *33*(10), 777-780.

Taylor, G. K., Grocott, J., Dashwood, B., Gipson, M., & Arévalo, C. (2007). Implications for crustal rotation and tectonic evolution in the central Andes fore arc: New paleomagnetic results from the Copiapó region of northern Chile, 26°–28° S. Journal of Geophysical Research: Solid Earth, 112(B1).

Thomas, N. A. (1967). Beitrag zur tektonik nord Chiles, Geol. Rundsch., 59,1013-10271, 970.

Thomas, W. A. (1977). Evolution of Appalachian-Ouachita salients and recesses from reentrants and promontories in the continental margin. *American Journal of Science*, *277*(10), 1233-1278.

Tomlinson, A.J., Maksaev, J., and Blanco, N., 1995, Cuadrangulo Cerro Jaspe, Region de Antofagasta: Servicio Nacional de Geologia y Mineria y Corporacion Nacional del Cobre, registered report, IR-95–07, map scale 1: 50,000.

Turienzo, M. (2010). Structural style of the Malargüe foldand- thrust belt at the Diamante River area (34°30′–34°50′S) and its linkage with the Cordillera Frontal Andes of central Argentina: Journal of South American Earth Sciences, v. 29,p.537–556, doi:10.1016/ j.jsames.2009.12.002.

Torsvik, T. H., Van der Voo, R., Preeden, U., Mac Niocaill, C., Steinberger, B., Doubrovine, P. V., ... & Meert, J. G. (2012). Phanerozoic polar wander, palaeogeography and dynamics. Earth-Science Reviews, 114(3-4), 325-368.

Uyeda, S., Kanamori, H. (1979). Back-arc opening and the mode of subduction. Journal of Geophysical Research: Solid Earth, 84(B3), 1049-1061.

Uyeda, S. (1982). Subduction zones: an introduction to comparative subductology. Tectonophysics, 81(3-4), 133-159.

Valenzuela, J. I., Herrera, S., Pinto, L., & Del Real, I. (2014). Carta Camiña, regiones de Arica-Parinacota y Tarapacá. Servicio Nacional de Geología y Minería. Carta Geológica de Chile, Serie Geología Básica, 170, 97.

Vásquez, P., Sepúlveda, F. A., & Quezada, A. (2015). 110 millones de años de volcanismo andesítico (Triásico Superior–Cretácico Inferior) en la Cordillera de la Costa (20 00′–21 15′ S): nuevas edades U/Pb. In XIV Congreso Geologico Chileno, La Serena, Chile (pp. 848-851).

Veloso, E. E., Gomila, R., Cembrano, J., González, R., Jensen, E., & Arancibia, G. (2015). Stress fields recorded on large-scale strike-slip fault systems: Effects on the tectonic evolution of crustal slivers during oblique subduction. Tectonophysics, 664, 244-255.

Vicente, J. C. (2006). Dynamic paleogeography of the Jurassic Andean Basin: pattern of regression and general considerations on main features. *Revista de la Asociación Geológica Argentina*, *61*(3), 408-437.

Victor, P., Oncken, O., Glodny, J. (2004). Uplift of the western Altiplano plateau: Evidence from the Precordillera between 20 and 21 S (northern Chile). Tectonics, 23(4).

Vila, T. (2010). Geología de los depósitos salinos andinos, Provincia de Antofagasta, Chile. Andean Geology, (2).

Wagner, L. S., Jaramillo, J. S., Ramírez-Hoyos, L. F., Monsalve, G., Cardona, A., Becker, T. W. (2017). Transient slab flattening beneath Colombia. Geophysical Research Letters, 44(13), 6616-6623.

Weil, A. B., Sussman, A. J. (2004). Classifying curved orogens based on timing relationships between structural development and vertical-axis rotations. In *Orogenic curvature: integrating paleomagnetic and structural analyses* (Vol. 383, pp. 1-15). Geological Society of America.

Wessel, P., Smith, W. H., Scharroo, R., Luis, J., & Wobbe, F. (2013). Generic mapping tools: improved version released. Eos, Transactions American Geophysical Union, 94(45), 409-410.

Weil, A. B., Gutiérrez-Alonso, G., Johnston, S. T., Pastor-Galán, D. (2013). Kinematic constraints on buckling a lithospheric-scale orocline along the northern margin of Gondwana: A geologic synthesis. *Tectonophysics*, *582*, 25-49.

Weil, A. B., Yonkee, A., & Schultz, M. (2016). Tectonic evolution of a Laramide transverse structural zone: Sweetwater Arch, south central Wyoming. Tectonics, 35(5), 1090-1120.

Xiao, W., Windley, B. F., Sun, S., Li, J., Huang, B., Han, C., Yuan, C., Sun, M., Chen, H. (2015). A tale of amalgamation of three Permo-Triassic collage systems in Central Asia: oroclines, sutures, and terminal accretion. *Annual review of earth and planetary sciences*, *43*, 477-507.

Yamada, Y., McClay, K. (2003). Application of geometric models to inverted listric fault systems in sandbox experiments. Paper 1: 2D hanging wall deformation and section restoration. Journal of structural geology, 25(9), 1551-1560.

Yáñez, G. A., Ranero, C. R., von Huene, R., Díaz, J. (2001). Magnetic anomaly interpretation across the southern central Andes (32–34 S): The role of the Juan Fernández Ridge in the late Tertiary evolution of the margin. Journal of Geophysical Research: Solid Earth, 106(B4), 6325-6345.

Yonkee, A., Weil, A. B. (2010). Quantifying vertical axis rotation in curved orogens: Correlating multiple data sets with a refined weighted least squares strike test. Tectonics, 29(3).

Zandt, G., Leidig, M., Chmielowski, J., Baumont, D., & Yuan, X. (2003). Seismic detection and characterization of the Altiplano-Puna magma body, central Andes. Pure and Applied Geophysics, 160(3-4), 789-807.

Zhang, G., Buatois, L. A., Mángano, M. G., & Aceñolaza, F. G. (1998). Sedimentary facies and environmental ichnology of a Permian playa-lake complex in western Argentina. Palaeogeography, Palaeoclimatology, Palaeoecology, 138(1), 221-243.

Zimmermann, U., Bahlburg, H., Mezger, K., Berndt, J., Kay, S. M. (2014). Origin and age of ultramafic rocks and gabbros in the southern Puna of Argentina: an alleged Ordovician suture revisited. International journal of earth sciences, 103(4), 1023-1036.

Anexos

Anexo A: Tablas de datos del capítulo 2

Table 1: Datos paleomagnéticos y promedio por localidades.

	North Vallenar - Andean Forearc														
			In Situ			Tilt corrected				Position					
	N	Declination	Inclination	a95	k	Declination	Inclination	a95	k	Latitude	Longitude	Rock	Age		Strike/Dip
L1	**Hornitos**														
08TX15	4	150.3	41.2	3.1	857	187.1	77.7	3.1	857	-27.83328	-70.22031	Tuff	67	My	228/40
08TX16	5	167.1	41.8	5.6	189	274.2	66.0	5.6	189	-27.83837	-70.20817	Tuff	67	My	233/62
08TX17	4	243.8	50.2	6.2	221	169.6	72.2	6.2	221	-27.81407	-70.19096	Tuff	66	My	131/49
08TX18	3	222.5	40.1	7.6	263	296.1	82.2	9.5	263	-27.82974	-70.20657	Tuff	66	My	304/47
mean:		193.9	50	37.4	7	**229.7**	**80.3**	**18**	**27**	**-27.815**	**-70.205**		**65**	**My**	
L2	**Sierra**	**de**	**Palmira**												
08TX01	7	130.3	68.7	2.4	631	286.0	52.3	2.4	631	-27.96513	-70.21885	Tuff	80	My	205/58
08TX03	5	139.6	30.7	6.4	145	220.2	64.1	6.4	145	-27.99544	-70.23946	Tuff	80	My	201/65
08TX04	5	142.7	31.2	2.1	1300	220.8	61.5	2.1	1300	-27.99552	-70.23939	Tuff	80	My	201/65
08TX05	4	143.4	33.1	2.9	998	224.5	60.6	2.9	998	-27.99555	-70.23933	Tuff	80	My	201/65
08TX06	8	162.7	34.9	6.2	80	226.2	44.7	6.2	80	-27.99567	-70.23917	Red Sandstone	80	My	201/65
08TX08	5	261.2	60.4	12.5	38	215.9	46.6	12.5	38	-27.98683	-70.24718	Red Sandstone	80	My	80/34
08TX10	5	18.5	-6.6	1.4	2916	25.3	-22.0	1.4	2916	-28.09138	-70.26638	Tuff	80	My	232/30
08TX13	3	223.4	49.0	9.0	188	253.0	30.6	9.0	188	-28.02601	-70.28806	Andesite	80	My	211/38
mean:		169.4	46.3	26.8	5	**230.5**	**50.5**	**16**	**13**	**-28.005**	**-70.256**		**80**	**My**	

L3	**Salitral**														
09TX09	6	36.0	-60.4	4.5	219					-28.27399	-70.26968	Diorite	54	My	0/0
09TX10	5	194.2	51.2	4.1	352					-28.286050	-70.288040	Diorite	54	My	0/0
09TX01	7	37.8	-59.5	4.9	156					-28.30811	-70.46288	Granodiorite	67	My	0/0
mean:		**208.2**	**57.5**	**13.6**	**83**					**-28.277**	**-70.283**		**55**	**My**	
L4	**Los**	**Morteros**													
07ES01	3	179	48.5	3.4	1299					-28.560770	-70.377900	Granodiorite	61	My	0/0
07ES02	5	199.4	50.9	4.7	266					-28.58831	-70.36909	Granodiorite	62	My	0/0
07ES04	5	214.8	59.8	3.0	645					-28.59867	-70.23895	Diorite	63	My	0/0
07ES06		14.7	-47.3	5.7						-28.61113	-70.27512	Diorite	63		0/0
07ES09	3	164.0	73.7	8.1						-28.493360	-70.178430	Tonalite	68	My	0/0
mean:		**192.6**	**56.9**	**13.8**	**32**					**-28.558**	**-70.271**		**65**	**My**	
L5	**Tres**	**Morros**													
07ES07	4	226.0	54.8	6.8	183					-28.46108	-70.06792	Granodiorite	40	My	0/0
07ES08	7	216.4	61.9	3.7	260					-28.44867	-70.08369	Granodiorite	39	My	0/0
09TX04	4	253.9	52.0	13.1	50					-28.49708	-70.03249	Granodiorite	49	My	0/0
mean:		**233.5**	**57.3**	**18.3**	**46**					**-28.469**	**-70.061**		**45**	**My**	
L6	**El**	**Morro**													
07VO45	4	260.9	28.8	4.1	511	232.9	43.5	4.1	511	-28.59533	-69.83553	Andesite	61	My	46/39
07VO46	6	280.9	29.8	2.4	751	248.2	36.5	2.4	751	-28.59533	-69.83553	Andesite	61	My	77/47
07VO47	3	255	50.7	3.2		195.2	38.9	3.2		28.591550	69.838180	Red Sandstone	150	My	55/54
mean:		**266.6**	**36.9**	**25.5**	**24**	225.8	41.9	33.4	15	**-28.585**	**-69.874**		**40**	**My**	
L7	**El**	**Morro**	**2**												
07VO48	11	45.3	-20.7	4.3	79	25.0	-33.0	4.3	79	-28.58246	-69.87859	Red Sandstone	150	My	18/40
07VO49	11	229.5	25.8	3.4	380	211.2	21.6	3.4	380	-28.59032	-69.87074	Red Sandstone	150	My	46/40
mean:		**226.7**	**22.4**	**5.6**	**482**	207.2	29.2	11.2	123	**-28.592**	**-69.840**		**40**	**My**	
	Isolated	**sites**													

05VO06	6	184.7	76.2	7.5	105	**246.8**	**60.2**	**7.5**	**105**	-28.72939	-70.22138	Basalt	220	My	195/20
05VO07		122.6	41.4	1.5		**215.7**	**45.4**	**1.5**		-29.00405	-70.29441	Tuff	151	My	170/75
05VO11	4	204.5	64.7	8.8	148					-28.69647	-70.55573	Intrusive	70	My	0/0
	North	**Vallenar**	**-**	**Eastern**	**Cordillera/Sierras**	**Pampeanas**									
L8	**Antofalla**														
06FP12	8	173.6	25.0	9.8	36	183.6	36.3	9.8	36	-25.807	-67.892	Red Sandstone	25	My	215/20
06FP13	7	170.0	43.3	11.6	28	188.9	42.5	11.6	28	-25.807	-67893	Red Sandstone	25	My	180/20
06FP14	16	173.4	33.0	6.4	34	183.3	40.4	6.4	34	-25.806	-67.900	Red Sandstone	25	My	210/15
06FP15	14	163.3	44.9	10.8	15	193.9	44.2	10.8	15	-25.846	-67.881	Red Sandstone	25	My	180/30
mean:		170.4	36.6	11.5	65	**187.3**	**40.9**	**5.8**	**255**	**-25.816**	**-67.888**		**25**	My	
L9	**Laguna**	**Verde**													
06FP04	5	200.2	65.9	2.5	958	202.9	42.4	2.5	958	-27.634	-68.718	Red Sandstone	25	My	117/23
06FP05	10	194.9	64.5	2.9	288	210.4	47.2	2.9	288	-27.40	-68.723	Red Sandstone	25	My	145/20
06FP06	9	204.9	68.8	3.2	255	201.0	45.6	3.2	255	-27.636	-68.715	Red Sandstone	25	My	108/23
06FP07	5	206.6	66.3	5.1	190	215.3	46.1	5.1	190	-27.630	-68.725	Red Sandstone	25	My	138/21
mean:		201.4	66.4	3.2	847	**207.3**	**45.5**	**5.8**	**253**	**-27.634**	**-68.723**		**25**	**My**	
L10	**Chascuil**														
06FP09	10	115.1	47.9	12.1	17	136.4	45.3	12.1	17	-27.745	-67.975	Red Sandstone	280-275	My	120/20
06FP10	14	179.7	50.0	5.5	53	156.0	63.1	5.5	53	-27.736	-67.966	Red Sandstone	280-275	My	310/20
06FP11	10	205.5	28.3	3.5	190	166.5	45.6	3.5	190	-27.726	-67.937	Red Sandstone	280-275	My	350/50
mean:		169.7	46.7	34.7	8	**163.5**	**50.7**	**21**	20	**-27.242**	**-66.837**		**5**	**My**	
	Isolated	**sites**													
L11	**Vinchina**														
06FP28	9	185.2	5.1	6.5	74	226	62.8	6.5	74	**-28.723**	**-68.239**	Red Sandstone	30	My	71/72
20	8	349.1	-19.8	5.3	111.5	22.9	-56.3	5.3	111.5	**-28.733**	**-68.000**	Red Sandstone	30	My	227/57
21	8	344.7	-11.1	8.1	48	17.6	-49.2	8.1	48	**-28.716**	**-68.194**	Red Sandstone	30	My	216/61
mean:		177.2	33	61.1	5	**207.1**	**56.7**	**16.1**	**60**	**-28.720**	**-68.150**		30	My	

	South	**Vallenar**	**-**	**Andean**	**Forearc**										
L12	**Las**	**Campanas**													
06FP40	5	176.7	65.1	3.5	472					-29.17200	-70.63200	Granite	75	My	0/0
06FP42	4	156.8	39.0	9.4	42	157.6	72.0	9.4	42	-29.13600	-70.57300	Andesite	80	My	245/33
05VO16	6	196.1	65.0	1.8	1314					-29.45142	-70.74343	Diorite	63	My	0/0
05VO18	3	181.0	60.5	14.0	79				79	-29.40669	-70.85665	Granodiorite	83	My	0/0
05VO19		26.6	-53.3	8.2						-29.36327	-71.01345	Andesite	80	My	0/0
06FP38	16	13.7	-48.8	5.4	453				453	-29.34300	-70.92500	Granite	90-96	My	70/9
06FP39	7	23.5	-48.8	4.0	229	47.2	16.0	4.0	229	-29.26000	-70.85000	Andesite	93	My	172/86
mean:		**191.7**	**53.5**	**10.5**	**25**	199.7	51.6	19.4	8	**-29.299**	**-70.815**		**65**	My	
L13	**Tulahuen**														
05VO40	5	188.8	52.5	9.1	55	207.8	50.9	9.1	55	-31.013	-70.632	Andesite	80-85	My	190/15
05VO41	3	352.5	-44.8	7.8	252					-31.022	-70.682	Diorite	39	My	0/0
05VO42	3	177.9	52.6	12.9						-30.973	-70.774	Granodiorite	39	My	0/0
05VO43	5	7.3	-43.5	5.9	129					-31.132	-70.822	Granodiorite	38	My	0/0
05VO37	3	195.7	69.1	8.1		243.5	61.8	8.1		-30.917	-70.482	Andesites	40	My	220/22
mean:		**183.2**	**52.7**	**10.9**	**50**	193.9	53.1	17.3	21	**-31.012**	**-70.678**		**40**	**My**	
Isolated															
05VO14		317	-41.7	1.7		309.7	-30.3	1.7		-29.225730	-71.01104	Andesite	80	My	0/15
06FP37	3	222.6	37.2	5.8	453.3				453.3	-28.96000	-71.04800	Granite	125	My	0/0
05VO20	5	337.4	-71.6	10.3	56	**337.4**	**-58.6**	**10.3**	**56**	-29.797	-70.762	Andesites	75	My	100/20
05VO21	5	49.6	-49.7	4.0	361	**31.9**	**-57.3**	**4.0**	**361**	-29.85697	-70.83154	Andesites	75	My	10/15
mean:															
	South	**Vallenar**	**-**	**Eastern**	**Cordillera/Sierras**	**Pampeanas**									
L14	**Los**	**Tambillos**													
06FP22	5	11.4	-51.3	10.4	64	0.9	-58.1	10.4	64	-29.371	-67.737	Red Sandstone	260	My	325/10

06FP08	9	343.5	-41.0	4.2	150	10.8	-41.7	4.2	150	-27.657	-68.238	Red Sandstone	260	My	180/30
06FP24	8	18.1	-44.5	7.4	67	11.3	-38.1	7.4	67	-29.475	-67.828	Red Sandstone	260	My	55/10
mean:		3.7	-46.7	21.7	**33**	**8.5**	**-46**	**17.4**	**52**	**-29.405**	**-67.805**		260	**My**	
L15	**Guandacol**														
06FP25	8	183.0	34.3	10.9	28	176.1	35.2	10.9	28	-29.477	-68.329	Red Sandstone	260	My	355/10
06FP26	8	47.0	-56.7	6.6	71	13.4	-50.1	6.6	71	-29.525	-68.419	Red Sandstone	260	My	45/25
06FP27	7	55.8	-35.5	7.7	62	33.7	-35.6	7.7	62	-29.525	-68.420	Red Sandstone	260	My	45/30
mean:		214	44.7	39.6	11	**194.4**	**41.4**	**26.5**	**23**	**-29.509**	**-68.380**		**260**	**My**	
L16	**Santo Domingo**														
06FP31	5	353.1	-0.3	9.5	66	12.2	-49.7	9.5	66	-28.576	-68.743	Red Sandstone	200	My	235/60
D36	3	343.5	-28.2	12.6	96	46.3	-46.1	12.6	96	-28.576	-68.743	Red Sandstone	200	My	206/70
D37	3	345.4	-20.9	12.7	95	36.2	-43.9	12.7	95	-28.576	-68.743	Red Sandstone	200	My	206/70
D39	4	354	-15.4	10	83	36.5	-49.6	10	83	-28.576	-68.743	Red Sandstone	200	My	222/65
mean:		350.6	-15.4	17.4	29	**33.2**	**-46.4**	**11.3**	**67**	**-28.576**	**-68.743**		**200**	My	
Isolated															
06FP23	14	147.6	50.2	1.8	487	**135.8**	**54.1**	**1.8**	**487**	-29.391	-67.790	Red Sandstone	260	My	325/10

Tabla 2: Resultados de Analisis geocronológicos

Sample	Rock type	Median $^{206}Pb/^{238}U$ age (Ma)*	Epoch (ICS, 2012)	# of spots included	MSWD
YB-35	leuco-granodiorite	67 $^{+1.5}/_{-1.5}$	Late Cretaceous Maastrichtian	15/27	2,3
M-7	hornblende-biotite granite	44.0 $^{+2.3}/_{-2.3}$	Eocene	20/30	3,4
M-14	monazite	54.3 $^{+1.2}/_{-1.2}$	early Eocene	21/29	1,7
YB-96	biotite granite	47.1 $^{+1.8}/_{-1.8}$	early Eocene	21/34	1,8
Sample	**Rock type**	**Median $^{206}Pb/^{238}U$ age (Ma)***	**Epoch (ICS, 2012)**	**# of spots included**	**Error confidence**
AT-03	welded tuff, dacitic	80.8 $^{+1.2}/_{-1.1}$ youngest age group (n=28) 81.3 ± 0.3 Ma	Late Cretaceous Campanian	14/28	94,30%
AT-10	glasy tuff, rhyolitic	80.8 $^{+1.1}/_{-0.7}$ youngest age group (n=2) 72.6 ± 0.9 Ma	Late Cretaceous Campanian	18/29	96,90%

		$^{40}Ar/^{39}Ar$ plateau age			
07ES01	Granodiorite	61.2 ± 0.2	Early Paleocene		
07ES02	Tonalite	61.9 ± 0.1	Early Paleocene		
07ES04	Granodiorite	63 ± 0.1	Early Paleocene		

*Median $^{206}Pb/^{238}U$ age (unweighted median age with asymmetric > 94%-confidence errors)

Tabla 3: Rotaciones tectónicas para las distintas localidades.

				Observed			VGP			Expected					
Locality	Age	Lat(º)	Long(º)	Dec	Inc	a95	Lat(º)	Long(º)	p95	Dec	Inc	Rot	¬±DR	Inc	¬±EI
L1	65	-27.815	-70.205	49.7	-80.3	18.0	82.0	193.7	3.6	351.0	-47.2	58.7	72.1	33.1	14.8
L2	80	-28.005	-70.256	50.5	-50.5	16.0	82.3	228.4	6.9	352.6	-41.8	57.9	21.4	8.7	14.8
L3	55	-28.277	-70.283	28.2	-59.4	17.8	82.7	145.3	4.1	354.9	-53.6	33.3	29.8	5.8	14.6
L4	65	-28.558	-70.271	11.9	-59.4	17.8	82.0	193.7	3.6	350.9	-48.1	21.0	29.7	11.3	14.6
L5	40	-28.469	-70.061	53.5	-57.3	18.3	82.0	126.5	5.3	357.2	-55.6	56.3	28.9	1.7	15.2
L6	40	-28.585	-69.874	86.6	-36.9	25.5	80.0	139.5	7.3	353.9	-56.6	92.7	27.1	-19.7	21.1
L7	40	-28.592	-69.840	46.7	-22.4	5.6	80.0	139.5	7.3	353.9	-56.6	52.8	8.8	-34.2	7.1
L8	25	-28.816	-67.888	7.3	-40.9	5.8	84.4	126.1	5.3	358.4	-53.7	8.9	8.0	-12.8	6.4
L9	5	-27.634	-68.723	21.4	-66.4	3.2	86.5	168.0	2.6	356.6	-48.5	24.8	6.8	17.9	3.5
L10	280	-27.675	-68.017	343.5	-50.7	21.0	64	170.4	2.8	331.6	-57.7	11.9	27.7	-7	16.9
L11	5	-27.242	-68.837	30.0	-54.8	15.4	86.5	168.0	2.6	356.6	-48.1	33.4	22.1	6.7	12.6
L12	65	-28.299	-70.815	9.8	-53.3	11.9	82.0	193.7	3.6	350.9	-47.7	18.9	16.5	5.6	10.1
L13	40	-31.012	-70.678	3.2	-52.7	10.9	80.0	139.5	7.3	353.5	-58.8	9.7	16.4	-6.1	10.2
L14	5	-29.405	-67.805	0.1	-50.9	28.2	86.5	168.0	2.6	330.8	-59.1	3.5	29.3	-17.7	21.3
L15	280	-29.509	-68.380	14.4	-41.4	26.5	64	170.4	2.8	334.2	-65.3	40.2	29.3	-23.9	21.3
L16	200	-28.576	-68.743	33.2	-46.4	11.3	74.4	58.7	2.8	15.5	-56.6	-18.3	13.5	-10.2	9.3
05VO04	45	-28.620	-69.967	32.0	-33.9	8.5	82.0	126.5	5.3	357.2	-55.7	34.8	9.8	-21.8	8.0
05VO06	220	-28.729	-70.221	66.8	-60.2	7.5	67.6	89.5	2.0	11.7	-66.7	55.1	12.4	-6.5	6.1
05VO11	70	-28.696	-70.555	24.5	-64.7	8.8	82.3	199.0	4.8	351.2	-47.3	33.3	17.3	17.4	8.4
05VO21	75	-29.856	-70.831	59.3	-40.9	4.0	83.6	170.6	7.2	353.3	-52.1	66.0	8.1	-11.2	6.9
06FP28	30	-28.723	-68.239	46.0	-62.8	6.5	83.5	163.8	5.3	353.9	-52.0	52.1	12.5	10.8	6.9

Anexo B: Tablas de datos del capítulo 3

Table 1: Datos paleomagnéticos y promedio por localidades.

Sites	**Domeyko** Latitude	**Range** Longitude	**Domain** Lithology	Age	IS Declination(IS)	IS Inclination(IS)	a95	Kappa	TC Declination (TC)	TC Inclination (TC)	a95	Kappa
L1	**Lluta**											
06dn80	-18.323.770	-69.840.000	Sandstone	65	323.5	-39.6	13.2		6.7	-47.2	13.2	
06dn77	-18.315.340	-69.801.480	Granodiorite	65	178.5	25.5	7.3					
06dn78	-18.324.480	-69.834.930	Limestone	65	340.9	-34.9	12.5		11.7	-33.1	12.5	
	-18.321.197	**-69.825.470**		**65**	161.9	34.2	25.2	26	**185.4**	**35.4**	**19**	**43**
L2	**Quebrada Cardones**											
06dn82	-18.445.900	-69.760.510	Granite	65	1.9	-37.2	8.4					
06dn81	-18.440.160	-69.749.450	Granite	65	352.4	-43.1	8					
06dn76	-18.312.480	-69.799.230	Granodiorite	65	158.9	38.4	6.2					
06dn75	-18.820.840	-69.692.670	Granodiorite	65	327.5	-62.5	1.5					
	-18.504.845	**-69.750.465**		**65**	**167.2**	**45.9**	**17.7**	**28**				
L3	**Camiña**											
C62 roperch	-19.228.000	-69.390.000	Sandstone	60-45	181.1	52	1.7		164.7	48.5	1.7	
C63a roperch	-19.307.000	-69.427.000	Sandstone	60-45	179.3	50	3.3		179.3	50	3.3	

C63b roperch	-19.307.000	-69.427.000	Sandstone	60-45	6.5	-27.9	5.9		6.5	-27.9	5.9	
06dn71	-19.168.690	-69.316.380	Dacite Prophiry	15	334.9	-41.5	6.3					
06dn72	-19.332.420	-69.478.310	Dacite Prophiry	65	8.5	-29.3	4.1					
	-19.268.622	**-69.407.738**		**15**	**178.7**	**40.8**	**14.7**	**28**	175.8	40.2	14.7	28
L4	**Chusmisa**											
06dn53	-19.854.560	-69.038.440	Granodiorite	40	206.1	28	11.7					
06dn51	-19.893.620	-69.107.350	Diorite	45	9.1	-39.6	7.1					
06dn48	-19.611.340	-69.168.280	Gabbro	40	181	51.9	1.7					
06dn46	-19.664.670	-69.158.550	Diorite	45	189.8	50.8	3.3					
	-19.756.048	**-69.118.155**		**40**	**192.7**	**43**	**15.8**	**35**				
L5	**Tarapaca**											
06dn50	-19.859.670	-69.370.630	Granite	70	350.4	-41.7	5.8					
06dn49	-19.844.840	-69.314.460	Andesite	60	49.6	-39.5	4.4		21.5	-59.4	4.4	
	-19.852.255	**-69.342.545**		**65**	31.2	-43.7	40.6	10	**8.4**	**-54.5**	**23.3**	**29**
L6	**Choja**											
06dn57	-19.982.260	-69.121.190	Sandstone	65	356.4	-46.7	9.9		348.4	-41.2	9.9	
06dn58	-20.020.120	-69.212.460	Sandstone	65	173	35.9	7.5		183.4	37.4	7.5	
06dn59	-20.057.380	-69.349.490	Sienogranite	65	15.1	-57.5	3					
06dn52	-19.895.280	-69.094.220	Sandstone	65	0.6	-45.6	6.1		10.5	-43.9	6.1	
	-19.988.760	**-69.194.340**		**65**	**180.1**	**46.7**	**12.4**	**56**	183.5	45.4	13.6	46
L7	**Pica**											
06dn62	-20.146.860	-69.061.640	Granodiorite	45	202.4	45.7	6.4					
06dn63	-20.168.790	-69.062.360	Monzodiorite	45	330.7	-72.5	2.9					
06dn64	-20.224.200	-69.046.300	Monzodiorite	45	148.4	52.2	3.1					

	-20.157.825	**-69.062.000**		**45**	**172**	**59.6**	**34.9**	**14**				
L8	**Montecristo**											
UK1	-22.300.000	-69.096.667	Conglomerate	63	193.3	54.4	6.5		160.2	57.5	6.5	
UK2	-22.301.667	-69.096.667	Conglomerate	63	179.2	47.6	4.6		155.5	55.4	4.6	
QM1	-22.301.667	-69.100.000	Monzodiorite	63	188.8	45.8	7.9					
06dn04	-22.296.240	-69.099.050	Andesite	80-65	180.8	46.3	3.7					
	-22.299.894	**-69.098.096**		**63**	**185.3**	**48.7**	**6.7**	**190**	172.9	52.1	13.3	49
	Isolated	**Sites**										
06dn22	**-21.858.950**	**-68.933.070**	**Granodiorite**	**230**	**153.7**	**53**	**5.2**					
06dn12	**-20.927.750**	**-68.913.140**	**Granite**	**65**	**341.9**	**-65.7**	**2.4**					
06dn01	**-22.289.220**	**-68.964.970**	**Granodiorite**	**40**	**327.6**	**-65**	**3.7**					
	Coastal	**Range**	**Domain**									
L9	**Chucumata**											
04IQ04	-20.612	-70.198	Andesite	170	13	-38.7	22.7		13	-28	22.7	
04IQ06	-20.766	-70.193	Diorite	155	344.9	-40.9	8.6					
04IQ08	-20.961	-70.142	Diorite	155	23.8	-30.6	9.4					
04IQ09	-20.995	-70.160	Diorite	155	359.4	-39.4	22.1					
04IQ11	-21.038	-70.162	Diorite	155	11.5	-31.6	7					
	-20.874	**-70.171**		**155**	**7.2**	**-37**	**12.2**	**40**	7.3	-34.8	12.7	37
L10	**Loa**											
04IQ14	-21.110	-70.119	Gabbro	155	353.6	-38.1	11.4					
04IQ16	-21.267	-70.078	Diorite	155	176.3	23.1	10.8					
04IQ21	-21.430	-70.032	Diorite	155	7.1	-22.2	11.8					
04IQ23	-22.014	-70.194	Diorite	160	192.3	41.9	26.3					
04MB18	-22.073	-70.164	Monzodiorite	160	189	34.9	10.2					

04MB17	-22.073	-70.164	Monzodiorite	160	204	38.8	20.3					
	-21.661	**-70.125**		**155**	**186.6**	**33.6**	**10.4**	**43**				
L11	**Cobija**											
04MB20	-22.434	-70.254	Diorite	160	213.1	6.4	15.9					
04MB19	-22.378	-70.236	Andesite	160	350.8	-18.1	23.2		343.9	-12.9	23.2	
04MB24	-22.610	-70.261	Monzodiorite	155	194.4	11.2	6.1					
04MB25	-22.620	-70.264	Monzodiorite	155	197.9	20.5	13.8					
	-22.511	**-70.254**		**155**	**194.3**	**14.5**	**21**	**20**	192.6	13.4	24.4	15
	Isolated	**Sites**										
04MB21	**-22.452**	**-70.258**	**Diorite**	**160**	**322.5**	**-63.6**	**14**					
04MB27	**-22.925**	**-70.302**	Diorite	**140**	**357.2**	**-49.2**	**14.6**					
04IQ07	**-20.880**	**-70.143**	**Andesite**	**155**	**223.9**	**60.8**	**13.5**		194.3	51.1	42.6	

Tabla 2: Rotaciones tectónicas para los datos analizados. A: Este trabajo; b: Roperch et al. (2006); c: Heki et al. (1985); d: Scalan & Turner (1992); e: Palmer et al. (1980); f: (Arriagada et al., 2003).

REF	SITE	AGE	LAT	LONG	DOBS	INC	A95	LAT	LON	P95	DEXP	INC	ROT	±DR	ERR_I	±EI
a	04IQ07	155	-20.880	-70.143	58	-59.6	11.5	87.3	39.6	3.8	2.7	-38.6	55.3	18.8	21	10.2
a	04mb21	160	-22.452	-70.258	322.5	-63.6	14	88.2	189.6	7.1	358.1	-40	-35.6	27.1	23.6	13.7
a	04MB27	140	-22.925	-70.302	357.2	-49.2	14.6	77.5	238.2	8.1	349.9	-27.9	7.3	19.4	21.3	15.9
a	06dn01	40	-22.289	-68.964	327.6	-65	3.7	80	139.5	7.3	354.5	-50.2	-26.9	9.8	14.8	7.1
a	06dn12	65	-20.927	-68.913	341.9	-65.7	2.4	82	193.7	3.6	351.5	-38.6	-9.6	5.6	27.1	4.5
a	06dn22	230	-21.858	-68.933	333.7	-53	5.2	68.7	101	2.6	5	-61.6	-31.3	7.5	-8.6	4.5
a	L1	65	-18.321	-69.825	5.4	-35.4	19	82	193.7	3.6	351.6	-34.6	13.8	19.1	0.8	15.8
a	L2	65	-18.504	-69.750	347.2	-45.9	17.7	82	193.7	3.6	351.6	-34.9	-4.4	20.9	11	14.8
a	L3	15	-19.268	-69.407	358.7	-40.8	14.7	84.8	136.7	3.2	357.5	-41.6	1.2	15.9	-0.8	12.2
a	L4	40	-19.756	-69.118	12.7	-43	15.8	80	139.5	7.3	354.6	-47.3	18.1	18.7	-0.3	14.4
a	L5	65	-19.852	-69.642	8.4	-54.5	23.3	82	193.7	3.6	351.5	-36.9	16.9	34.5	17.6	19.1
a	L6	65	-19.988	-69.194	0.1	-46.7	12.4	82	193.7	3.6	351.5	-37.2	8.6	14.9	9.5	10.8
a	L7	45	-20.157	-69.062	151	59.2	17.8	82	126.5	5.3	357.6	-46.6	-26.6	29.7	12.6	15.1
a	L8	60	-22.299	-69.098	5.3	-48.7	6.7	82.4	168.5	4.3	352.9	-44.6	12.4	9	4.1	6.9
a	L9	155	-20.689	-70.196	7.2	-37	12.2	87.3	39.6	3.8	2.7	-38.3	4.5	12.7	-1.3	10.7
a	L10	155	-21.661	-70.125	6.6	-33.6	10.4	87.3	39.6	3.8	2.8	-39.7	3.8	10.5	-6.1	9.3
a	L11	155	-22.511	-70.254	14.3	-14.5	21	87.3	39.6	3.8	2.8	-40.9	11.5	17.7	-26.4	17.3
b	suca	100	-18.900	-70.000	351.2	-38	3	87.8	29.2	11.5	2.3	-34.9	-11.1	10.2	3.1	14.1
c	AricaDykes	105	-18.600	-70.300	345	-26	3.3	88	179.8	24.6	358	-35	-13	21.1	-9	29.8
c	Atajaï¿½a	120	-18.800	-70.300	345	-26	4.1	83.9	238.5	3.1	355.1	-28	-10.1	4.5	-2	5.3
d	Cuya	140	-19.200	-70.300	351	-40	7	77.5	238.2	8.1	350.1	-21.6	0.9	9.9	18.4	12.9

e	Camaraca	155	-18.600	-70.300	339	-37	6	87.3	39.6	3.8	2.7	-35.3	-23.7	6.8	1.7	6.6
f	La Negra	180	−22.2	−70.2	9.1	−39.2	12	81.6	21.4	8.6	6.9	-36.2	−2.2	13.3	3	11.2

Anexo C: Resumen presentado en AGU Fall Meeting (2015). San Francisco, EEUU. T23A-2909.

The open scars of Latin America: The Bolivian Orocline as a basament-related hinge, and the influence of accreted terranes on the paleomagnetic rotational patterns of the Chilean forearc.

We made a paleomagnetic study in two separate zones of the Chilean forearc, between 18-22ºS and between 28-32ºS, sampling igneous and sedimentary rocks with ages ranging from Triassic to Miocene. More than 500 samples showed a stable magnetization, with hematite and magnetite being the principal carriers of magnetism. The rotation pattern obtained, together with previously published paleomagnetic data, show a continuous database for the Chilean forearc, between 19 and 35ºS, allowing us to separate distinct patterns in 4 major rotational zones: (1) Between 18-19.5ºS there is a strong anticlockwise rotational pattern, in agreement with the data known in southern Peru. (2) Between 19.5-22.5ºS, there is little to no rotation, with the southern limit being related to a major structural feature: The Antofagasta–Calama Lineament. (3) Between 22.5-29ºS there is a strong regional clockwise rotation pattern of nearly 30º. (4) Between 29-32ºS there is again a little to non-rotational pattern, in the area of the Pampean flat-slab. Overlapping these zones and the recognized accreted terranes boundaries shows a clear spatial relationbetween these and the limits of the rotated zones. We propose that all these zones are related to basament-related inherited structures, which acted as hinges, being weakness zones that helped to create the margin curvatures observed today. Under this model, the bolivian orocline would be the result of the opening of a hinge, helped by other geodynamics features like sea mountains and ridges, at the limit between the old accreted paleozoic terranes of Antofalla and Arequipa.

Anexo D: Resumen presentado en en XIV Congreso Geológico Chileno (2015). La Serena, Chile.

Los limites del CARP: rotaciones tectonicas en el antearco chileno entre los 18-32ºS

Matias Peña*, **Iván Gómez y Cesar Arriagada.**

Departamento de Geología, Facultad de Ciencias Físicas y Matemáticas, Universidad de Chile, Plaza Ercilla 803, Santiago, Chile.

mapena@ing.uchile.cl

Resumen. Con el fin de completar la base datos paleomagnéticas, se realizó una compilación de datos desde los 18 hasta los 32°S, con datos de trabajos anteriores y con nuevos datos presentados en esta contribución. Los datos analizados muestran que el patrón de rotaciones horarias de los Andes Centrales (CARP) empieza alrededor de los 23°S y termina alrededor de los 29°S, así como que entre los 19.5°S y los 22°S existen rotaciones mínimas o nulas. Estos nuevos datos pueden apuntar al mecanismo y a la causa de la formación del Oroclino Boliviano

Palabras Claves: Paleomagnetismo, rotaciones tectónicas, Oroclino.

1 Introducción

Si bien se conoce bastante bien cómo cambia el patrón de rotaciones paleomagnéticas alrededor del Oroclino Boliviano (Arriagada et al., 2006; Roperch et al., 2010), no se conoce en detalle cuales son los limites espaciales del patrón de rotaciones horarias de los andes Andes Centrales (CARP). Con el fin de obtener el comportamiento del patrón de rotaciones horarias en todos sus límites, se realizó un estudio en rocas desde el Triásico hasta el Mioceno (SERNAGEOMIN, 2003) a través de la Precordillera y la Cordillera de la Costa de Chile entre los 19°S y los 32°S.

2 Métodología, muestreo, resultados

El muestreo paleomagnético fue realizado en más de 2000 muestras orientadas, entre los 18-23ºS (Figura 1) y entre los 27-32ºS (Figura 2). Se midió remanencia magnética con magnetómetros de rotación (Molspin y JR5 de AGICO), mientras que la susceptibilidad magnética fue medida con un susceptibilimetro Bartington, en el Laboratorio de Tectónica y Paleomagnétismo del Departamento de Geología de la Universsidad de Chile. Para constreñir de mejor forma la mineralogía magnética, se realizaron experimentos de magnetización isotermal remanente (IRM) y de variación de susceptibilidad durante el calentamiento (análisis de Curie) en ciertas muestras. Estos experimentos se realizaron con un susceptibilimetro AGICO KLY3-CS3. Las muestras orientadas fueron sujetas a demagnetización, por calentamiento paulatino o aplicando campos magnéticos alternos, midiendo tanto la magnetización remanente como la susceptibilidad en cada paso de demagnetización, para controlar cambios mineralógicos y del vector magnético remanente.

Con el fin de concluuir implicancias tectónicas de los datos paleomagnéticos y detectar posibles rotaciones, los sitios que pertenecen a un bloque tectónico homogéneo fueron agrupados en localidades de acuerdo a la naturaleza y edad de magnetización. Se utilizaron los polos de referencia de Besse y Courtillot (2002) para calcular las rotaciones tectónicas para las distintas localidades.

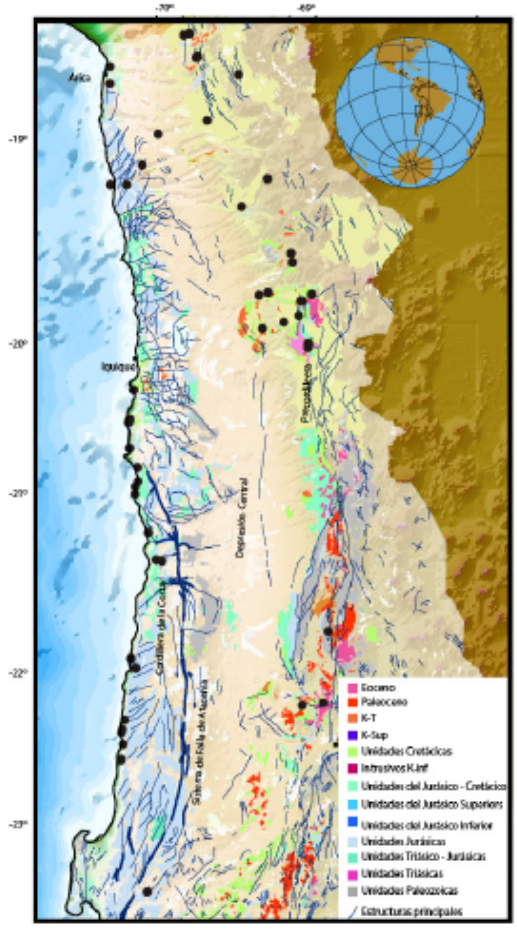

Figura 1. Mapa geológico simplificado de la zona de estudio, modificado del mapa 1:1000000 de SERNAGEOMIN (2003), entre Arica y Antofagasta. Los círculos negros representan los sitios de muestras paleomagnéticos.

2 Marco Tectónico

La región estudiada se localiza entre los 19°-32S, partiendo desde el Oroclino Boliviano hasta el límite sur del sector de Flat Slab Pampeano de Chile y Argentina (Cahill & Isacks, 1992). Esta área representa las zonas de antiguas acreciones de los terrenos de Cuyania y Arequipa - Antofalla, que terminaron sus procesos acrecionales en el Cámbrico (Ramos, V.A., 2008), y del terreno de Chilenia (Alvarez et al., 2013). Un intenso magmatismo Permo-Triásico afectó la actual Cordillera Frontal y de Domeyko (Maksaev et al., 2014). Desde el Triásico hasta el Cretácico Temprano, cuencas extensionales se formaron estas zonas, controlando secuencias sedimentarias de carácter marino y continental a lo largo del norte de Chile (Charrier et al., 2007). Desde el Cretácico Superior hasta el Mioceno en adelante, la región ha sufrido deformación mayormente compresiva, que se apoya en antiguas estructuras que controlaron las cuencas mesozoicas, provocando el levantamiento de la Cordillera de la Costa, luego de la cordillera de Domeyko y, por último, la Cordillera Frontal, a lo largo de toda la franja andina. Por ultimo, existen evidencias de pulsos extensionales locales en zonas como el Salar de Atacama, en el Oligoceno-Neogeno, que culminarían la evolución estructural de la región (Arriagada et al., 2006a; Bascuñan et al., 2015; Martinez et al., 2015; Rubilar et al., este congreso).

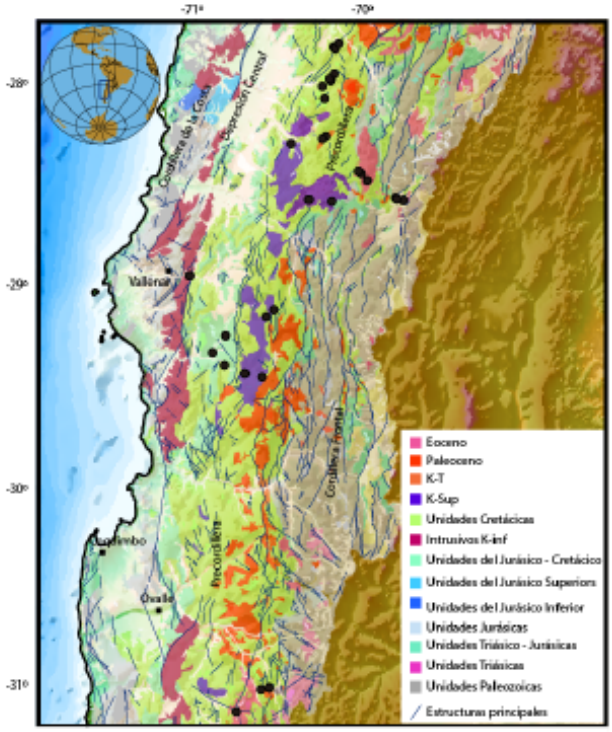

Figura 2. Mapa geológico simplificado de la zona de estudio, modificado del mapa 1:1000000 de SERNAGEOMIN (2003), entre Copiapó y Vallenar. Los círculos negros representan los sitios de muestras paleomagnéticos.

3 Resultados y discusiones

Más de 650 muestras orientadas arrojaron magnetización estable, con mineralogías como hematita y magnetita como principales acarreadoras de la magnetización. Las muestras y sitios fueron agrupadas en localidades de acuerdo a su edad y naturaleza magnética, resultando en una sectorización de los patrones paleomagnéticos rotacionales de la siguiente forma: entre los 16-19.5°S existe un patrón de rotaciones paleomagnéticas antihorarias de alrededor de 30° que se observan desde el sur de Perú (Roperch et al., 2010) hasta el comienzo del norte de Chile (Figura 3). Desde los 19.5°S hasta los 23°S se observa un patrón de rotaciones mínimas o nulas, tanto en la Cordillera de Domeyko como en Cordillera de la Costa. Entre los 23-29°S existe un patrón de rotaciones horarias, de alrededor de 35°, que se habría producido antes del Mioceno (Somoza et al., 2012). Por último, entre los 29-33°S, en la zona del Flat-Slab pampeano, existe otro patrón de rotaciones nulas o mínimas (Arrigada et al., 2013).

Con este conjunto de datos es posible establecer límites claros para los largamente estudiados patrones de rotaciones horarios y antihorarios de los Andes centrales. El CARP tendría su límite norte alrededor del lineamiento de la carretera Antofagasta-Calama (Arriagada et al., 2003) y su límite sur en el Oroclino de Vallenar (Peña et al., 2011). Existe un patrón de rotaciones mínimas o nulas, entre la línea de Gephart (Gephart, 1994) y el lineamiento de la carretera, así como entre el Oroclino de Vallenar y el Oroclino del Maipo. Con estas sectorizaciones podemos decir que: (1) El dominio de la deformación de escala regional causada por el Oroclino Boliviano en los patrones de rotaciones tiene un límite sur en el Oroclino de Vallenar. (2) Las rotaciones mínimas o nulas, entre los 19.5-23°S en la Cordillera de la Costa muestran, con los resultados preliminares de este trabajo, que el Sistema de Fallas de Atacama pareciera no causar grandes rotaciones a su alrededor. (3) La edad de las rotaciones va entre el Cretácico Tardío hasta el Eoceno, coincidiendo con los mayores pulsos de deformación de los Andes Centrales. (4) Existe una fuerte correlación entre los límites de las zonas de rotación y los grandes basamentos paleozoicos acrecionados, posiblemente permitiendo que los límites entre estos hayan actuado como zonas de debilidad para la formación de las futuras flexuras en el margen occidental Sudamericano.

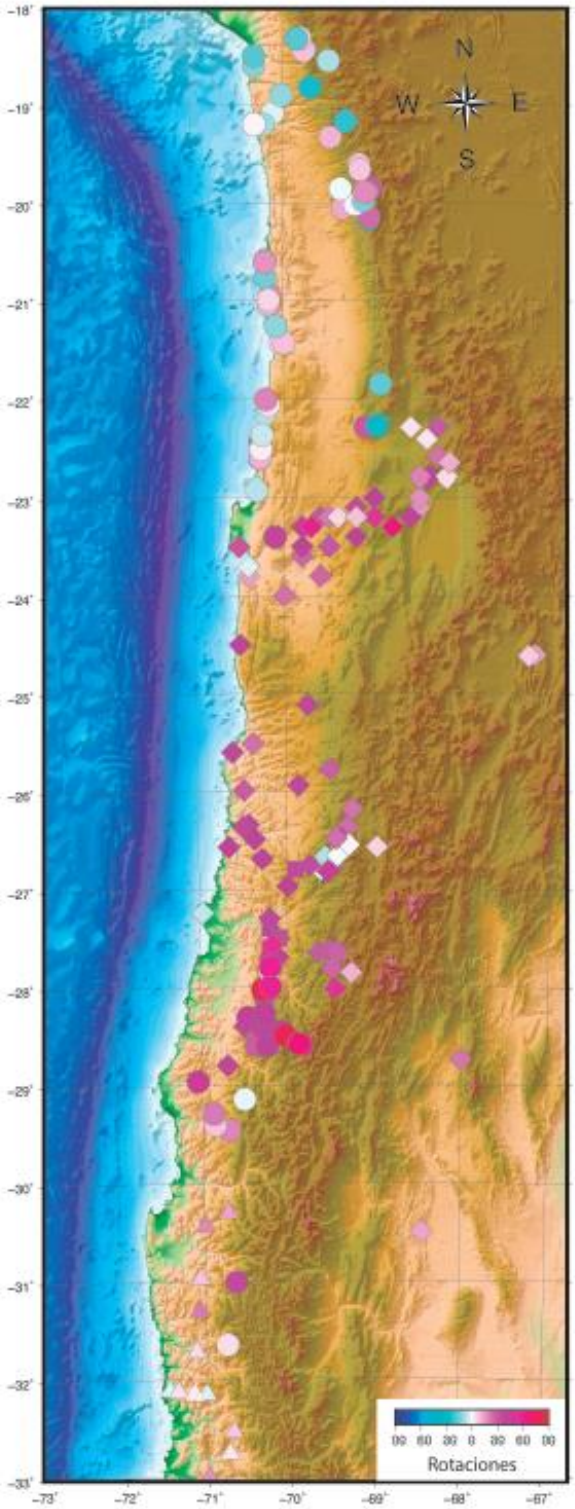

Figura 3. Resumen de las rotaciones tectónicas en el norte de Chile, los rombos corresponden a datos de Arriagada et al. (2006), los cuadrados a Taylor et al., (2007) y los triángulos a Arriagada et al. (2013). Los círculos corresponden a los datos de este trabajo.

Agradecimientos

Los autores desean agredecer a Sergio Villagran y Marco Vaccaris por su apoyo en terreno. Matias Peña agradece la beca doctoral CONICYT, con la cual fue posible la realización de este trabajo.

Referencias

Álvarez, J., Mpodozis, C., Blanco-Quintero, I., García-Casco, A., Arriagada, C., & Morata, D. (2013). U–Pb ages and metamorphic evolution of the La Pampa Gneisses: Implications for the evolution of the Chilenia Terrane and Permo-Triassic tectonics of north Central Chile. Journal of South American Earth Sciences, 47, 100-115.

Arriagada, C., Roperch, P., Mpodozis, C., Dupont-Nivet, G., Cobbold, P. R., Chauvin, A., & Cortés, J. (2003). Paleogene clockwise tectonic rotations in the forearc of central Andes, Antofagasta region, northern Chile. Journal of Geophysical Research: Solid Earth (1978–2012), 108(B1).

Arriagada, C., Roperch, P., Mpodozis, C., Fernández, R., 2006, Paleomagnetism and tectonics of the southern Atacama Desert (25-28°S), northern Chile, Tectonics, 25, TC4001, doi:10.1029/2005TC001923.

Arriagada, C., Mpodozis, C., Yáñez, G., Charrier, R., Farías, M., & Roperch, P. (2009, November). Rotaciones tectónicas en Chile central: El oroclino de Vallenar y el 'megakink'del Maipo. In Congreso Geológico Chileno (Vol. 12, pp. S9-009).

Bascuñán, S., Arriagada, C., Le Roux, J., & Deckart, K. (2015). Unraveling the Peruvian Phase of the Central Andes: stratigraphy, sedimentology and geochronology of the Salar de Atacama Basin (22° 30–23° S), northern Chile. Basin Research.

Besse, J., & Courtillot, V. (2002). Apparent and true polar wander and the geometry of the geomagnetic field over the last 200 Myr. Journal of Geophysical Research: Solid Earth (1978–2012), 107(B11), EPM-6.

Cahill, T., & Isacks, B. L. (1992). Seismicity and shape of the subducted Nazca plate. Journal of Geophysical Research: Solid Earth (1978–2012), 97(B12), 17503-17529.

Charrier, R., Pinto, L., & Rodríguez, M. P. (2007). Tectonostratigraphic evolution of the Andean Orogen in Chile. The geology of Chile (Moreno, T.; gibbons, W.; editors). The geological Society, 21-114.

Gephart, J. W. (1994). Topography and subduction geometry in the central Andes: Clues to the mechanics of a noncollisional orogen. Journal of Geophysical Research: Solid Earth (1978–2012), 99(B6), 12279-12288.

Maksaev, V., Munizaga, F., & Tassinari, C. (2014). Temporalidad del magmatismo del borde paleo-Pacifico de Gondwana: geocronologia U-Pb de rocas ígneas del Paleozoico tardio a Mesozoico temprano de los Andes del norte de Chile entre los 20° y 31° S. Andean geology, 41(3), 447-506.

Martinez, F., Arriagada, C., Valdivia, R., Deckart, K., & Peña, M. (2015). Geometry and kinematics of the Andean thick-skinned thrust systems: Insights from the Chilean Frontal Cordillera (28°-28.5° S), Central Andes. *Journal of South American Earth Sciences*.

Somoza, R., Singer, S., & Coira, B. (1996). Paleomagnetism of upper Miocene ignimbrites at the Puna: An analysis of vertical-axis rotations in the Central Andes. Journal of Geophysical Research: Solid Earth (1978–2012), 101(B5), 11387-11400.

Ramos, V. A. (2008). The basement of the Central Andes: the Arequipa and related terranes. Annu. Rev. Earth Planet. Sci., 36, 289-324.

Roperch, P., Sempere, T., Macedo, O., Arriagada, C., Fornari, M., Tapia, C., Gracia, M., Laj, C., 2006, Counterclockwise rotation

of late Eocene-Oligocene fore-arc deposits in southern Peru and its significance for oroclinal bending in the central Andes. Tectonics, 25, tc3010, doi:10.1029/2005tc001882.

Roperch, P., Carlotto, V., Ruffet, G., & Fornari, M. (2011). Tectonic rotations and transcurrent deformation south of the Abancay deflection in the Andes of southern Peru. Tectonics, 30(2).

Rubilar, J. F.; Becerra, J.; Arriagada, C. 2015. Structure of the Cordillera de la Sal: A key tectonic feature for the Oligocene-Neogene evolution of the Salar de Atacama basin, Central Andes of Northern Chile. This congress

Servicio Nacional de Geología y Minería, 2003. Mapa Geológico de Chile, Escala 1:1000000. N° Mapa:M61.

Taylor, G.K., Grocott, J., Dashwood, B., Arévalo, C., 2007, Implications for crustal rotation and tectonic evolution in the Central Andes forearc: New Paleomagnetic results from the Copiapó region in northern Chile, 26° to 28°, J. Geophys. Res., 112, NO B11, BO1102. doi:10.1029/2005JB003950.

Anexo E: Resumen presentado en el XV Congreso Geológico Chileno (2018). Concepción, Chile. P.1267.

XV CONGRESO GEOLÓGICO CHILENO
"GEOCIENCIAS HACIA LA COMUNIDAD"
18 AL 23 DE NOVIEMBRE DE 2018. UNIVERSIDAD DE CONCEPCIÓN.
CONCEPCIÓN, CHILE

SINT-1: Procesos de deformación en márgenes activos: terremotos y tectónica

Seismotectonic and geometric control of subducted Nazca plate on the Central Andes deformation styles.

Matias Alberto Peña[2,1], Andrei Maksymowicz[3], Sergio Ruiz[3].
(1) Geología, Facultad de Ciencias físicas y matemáticas, Universidad de Chile, Santiago , Chile
(2) Escuela de Geología, Facultad de Ciencias, Universidad Mayor, Santiago, Chile
(3) Geofísica, Facultad de Ciencias físicas y matemáticas, Universidad de Chile, Santiago, Chile

Along the Nazca-South America convergent margin, the slab in-homogeneities, seamounts chains, spreading centers and fractures zones correlates with the seismicity from small magnitude events to large megathrust earthquakes. In addition, the impact of the subducted slab geometry on the upper plate structure is evidenced, for instance, by the relation between the flat-slab segments and the migration of the continental deformation to the back-arc. In general, the continental plate shows tectonics longitudinal and latitudinal segmentations, which can be paired with the variability of shortening rates, styles and tectonic rotations along the South American margin. From small anticlockwise rotations, linked to the Miocene Peruvian flat-slab, to strong anticlockwise rotations, linked to Eocene-Oligocene bending of the Bolivian Orocline, in southern Peru, and Eocene-Miocene shortenings with some strike-slip deformation, to a big Eocene-Oligocene shortening age around 18°S, followed by the uplift of the Altiplano-Puna Plateau and deformation of the Sub-Andean range. From 18°S to 23°S there is small clockwise tectonic rotation, changing the deformation style again around 23°S, with strong clockwise rotations and Upper Cretaceous-Oligocene shortenings. Around 29°S another strong change in the rotational pattern occurs, changing from strong to small clockwise rotations, simultaneous to the Pampean flat-slab subduction and a thick skin tectonic style. By a joint analysis of the seismicity catalogues, bathymetry/topography, potential field maps and structural deformation data, along the Central Andes (5°S-34°S), we derive new insights about the Nazca-south America subduction process. Results highlights: (1) the high correlation between seismicity and subducted oceanic features, in particular, the relevance of the fracture zones in the subducted slab geometry, (2) the good correlation between intermediate depth seismicity and the upper plate tectonic limits of the Altiplano-Puna deformation zone, which suggests a direct relation between continental thickness/rheology and subducted plate geometry, (3) the presence of a strong change in the Central Andean Rotational Pattern (CARP), around 28-29°S, which can be correlated spatially and temporally with the subduction of the Challenger fault zone and other oceanic features. These observations raise important questions about the first order multiscale feedbacks between subducted plate and continental deformation process.

Anexo F: Publicaciones de Coautor en revistas indexadas

Journal of South American Earth Sciences 64 (2015) 261–272

Contents lists available at ScienceDirect

Journal of South American Earth Sciences

journal homepage: www.elsevier.com/locate/jsames

Paleomagnetism of Permo-Triassic and Cretaceous rocks from the Antofagasta region, northern Chile

K. Narea [a], M. Peña [a], S. Bascuñán [a], J. Becerra [a], I. Gómez [a], K. Deckart [a], F. Munizaga [a], V. Maksaev [a], C. Arriagada [a, *], P. Roperch [b]

[a] Departamento de Geología, Facultad de Ciencias Físicas y Matemáticas, Universidad de Chile, Chile
[b] Géosciences Rennes, Université de Rennes 1, CNRS, Rennes, France

ARTICLE INFO

Article history:
Received 28 April 2015
Received in revised form
8 September 2015
Accepted 10 September 2015
Available online 25 September 2015

Keywords:
Paleomagnetism
Central Andes
Northern Chile
Tectonics
Permo-Triassic
Antofagasta region

ABSTRACT

New paleomagnetic data from Permo-Triassic and Late Cretaceous rocks yield a consistent trend of vertical-axis-tectonic-rotations which are consistent with the Central Andean Rotation Pattern (CARP). However, three sites in the Tuina Formation and one site in the Purilactis Group record large rotations (80°). These mayor rotations are probably due to dextral-transpressive deformation occurring in close relation with the Incaic tectonic phase. Consequently, it is possible to infer that previous tectonic phases Peruvian and K-T would not have produced significant tectonic rotations in the area.

1. Introduction

The central Andes, a noncollisional orogeny, are a prime example of oroclinal bending (Isacks, 1988), the idea that mountain ranges form initially in a linear geometry and then are bent into their more highly curved configuration (Carey, 1955). The "Bolivian Orocline" is the change in trend of the Andes from NW to N near 18°S. The origin of the Bolivian Orocline has traditionally been studied with paleomagnetic data (e.g., Arriagada et al., 2003, 2006a, 2008; Beck, 1987; Coutand et al., 1999; Lamb, 2001; McFadden, 1990; Roperch and Carlier, 1992; Scanlan and Turner, 1992; Somoza and Tomlinson, 2002). Counterclockwise rotations with respect to stable South America are found along the Peruvian margin (Heki et al., 1984, 1985; May and Butler, 1985; Roperch and Carlier, 1992; Roperch et al., 2011) while clockwise rotations characterize the Chilean margin (Forsythe et al., 1987; Hartley et al., 1992a; Riley et al., 1993; Roperch et al., 1997). This pattern of tectonic rotations is usually called Central Andean Rotation Pattern (CARP) (Beck, 2004; Taylor et al., 2005; Roperch et al., 2006; Arriagada et al., 2008).

Mountain building in the Central Andes occurred mainly during the Cenozoic and this is the reason why paleomagnetic studies along the margin of northern Chile and Peru have been focused on essentially Jurassic, Cretaceous and Tertiary units (Fig. 1). While there are numerous paleomagnetic studies in Paleozoic rocks of the Argentinan Andes (Geuna and Ecosteguy, 2004), few studies have been reported for the Paleozoic-Triassic basement in the Andes of Northern Chile (Jesinkey et al., 1987). However, in the study of Jesinkey et al. (1987) there is no paleomagnetic data on Tertiary rocks to test the rotation history of this area.

In the present contribution, we will present paleomagnetic results from the Permo-Triassic Tuina Formation in an area where Cretaceous and Tertiary red beds have already been studied (Hartley et al., 1992a; Arriagada et al., 2000; Somoza and Tomlinson, 2002; Arriagada et al., 2003).

2. Tectonic setting

The oldest rocks found here correspond to a succession of andesitic lavas, tuffs and sandstones (Tuina Formation) deposited in a continental, volcanic environment (Mundaca, 1982). Continental sedimentary rocks of Albian to Maastrichtian-Danian age (Tonel,

* Corresponding author. Departamento de Geología, Facultad de Ciencias Físicas y Matemáticas, Universidad de Chile, Santiago, Chile.
E-mail address: cearriag@cec.uchile.cl (C. Arriagada).

http://dx.doi.org/10.1016/j.jsames.2015.09.008
0895-9811/

Tectonophysics 667 (2016) 144–162

Contents lists available at ScienceDirect

Tectonophysics

journal homepage: www.elsevier.com/locate/tecto

Tectonic styles and crustal shortening of the Central Andes "Pampean" flat-slab segment in northern Chile (27–29°S)

Fernando Martínez [a,*], César Arriagada [a], Matías Peña [a], Katja Deckart [a,c], Reynaldo Charrier [a,b,c]

[a] Departamento de Geología, Facultad de Ciencias Físicas y Matemáticas, Universidad de Chile, Santiago, Chile
[b] Escuela de Ciencias de la Tierra, Universidad Andrés Bello, Santiago, Chile
[c] Advanced Mining Technology Center, Avda. Tupper 2007, Universidad de Chile, Santiago, Chile

ARTICLE INFO

Article history:
Received 25 August 2015
Received in revised form 14 October 2015
Accepted 8 November 2015
Available online 10 December 2015

Keywords:
Flat-slab segment
Doubly vergent fault system
Inverted fault
Mesozoic extensional fault systems

ABSTRACT

The Andean orogenic belt, located in the Central Andes "Pampean flat-slab" segment in northern Chile (27–29°S), is composed of two major tectonic regions: the Coastal Cordillera and the Frontal Cordillera. To understand their internal tectonic styles, history of growth and the shortening absorbed by the upper crustal structure of this segment, we combined regional geological mapping data, new ages obtained from radiometric U–Pb dating, and a semibalanced and restored cross-section 225.18 km in length. The results as shown in the previous Mesozoic extensional fault systems, established in northern Chile by the Gondwana breakup, have played a fundamental role in the orogenic buildup. The central structure is characterized by an asymmetric basin (Upper Cretaceous–Paleocene) confined by a doubly vergent fault system composed of inverted faults related to the edges of the Mesozoic Chañarcillo and Lautaro Basins. The U–Pb geochronological data obtained from synorogenic volcano-sedimentary deposits and the angular unconformities recorded between the Cenozoic geological units have revealed that the compressive deformation in this segment started at around ~80 Ma by tectonic inversion in the eastern Coastal Cordillera and western Frontal Cordillera, however, the presence of Paleocene and Miocene synorogenic successions at the footwall of the basement reverse faults of the Frontal Cordillera suggests a migration of Andean deformation from the west to the east during the Paleocene–Miocene by propagation of ramps involving inherited basement highs. The pre-compression restoration makes it possible to estimate 40.94 km of minimum shortening, concentrated by inversion anticlines and fault-controlled basement highs across the Frontal Cordillera.

1. Introduction

The Central Andes (Fig. 1) is an orogenic belt produced by crustal shortening, thickening, and magmatism related to the subduction of the oceanic Nazca Plate beneath continental South America (Ramos, 2009). The segmentation of the Nazca Plate beneath the Central Andes (steep subduction segment (15–24°S) and the flat-slab or "Pampean" subduction segment (28–33°S); Fig. 1) (Baraganzi and Isacks, 1976; Bevis and Isacks, 1984; Cahill and Isacks, 1992; Isacks, 1988; Jordan et al., 1983) has induced notable differences in the along-strike tectonic style, as well as the presence or absence of active volcanism in this orogenic belt. The tectonic styles and the geological processes related to the flat-slab subduction segment in the Central Andes have been better recorded on the eastern side of this orogenic belt (Fig. 1), as a result of the combination of a more advanced structural stage of evolution of this segment and an outstanding level of exposure due to the aridity of the mountains at these latitudes. A significant amount of the structural knowledge of this Andean segment has been derived from the large Sierras Pampeanas (SP in Fig. 1) and the petroliferous basins located in northwestern Argentina, between 24° and 33°S (e.g., the Santa Bárbara System, the Cordillera Oriental, the Tucumán Basin, the El Metán Basin, and others). These basins were initiated as NE and NW back-arc rift systems during the Cretaceous crustal stretching of the western South America, which occurred coeval with the opening of the South Atlantic Ocean and finally were deformed by the Andean compression during Cenozoic times (Grier et al., 1991; Kley and Monaldi, 1998; Ramos, 2009; Iaffa et al., 2011, among others).

Previous studies of this segment have taken advantage of two-dimensional (2-D) and three-dimensional (3-D) seismic information and deep oil well data, which have made it possible to identify special structural features, such as thick-skinned thrust systems, characterized by steeper faults in the crystalline basement, basement-involved compressive folds, reactivated faults, and shortening estimates of no more than 150 km (Carrapa et al., 2011; Coutand et al., 2001; DeCelles et al.,

* Corresponding author at: Departamento de Geología, Facultad de Ciencias Físicas y Matemáticas, Universidad de Chile, Plaza Ercilla 803, Santiago, Chile.
E-mail addresses: martinezfjh@hotmail.com (F. Martínez), cearriag@ing.uchile.cl (C. Arriagada), geodeckart@gmail.com (M. Peña), kdeckart@ing.uchile.cl (K. Deckart), rcharrie@ing.uchile.cl (R. Charrier).

http://dx.doi.org/10.1016/j.tecto.2015.11.019
0040-1951/

Contents lists available at ScienceDirect

Journal of Geodynamics

journal homepage: www.elsevier.com/locate/jog

Late Cretaceous to Cenozoic deformation and exhumation of the Chilean Frontal Cordillera (28°–29°S), Central Andes

Fernando Martínez[a,*], Mauricio Parra[b], César Arriagada[c], Andrés Mora[d], Sebastián Bascuñan[c], Matías Peña[c]

[a] Departamento de Ciencias Geológicas, Facultad de Ingeniería, Universidad Católica del Norte, Angamos 0610, Antofagasta, Chile
[b] Institute of Energy and Environment, University of Sao Paulo, Sao Paulo, Brazil
[c] Departamento de Geología, FCFM, Universidad de Chile, Chile
[d] Ecopetrol S.A. – Instituto Colombiano del Petróleo, Piedecuesta, Colombia

ARTICLE INFO

Keywords:
Frontal Chilean Cordillera
Incaic deformation
Tectonic inversion
Basement-involved deformation

ABSTRACT

The Frontal Cordillera in northern Chile is located over the flat-slab subduction segment of the Central Andes. This tectonic province is characterized by a thick-skinned structural style showing evidence of tectonic inversion and basement-involved compressive structures. Field data, U-Pb geochronological and apatite fission track data were used to unravel partially the tectonic history of the area. Previous U-Pb ages of synorogenic deposits exposed on the flanks of basement-core anticlines indicate that Andean deformation started probably during Late Cretaceous with the tectonic inversion of Triassic and Jurassic half-grabens. New U-Pb ages of the synorogenic Quebrada Seca Formation suggest that this deformation continued during Paleocene (66-60 Ma) with the reverse faulting of pre-rift basement blocks. The analysis of new apatite fission-track data shows that a rapid and coeval cooling related to exhumation of the pre-rift basement blocks occurred during Eocene times. This exhumation event is interpreted for first time in the Chilean Frontal Cordillera and it could have occurred simultaneously with the propagation of basement-involved structures. The age of this exhumation event coincides with the Incaic orogenic phase, which is interpreted as the most important to the Central Andes in terms of shortening, uplift and exhumation.

1. Introduction

The Central Andes of northern Chile between 27° and 28°S (Fig. 1) are located over the so-called "Pampean" flat-slab subduction segment defined originally by Baraganzi and Isacks (1976), which is mainly characterized by a volcanic gap on the Chilean side, as well as by the occurrence of a mixed thick- and thin-skinned deformation style (Jordan et al., 1983; Moscoso and Mpodozis, 1988; Mpodozis and Kay, 1990; Ramos et al., 2002; Martínez et al., 2016, among others). Here, the deformed belt is divided into two large, NNE-oriented tectonic provinces: the Coastal Cordillera and the Frontal Cordillera (Fig. 1). The tectonic evolution of both provinces was marked by a series of geological processes that include extensional deformation creating back-arc basins during Mesozoic times (Triassic-Jurassic; Mpodozis and Ramos, 2008), and compressional tectonic episodes and magmatism, which created thrust systems that led to shortening and thickening of the continental margin during the Cenozoic (Mpodozis and Ramos, 1989; Ramos et al., 2002; Ramos, 2009). Both tectonic processes (extension and compression) are mostly associated with the westward South America plate motion, changes in the convergence rate between the oceanic pacific plate and South America, as well as by the coupling between both plates (Moscoso and Mpodozis, 1988; Mpodozis and Ramos, 1989; Ramos et al., 2002; Ramos, 2010; Ramos and Folguera, 2009).

The Chilean Frontal Cordillera (Figs. 1 and 2) consists of a series of large (≥ 50 km-long) Permo-Triassic crystalline basement blocks, that are well-exposed along an extensive belt that forms part of a group of Upper Paleozoic to Low Mesozoic intrusives, similar to those the form the Cordillera Real in Ecuador and the Cordillera Real of Bolivia (Mpodozis and Ramos, 1989; Mpodozis and Kay, 1990; Gregori et al., 2003; Chew et al., 2007; Hervé et al., 2014). In northern Chile (Fig. 2), these basement blocks lie intercalated with NNE-striking belts made of Mesozoic and Cenozoic volcanic and sedimentary successions (Fig. 2) that record the successive episodes of deformation within this Andean segment (Jensen, 1976; Moscoso and Mpodozis, 1988; Moscoso et al., 2010; nez et al., 2015, 2016; nez et al., 2015, 2016). The present-day

* Corresponding author.
E-mail address: martinezfjh@hotmail.com (F. Martínez).

http://dx.doi.org/10.1016/j.jog.2017.08.004
Received 24 April 2017; Received in revised form 21 August 2017; Accepted 22 August 2017
Available online 08 September 2017

Received: 18 January 2021 | Revised: 18 May 2021 | Accepted: 25 May 2021

DOI: 10.1111/bre.12580

RESEARCH ARTICLE

Basin Research | EAGE | WILEY

Contraction and exhumation of the western Central Andes induced by basin inversion: New evidence from "Pampean" subduction segment

Fernando Martínez[1] | **Matías Peña**[2] | **Mauricio Parra**[3] | **Cristopher López**[1]

[1]Departamento de Ciencias Geológicas, Facultad de Ingeniería, Universidad Católica del Norte, Antofagasta, Chile

[2]Universidad Mayor, Escuela de Geología, Santiago, Chile

[3]Institute of Energy and Environment, University of Sao Paulo, Sao Paulo, Brazil

Correspondence
Fernando Martínez, Departamento de Ciencias Geológicas, Facultad de Ingeniería, Universidad Católica del Norte, Antofagasta, Chile.
Email: fernando.martinez@ucn.cl; martinezfjh@gmail.com

Funding information
Fondo Nacional de Desarrollo Científico, Tecnológico y de Innovación Tecnológica

Abstract

In this study, we conducted an integrated analysis supported by previous regional and mesoscopic field observations, new U–Pb chronological data of synorogenic deposits and thermochronological data from syncontractional granitic rocks. The objective is understanding the main mechanism and timing of crustal uplift of the western Central Andes on the modern flat-slab segment of northern Chile. The first-order structural styles identified in several basins of northern Chile consisted mostly of large reverse-reactivated Mesozoic normal faults, which formed large kilometer-scale inverted anticlines and localized doubly verging basement reverse faults depending on the degree of tectonic inversion. The observations indicate that crustal shortening experienced in the region was distributed along with the pre-orogenic half-graben structures of the Triassic to Jurassic basement. The wide distribution of Upper Cretaceous–Paleocene synorogenic deposits over the syn-rift Mesozoic deposits along inverted structures in both the Coastal and Frontal cordilleras indicate that the Andean orogenesis in the region was initiated during this period. Our field and geochronological interpretations suggest that basin inversion of the ancient Mesozoic half-graben structures was frequently accompanied by the emplacement of Upper Cretaceous and Paleocene intrusive granitic bodies hosted in the core of the anticline and syncline folds. Their crystallization ages correlated with those reported by the synorogenic deposits, thereby suggesting that both basin inversion and magmatism occurred simultaneously. The thermal history of the intrusives also indicates that they were rapidly exhumed at 53–57 Ma, possibly during the final episodes of the basin inversion.

KEYWORDS

Andean tectonics, basin analysis, basin inversion, fold and thrust belts, orogenic belt

1 | INTRODUCTION

The Central Andes of South America (Figure 1) corresponds to an active orogen with an area of approximately 500,000 km^2. It is considered to be associated with the subduction of the oceanic plate under the continental margin. The topographic and tectonic features of the orogen were formed due to crustal shortening during Cenozoic, which underwent alteration with local extension, strike-slip deformation and magmatism in certain places (Allmendinger

Tectonics

RESEARCH ARTICLE

10.1029/2020TC006499

Architecture, Kinematics, and Tectonic Evolution of the Principal Cordillera of the Andes in Central Chile (~33.5°S): Insights From Detrital Zircon U-Pb Geochronology and Seismotectonics Implications

Verónica Mardones[1], Matías Peña[1,2], Sebastián Pairoa[1], Jean Baptiste Ammirati[1], and Mathieu Leisen[1]

[1]Departamento de Geología, Universidad de Chile, Santiago, Chile, [2]Facultad de Ciencias, Escuela de Geología, Universidad Mayor, Santiago, Chile

Abstract We assess the role of inherited structures on the Meso-Cenozoic tectonic evolution of the main Andean Cordillera in central Chile (33°30′S-34°S). Based on extensive field mapping, U-Pb geochronology and palinspastic restorations along the Yeso and Volcán river valleys, we propose a tectono-stratigraphic model for the evolution of a hybrid fold-and-thrust belt, originated from the inversion of Mesozoic extensional basins. With these results, we highlight the structural graben configuration of the Yeguas Muertas and Nieves Negras depocenters, as evidenced by synextensional deposition of the Río Damas and Lo Valdés Formations, controlled by normal faulting. The uppermost Cretaceous evolution can be approached through the analysis of the Las Coloradas Unit (ULC), which overlies the volcanic rocks of the upper Colimapu Formation and can be correlated, north of 32°S, with the Juncal Formation, and south of 35°S, with the Plan Los Yeuques Formation. The contractional Neogene-Quaternary deformation in the fold-and-thrust belt domain studied in this work, accommodated 27–28 km of minimum crustal shortening. The Neogene-Quaternary deformation that generated the final uplift of the Andes, has a close relationship with preexisting inverted Mesozoic structures. These structures deform the volcano-sedimentary Abanico Formation, deposited since the late Eocene, based on new U-Pb detrital zircon data. We propose that the active seismicity observed in the eastern border of the Principal Cordillera, located to the east of Santiago, can be associated with major crustal faults, as the Estero de Yeguas Muertas-Baños Colina fault system and the Chacayes-Yesillo fault.

Key Points:

- The geochronological new data confirm the Andean Jurassic arc as a sediment source for the Río Damas Formation
- The geometry of the western AFTB is controlled by heterogeneities inherited from the Neuquén Basin
- The Chacayes-Yesillo fault and the foot of the Estero de Yeguas Muertas-Baños Colina fault system concentrate the recent seismic activity

Supporting Information:

Supporting Information may be found in the online version of this article.

Correspondence to:

V. Mardones,
veronica.mardones@ug.uchile.cl

Citation:

Mardones, V., Peña, M., Pairoa, S., Ammirati, J. B., & Leisen, M. (2021). Architecture, kinematics, and tectonic evolution of the principal cordillera of the Andes in central Chile (~33.5°S): Insights from detrital zircon U-Pb geochronology and seismotectonics implications. *Tectonics*, 40, e2020TC006499. https://doi.org/10.1029/2020TC006499

Received 24 SEP 2020
Accepted 26 MAY 2021

1. Introduction

The South American western margin has recorded an active and continuous subduction since the Carboniferous (Coloma et al., 2017; Del Rey et al., 2016, 2019; Oliveros et al., 2020). This process has driven the complex evolution of different segments of the Andean orogen, which generated the series of latitudinal and longitudinal variations observed in the present day (Cembrano & Lara, 2009; Cobbold et al., 2006; Mpodozis & Ramos, 1989; Ramos, 1996). Latitudinal variations in the amount of tectonic shortening and deformation style may have been controlled by regional heterogeneities in the upper continental crust and subducted slab (Jordan et al., 1983; Mpodozis & Ramos, 1989). Among these, the Pampean flat-slab subduction zone (27°S-33°S) is one of the most remarkable features in this orogen (Cahill & Isacks, 1992; Gutscher et al., 2000). It is characterized by a series of tectonic domains, with an accretionary wedge in the Coastal Cordillera, Quaternary deposits in the Central Valley, a hybrid thrust belt in the Principal Cordillera, a rigid block uplift in the Frontal Cordillera, basement uplift in the Precordillera and the Sierras Pampeanas, and a series of Neogene-Quaternary broken foreland basins (Alvarado et al., 2009; Giambiagi et al., 2015; Lossada et al., 2020; Martinez et al., 2016; Ramos et al., 2002, 2004; Rodriguez et al., 2018; Suriano et al., 2017). A decrease of volcanic activity since the early and middle Miocene (Jones et al., 2016; Kay & Abbruzzi, 1996; Litvak et al., 2007; Ramos et al., 2002), and a complex history of shortening and exhumation (Barrionuevo et al., 2019; Lossada et al., 2017, 2020; Martos et al., 2020; Rodriguez et al., 2018; Suriano et al., 2017) is also one of the main features of this area. The transition between the Pampean flat-slab and the southern normal subduction zone is observed along the Aconcagua fold-and-thrust belt (AFTB; Figure 1), characterized by a mixture of thin- and thick-skinned tectonic styles (Giambiagi & Ghiglione, 2009; Giambiagi et al., 2003a,

Journal of South American Earth Sciences 106 (2021) 102981

Contents lists available at ScienceDirect

Journal of South American Earth Sciences

journal homepage: www.elsevier.com/locate/jsames

Spatio-temporal variation of the strain field in the southern Central Andes broken-foreland (27°30′S) during the Late Cenozoic

R. Quiroga [a,*], M. Peña [b,c,d], F. Poblete [b,c], L. Giambiagi [a], J. Mescua [a,f], I. Gómez [b,c], A. Echaurren [a], S. Perroud [b], J. Suriano [a], F. Martínez [e], D. Espinoza [e]

[a] Grupo de Tectónica, IANIGLA, CCT Mendoza, CONICET, Argentina
[b] Departamento de Geología, Universidad de Chile, Plaza Ercilla 803, Santiago, Chile
[c] Laboratorio de Paleomagnetismo, Departamento de Geología, Universidad de Chile, Plaza Ercilla 803, Santiago, Chile
[d] Escuela de Geología, Universidad Mayor, Santiago, Chile
[e] Departamento de Ciencias Geológicas, Universidad Católica del Norte, Antofagasta, Chile
[f] Facultad de Ciencias Exactas y Naturales, Universidad Nacional de Cuyo, Argentina

ARTICLE INFO

Keywords:
Anisotropy of magnetic susceptibility
Broken foreland
Fiambalá basin
Strain field
NW Sierras Pampeanas
Kinematic analysis

ABSTRACT

We present an integrated structural and Anisotropy of Magnetic Susceptibility (AMS) study focused on the characterization of the spatio-temporal variation of the strain field during the main Neogene deformation, of the Argentine Precordillera and the northern Sierras Pampeanas, immediately to the south of the Puna plateau (27°30′S). The AMS from 43 sites and fault-slip data analysis from mesoscale faults (n = 540) were carried out in Lower Miocene to Middle Pliocene sedimentary and volcaniclastic rocks. The AMS results show moderate values of anisotropy degree near to deformation zones, and low and high values of bulk susceptibility. The most predominant magnetic fabric is sedimentary type I and II, with a weak magnetic lineation. In areas where the rocks are deformed, the incipient magnetic lineation are subparallel to the regional structural trend and present a main N–S orientation in the Precordillera and Fiambalá basin, while in the Sierras Pampeanas they are mostly NE-oriented. Combining these results with kinematic analysis from fault-slip data, we identify, in the Precordillera and Fiambalá basin areas, a contractional event with E-W main direction, from ~23 Ma to 5 Ma, mostly active from the onset of deposition of Neogene sequences. During this period, in the NW Sierras Pampeanas, the contraction directions follow a NW orientation. The onset of N–S to NNW contraction, mostly recognized in rocks younger than 5 Ma, exposed in the northern areas of Precordillera and Sierra Pampeanas, documents a change of the strain field during the Early-to-Middle Pliocene, associated with a shift in the contractional direction from E-W to N–S. We relate the change to the rapid uplift of the southern Puna, generating a juxtaposition of an area under N–S extension, affecting the topographically-higher Puna, with the other area under N–S contraction in the adjacent Precordillera and Sierras Pampeanas. We associate these two events as part of the evolution of this segment of the Andes, where the broken foreland setting is active during this time. By combining the AMS and kinematic analysis results, we obtain a timing for the spatio-temporal change of contraction directions, which allows us to compare both the broken-foreland and foreland basins to understand spatio-temporal strain variations.

1. Introduction

In subduction zones, deformation of the continental lithosphere has been interpreted as a response to a regional stress field induced by plate tectonics dynamics (Zoback, 1992; Hu et al., 1996). In this tectonic setting, the cordilleran orogenic system corresponds to a trench-parallel elongated morphostructural belt, which evolution is registered by deformation, magmatism and sedimentation (DeCelles et al., 2009) developed with variable crustal architecture and surface morphology. The Andes, the largest of these non-collisional orogenic systems, have suffered several episodic deformational events through their Late Paleozoic to Cenozoic evolution, leading to the construction of a highly-segmented orogen (e.g., Mpodozis and Ramos, 1989; Kley et al., 1999; Horton, 2018). The Altiplano-Puna plateau in the Central Andes,

* Corresponding author.
E-mail address: rquiroga@mendoza-conicet.gob.ar (R. Quiroga).

https://doi.org/10.1016/j.jsames.2020.102981
Received 27 May 2020; Received in revised form 24 September 2020; Accepted 20 October 2020
Available online 25 November 2020
0895-9811/